Vol. 99 No. 1 July 1, 1978

ISSN 0003-2670

ANALYTICA CHIMICA ACTA

International journal devoted to all branches of analytical chemistry

ELSEVIER SCIENTIFIC PUBLISHING COMPANY

ANALYTICA CHIMICA ACTA

International journal devoted to all branches of analytical chemistry
Revue internationale consacrée à tous les domaines de la chimie analytique
Internationale Zeitschrift für alle Gebiete der analytischen Chemie

PUBLICATION SCHEDULE FOR 1978 (incorporating the section on Computer Techniques and Optimization).

	J	F	M	A	M	J	J	A	S	O	N	D
Analytica Chimica Acta	96/1	96/2	97/1	97/2	98/1	98/2	99/1	99/2	100	101/1	101/2	102
Section on Computer Techniques and Optimization			103/1			103/2			103/3			103/4

Scope. *Analytica Chimica Acta* publishes original papers, short communications, and reviews dealing with every aspect of modern chemical analysis, both fundamental and applied. The section on *Computer Techniques and Optimization* is devoted to new developments in chemical analysis by the application of computer techniques and by interdisciplinary approaches, including statistics, systems theory and operation research.

Submission of Papers. Manuscripts (three copies) should be submitted to:
for *Analytica Chimica Acta:* Dr. A. M. G. Macdonald, Department of Chemistry, The University, P.O. Box 363, Birmingham B15 2TT, England;
for the section on *Computer Techniques and Optimization:* Dr. J. T. Clerc, Laboratorium für Organische Chemie, Swiss Federal Institute of Technology, Universitätstrasse 16, CH-8092 Zürich, Switzerland.

Information for Authors. Papers in English, French and German are published. There are no page charges. Manuscripts should conform in layout and style to the papers published in this Volume. Authors should consult Vol. 93, p. 379 for detailed information. Reprints of this information are available from the Editors or from: Elsevier Editorial Services Ltd., Mayfield House, 256 Banbury Road, Oxford OX2 7DE (Great Britain).

Reprints. Fifty reprints will be supplied free of charge. Additional reprints (minimum 100) can be ordered. An order form containing price quotations will be sent to the authors together with the proofs of their article.

Advertisements. Advertisement rates are available from the publisher.

Subscriptions. Subscriptions should be sent to: Elsevier Scientific Publishing Company, P.O. Box 211, 1000 AE Amsterdam, The Netherlands. The section on *Computer Techniques and Optimization* can be subscribed to separately.

Publication. *Analytica Chimica Acta* (including the section on *Computer Techniques and Optimization*) appears in 8 volumes in 1978. The subscription for 1978 (Vols. 96–103) is Dfl. 1000.00 plus Dfl. 120.00 (postage) (Total approx. US $486.96). The subscription for the *Computer Techniques and Optimization* section only (Vol. 103) is Dfl. 125 plus Dfl. 15.00 (postage) (Total approx. US $60.87). Journals are sent automatically by air mail to the U.S.A. and Canada at no extra cost and to Japan, Australia and New Zealand for a small additional postal charge. All earlier volumes (Vols. 1–87) are available at Dfl. 115.00 (plus postage).

Claims for issues not received should be made within three months of publication of the issue, otherwise they cannot be honoured free of charge.

Customers in the U.S.A. and Canada who wish to obtain additional bibliographic information on this and other Elsevier journals should contact our Journal Information Center, 52, Vanderbilt Avenue, New York, NY 10017. Tel: (212) 867-9040.

on-Selective Electrodes

onference held at Budapest, Hungary, 5-9 September, 1977

PUNGOR and **I. BUZAS** (Editors)

ıis volume, containing 55 papers presented by participants from 18 countries, ovides an account of recent results in this rapidly developing field of electro- ıalytical chemistry. The 7 plenary lectures cover current trends of research in e field of ion-selective electrodes, theoretical problems related to the mechanisms the electrode response and results in the field of new electrode constructions, well as the standardization of ion-selective electrodes and their application at gh temperatures.

ıe 48 discussion papers concentrate mainly on the analytical applications of ion- lective electrodes. Some topics of special interest are discussed, such as:

ransport characteristics and dynamic behaviour of glass membrane electrodes
nzyme electrodes
iquid membrane electrodes
on-exchanger electrodes
roblems of the incorporation of ion-selective electrodes into automatic systems
ecently developed analyzers and electrode types

ıis volume will not only be of value to researchers concerned with the theory of n-selective electrodes, but also to analytical chemists working in a wide range fields and those dealing with the technical aspects of instrument development.

pril 1978 624 pages US $75.00/Dfl. 180.00 ISBN 0-444-99799-7

odd's Chemistry of Carbon ompounds (Second Edition)

COFFEY (editor)

OLUME IV: HETEROCYCLIC COMPOUNDS

ırt H: Six-membered heterocyclic compounds with (a) a nitrogen atom common two or more fused rings; (b) one hetero-atom in each of two fused rings. Six- embered ring compounds with two hetero-atoms from Groups VI B, or V B and I B of the Periodic Table, respectively. Isoquinoline, lupinane and quinolizidine kaloids

ıe wide and varied range of compounds considered in this volume makes it of ıecial interest not only to organic chemists, but also to a much wider circle of aders.

lay 1978 xx + 576 pages US $106.95/Dfl. 245.00 ISBN 0-444-41575-0

ELSEVIER

P.O. Box 211, Amsterdam
The Netherlands
52 Vanderbilt Ave
New York, N.Y. 10017

e Dutch guilder price is definitive. US $ prices are subject to exchange rate fluctuations.

7091

JOURNAL OF CHROMATOGRAPHY
BIOMEDICAL APPLICATIONS

An international journal devoted to new developments and advances in biomedical applications of chromatography and electrophoresis.

Specimen copies are available upon request.

Aims and Scope

The journal publishes papers dealing with the following aspects:
- developments in, and applications of chromatographic and electrophoretic techniques related to clinical diagnosis (including the publication of normal values).
- screening and profiling procedures with special reference to metabolic disorders.
- results from basic medical research with direct consequences in clinical practice.
- combinations of chromatographic and electrophoretic methods with other physico-chemical techniques such as mass spectrometry.

Furthermore, the journal encourages contributions that give new information concerning the composition of tissues and body fluids. Manuscripts dealing with drug and metabolic levels, with special reference to blood, urine and other body fluids, particularly when related to therapy, are welcome. Also acceptable are papers describing new chromatographic and electrophoretic techniques devoted to clinical toxicology, and the determination of toxic levels of commonly used pharmaceuticals, but excluding toxicological studies per se. Chromatographic and electrophoretic studies on environmental hazards are considered for publication, providing they are directly related to clinical analysis.

Types of Contributions

Original papers
Short communications
Review articles (following a preliminary agreement with the editor).
Information regarding new instrumentation, chromatographic and electrophoretic materials and accessories, forthcoming events, etc., which are published in the News Section.
Reviews of books within the scope of the journal.

Publication Schedule

The JOURNAL OF CHROMATOGRAPHY, BIOMEDICAL APPLICATIONS is published bimonthly, six issues per year constituting two volumes.

Subscription Information

The journal forms an integral part of the Journal of Chromatography. However, it can be subscribed to separately. The subscription price for 1978 (Volumes 2 and 3 totalling six issues) is US $119.25/Dfl. 274.00 including postage.

Journals are automatically sent by air to the U.S.A. and Canada at no extra cost, and to Japan, Australia and New Zealand with a small additional postal charge.

ELSEVIER

P.O. Box 211, Amsterdam
The Netherlands
52 Vanderbilt Ave
New York, N.Y. 10017

The Dutch guilder price is definitive. US $ prices are subject to exchange rate fluctuations.

7088

ANALYTICA CHIMICA ACTA
VOL. 99 (1978)

ANALYTICA CHIMICA ACTA

International journal devoted to all branches of analytical chemistry

ELSEVIER SCIENTIFIC PUBLISHING COMPANY

Anal. Chim. Acta, Vol. 99 (1978)

Printed in The Netherlands

Analytica Chimica Acta, 99 (1978) 1—36

Review

POLYURETHANE FOAMS AND MICROSPHERES IN ANALYTICAL CHEMISTRY
Improved Liquid—Solid, Gas—Solid and Liquid—Liquid Contact via a new Geometry of the Solid Phase

T. BRAUN* and A. B. FARAG**

Institute of Inorganic and Analytical Chemistry, L. Eötvös University, P.O. Box 123, 1443 Budapest (Hungary)

(Received 2nd February 1978)

SUMMARY

This review covers the following aspects: the preparation and properties of polyurethane foams and of open-pore polyurethane microspheres; the use of unloaded polyurethane foams for the separation and enrichment of inorganic and organic species in aqueous solution, and for the collection of pesticide vapours in air; and the application of polyurethane foams with physically immobilized reagents (hydrophobic reagents such as organic extractants and chelating agents, heterogeneous ion-exchange foams and inorganic precipitates). Polyurethane foams with anchored functional groups and specially treated polyurethane foams are then discussed. Finally the use of open-pore polyurethane microspheres in gas—solid chromatography, gas—liquid chromatography, and low pressure liquid chromatography is outlined.

Natural sponge (a material of foam-like geometry) treated with olive oil was used, more than four centuries ago, for the purification of ethanol in a distillation system [1]. This method is a true foam separation method and can be considered as a precursor of gas—liquid partition chromatography in which the sponge material is the solid support, olive oil the stationary phase and the ethanol vapours the mobile phase. This technique was checked by Bayer [2] in 1962 and proved to operate well.

The extraction of trace elements from sea water with natural sponges supporting an iron(III) hydroxide precipitate has also been reported [3]. Many elements (e.g., Si, Be, Al and Ti) could be enriched by towing iron(III) hydroxide-impregnated sponge through coastal sea-water.

During the past decade, foamed plastics (mainly polyurethanes) have been tested [4] as supports in reversed-phase extraction chromatography [5], and in gas—solid and gas—liquid partition chromatography [6]. The high available surface area and cellular structure of polyurethane foam makes it very suitable

**Permanent address: Chemistry Department, Faculty of Science, Mansoura University, Mansoura, Egypt.

as an adsorbent and absorbent and as a column-filling material. Polyurethane in foamed and microspherical form has an excellent capacity for firmly retaining various loading and extracting agents. The hydrodynamic properties of foam-filled columns have been shown [5] to be very favourable, and relatively high flow-rates can be attained simply by gravity flow.

The absorption capabilities of untreated polyurethane foams for inorganic and organic species in aqueous solution and also in the gaseous state have been investigated [7, 8, 18].

Polyurethane foams immobilizing various hydrophobic reagents [9—12], powdered ion-exchangers [13, 14] and finely divided precipitates [15, 16] have been recommended for several analytical applications. Foam materials to which certain functional groups are anchored have also been prepared [13, 17].

In general, the membrane-like structure of polyurethane foam facilitates the kinetics of the absorption and extraction processes in solid—liquid, solid—gas and liquid—liquid contact. The possibilities of using untreated polyurethane foams and specially treated ones for the separation, preconcentration and detection of various metal ions from aqueous solutions have been emphasized [18—20]. The advantages of precipitated open-pore polyurethane microspheres in gas and liquid chromatographic operations have also been demonstrated [21].

A systematic review of the potentialities of using polyurethane foams and precipitated open-pore polyurethane for analytical separations is presented in this paper.

PREPARATION AND PROPERTIES

Polyurethane foams

In general, cellular (foamed) plastics can be defined [22] as plastic materials in which a proportion of the solid phase is replaced by gas in the form of numerous small cells. The gas may be in continuous phase to give an open-cell material or it may be discontinuous, i.e. in the form of discrete, non-communicating cells. From the geometrical point of view, if the gas bubbles occupy a volume smaller than 76%, they may be spherical; if they occupy a larger volume, they will be distorted into polyhedra [23] (pentagonal dodecahedra on average). Figure 1 shows a typical polyurethane foam in which the bubbles (cells) occupy 97% of the volume.

The cell structure (i.e. presence or absence of windows in the cells or the number of windows per cell) is a function of the process by which the cellular material is made [24]. Polyurethane foams can be prepared in soft, flexible or rigid forms [25] and have been prepared from a variety of polyesters and polyethers. The two most important reactions in the preparation of urethane foams are the reaction between isocyanate and hydroxyl compounds (polyester or polyether polyols) and the reaction between isocyanate and water. For the formation of urethane groups, the former reaction can be considered as the chain-propagating reaction.

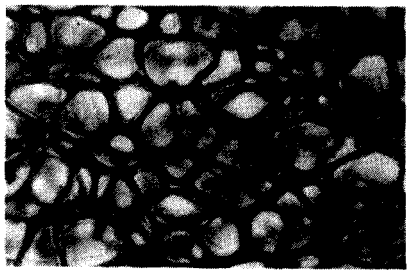

Fig. 1. Typical polyurethane foam structure (97% void).

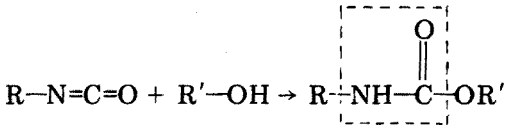

urethane (1)

The water—isocyanate reaction is responsible for the foam formation by the liberation of carbon dioxide as an in situ blowing agent. The first step of this reaction is the formation of the unstable carbamic acid which decomposes to form carbon dioxide and amine; the latter may react with an additional isocyanate to produce a substituted urea:

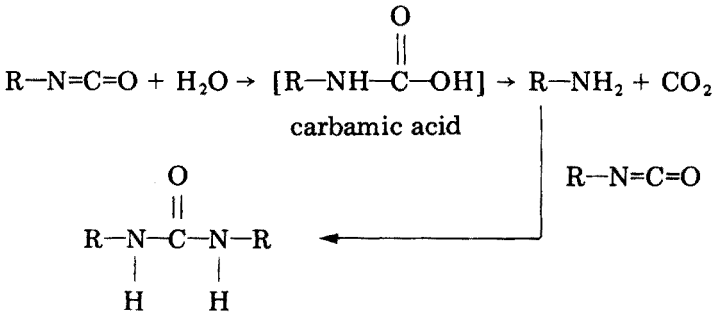

carbamic acid

substituted urea (2)

Alternatively, the carbamic acid may react with another isocyanate molecule to produce a carbamic acid anhydride which decomposes to a substituted urea and carbon dioxide

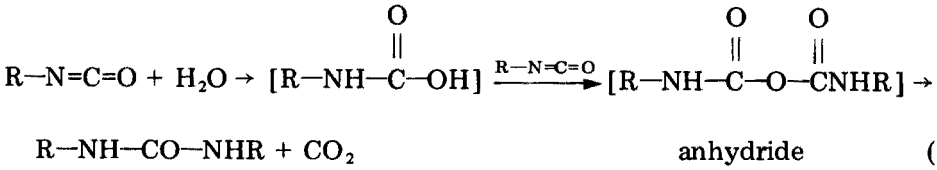

anhydride (3)

The main reactions which lead to branching and cross-linking are the isocyanate—urethane reaction producing allophanate linkages (eqn. 4) and the isocyanate—urea reaction which produces biuret (eqn. 5).

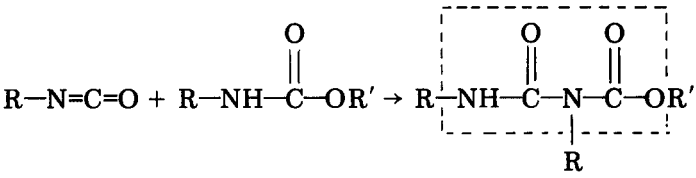

(4)

allophanate

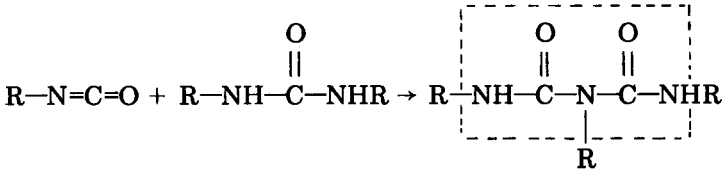

(5)

biuret

Polyol represents the largest single component in foam preparation. Many polyols are commercially available under various trade names. In general, polyols in the molecular weight range 400—6000 are employed [24, 26]. The propylene oxide adduct of glycerol with more than 90% secondary hydroxyl terminal groups (m.w. 3000) is an example of the most widely used polyol (polyether) for the production of polyether-type polyurethane foam. The second largest component of the foam formulation is the isocyanate compound. The most widely used isocyanate is toluene diisocyanate; the toluene diisocyanates usually employed are 80/20 and 65/35 mixtures of the 2,4- and 2,6-isomers. In industrial preparations, catalysts are employed to increase the reaction rate and to establish the proper balance between the chain extension and the foaming reaction. The catalysts most commonly used [25] are tertiary amines and organometallic compounds, e.g. organotin compounds.

Generally, the physical properties of polyurethane foam depend mainly on the method by which the foam is prepared. For example, the windows may or may not be ruptured in the final stage of expansion, depending on the relative rate of molecular growth (gelation) and gas reaction, giving rise to flexible (open cell) or rigid (closed cell) foam. In polyurethane foam preparation, the variety in choice of simple molecules is great and consequently the properties of the product are wide. The choice of the polyol has a major effect on the foam properties, especially its rigidity and flexibility [25]. The cross-link density of the urethane polymer determines whether the foam will be flexible (low cross-link density) or rigid (high cross-link density). Flexible foams are prepared from polyols of moderately high

molecular weight with a low degree of branching, while rigid foams are prepared from highly branched resins of low molecular weight.

The chemical properties of polyurethane foams are also a function of the preparation process. For example, the solvent resistance of polyurethane structures increases at higher cross-link densities, appears to be unaffected by the type of aromatic diisocyanate, and is reduced by the use of a large excess of isocyanate [27].

Bowen [7] examined the chemical resistance of some batches of commercial polyurethane foams and claimed that they are rather stable and inert. The foam batches tested degraded when heated between 180°C and 220°C, and slowly turned brown in ultraviolet light. They were dissolved by concentrated sulphuric acid and destroyed by concentrated nitric acid; they reduced alkaline potassium permanganate. They are mostly unaltered, apart from reversible swelling, by water, hydrochloric acid up to 6 M, sulphuric acid up to 2 M, glacial acetic acid, 2 M ammonia and 2 M sodium hydroxide solutions, as well as by solvents such as light petroleum, benzene, carbon tetrachloride, chloroform, diethyl ether, diisopropyl ether, acetone, isobutyl methyl ketone, ethyl acetate, isopentyl acetate and alcohols. It was also noted [7] that polyurethane foams can be dissolved in hot arsenic(III) chloride solution.

Open-pore polyurethane microspheres

In contrast to polyurethane foam, open-pore microspherical polyurethane is composed of agglomerated spherical particles (1—10 μm in diameter) bonded to each other in a rigid, highly permeable structure [28]. This material is formed by relatively slow precipitation from a quiescent, homogeneous, diluted mixture of the reactants (an isocyanate and a polyol in 60:40 toluene—carbon tetrachloride solution). In situ precipitation of open-pore polyurethane in various chromatographic columns of different shape, diameter and length has been described [21]. The solvent composition is selected on the basis of density so that the polymerized open-pore polyurethane particles remain suspended in the solvent, rather than floating or sinking [28]. It was reported that materials with specific density, porosity and surface characteristics can be prepared by controlling the reaction conditions.

The isocyanate can also react with other active hydrogens, e.g. in amines, glycols, organic acids and water. Open-pore polyurethane can be tailored to specific separation applications by chemically bonded functional groups at the —OH and —OCN sites.

The compatibility of open-pore polyurethane foam with various organic solvents has been measured [28]. Open-pore polyurethane is compatible with organic solvents, as well as water and dilute acids, but exposure to dilute bases causes the polyurethane—glass column bond to break easily. Open-pore polyurethane microspheres were also found to have no cation-exchange properties, but exhibit low-capacity, weak-base anion-exchange characteristics.

In general, the polyurethane product has excellent gas-flow permeability properties. Liquid phases can be incorporated in the precursor chemicals or by adding a stationary phase after the formation of the support.

UNLOADED POLYURETHANE FOAMS

Separation and enrichment of inorganic species in aqueous solution

The absorption and recovery of a number of substances from dilute aqueous solutions onto flexible polyether polyurethane foams was discovered and investigated by Bowen [7], who reported that there are two classes of substances which are strongly extracted from aqueous solution by the foam. These are substances which exist in aqueous solution as free molecules with high polarizability, e.g. iodine, aromatic compounds, metal dithizonates, and univalent anions with high polarizability, e.g. $AuCl_4^-$, $TlCl_4^-$ and $FeCl_4^-$.

The surface areas of several polyurethane foam samples (of the polyether type) have been measured; the uptake of different components from aqueous solution is due to absorption rather than adsorption phenomena [7, 29]. This has been confirmed by microscopic examination of a cross-section of foam fibers after absorption of iodine; the iodine colour is uniformly distributed in the foam section and is not apparent only on its surface.

The absorption isotherms of some elements have been measured [7] and the distribution ratios and absorption capacities for these elements have been determined (Table 1).

TABLE 1

Distribution ratios and absorption capacities for foam extractions [7]

Substance	Solvent	Distribution ratios	Absorption capacities (mol kg^{-1})	Formula of complex
Iodine	Water	700—3500	0.67—1.36	I_2
Chloroform	Water	260—420	0.17—0.25	$CHCl_3$
Benzene	Water	60—140	0.45—1.79	C_6H_6
Phenol	Water	45—410	$\geqslant$0.032	PhOH
Mercury(II)	0.2 M HCl	30—125	$\geqslant$0.060	n.d.
Gold(III)	0.2 M HCl	45—3900	0.33—1.27	$AuCl_4^-$
Gold(III)	0.2 M HBr	140—570[a]	0.71—1.07	$AuBr_4^-$
Gold(III)	0.2 M HI	250—590[a]	0.76—1.68	AuI_4^-
Iron(III)	6 M HCl	40—1400	0.38—0.77	$FeCl_4^-$
Rhenium(III)	6 M HCl	340[a]	$\geqslant$0.043	n.d.[b]
Thallium(III)	6 M HCl	170—3700	0.29—0.46	$TlCl_4^-$
Antimony(V)	6 M HCl	75—500	0.25—0.59	$Sb_2Cl_5O_n^{m-}$
Molybdenum(VI)	6 M HCl	27—41[a]	0.10—0.42	n.d.
Uranium(VI)	Sat. $Al(NO_3)_3$	25—100	$\geqslant$0.16	n.d.

[a]Only one foam tested. [b]n.d. = not determined.

The efficiency of collection of radioactive gold(III) from mineral waste-waters on polyurethane foam has been compared [30] with the conventional coprecipitation method based on lead sulphide prepared by various techniques. Polyurethane foam has a specific gold-absorbing property and thus can be recommended for gold separation. In another comparative study [31], the separation of gold(III) chloride from natural waters by coprecipitation with iron(III) hydroxide, lead sulphide or aluminium hydroxide, and by separation with Dowex 1-X8 resin and flexible polyurethane foam was examined. Lead sulphide and polyurethane foam are the most efficient collectors. Gold at the ppb level ($\mu g\ l^{-1}$) can be collected quantitatively from aqueous solution onto polyurethane foam by shaking the mixture for 90 min. The recovery of the gold—thiourea complex ($Au(thiourea)_2^+$) from acidic perchlorate solution on polyurethane foam (polyether and polyester types) has been investigated [31]. Both types of foam extract this cationic complex but the absorption capacity of the polyether type is generally greater than that of the polyester one. The uptake of the gold—thiourea complex by the different polyether polyurethane foam samples depends to some extent on cell dimension; the uptake decreases as the cell size decreases.

The efficiency of extraction of the gold—thiourea complex on polyurethane foam (polyether, open cell) has also been compared with that on active carbon [32]. Although the uptake of the gold complex by 10 g of foam material is approximately equal to the uptake of 0.2 g of active carbon under identical experimental conditions, the application of the cheap foam material is advantageous [31] as it eliminates the filtration necessary in the case of carbon [32]. Figure 2 shows the effect of foam charge on the recovery of gold from acidic thiourea solution; gold-free solution can be obtained by using a foam charge of ca. 30 $g\ l^{-1}$, which again is about 50 times greater than the amount of carbon required [32].

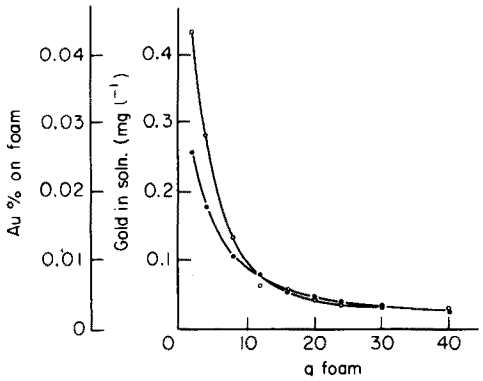

Fig. 2. Effect of foam charge (unloaded polyether polyurethane) on the sorption of gold from acidic thiourea solution. [Au] = 5×10^{-6} M. [Thiourea] = 3%. [$NaClO_4$] = 1%. [$HClO_4$] = 0.1 M. (○) Gold in soln., (●) gold on foam.

Further work on the recovery of gold by polyurethane foam has been carried out by Sukiman [12] who described the application of polyether polyurethane foam for the extraction of gold(III) chloride from acidic aqueous solution, using the dynamic technique. Gold(III) at trace levels (0.02—25 ppm) was quantitatively collected from acidic aqueous solution by percolating the solution through a short foam column at relatively high flow-rates (10—13 ml cm^{-2} min^{-1}*). Acetone has been employed for the recovery of gold from the foam column at a flow-rate of 1 ml cm^{-2} min^{-1}. It was reported [12] that 0.3 M thiourea solution in 1 M HCl could be used for the recovery of the absorbed gold at 50°C, but the acetone elution was recommended as it is not convenient to work at high temperatures. The polyurethane foam method was then applied to extract gold from natural waters.

Gesser et al. [33] have shown that open-cell polyurethane foam of the polyether type can be used as a convenient solid substitute for liquid diethyl ether in extraction systems. They investigated the extraction and recovery of gallium from acidic chloride solutions. The effect of hydrochloric acid concentration on the extraction efficiency is more or less similar to that found in diethyl ether extractions. It was proved that the open-cell foam is more efficient than the closed-cell rigid foam. However, silicone rubber sponge does not extract gallium under similar experimental conditions. Water or weakly basic solution is very effective in removing gallium from the foam columns [33]. Figure 3 shows the effect of acid and base strengths on the recovery of gallium from the foam column.

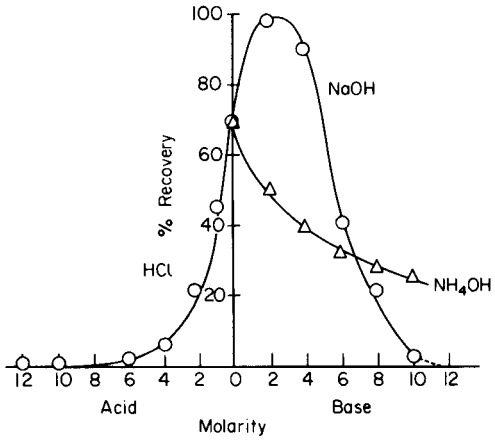

Fig. 3. Effect of acid and base concentrations on the recovery efficiency for gallium from a foam plug [33].

*It is necessary to include the cross-sectional area of the column in specification of the flow-rate, which thus has the dimensions of a linear flow-rate.

The effects of temperature and flow-rate on the extraction and recovery of gallium have also been investigated. Generally, the extraction and recovery efficiencies are increased by decreasing the flow-rate. After a detailed experimental study, Gesser et al. [33] concluded that foam column efficiency for extracting gallium can be increased either by passing the solution through several foam plugs or by passing the same solution through the foam several times. Under optimal experimental conditions, it was possible to absorb gallium in the foam to the extent of 10% by weight. This relatively high absorption capacity is due mainly to dissolution of the gallium chloride complex in the foam material rather than to adsorption on the foam surfaces. That is, the foam material acts as a polymeric solid extractant for gallium. This method can be applied for the separation of gallium and iron from aluminium in acidic chloride solutions.

In a recent paper [34], the thermodynamic properties of open-cell polyurethane foam as a solid extractant for gallium from acidic chloride solution are described in terms of the acid, chloride and gallium concentrations. It was proved that the diffusion of gallium into the foam membrane is consistent with the solubility of the $HGaCl_4$ complex in polyurethane foam.

Further proof that open-cell polyether-type polyurethane foam can act as a solid ether solvent has recently been provided by Braun and Farag [35]. In this connection, the extraction of thiocyanate complexes of iron and cobalt was investigated. The extraction rates of cobalt(II) and iron(III) from acidic thiocyanate solutions are quite fast, and this system can be applied in column operations. It is noteworthy that cobalt and iron cannot be extracted from acidic aqueous thiocyanate media with polyester-type polyurethane foam.

The effect of flow-rate on the extraction efficiency of the polyether-type polyurethane foam columns has been investigated [35]. More or less complete extraction of 2 μg of cobalt or iron can be obtained from acidic thiocyanate solutions onto the foam columns at flow-rates as high as 8 ml cm^{-1} min^{-1}. Also, quantitative recoveries of cobalt and iron, in concentrations ranging between 0.2 and 200 μg can be obtained at flow-rates of 4 ml cm^{-2} min^{-1}. These high capacities prove that the foam material acts as a solid polymeric extractant for these complexes.

The polyurethane foam columns are also useful for the preconcentration of 1 μg of cobalt or iron in 1-l volumes of aqueous thiocyanate solutions at flow rates of 6 ml cm^{-2} min^{-1}.

Separation and enrichment of organic species in aqueous solution

Gesser et al. [18] initiated the application of unloaded polyurethane foam (polyether type) for the extraction and recovery of organic contaminants from water. Polychlorinated biphenyls at various concentrations (2—20 μg l^{-1}) can be collected successfully by passing the aqueous solution through polyurethane foam plugs designed as culture tube stoppers. It was claimed that 95% of the polychlorinated biphenyls is retained by the first foam plug and

a few percent retained by the second plug at a flow-rate as high as 80 ml cm^{-2} min^{-1}. Acetone and hexane are employed for elution of the absorbed biphenyls. The eluent is then concentrated in a rotary evaporator and the concentration of polychlorinated biphenyls is determined by gas chromatography.

Polyurethane foam placed in a standard carbon adsorption metering apparatus has been used [36] to monitor organic matter in drinking water. A certain volume of water (1—2 l) is percolated through the foam columns at 2—4 ml cm^{-2} min^{-1}. The foam plugs are then extracted with pesticide-grade hexane in a Soxhlet extractor to wash out the absorbed organic compounds. Gas chromatography is used to analyze the hexane extract after suitable concentration in a flash evaporator. Figure 4 shows typical chromatograms obtained by this method.

A detailed study on the different factors affecting the extraction and recovery of various organochlorine insecticides and polychlorinated biphenyls with polyurethane foam columns has been carried out by Musty and Nickless [37], who examined six different foam samples of different surface areas and bulk densities. It was found that the efficiency of adsorption of methylene blue from aqueous solution by the foam material can be used as a criterion for the relative efficiency of extraction of organic insecticides from aqueous solution. The higher the amount of methylene blue adsorbed, the higher the efficiency of the foam material for recovering insecticides from water. Polyurethane foams adsorbing ca. 250 mmol kg^{-1} of methylene blue in 24 h were recommended for use in the extraction of chlorinated insecticides and polychlorinated biphenyls. The effect of flow-rate on the efficiency of a polyurethane-foam column for extracting various insecticides is shown in Table 2. Essentially quantitative recoveries for 13

TABLE 2

The effect of flow-rate on the recovery of different insecticides from aqueous solution by the unloaded foam [37]

Insecticide	Concentration (ppm)	Recovery (%)[a]		
		10 ml min^{-1}	30 ml min^{-1}	250 ml min^{-1}
α-BHC	1	101	95	49
Lindane	1	101	91	40
β-BHC	1	101	86	44
Aldrin	1	99	73	46
p,p'-DDE	2	106	77	68
Dieldrin	1	106	77	58
Endrin	10	100	94	54
o,p'-DDT	10	113	84	43
p,p'-DDD	2	102	89	57
p,p'-DDT	10	114	100	26

[a]With glass columns of 2-cm diameter and 20-cm length.

insecticides from water can be obtained [37] on polyurethane foam columns at a flow rate of ca. 32 ml cm^{-2} min^{-1}. The effect of the pH of the water on the recovery of the different insecticides was also examined, and a pH value in the range 6—9 was recommended for quantitative recoveries. Acetone and hexane are satisfactory for elution of the extracted insecticides from the foam column and gas chromatography is suitable for analyzing the eluent.

The extraction and recovery of phthalate esters from water with porous polyurethane foam have also been investigated [38]. Polyurethane foam was successfully used to remove some phthalate esters from water at $\mu g\ l^{-1}$ concentrations. Various foam samples were tested; the results presented in Table 3 show the recovery of different phthalates (with side chains varying in length from 1 to 10 carbons). Again, acetone and hexane were employed as eluents before the final gas chromatographic procedure.

Polyurethane foam has been used [39] for the absorption of alkylbenzene sulphonates from aqueous solution. Trace amounts of alkylbenzene sulphonate in aqueous solution containing crystal violet or methylene blue are selectively absorbed on flexible polyurethane foam; the colour intensity of the foam absorbing the alkylbenzene sulphonate—crystal violet or alkylbenzene sulphonate—methylene blue ion-association complexes is proportional to the concentration of alkylbenzene sulphonate and thus the concentration of the latter can be determined visually by a standard series method. It was claimed that the alkylbenzene sulphonate can also be determined by eluting the complex from the foam with methanol and measuring the absorption of the eluent spectrophotometrically; when this static method is used, as little as

TABLE 3

Recovery of a series of phthalate esters under flow conditions
(For each test 100 ml of water spiked with 0.1 μg of each phthalate was run on a column of 5 foam plugs at 10 ml min^{-1}. The internal diameter of the column was 15 mm [38].)

Phthalate	Recovery (%)[a]	
	Foam sample A	Foam sample B
Dimethyl phthalate (DMP)	20 ± 5	8 ± 1
Diethyl phthalate (DEP)	84 ± 8	80
Di-n-butyl phthalate (DnBP)	102 ± 4	101 ± 1
Diisobutyl phthalate (DiBP)	93 ± 2	99 ± 2
Diamyl phthalate (DPA)[b]	85	80
Di-n-hexylphthalate (DnHxP)	34 ± 2	33 ± 2
Di-n-heptyl phthalate (DnHpP)	23 ± 2	25 ± 2
Di-2-ethylhexyl phthalate (DEHP)	—	—
Dioctyl phthalate (DOP)	—	—
Diisodecyl phthalate (DiDP)	—	—
Butylbenzyl phthalate (BBP)	70 ± 3	86 ± 3

[a]Foam sample A has a density of 0.030 g ml^{-1}. Foam sample B has a density of 0.019—0.022 g ml^{-1}. [b]One run only.

TABLE 4

Determination of alkylbenzene sulphonate in river waters [39]

Sample taken[a] (ml)	Alkylbenzene sulphonate added (ppm)	Alkylbenzene sulphonate found (ppm)	
		Visual method	Spectrophotometric method
20	—	5	5.7
40	—	5	5.5
20	5	10	11.0
20	10	15	13.8

[a]From a small river in Ikeda City, pH 7; Alkylbenzene sulphonate content: 6.4 ppm (by methylene blue method.)

0.5 ppm alkylbenzene sulphonate can be determined. Table 4 shows the results obtained for the determination of alkylbenzene sulphonate in actual river water. The limit of detection of this method can be decreased to 0.1 ppm by using the foam material in a dynamic system [39].

Collection of pesticide vapours in air

The collection of polychlorinated biphenyl vapours from atmospheric samples by polyurethane foam has been investigated [40, 41]. The cellular structure of the foam material offers little resistance to air passage and therefore is compatible with high-volume sampling apparatus. An efficient collection system for polychlorinated biphenyl vapours which allows hundreds of cubic meters of air to be sampled per day, has been described [40].

Polyurethane foam plugs (10 cm diameter and 5 cm long) placed in an aluminium cylinder proved to have an excellent collection efficiency for the tri-, tetra-, and pentachlorobiphenyl isomers. The extracted polychlorinated biphenyls were stripped from the foam with petroleum ether in a Soxhlet extractor, and then determined by gas chromatography. The efficiency of the foam material was found [40] to be superior to that of the Greenburg—Smith impinger containing ethylene glycol [42]. The foam method was employed for the collection of polychlorinated biphenyls from typical atmospheric samples. Comparison with Aroclor standards indicated that subnanogram amounts can be determined.

The trapping efficiency of open-cell polyester polyurethane foam for pesticide vapours in air has recently been investigated in detail by Turner and Glotfelty [8]. Polyurethane foam seems to be a nearly ideal trapping medium, since it is both highly efficient and can readily be extracted with boiling organic solvent. Foam plugs (4.5 cm diameter and 5 cm long) have both a great capacity to trap and retain high concentrations, and this high trapping efficiency was found to be independent of the vapour concentration of the six pesticides examined (dieldrin, heptachlor, *trans*-chloradane

and lindane as insecticides, and trifluralin and dacthal as herbicides). In all cases a single plug could trap 98% or more of the total pesticide vapour added. The highest amount tested (300 μg) was trapped as efficiently as lower concentrations, and was retained even when pesticide-free air was drawn through the exposed plug for an additional 18 h.

The proposed foam method can be successfully applied to field air samples. For example, it has been used to establish trifluralin and heptachlor concentration profiles obtained within 200 cm of the surface of treated fields 1 h and 24 h after application of the pesticides [8].

The application of polyurethane foam in a high-volume air sampler to the collection of a broad spectrum of pesticides, polychlorinated biphenyls and polychlorinated naphthalenes has been evaluated by Lewis et al. [43]. The sampler draws air through a glass module equipped with a particulate filter and a polyurethane foam vapour trap at controlled flow rates of 100 to 25 l min^{-1}. Up to 360 m^3 of air can be sampled in a 24-h period, providing theoretical collection limits of less than 0.1 $\mu g\ m^{-3}$ for some individual compounds.

The collection of phthalate esters from air by polyurethane foam has been investigated recently by Yamasaki and Kuwata [44]. Air was sampled at 28 l min^{-1} for 24 h through a glass tube with a glass fibre filter (20 mm diameter) and two polyurethane foam plugs (density 0.024 g cm^{-3}, 23-mm diameter, 50-mm length) in series. The filter and the first plug were extracted

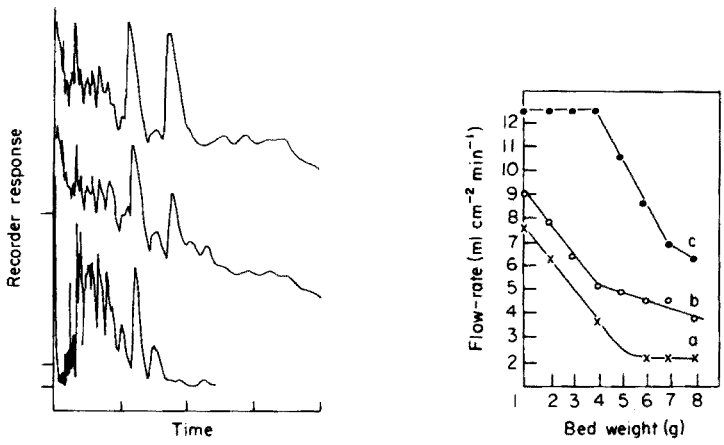

Fig. 4. A comparison of three chromatograms [36]. Top: river water extracted by polyurethane foam and concentrated to 5 ml of hexane; middle: treated municipal drinking water extracted by polyurethane foam and concentrated to 5 ml of hexane. Bottom: 2 $\mu g\ ml^{-1}$ polychlorinated biphenyls in hexane. Each sample was 5 μl.

Fig. 5. Flow-rate vs. weight of loaded foam and Voltalef powder. (a) Voltalef packed by the normal method; (b) Voltalef packed by the vacuum method; (c) foam packed by the vacuum method [46].

in a Soxhlet extractor with 5% petroleum ether in n-hexane, and the phthalate esters were determined by gas chromatography.

POLYURETHANE FOAM WITH PHYSICALLY IMMOBILIZED REAGENTS

Braun and Farag [9] discovered that open-cell flexible polyurethane foams are able to immobilize efficiently various organic extractants, chelating agents and inorganic precipitates on the thin membrane and strands forming the skeleton of the foam material. The reagent foams produced have been used successfully for various analytical applications.

Polyurethane foams with immobilized organic extractants

A detailed study [31] has been made on the loading properties of different types of polyurethane foam for the organic extractant TBP (tri-n-butyl phosphate). Polyurethane foams generally retain TBP much more efficiently than, for example, granular Voltalef which is considered one of the best granular supports in extraction chromatography. Foams of the polyether type retain TBP more efficiently than the polyester type.

However, the uptake of TBP by polyether foams can be increased slightly by decreasing the cell dimensions of the foam material (see Table 5). Obviously, the higher the uptake of the organic extractant, the higher will be the retention (extraction) capacity of the loaded support.

TABLE 5

The TBP-loading capacity of various types of polyurethane foam (In each case, 5 g of dry foam was taken.) [31]

Sample No.	Type of foam[a]	Weight of loaded foam (g)	TBP in loaded support (%)
1	Polyurethane foam polyether, more than 95% open cell (HI)	14.9516	66.6
2	Polyurethane foam, polyether, more than 95% open cell (H2)	15.9490	68.7
3	Polyurethane foam, polyether, ca. 100% open cell (W8100)	14.4372	65.4
4	Polyurethane foam, polyether, ca. 100% open cell (W8300)	14.5991	65.8
5	Polyurethane foam, polyether, ca. 100% open cell (W8600)	15.8234	68.4
6	Polyurethane foam, polyether, ca. 100% open cell (PPI-80 nFR)	10.3270	50.7

[a]Cell dimensions of sample 1 > sample 2 = sample 3 > sample 4 > sample 5.

Because column preparation is of capital importance in all types of chromatographic techniques, a vacuum method for foam column packing has been developed [45, 46]. The method described is suitable for the preparation of homogeneous foam columns of various lengths and diameters, and at the same time produces columns with good performance and suitable flow characteristics.

Figure 5 shows plots of the flow-rate (attained by gravity flow) as a function of bed weight of TBP-loaded foam and TBP-loaded Voltalef packed by the above-mentioned vacuum method. Evidently, the flow-rate is decreased by the increase in bed weight, but foam columns generally allow higher flow-rates.

Polyurethane foam loaded with TBP has been used for the separation of various inorganic species from aqueous solution. Braun and Farag [5] made several comparative investigations on TBP-loaded foam and TBP-loaded Voltalef powder, and demonstrated the practical advantages of using TBP-loaded foam in many separation systems.

Palladium(II), bismuth(III) and nickel(II) in a thiourea—perchloric acid system can be separated on TBP-loaded foam [45]. The extraction behaviour of the three metal ions onto polyurethane foam was examined in batch and column operations.

The rate of extraction of the Pd—thiourea complex by TBP-loaded foam is quite fast, as indicated by the value of the half-life of equilibrium absorption ($t_{1/2}$ = 0.5 min). There is a good linear correlation between the concentration of palladium on the foam and in aqueous solution over a relatively wide range of concentrations.

Retention of the Pd—thiourea complex by a TBP-loaded foam and its elution have also been tested. The complex is retained quantitatively as a narrow yellow band at the top of the column bed. Complete elution is effected by water and the elution curves are symmetrical with a relatively sharp peak. The height equivalent to a theoretical plate (HETP) calculated [47] from the elution curve of palladium was found [45] to be 1.7 mm, for Voltalef columns the HETP determined under the same experimental conditions was 2.8 mm. The effect of temperature and flow-rate on the HETP and V_{max} was investigated for the TBP-loaded foam columns. The increase in plate height (decrease in column performance) with increasing flow-rate in the range 1—5 ml cm^{-2} min^{-1} is pronounced only at 25°C. The V_{max} value is not affected by flow-rate but decreases with increasing temperature.

Generally, the capacity of the TBP-loaded foam is about double that of the TBP-loaded Voltalef. Quantitative separations of palladium from various concentrations of nickel and bismuth in a thiourea—perchloric acid system are possible on the TBP-loaded foam columns. An elution curve of the three metal ions is shown in Fig. 6.

The gold—thiourea complex can be extracted [48] with TBP under suitable conditions; the formula of the extracted species is [Au(thiourea)-

$ClO_4 \cdot 4TBP$]. The rate of extraction of the gold—thiourea complex on TBP-loaded foam was found to be quite high and was not affected significantly by the presence of various possible interfering elements. A detailed study of the effect of flow-rate on the retention efficiency when different concentrations of TBP in toluene were used to load the dry polyurethane foam showed that the extraction efficiency generally decreases with increasing flow-rates. However, when undiluted TBP solution is used to load the foam, relatively high flow-rates (up to 20 ml cm^{-2} min^{-1}) can be applied without appreciable loss in column performance. A column packed with 5 g of TBP-loaded foam has a total capacity of 10 mg of gold(III) when 1 l of aqueous solution is passed at a flow-rate of 10—12 ml cm^{-2} min^{-1} and at room temperature.

The practical utility of the foam-filled columns has been tested by studying their ability to separate quantitatively trace amounts of gold from high concentrations of Zn^{2+}, Co^{2+}, Ni^{2+}, Fe^{3+}, Sb^{3+}, Cu^{2+}, Bi^{3+} and Pd^{2+}. The chemical enrichment of gold from dilute aqueous solutions (spiked with radioactive gold-198) has also been investigated [48]. Gold can be collected quantitatively on passing the solution through a short foam column at a flow rate of 10—12 ml cm^{-2} min^{-1}, and can be recovered by dissolving the foam in hot concentrated nitric acid.

Separation of iron(III) from cobalt(II), copper(II) or nickel(II) has been investigated [49], by reversed-phase foam chromatography in a TBP—HCl system. The analytical use of tri-n-octylamine (TNOA)-loaded polyurethane foam has been examined [11] for the separation of cobalt from nickel in hydrochloric acid medium under a wide range of relative concentrations.

Polyurethane foams immobilizing methyl isobutyl ketone, diethyl ether, isopropyl ether or ethyl acetate have been examined [12] for the extraction of gold(III) chloride from aqueous solutions. For rapid collection of gold at trace concentrations (0.06—25 ppm), percolation of the aqueous solution through short columns packed with these loaded foams was recommended (Table 6). Gold was eluted from the foam column with acetone.

Various treated polyurethane foams have also been tested for the extraction of several organic compounds from aqueous solution. Gesser and

TABLE 6

Uptake of gold by different treated foams when 200 ml of solution was passed through the column [12]

Solvent used for treatment	^{198}Au (0.06 ppm)	Au (25 ppm)	
	Uptake (%)	Uptake (%)	Recovery (%)
Methyl isobutyl ketone	98.6	100	97.8
Diethyl ether	99.3	100	111.0
Isopropyl ether	99.1	100	101.8
Ethyl acetate	99.5	100	100.4

co-workers [10] started the work in this direction by application of grease-loaded foam for the extraction and recovery of some organochlorine pesticides. They prepared the foam by dipping and squeezing cylindrical polyurethane foam plugs in a 0.5% solution of the coating grease in pesticide-grade solvent. The columns were prepared by pushing down the required number of foam plugs in glass columns containing aqueous 70% ethanol. Several chromatographic-grade greases loaded on polyurethane foams were tested for the recovery of pesticides from aqueous solution. DC-200 grease proved to be the best and was recommended for quantitative recoveries. In collection of the different pesticides from water, fast flow rates (ca. 80 ml cm^{-2} min^{-1}) can be employed, but low flow-rates (ca. 10 ml cm^{-2} min^{-1}) are necessary for collection from suspensions. Generally, the DC-200 loaded foam columns (loaded with DC-200 grease) extract several pesticides from water almost quantitatively. However, in the case of suspensions, some pesticides (e.g., *pp'*—DDE) are not extracted completely, probably because they are adsorbed on the suspension. In all cases, the extracted pesticides can be eluted from the foam column with acetone and n-hexane, for determination by gas chromatography [10].

Further work on the extraction of organochlorine insecticides and polychlorinated biphenyls from water with silicone oil DC-200-coated polyurethane foam has been carried out by Musty and Nickless [37]. They examined the extraction efficiency of six foams with different surface areas and bulk densities, and also compared the efficiency of grease-coated foams and uncoated ones. In general, higher recoveries are obtained with the uncoated foams at flow-rates of 3—10 ml cm^{-2} min^{-1}, while the coated foam columns are the more efficient at a flow-rate of 80 ml cm^{-2} min^{-1}. For

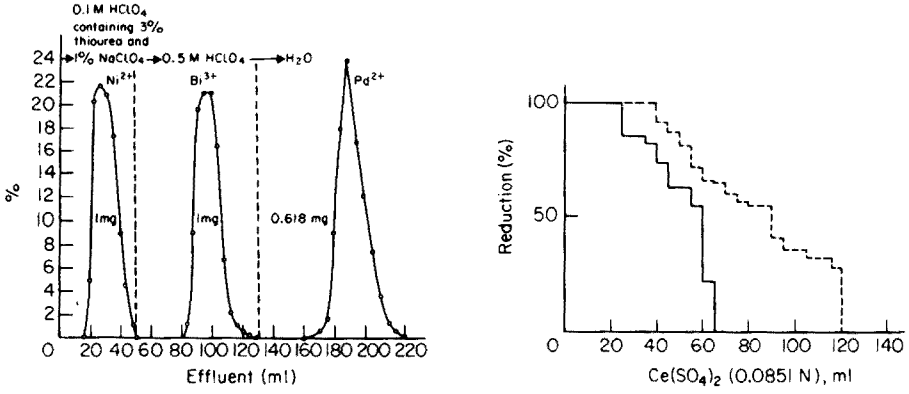

Fig. 6. Separation of Ni—Bi—Pd on TBP-loaded foam at room temperature. Bed height was 100 mm; flow-rate 2.5 ml min^{-1} [45].

Fig. 7. Break-through capacity curve of cerium(IV) reduction on columns packed with open-cell polyurethane foam loaded with various amounts of chloranil (——) 1 g of chloranil per 3 g of dry foam; (--------) 3 g of chloranil per 3 g of dry foam [15].

TABLE 7

Recovery of phthalate esters on foam coated with 5 mg of DOW-200 silicone oil per plug [38]

Phthalate	Recovery (%)
Dimethyl phthalate (DMP)	13
Diethyl phthalate (DEP)	70
Di-n-butyl phthalate (DnBP)	98
Diamyl phthalate (DAP)	49
Di-n-octyl phthalate (DOP)	9.0
Butylbenzyl phthalate (BBP)	74

quantitative recovery of the different organochlorine insecticides and polychlorinated biphenyls, the aqueous solutions should have a pH value in the range 6—9.

In some preliminary experiments [38], polyurethane foam loaded with DOW-200 silicone oil was found to extract, to various extents, different phthalate esters (see Table 7).

Polyurethane foam with immobilized tetrachlorohydroquinone

Redox reactions have been investigated on polyurethane foam columns supporting tetrachlorohydroquinone [15]. The foam retains chloranil (tetrachloro-*p*-benzoquinone) more efficiently than Kel-F powder [50, 51]. To test the usefulness of the chloranil-loaded foam, the breakthrough capacity was measured with cerium(IV) solution, for two columns containing the same amount of dry foam but treated with different concentrations of chloranil-loading solutions. The break-through curve of the column loaded was chloranil solution of lower concentration was sharper (Fig. 7).

A useful development of the foam technique seems to be the pulsed column operation [52], which depends on the flexible character of open-cell plastic foams — a property not found in any other kind of column filling — and on the rapid reaction between the metal ion in solution and the reagent on the foam. The pulsed column method is realized simply by packing the reagent-loaded foam into a medical syringe. Pressing the glass plunger compresses the foam; when the tip of the column is kept in a given solution and the plunger is gradually released, the solution penetrates into the column and the foam material returns to its original volume. Repetition of this process allows the external solution to come in contact with the reagent several times, so that the reaction between the metal ion in solution and the reagent on the foam can proceed.

Quantitative reduction of Ce(IV), V(V) and Fe(III) has been achieved by the pulsed column technique. The reduction efficiency of pulsed columns packed with swollen foam material (immobilizing the redox reagent in chlorobenzene solution) is better than that of pulsed columns packed

with dry foam (i.e., immobilizing the redox reagent in a microcrystalline state). Also, the reduction of Ce(IV), V(V) and Fe(III) is more effective if the aqueous metal ion solution is heated to about 80°C before reaction. Application of the pulsed foam column for the determination of various amounts (2—20 mg) of cerium(IV), vanadium(V) and iron(III) gave quantitative results [52].

Polyurethane foams with immobilized chelating agents

Braun and Farag [53] have used open-cell polyurethane foam for immobilizing various chelating agents for the separation as well as preconcentration of several metal ions from aqueous solution. The plasticized reagent foam is prepared by dissolving hydrophobic organic reagents in a plasticizer solution and then immobilizing the solution on an open-cell polyurethane foam by swelling. The plasticizer has a dual purpose [53]: it acts as an efficient non-volatile solvent for chelating agents, as well as a plasticizer for the foam plastic itself. Several hydrophobic organic reagents (e.g. dithizone, 1-nitroso-2-naphthol, diethylammonium diethyldithiocarbamate, 1-(2-pyridylazo-2-naphthol) (PAN)) dissolve in various plasticizers (e.g., TBP, α-di-n-nonyl phthalate, di-n-octyl phthalate and dibutyl adipate). Accordingly, plasticized foams with zinc dithizonate [53, 54], 1-nitroso-2-naphthol [55], diethylammonium diethyldithiocarbamate [55] and PAN [20] have been prepared. These foams have reasonable capacities and are suitable for the separation and preconcentration of metal ions from aqueous solutions.

The collection of traces of silver and mercury on zinc dithizonate foam has been examined [53, 54]. The collection rates with the plasticized zinc dithizonate foams are generally better than with the unplasticized ones. This can be attributed to the high mobilities of metal ions in the plasticized reagent foams. Figure 8 shows, for example, the effect of plasticizer on the rate of collection of silver on zinc dithizonate foams. Silver can be extracted from acidic and neutral aqueous solutions on the reagent foam, but the rate of extraction from aqueous solutions of pH 4.5—6.5 is better than that from more acidic solutions [53]. Although mercury can be extracted quantitatively even from 2 M nitric acid solution, the rate of extraction from neutral aqueous solution (pH ~ 6) is again faster than that from acidic media. The optimum dithizonate concentration for the extraction and recovery of both silver and mercury is about 4×10^{-3} M (in the loading solution).

The break-through and overall capacities of plasticized dithizonate foam columns are quite reasonable for both silver and mercury. The capacities are higher than those reported for other dithizone-loaded supports [56, 57]. The overall capacity for mercury was found to be 22.3 μeq g^{-1} (loaded foam).

Trace amounts of silver can be separated from a wide range of relative concentrations of lead and copper, when EDTA is used as a masking agent for the interfering ion. The results obtained are presented in Table 8.

The preconcentration of small amounts of silver (1.0 $\mu g\ l^{-1}$) and mercury

TABLE 8

Collection of traces of silver in the presence of various concentrations of lead and copper [53]

Matrix	Amount		Ag in matrix (ppm)	Av. Ag^+ in aq. soln. (%)	Av. Ag^+ on foam (%)	S.d. (s)	Bias
	Ag^+ (μg)	Matrix (mg)					
H_2O	100	—	10	0.7	99.3	0.224	−0.7 ± 0.06
H_2O	1	—	0.1	1.4	98.6	0.656	−1.4 ± 1.06
H_2O	0.01	—	0.001	1.2	98.8	0.663	−1.2 ± 1.08
H_2O	carrier-free	—	—	1.9	98.1	0.800	−1.9 ± 1.29
Cu^{2+}	0.01	0.1	100	1.6	98.4	0.600	−1.6 ± 0.97
Cu^{2+}	0.01	1.0	10	2.2	97.8	0.509	−2.2 ± 0.83
Cu^{2+}	0.01	10.0	1	2.5	97.5	1.565	−2.5 ± 2.57
Cu^{2+}	carrier-free	1.0	—	2.0	98.0	0.761	−2.0 ± 1.24
Pb^{2+}	0.01	0.1	100	2.3	97.7	0.583	−2.3 ± 0.95
Pb^{2+}	0.01	1.0	10	1.8	98.2	1.179	−1.8 ± 1.91
Pb^{2+}	0.01	10.0	1	2.9	97.1	1.887	−2.9 ± 3.09
Pb^{2+}	carrier-free	1.0	—	0.8	99.2	0.265	−0.8 ± 0.42

(0.72 μg l^{-1}) has successfully been achieved by percolating the aqueous metal ion solution through the plasticized foam column at a flow-rate of 8—12 ml cm^{-2} min^{-1}. Quantitative recoveries of silver and mercury from the plasticized zinc dithizonate foam are obtained by elution with sodium thiosulphate solution [53, 54].

The preparation of plasticized silver dithizonate foam suitable for isotope exchange separations has also been described [58]. Radio-silver can exchange from acidic solutions (pH < 2) on polyurethane foam immobilizing the primary silver dithizonate complex. The isotope exchange reaction can be represented by

$$*Ag(aq.) + AgHDz\ (foam) \rightleftharpoons Ag^+ + *AgHDz\ (foam)$$

where the asterisks denote the radioisotope of silver. The rate of isotope exchange of radio-silver on TBP-plasticized silver dithizonate foam is quite high and the reagent foam is useful in column operations. Collection of various concentrations of radio-silver by this exchange reaction in columns of silver dithizonate foam is possible at a flow-rate of 3 ml cm^{-2} min^{-1}.

Chow and Buksak [59] have described a method for the collection of mercury(II) and methylmercury(II) chloride on dithizone-treated polyurethane foam. They prepared the reagent foam by soaking the polyurethane plugs in a solution of dithizone in acetone (0.1 mg ml^{-1}) for 1 h, draining the foam material and drying overnight in a vacuum desiccator. Mercury(II) chloride is extracted efficiently at pH 5—10, while methylmercury(II) chloride is best extracted at pH 1.2. Low flow-rates (ca. 0.3 ml cm^{-2} min^{-1})

are needed to obtain more or less quantitative collection of both mercury compounds; at slightly higher flow-rates (1 ml cm^{-2} min^{-1}), the results are variable and less quantitative. Recoveries of mercury(II) chloride and methylmercury(II) chloride in concentrations ranging between 0.002 ppb to 100 ppm are reported to be complete. Both mercury compounds can be eluted from the foam column by acetone which also washes out the reagent.

The collection of traces of cobalt from aqueous solution on plasticized 1-nitroso-2-naphthol and diethylammonium diethyldithiocarbamate foams has been tested [55]. The optimal pH values of the aqueous solutions for the collection of cobalt(II) are 6.6—9.0 and 4.5—5.5, respectively, for these two foams. The presence of buffer in the aqueous solution has a serious effect on the collection of cobalt in the case of the dithiocarbamate foam, therefore adjustment of the pH with NaOH and HCl is recommended. The rate of collection on both treated foams is quite rapid so that reasonable flow-rates (5 -6 ml cm^{-2} min^{-1}) are possible for quantitative collection of cobalt (1—1000 μg) by the columns. Table 9 shows, for example, the results obtained with the dithiocarbamate foam columns; recoveries are complete even from the carrier-free solution. Results are of the same level of accuracy with the plasticized 1-nitroso-2-naphthol foam columns [55].

Lypka et al. have investigated the extraction and separation of copper and cadmium with benzoylacetone-loaded polyurethane foam [60], which was prepared by soaking the washed and dried foam in an acetone solution of benzoylacetone and then drying under vacuum. The extraction is pH-dependent, the extraction curves resembling those for liquid—liquid extraction. Table 10 shows the effect of flow-rate on the completeness of the extraction of copper and cadmium. Recovery of cadmium and copper from the treated foam was achieved by elution with 1.5 M hydrochloric acid.

Separation of the copper—cadmium system is possible on the basis of extraction with consecutive reagent foam plugs [60]. If the solution is

TABLE 9

Collection of cobalt(II) on columns packed with TBP-plasticized diethylammonium diethyldithiocarbamate foam [55]
(Flow-rate, 5—6 ml cm^{-2} min^{-1})

Amount of Co taken (μg)	Average[a] Co retained on foam ($\bar{x}$, %)	Relative accuracy of the mean (%)	S.d. (s)	Confidence limit ($\bar{x} \pm tsn^{-1/2}$) t 0.95
Carrier-free	97.7	—2.3	1.544	97.7 ± 2.5
1.0	98.6	—1.4	0.532	98.6 ± 0.8
10.0	99.6	—0.4	0.250	99.6 ± 0.4
100.0	99.3	—0.7	0.655	99.3 ± 1.0
1000.0	99.4	—0.6	0.512	99.4 ± 0.8

[a]Average of 4 determinations.

adjusted to pH 4.86 and extracted with 5 foam plugs, 99.8 ± 0.2% of copper is extracted, together with less than 1.0 μg of cadmium. However, separation by elution in a dynamic system utilizing the pH-dependent nature of the extraction curves is less effective [60].

Polyurethane foam immobilizing dimethylglyoxime has been suggested by Lee and Halmann [61] for the quantitative and selective separation of nickel from aqueous solution, even from very dilute solutions (ca. 10^{-5} M). This reagent is immobilized on the foam by shaking open-cell flexible

TABLE 10

Extraction of copper and cadmium by benzoylacetone-treated polyurethane foam [60]

Flow-rate (ml min^{-1})[a]	Amt. Cu extracted (μg)[b]	% Cu extracted[b]	Amt. Cd extracted (μg)[c]	% Cd extracte
1.5	175.5	100	174.4	99.4
2.0	175.5	100	—	—
3.0	175.5	100	174.1	99.2
6.0	170.5	97.2	174.1	99.2
12	158.5	90.4	174.1	99.2
18	152.5	87.0	174.1	99.2
250	123.5	70.4	160.1	91.2

[a]The column diameter was 40 mm. [b]At pH 8.0. [c]At pH 10.53

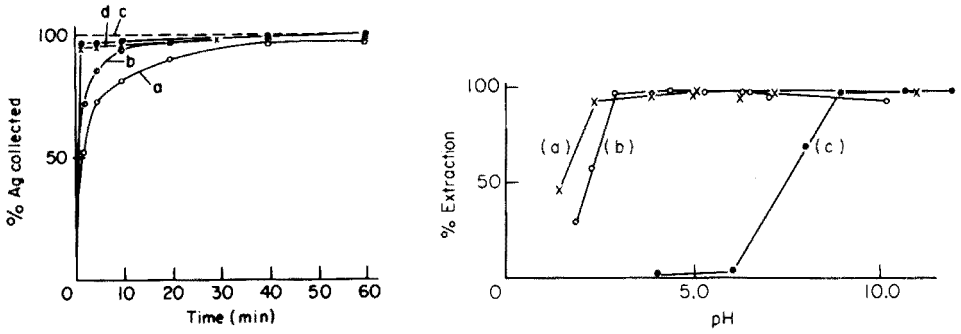

Fig. 8. Effect of shaking time on the collection of silver by polyurethane foam loaded with zinc dithizonate in various plasticizers and chloroform. The loaded foam contained 1% zinc dithizonate in (a) $CHCl_3$, (b) di-n-octyl phthalate, (c) TBP and (d) α-di-n-nonyl phthalate [53].

Fig. 9. Extraction of cobalt, iron and manganese as a function of pH. (a) Iron, (b) cobalt, (c) manganese [20].

polyurethane foam cubes or cylinders with the appropriate concentration of the reagent in acetone for about 1 h. The treated foam is first dried between sheets of filter paper and then at room temperature in a vacuum desiccator. The optimal pH for the extraction of nickel lies in the range of 8—10, but quantitative extraction is possible from solutions of slightly lower or higher pH, if the reagent foam contains an excess of dimethylglyoxime. Nickel(II) reacts with the dimethylglyoxime-impregnated foam immediately to form the red complex, but takes some time to be bound quantitatively. The extraction is unaffected by temperature in the range 20 to 60°C. Foreign ions such as Fe(II), Fe(III), Cu(II), Cd(II), Zn(II) and Co(II) do not interfere. Separation of low concentrations of nickel(II) (less than 5 ppm) is reported to be very efficient by both the static and dynamic methods. The nickel(II) is eluted from the foam column with a mixture of 1 M HCl and ethanol (1:1). In both extraction and elution processes, a flow-rate of less than 1 ml cm^{-2} min^{-1} is necessary.

It is worth mentioning that a method for the preparation of silicone-rubber foam and its treatment with dimethylglyoxime has also been described [62]. Open-cell silicone-rubber foam treated with dimethylglyoxime was found to be very suitable for the separation of platinum and palladium from aqueous solutions.

The feasibility of using plasticized and unplasticized 1-(2-pyridylazo)-2-naphthol (PAN) foams in batch and column operations has been tested [20, 63]. The collection of cobalt and iron is essentially complete from aqueous solutions of pH 4—9, but manganese is completely extracted only above pH 9; below pH 6 the extraction of manganese is negligible (Fig. 9). The effects of 23 anions on the extraction of cobalt, iron and manganese with plasticized PAN-foam have been examined. In general, cyanide, peroxide, periodate and citrate mask all the three metal ions. Borate, fluoride, phosphate and tartrate mask iron more than cobalt, but have no effect on manganese.

The extraction rate of cobalt on PAN-polyester polyurethane foam is very high from aqueous thiocyanate medium, but the extraction rate for iron is highest from water. Anions which do not mask manganese(II) do not affect its extraction rate. Generally, the extraction rate for manganese with PAN-foam is slower than that for cobalt, but is still slightly better than that of iron. Microgram amounts of cobalt are quantitatively collected on plasticized and unplasticized PAN-polyester foam columns from aqueous thiocyanate solution at flow-rates of up to ca. 3 ml cm^{-2} min^{-1} (Table 11). In the case of manganese, complete recovery can be obtained only at flow-rates up to ca. 1 ml cm^{-2} min^{-1}. However, iron is not extracted quantitatively by the foam column even at flow-rates as low as 0.3 ml cm^{-2} min^{-1} Cobalt can be separated from various concentrations of manganese by pH control; at pH 4—5 cobalt is quantitatively extracted by the foam while manganese moves with the solvent front. Acetone is then employed for the elution of cobalt.

TABLE 11

Collection of various concentrations of cobalt or manganese on plasticized and unplasticized PAN-polyester polyurethane foam columns [20]

Amount of metal taken (μg)	Average extracted ($\bar{x}$, %)	Relative accuracy of the mean (%)	Standard deviation (s)	Confidence limit $\bar{x} + tsn^{-1/2}$ $t = 0.95$
Cobalt				
Carrier-free	98.7[b]	−1.4	0.235	98.6 ± 0.3
	98.6[a]	−1.3	0.497	98.7 ± 0.6
0.2	98.6[b]	−1.4	0.273	98.6 ± 0.4
		−1.4	0.187	98.6 ± 0.2
2.0	98.8[a]	−1.2	0.464	98.8 ± 0.6
	98.6[b]	−1.4	0.141	98.6 ± 0.2
20.0	99.2[a]	−0.8	0.212	99.2 ± 0.2
	98.7[b]	−1.3	0.570	98.7 ± 0.7
200.0	95.8[a]	−4.2	1.868	95.8 ± 2.0
	97.1[b]	−2.9	0.540	97.1 ± 0.7
Manganese				
0.2	98.5[a]	−1.5	0.700	98.5 ± 0.4
2.0	98.4[a]	−1.6	0.510	98.4 ± 0.3
20.0	98.2[a]	−1.8	0.866	98.2 ± 0.5
200.0	96.7[a]	−3.3	1.520	96.7 ± 0.9

[a]Plasticized. [b]Unplasticized.

A method of concentrating antimony from natural water on polyurethane foams loaded with a 1% solution of 1,2-ethanedithiol in benzene has been described by Valente and Bowen [64]. When this reagent foam is used in batch experiments, absorption of antimony is 50% complete after shaking for 1 min, and 95% complete after 3 min. The absorption is independent of the type of water used and the oxidation state of antimony. More than 97% of the antimony can be extracted from aqueous solution at pH 1—2.5; above pH 4, the percentage extracted decreases sharply. Quantitative collection of antimony is possible in flow experiments at flow-rates of ca. 2.5 ml cm^{-2} min^{-1}. Antimony can be removed from the foam columns by eluting with acetone at a flow-rate of 0.5 ml cm^{-2} min^{-1}. The effects of various possible interfering elements (Na, Br, Hg, Sn, Cd and As) on the retention of antimony have been reported [64].

The separation of antimony(III) and antimony(V) in solution has also been tested [65] with sodium diethyldithiocarbamate loaded on polyurethane foam in static and dynamic systems. Separation can be achieved by adjusting the pH of the aqueous solution (containing an excess of reagent) to 9.5 and shaking with the reagent foam. At this pH value, the antimony(III) complex is quantitatively retained while the antimony(V) complex is not extracted at all. The $Sb(DDC)_3$ complex retained by the foam can be eluted completely with acetone.

One of the most attractive and useful applications of reagent foams seems to be their utilization for the qualitative and semiquantitative detection of some species. Plasticized polyurethane foams immobilizing chromogenic hydrophobic organic reagents have been suggested for rapid detection and semiquantitative determination of very low concentrations of metal ions in aqueous solution [19]. The name "Chromofoam" was proposed, and it was claimed that the organic reagent solution, which is homogeneously distributed on the large available surface area of the plasticized reagent foam (chromofoam), can function as an effective collector for metal ion traces from relatively high volumes of aqueous solution. This, together with the relative ease of observing the reaction products on the surface of the foam material, allows the detection of traces of metal ions with a chromofoam by shaking one small cube of it with the aqueous solution.

The detection and semiquantitative determination of zinc(II) and lead(II) with plasticized dithizone foam, and of copper(II) and cobalt(II) with rubeanic acid and Amberlite LA-1 foams, respectively, are very sensitive. In general, the sensitivity of the foam test is better than, or equal to, that of the usual spot tests [66] on a spot plate or filter paper. The detection of cobalt(II) with Amberlite LA-1 foam in the presence of thiocyanate ions is more sensitive than the resin spot tests [67]. The selectivity of the chromofoam test for 1 μg of cobalt in the presence of up to 10 mg of more than 40 elements is quite satisfactory.

A further advantage of chromofoams is that columns homogeneously packed with them can be used for the detection and semiquantitative determination of metal ions at the $\mu g\ l^{-1}$ level. This is achieved simply by passing large known volumes of the aqueous solution through the reagent foam column at a flow-rate of 10—15 ml $cm^{-2}\ min^{-1}$ and measuring (in comparison with standards) the length of the coloured zone.

Polyurethane foams with immobilized iodine

Iodine is satisfactorily dissolved in TBP and the resulting iodine solution can easily be immobilized, and retained firmly, in open-cell polyurethane foam [58]. Plasticized iodine foam has been tested for the separation of radio-iodide by isotope exchange in batch and flow experiments. The reaction of radio-iodide and the immobilized iodine in the foam can be represented by

$$2{*}I^- (aq) + I_2 (foam) \rightleftharpoons 2I^- (aq) + {*}I_2 (foam)$$

where the asterisk denotes the radio-isotope of iodine.

The percentage exchange of iodide on this iodine foam, investigated with carrier-free ^{131}I as tracer, is quite fast and the equilibrium value is reached after less than 10 min of shaking. The mobility of the iodide in the plasticized foam, checked by an isotope-exchange method [68], is quite high [58]. This means that the whole iodine-coated membranes of the plasticized foam and not only their surfaces are involved in the exchange

TABLE 12

Collection of various concentrations of radio-iodide by isotope exchange reaction on columns packed with TBP-plasticized iodine foam (Flow-rate, 3—4 ml cm^{-2} min^{-1}) [58]

Amount of I_2 taken (μg)	Average I exchanged on foam[a] ($\bar{x}$, %)	Relative accuracy of the mean (%)	Standard deviation (s)	Confidence limit ($\bar{x} + tsn^{1/2}$) $t = 0.95$
Carrier-free	98.1	—1.9	0.171	98.1 ± 0.3
0.1	97.9	—2.1	0.096	97.9 ± 0.2
1.0	98.1	—1.9	0.350	98.1 ± 0.6
10.0	98.0	—2.0	0.126	98.0 ± 0.2
100.0	98.7	—1.3	0.222	98.7 ± 0.4
1000.0	98.8	—1.2	0.572	98.8 ± 0.9

[a]Average of 4 determinations.

process under the experimental conditions used. The selectivity of the iodine foam has been examined by studying the effects of some interfering elements (e.g. Na^+, K^+, Cl^- and Br^-) on the retention of radio-iodide in column experiments. In all cases extraneous ions are eliminated by washing with water without affecting the retention of radio-iodide. The collection of various concentrations of radio-iodide from aqueous solutions is quantitative above pH 5 (Table 12).

The possibilities of rapid separation of radio-iodide with iodine solution in toluene (with or without TNOA dissolved) immobilized in polyurethane foam have been examined by Palágyi and Bilá [69]. Batch experiments show that the rate of exchange is quite high; equilibrium is attained in less than 10 min. The presence of TNOA generally increases the efficiency of separation. In separations under dynamic conditions, the separation efficiency decreases with increasing flow-rate, but the efficiency obtained at quite high flow-rates (ca. 190 ml cm^{-2} min^{-1}) is only slightly lower than that obtained at 10-times lower flow-rates (19 ml cm^{-2} min^{-1}). The dynamic exchange gives higher separation efficiency than the static one at the same degree of volume concentration. With 1 g of treated foam, it is possible to separate ^{131}I from a 1-l sample of water into 3.5 ml of foam with 90% separation efficiency in about 10 min.

Polyurethane foam columns immobilizing a solution of iodine in Alamine 336 in toluene have been used [70] for the separation of radio-iodide from milk samples. The method is suitable for the rapid determination of ^{131}I in fresh milk, as well as in formaldehyde-preserved milk. The effects of various parameters on the isotope exchange process have been examined, and a method ha been described for the separation of radio-iodine from 1 l of milk with a separation efficiency of about 80% in 15—20 min.

The preparation of plasticized polyurethane foam immobilizing bromine and its application for the collection of radio-bromide has also been tested [71].

The polyurethane foam sample used is attacked to some extent by bromine, but the results obtained for the isotope-exchange separation of radio-bromide are quite promising.

Heterogeneous ion-exchange foams

There has been continuous interest in preparing ion-exchange materials with reduced solid-phase mass transport in order to increase the rate of exchange processes. Preparations of pellicular resins [72, 73], in which a solid core is surrounded by a thin film of cross-linked ion-exchange material, and superficially sulphonated resins [74—76] have been described. The results obtained with these ion exchangers were promising, but their low capacities have proved a serious disadvantage. Exchange processes on finely pulverized ion exchangers proceed substantially faster than the same processes on beads of the same composition [77]. However, the use of columns filled with fine grains requires the employment of forced flow to attain reasonable flow-rates. A possible solution to this problem seemed to be the preparation of heterogeneous ion-exchange foams in which finely ground commercial ion-exchange resins (e.g. Varion KS) are built into a polyurethane foam matrix of the open-cell polyether type. Heterogeneous ion-exchange foams containing various percentages of the powdered ion-exchange resin (up to 40%, w/w) have been prepared [13]. The mechanical properties of these ion-exchange foams are the same as those of foam containing no ion-exchange resin, and the distribution of the exchanger grains is uniform.

The possibility of using polyurethane-Varion KS heterogeneous cation-exchange foam for rapid separations in aqueous and alcoholic solution has been investigated [14]. The slope of the break-through capacity curve of a column packed with cation-exchange foam, determined for copper(II) sulphate solution, is quite sharp. Sorption of copper occurs in one fast step (Fig. 10), i.e. gel diffusion is not the rate-controlling step as in the case of ordinary ion-exchange beads. The $t_{1/2}$ value for equilibrium sorption on the cation-exchange foam, calculated from the rate curve for copper(II), is

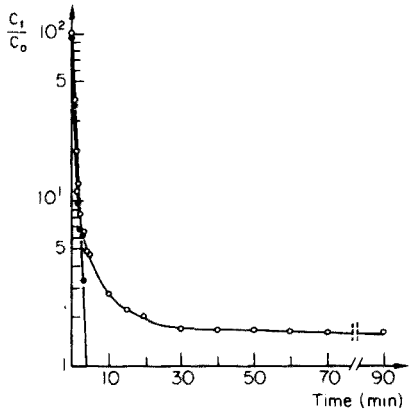

Fig. 10. Rate of sorption of copper(II) (5 mg) on ion-exchange foam at room temperature [14].

0.6 min. However, the capacity of the cation-exchange foam is much higher than that of surface-sulphonated resin beads.

These kinetic results have been confirmed by the elution of copper from the ion-exchange foam column with hydroxylammonium chloride solution at 50°C for various flow-rates. Figure 11 shows the effect of flow-rate on the elution of copper(II) from an ion-exchange foam column and an ion-exchange bead column. Clearly, the foam column is much superior to the conventional bead column. With foam columns, microgram and milligram amounts of copper can be retained and eluted quantitatively with hydroxylammonium chloride solution. The overall capacity of the ion-exchange foam is about 40% of the original capacity of beads.

A comparative study has shown that the selectivities of cation-exchange beads (Varion KS) and cation-exchange foam are about the same; the distribution coefficients of cadmium(II), zinc(II), iron(III) and calcium(II) were determined for the two exchangers.

Inorganic precipitates

Radiochemical separations based on isotope exchange between a dissolved ion and its fairly insoluble precipitate have been widely applied [78—80]. The use of precipitates of very small particle size (a few μm) has been recommended [81] for quantitative retention of the common radionuclides by isotope exchange on the precipitates (packed in columns) at reasonable flow-rates. The precipitates have to be powdered carefully to obtain the necessary particle size.

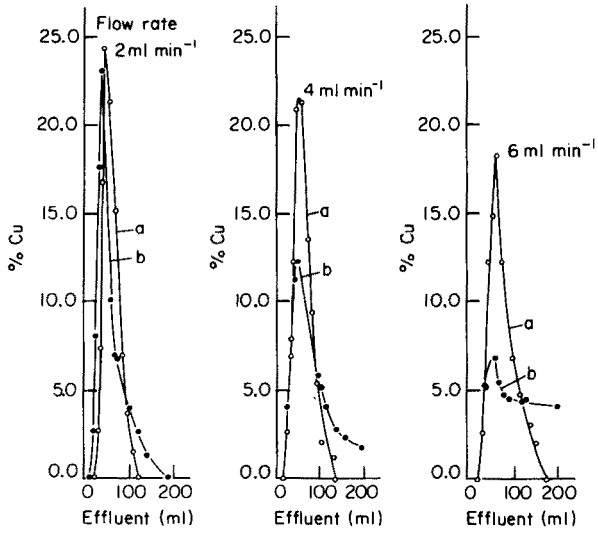

Fig. 11. Effect of flow-rate on the elution of copper(II) with 0.5 M hydroxylammonium chloride solution at 50°C. (a) Ion-exchange foam column; (b) ion-exchange bead column [14].

Polyurethane foam immobilizing a very fine precipitate, e.g. silver sulphide, suitable for isotope-exchange separation of radio-silver, has been suggested [16]. Silver sulphide foam can be prepared by loading heterogeneous cation-exchange foam with silver ion and then precipitating silver sulphide in the foam matrix with sodium sulphide solution. Repeated precipitation of silver sulphide on the foam is possible because the exchange capacity of the foam exchanger is completely recovered after precipitation. Separation of radio-silver on this foam can be done by batch or column methods. The exchange yield is equal to or higher than 99% from acid solutions up to 2 M HNO_3, but then decreases as the nitric acid concentration increases. The rate of retention of radio-silver on Ag_2S foam is high, the exchange yield reaching 99% after less than 10 min. Columns packed with Ag_2S foam retain radio-silver completely even at flow-rates as high as 20 ml cm^{-2} min^{-1} (see Table 13).

The preparation of polyurethane foam immobilizing finely divided copper has also been described [82]. The copper foam is prepared by treating heterogeneous cation-exchange foam [13] with copper sulphate solution and reducing the copper(II) in the foam to the metal with sodium dithionate ($Na_2S_2O_4$) solution.

Redox-exchange separation of radio-silver on this copper foam has been investigated. The retention efficiency is highest from 2 M nitric acid solutions and the rate of retention is reasonably rapid. In column experiments, flow-rates up to 10—12 ml cm^{-2} min^{-1} can be used without affecting the completeness of separation.

POLYURETHANE FOAM WITH ANCHORED FUNCTIONAL GROUPS

All the reagent foams described in the previous sections were prepared by direct physical immobilization of the required reagent on open-cell polyurethane foam. The preparation of cellular (foamed) plastics to which specific functional groups are chemically bonded has also been attempted [13, 17]. Gesser and co-workers [17] described a method for the preparation

TABLE 13

Collection of radio-silver by isotope-exchange reaction on columns packed with Ag_2S foam [16]

Ag taken (μg)	Av. Ag exchanged on foam ($\bar{x}$, %)[a]	Relative accuracy of the mean (%)	S.d. (s)	Confidence limit $\bar{x} \pm tsn^{-1/2}$ (t = 0.95)
0.1	99.2	0.8	0.416	99.2 ± 0.7
1.0	98.6	1.4	0.316	98.6 ± 0.5
10.0	98.8	1.2	0.625	98.8 ± 1.0
100.0	98.7	1.3	0.594	98.7 ± 0.9

[a] Average of 4 determinations.

of SH-polyurethane foam, based on treatment of polyether-type polyurethane with hydrogen sulphide in a discharge tube.

Columns packed with the SH-foam were evaluated for the adsorption of mercury(II) chloride and methylmercury(II) chloride from extremely dilute aqueous solutions. Mercury at concentrations of 0.4—0.0004 ppm can be quantitatively collected on these foam columns from 100 ml of aqueous solution passed at flow-rates of about 13 ml cm^{-2} min^{-1}. At higher mercury concentration (e.g. 4 ppm), the retention efficiency decreases because of oversaturation. The effectiveness of the SH-foam is said to be unaffected by the storage time before use. Freshly prepared and 1-month old foams gave similar adsorption values for 0.04 ppm of mercury(II) [17].

Generally, the effective capacity of the foam columns is much lower for methylmercury(II) chloride than for mercury(II) chloride. This was attributed [17] to the steric hindrance effect of the methyl group. The fraction of mercury absorbed on the foam column generally increases as the concentration decreases. Mercury can be recovered from the SH-foam by extraction with 2 M hydrochloric acid in a Soxhlet extractor.

Although the SH-treated polyurethane foam has low capacity and its preparation is quite complex, yet the preparation of such a foam is a valuable contribution to studies of anchoring functional groups on the foam matrix.

Braun et al. [13] have described various methods for the direct and indirect introduction of functional groups (ionogenic groups) into the skeleton structure of the foam. They prepared phenol—formaldehyde resin foam to which sulphonic acid groups were bonded by direct sulphonation of a commercially available phenol—formaldehyde foam. The mechanical properties of the original phenol—formaldehyde foam were not much changed by sulphonation, and the ion-exchange capacity of the foams was reasonable (1.85 meq g^{-1}).

Indirect introduction of the ionogenic groups into the foam material has also been reported [13]. Two different methods are possible. The first method is based on a polymer analogue reaction after the foam has been joined to an easily transformable polymer. Styrene—polyurethane copolymer foam can be prepared by this method and the anion-exchange groups then introduced by chloromethylation and amination. The mechanical properties of the foams depend on the polymerization conditions and on the quality of the initiator used. A typical capacity of such foams is 2.0—2.2 meq g^{-1}. The second method is based on radiation grafting of open-cell polyurethane foams with methacrylic acid; this process fixes an ionogenic group on the foam backbone, and so leads to the final product in a single step. Foams prepared by this method are weak carboxylic ion-exchange foams with excellent properties and good ion-exchange capacities (4 meq g^{-1}).

The preparation and application of foams with anchored (bonded) functional groups is still an open and promising field and requires further study to obtain various foam materials with specific properties.

SPECIALLY-TREATED POLYURETHANE FOAMS

Bauman et al. [83, 84] reported that open-cell polyurethane foam can be used as a support for starch gel containing enzymes. They described a method for the preparation of immobilized horse-serum cholinesterase products in which the enzyme in the starch gel is physically entrapped on the surface of open-cell polyurethane foam pads. The immobilized enzyme pad can be used to monitor water and air continuously for atmospheric pollutants which inhibit cholinesterase. In this system the air being sampled and a solution of substrate for the enzyme are pumped simultaneously and continuously through the immobilized enzyme product; the activity of the enzyme is monitored continuously by passing an electric current through platinum electrodes in contact with the immobilized enzyme product and observing changes in the electrode potential.

On the basis of this work, Goodson and Jacobs [85] designed an automatic system for monitoring water supplies for the presence of organophosphates. Ten gallons of river water can be passed through an enzyme pad without any detectable loss in enzyme activity. In one test, they pumped city tap water through a single enzyme pad for 68 h; more than half of the enzyme activity was lost, but the residual enzyme activity was still enough to produce an alarm in their instrument.

Several proteins and aluminium hydroxide have been tested [86] for adsorption of cholinesterase to increase its retention by a starch gel matrix. The adsorbed cholinesterase was then applied to sheets of open-pore polyurethane foam for evaluation. Enzyme pads prepared by coprecipitation of cholinesterase with aluminium hydroxide gel followed by entrapment in starch gel on the surface of open-pore polyurethane foam gave improved activity and wash-out resistance. These foam pads have high enzyme activity, and are easy to prepare in large quantities, uniform in their activities, and suitable for use in the electrochemical cell system for monitoring either air or water for cholinesterase inhibitors. When 2700 l of water were pumped through an enzyme pad to monitor organophosphates in a water supply, a useful quantity of enzyme remained in the pad at the end of the test period.

A detailed study [87] has been made of the sensitivity of the "Continuous Aqueous Monitor System" with cholinesterase-treated polyurethane foam pads, for a variety of pesticides. The sensitivity of the system is greater for P=O than for P=S compounds. Response of the system to carbamate-type insecticides is good, and there is no response to chlorinated hydrocarbon insecticides, herbicides, fungicides or rodenticides.

Reticulated polyester polyurethane foam, the cells of which are free of residual membranes, have been proved [88] to be a suitable matrix for immunoadsorption of cells. The foam material has pores sufficiently large to allow passage of cells without appreciable mechanical entrapment. Although the untreated foam has a high affinity for guinea pig erythrocytes,

yet the adsorption is not specific. The non-specific affinity can be greatly reduced by pretreating the foam with various polyanions, e.g. carboxymethyl cellulose, polyacrylic acid, gammaglobulin and gum arabic. Immunospecific binding of erythrocytes can be achieved by adding antierythrocyte antibody to a gum arabic solution used to protect the foam. The foam columns are mounted in a horizontal position and rotated centrifugally to prevent rapid sedimentation of cells before they come in contact with the foam surfaces. A single antibody-coated foam disk (1-in. diameter, 0.5-in thick) can bind up to 3×10^8 guinea pig erythrocytes. The specificity of this method was further proved by the finding that erythrocytes coated with haptens were bound specifically to foam coated with their corresponding antihapten antibodies, with a low background of cross-reactivity.

OPEN-PORE POLYURETHANE MICROSPHERES

In the previous sections the use of many types of open-cell foamed polyurethanes in liquid—solid or liquid—liquid separation systems has been described. The work presented in this section concerns the application of precipitated porous polyurethane microspheres in gas—solid, gas—liquid and low-pressure liquid chromatographic methods [6].

Gas—solid chromatography

The application of uncoated open-pore polyurethane microspheres for gas—solid chromatographic separations was suggested in 1970 [21, 89, 90]. It was reported [21] that apolar compounds, e.g. hydrocarbons, are generally separated on the uncoated polyurethane column in the order of their boiling points; this was proved for C_6—C_9 normal aliphatic hydrocarbons on a 20 × 0.25-in column. Polar compounds capable of hydrogen bonding are broadened and eluted in the order shown in Table 14.

Uncoated polyurethane microspheres have been used advantageously in the separation of geometrical isomers of various metal chelates. For example, in the separation of the *trans* and *cis*-isomers of chromium trifluoroacetylacetonate [$Cr(tfa)_3$], the elution times were about 2.2 and 5 min, respectively from a 25-cm column (4-mm i.d.) at 100°C with a helium flow-rate of 40 ml min^{-1} [89].

TABLE 14

Relative retention data on uncoated polyurethane [21]

Compound	Relative retention time	B.p. (°C)	Compound	Relative retention time	B.p. (°C)
2-Propanol	1.0	82.5	CCl_4	1.0	77
Ethanol	2.0	78.3	$CHCl_3$	1.05	61
Methanol	9.6	64.5	CH_2Cl_2	1.6	40

Pre-powdered porous polyurethane has also been used [90] in gas—solid chromatographic columns for the other separation of aliphatic hydrocarbons. Other pre-powdered porous plastics have also been tested [90].

Gas—liquid partition chromatography

Stationary phases can be incorporated successfully into the polymer by addition to the precursor solutions or by coating [21, 89]. Coating the open-pore microspheres with a stationary phase masks the gas—solid properties completely, so that the material adopts the characteristics of a gas—liquid substrate; that is, the polar sites of polyurethane are completely masked by the liquid phase.

Several separations have been successfully carried out with this system. Figure 12 shows a chromatogram of n-hexane and three aromatic compounds (benzene, toluene and xylene) on DC 550-treated open-pore polyurethane column. Gas-chromatographic separation of metal chelates on polyurethane microspheres coated with DC-550 has also been carried out [89]. Separation of aromatic hydrocarbons on a microsphere-filled column coated with Carbowax 400 has been tested.

High-resolution, low-pressure liquid chromatography

The advantages of open-pore polyurethane as a support in high-resolution, low-pressure liquid chromatography have been recently described [91]. The chemical and physical stability of the polyurethane, together with its homogeneous particle size and the possibility of preparing columns with specially designed porosity and functionality, make this material a nearly ideal support

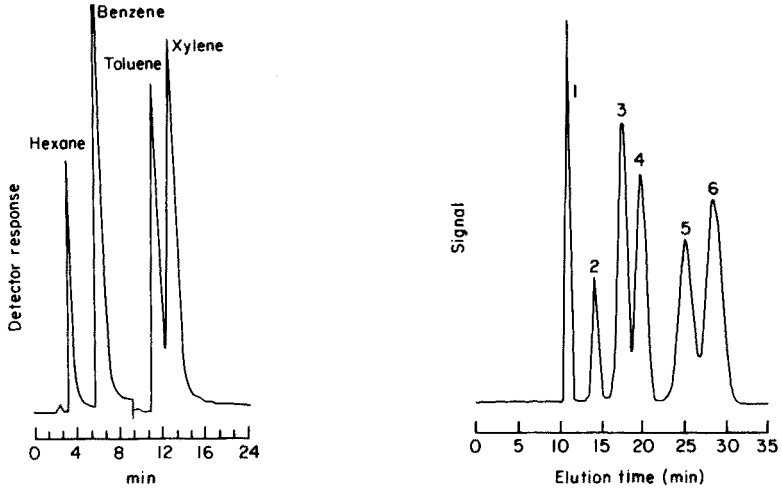

Fig. 12. Separation of n-hexane, benzene, toluene and xylene on incorporated DC 550 [89].

Fig. 13. Liquid chromatograms of the separation of dichloroanilines [91]. (1) Benzene; (2) 2,6-dichloroaniline; (3) 2,4-dichloroaniline; (4) 2,3-dichloroaniline; (5) 3,5-dichloroaniline; (6) 3,4-dichloroaniline.

for liquid chromatography. The mechanical properties of polyurethane microspheres allow the injection of samples directly on the column material. Also, column inlet and outlet porous filters are eliminated and relatively sharp peaks are obtained. Figure 13 shows, for example, the separation of dichloroanilines. The separation of acetone and *o*-aminophenol on an open-pore polyurethane column has also been reported.

REFERENCES

1 H. Brunschwig, Liber de Arte Distillandi, 1512 (see also A. Bittel, Dissertation, Tübingen, 1957).
2 E. Bayer, Gaschromatographie, 2nd edn., Springer-Verlag, Heidelberg, 1962, p. 4.
3 D. Lal, J. R. Arnold and B. L. K. Somayajulu, Geochim. Cosmochim. Acta, 28 (1964) 1111.
4 T. Braun and A. B. Farag, Talanta, 22 (1975) 699.
5 T. Braun and A. B. Farag, in T. Braun and G. Ghersini (Eds.), Extraction Chromatography, Elsevier, Amsterdam, and Akadémiai Kiadó, Budapest, 1975.
6 W. D. Ross, Sep. Purif. Methods, 3 (1974) 111.
7 H. J. M. Bowen, J. Chem. Soc. A, (1970) 1082.
8 B. C. Turner and D. E. Glotfelty, Anal. Chem., 49 (1977) 7.
9 T. Braun and A. B. Farag, Talanta, 19 (1972) 828.
10 J. F. Uthe, J. Reinke and H. D. Gesser, Environ. Lett., 3 (1972) 117.
11 T. Braun, É. Huszár and L. Bakos, Anal. Chim. Acta, 64 (1973) 77.
12 S. Sukiman, Radiochem. Radioanal. Lett., 18 (1974) 129.
13 T. Braun, O. Békeffy, I. Haklits, K. Kádár and G. Majoros, Anal. Chim. Acta, 64 (1973) 45.
14 T. Braun and A. B. Farag, Anal. Chim. Acta, 68 (1974) 119.
15 T. Braun, A. B. Farag and A. Klimes-Szmik, Anal. Chim. Acta, 64 (1973) 71.
16 T. Braun and A. B. Farag, Radiochem. Radioanal. Lett., 19 (1974) 275.
17 M. A. J. Mazurski, A. Chow and H. D. Gesser, Anal. Chim. Acta, 65 (1973) 99.
18 H. D. Gesser, A. Chow, F. C. Davis, J. F. Uthe and J. Reinke, Anal. Lett., 4 (1971) 883.
19 T. Braun and A. B. Farag, Anal. Chim. Acta, 73 (1974) 301.
20 T. Braun, A. B. Farag and M. P. Maloney, Anal. Chim. Acta, 93 (1977) 191.
21 W. D. Ross and R. T. Jefferson, J. Chromatogr. Sci., 8 (1970) 386.
22 C. R. Thomas, British Plastics, (1965) 552.
23 Cellular Plastics, Proceedings of a Conference, Natick, Massachusetts, 1966, NAS-NRC, Washington, D.C., 1967.
24 C. J. Benning, Plastic Foams: The Physics and Chemistry of Product Performance and Process Technology, Vol. 1, Chemistry and Physics of foam formation, J. Wiley, New York, 1969.
25 S. Gross (Ed.), Modern Plastics Encyclopaedia, Vol. 46, McGraw-Hill, New York, 1969, p. 248.
26 D. J. David and H. B. Staley, Analytical Chemistry of the Polyurethanes, Vol. XVI, Part III, J. Wiley, New York, 1969.
27 T. H. Ferrigno, Rigid Plastic Foams, Reinhold, New York, 1963.
28 J. D. Navratil and R. E. Sievers, Int. Lab., Nov./Dec., (1977) 26.
29 H. J. M. Bowen, Radiochem. Radioanal. Lett., 2 (1969) 169.
30 H. J. M. Bowen, Radiochem. Radioanal. Lett., 7 (1971) 71.
31 T. Braun and A. B. Farag, Anal. Chim. Acta, 66 (1973) 419.
32 N. V. Lodeishchikov and A. F. Panchenko, Isvetn. Met., 41 (1968) 25.
33 H. D. Gesser, E. Bock, W. G. Baldwin, A. Chow, D. W. McBride and W. Lipinsky, Sep. Sci., 11 (1976) 317.

34 H. D. Gesser and G. A. Horsfall, J. Chim. Phys., 82 (1977) 1.
35 T. Braun and A. B. Farag, Anal. Chim. Acta, in press.
36 H. D. Gesser, A. B. Sparling, A. Chow and C. W. Turner, J. Am. Water Works Assoc., 65 (1973) 220.
37 P. R. Musty and G. Nickless, J. Chromatogr., 100 (1974) 83.
38 K. M. Gough and H. D. Gesser, J. Chromatogr., 115 (1975) 383.
39 T. Tanaka, K. Hiiro and A. Kawahara, Jpn. Anal., 24 (1973) 320.
40 T. F. Bidleman and C. E. Olney, Bull. Environ. Contam. Toxicol., 11 (1974) 442.
41 T. F. Bidleman and C. E. Olney, Science, 183 (1974) 516.
42 J. F. Thompson (Ed.), Analysis of Pesticide Residues in Human and Environmental Samples, Perrine Primate Res. Labs., Environ. Protect. Agency, Perrine, Fla., 1971.
43 R. G. Lewis, A. R. Brown and M. D. Jackson, Anal. Chem., 49 (1977) 1668.
44 H. Yamasaki and K. Kuwata, Bunseki Kagaku, 26 (1977) 1.
45 T. Braun and A. B. Farag, Anal. Chim. Acta, 61 (1972) 265.
46 T. Braun and A. B. Farag, Anal. Chim. Acta, 62 (1972) 476.
47 E. Glueckauf, Trans. Faraday Soc., 51 (1955) 34.
48 T. Braun and A. B. Farag, Anal. Chim. Acta, 65 (1973) 115.
49 T. Braun, L. Bakos and Zs. Szabó, Anal. Chim. Acta, 66 (1973) 57.
50 E. Cerrai and C. Testa, Anal. Chim. Acta, 28 (1963) 205.
51 R. Belcher, J. R. Majer and G. A. H. Roberts, Talanta, 14 (1967) 1245.
52 T. Braun and A. B. Farag, Anal. Chim. Acta, 65 (1973) 139.
53 T. Braun and A. B. Farag, Anal. Chim. Acta, 69 (1974) 85.
54 T. Braun and A. B. Farag, Anal. Chim. Acta, 71 (1974) 133.
55 T. Braun and A. B. Farag, Anal. Chim. Acta, 76 (1975) 107.
56 D. E. Carrit, Anal. Chem., 25 (1953) 1927.
57 T. B. Pierce and P. F. Peck, Analyst, 86 (1961) 580.
58 T. Braun and A. B. Farag, J. Radioanal. Chem., 25 (1975) 5.
59 A. Chow and D. Buksak, Can. J. Chem., 53 (1975) 1373.
60 G. N. Lypka, H. D. Gesser and A. Chow, Anal. Chim. Acta, 78 (1975) 367.
61 D. W. Lee and M. Halmann, Anal. Chem., 48 (1976) 2214.
62 D. C. Gregoire and A. Chow, Talanta, 22 (1975) 453.
63 M. Maloney, G. J. Moody, J. D. R. Thomas, T. Braun and A. B. Farag, Paper presented at the 4th SAC Conference, Birmingham, July, 1977.
64 I. Valente and H. J. M. Bowen, Analyst, 102 (1977) 842.
65 I. Valente and H. J. M. Bowen, Anal. Chim. Acta, 90 (1977) 315.
66 F. Feigl and V. Anger, Spot Tests in Inorganic Analysis, 6th Edn., Elsevier, Amsterdam, 1972.
67 M. Fujimoto and Y. Nakatsukasa, Anal. Chim. Acta, 27 (1962) 373.
68 W. Eckhardt, G. Herrmann and H.-D. Schüssler, Fresenius Z. Anal. Chem., 226 (1967) 71.
69 S. Palágyi and E. Bilá, Radiochem. Radioanal. Lett., 32 (1978) 87.
70 S. Palágyi and R. Markusová, Radiochem. Radioanal. Lett., 32 (1978) 103.
71 T. Braun and A. B. Farag, unpublished work.
72 J. J. Kirkland, J. Chromatogr. Sci., 7 (1969) 361.
73 G. G. Horvath, B. A. Preiss and S. R. Lipsky, Anal. Chem., 39 (1967) 422.
74 M. Skafi and K. H. Lieser, Fresenius Z. Anal. Chem., 249 (1970) 182.
75 M. Skafi and K. H. Lieser, Fresenius Z. Anal. Chem., 250 (1970) 306.
76 M. Skafi and K. H. Lieser, Fresenius Z. Anal. Chem., 251 (1970) 177.
77 T. A. Pinfold and B. L. Karger, Sep. Sci., 5 (1970) 183.
78 D. N. Sunderman and W. W. Meinke, Anal. Chem., 29 (1957) 1578.
79 I. H. Qureshi, M. S. Shahid and S. M. Hasany, Talanta, 14 (1967) 951.
80 M. Rakovic and A. Glagolicová, Radiochem. Radioanal. Lett., 15 (1973) 387.
81 O. Gimesi, E. Bányai, M. Csajka and A. Szabadházy, Talanta, 17 (1970) 1183.
82 T. Braun and A. B. Farag, Radiochem. Radioanal. Lett., 19 (1974) 377.

83 E. K. Bauman, L. H. Goodson, G. G. Guilbault and D. N. Kramer, Anal. Chem., 37 (1965) 1378.
84 E. K. Bauman, L. H. Goodson and J. R. Thomson, Anal. Biochem., 19 (1967) 587.
85 L. H. Goodson and W. B. Jacobs, Proceedings, National Conference on Control of Hazardous Material Spills, Houston, Texas, March, 1973, Environmental Protection Agency, p. 129.
86 L. H. Goodson, W. B. Jacobs and A. W. Davis, Anal. Biochem., 51 (1973) 362.
87 L. H. Goodson and W. B. Jacobs, Proceedings, National Conference on Control of Hazardous Material Spills, American Institute of Chemical Engineers, New Jersey, 1974, Environmental Protection Agency, p. 292.
88 W. H. Evans, M. G. Mage and E. A. Petersen, J. Immunol., 102 (1969) 899.
89 F. D. Hileman, R. E. Sievers, G. G. Hess and W. D. Ross, Anal. Chem., 45 (1973) 1126.
90 H. Schnecko and O. Bieber, Chromatographia, 4 (1971) 109.
91 T. R. Lynn, D. R. Rushneck and A. R. Cooper, J. Chromatogr. Sci., 12 (1974) 76.

Analytica Chimica Acta, 99 (1978) 37—76

FLOW INJECTION ANALYSIS
Part X. Theory, Techniques and Trends†

J. RŮŽIČKA* and E. H. HANSEN

Chemistry Department A, Building 207, The Technical University of Denmark, 2800 Lyngby (Denmark)

(Received 20th January 1978)

SUMMARY

The dispersion of sample zones in Flow Injection systems is described by analogy with the mixing of fluids in large-scale chemical reactors. This comparison has resulted in a definition of the sample zone dispersion, its mathematical description, and the identification of the main parameters which can be used to effect the desired degree of mixing. The miniaturized Flow Injection system, designed with the aid of the rules derived on the basis of the theory of dispersion, uses only 5—30 μl of sample solution and gives the analytical readout within 5—30 s after sample injection. The most recent Flow Injection methods, such as pH measurements at limited dispersion, voltammetry (including anodic stripping at trace levels), solvent extraction, and a new approach to enzymatic assays, are briefly reviewed to illustrate the trends towards future developments in continuous analysis in unsegmented streams.

It might appear that the sole reason for automation of chemical analysis is the need to analyse a large number of samples rapidly with minimum expense of labour. This is indeed so in most clinical and many industrial laboratories, where the increased precision, inherent to automated handling, is also appreciated. From a research or academic viewpoint, automation is, unfortunately, often considered as a mere mechanization of existing procedures which does not offer much opportunity for innovation. This is true for most batch analysers (with the exception of the centrifugal analysers), but does not apply to continuous flow systems which are more flexible, and where the flow of liquids and the mixing patterns at the interfaces between regions of different concentrations offer many new aspects for performing chemical analysis. Yet, within the past 20 years, during which the air-segmented continuous flow systems based on Skeggs's concept [1] have been in use, only a small fraction of the several thousand published papers on Auto-Analyzer systems has dealt with the theory, the most significant contributions being those of Thiers et al. [2, 3], Begg [4, 5] and of the Technicon group [6—8]. Even these authors, however, have focussed their attention entirely

†Part of this text was presented in two plenary lectures at the "Workshop on Flow Injection Analysis", Oct. 1977, Uppsala, Sweden, organized by the Swedish Chemical Society.

on the most effective means of limiting the dispersion of the sample rather than trying to use the dispersion patterns for various analytical purposes.

Although it might appear that the main feature of the Flow Injection method [9] is the absence of air segmentation, or perhaps the feat of injecting the sample into a system, it is important to realize that this technique is founded on a combination of the following three principles: (1) sample injection, (2) reproducible timing, and (3) controlled dispersion.

The purpose of the sample injection is to place a well-defined sample zone into a continuously moving stream (Figs. 1 and 2) in such a way that the movement of this stream is not disturbed. The amount of sample, although it need not be accurately known, has to be injected with a high precision so that the volume and length of the sample zone at the point of injection is reproducible. The injection technique has progressively evolved from the use of a syringe and a flap valve [9—11] to a sample loop operated by a set of magnetic valves, and finally to the use of a rotary valve with a bore, which acts as the sample container and is furnished with a bypass of a higher hydrodynamic resistance than the sampling volume (Fig. 3). In the latter device, the carrier stream flows entirely undisturbed while the volumetric bore is filled, because the pumped stream bypasses the valve through a shunt; only after the core of the valve has been turned is the sample zone injected into the system by the stream which now follows the flow path of lower resistance. This way of injecting the sample into a continuously flowing stream is more reproducible than the aspiration technique used in the air-segmented systems, and therefore the injection technique allows the conventional concept of the "steady-state signal" to be abandoned and the sampling frequency to be substantially increased, while the sample consumption is reduced.

As the signal is no longer to be read at the flat part of the response curve, but on its steep ascending part, a highly reproducible timing is essential, because any imprecision in residence time of the sample on its way to the detector will be reflected in the readout. It is well recognized that precise timing is vital in continuous flow analysis, where the chemical reactions employed are very seldom allowed to reach equilibrium. Therefore — in addition to purely physical reasons related to the length of the sample zone and its dispersion as it flows towards the detector — the chemistry involved

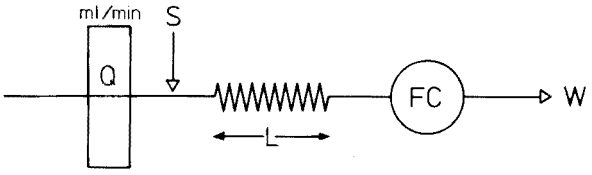

Fig. 1. The outline of a simple Flow Injection system, consisting of a pump which propels a carrier stream at pumping rate Q, an injection port through which a sample solution S is introduced, a reaction coil of length L, and a flow-through detector FC from which the measured stream flows to waste (W).

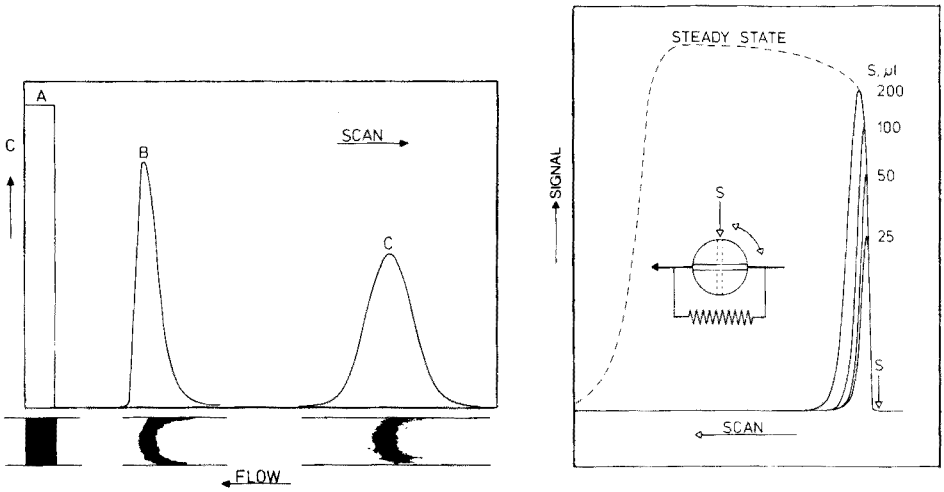

Fig. 2. Typical peak forms and corresponding concentration profiles observed: (A) at the point of injection; (B) shortly after injection; and (C) after passage through an open narrow tube.

Fig. 3. The principle of the injection valve, furnished with a bypass of higher hydrodynamic flow resistance; and peaks obtained by injecting, at point S, increasing volumes of sample solutions (S, μl).

also requires a reproducible travel pattern of the sample from the point of introduction to the detector. Yet, because of the inherent compressibility of air, any segmented stream pulsates and therefore neither the tube diameter nor the tube length can be decreased beneath a certain value if these pulsations are not adversely to affect the reproducibility of the timing required by the pertinent chemistry. Additional adverse factors are the addition and removal of air from systems and the irregularity of the bubble pattern. In contrast, the only source of pulsation in an unsegmented stream can be attributed to the use of an imperfect pump. Moreover, because the sample does not pass through a pump on its way to the detector, its path through the system is well defined, and the dispersion of the sample zone and the residence time can be chosen at will to suit exactly the requirements of the chemistry involved. Not only long but extremely short residence times can be maintained reproducibly.

The controlled dispersion of the sample zone which occurs during its passage through the system towards the detector results in a response curve (Fig. 2) which has a peak shape characteristic of the Flow Injection system. Naturally, the sample zone broadens as it moves downstream and changes from the original asymmetrical shape to a more symmetrical and eventually Gaussian form. By changing the flow parameters, the dispersion can be easily manipulated to suit the requirements of a particular analytical procedure so that optimum response is obtained at minimum time and reagent expense. Furthermore, the concentration gradients in the interfacial regions

between the sample and the carrier solution can be employed to develop entirely new analytical techniques. Generally, dispersion can be classified as limited, medium and large, and can be employed in the following ways.

If the original composition of the sample solution is to be measured, e.g., pH, pCa or conductivity, a limited dispersion of the sample zone is required, in order to ensure that the readout as obtained at the centre of the sample zone is not affected by any mixing with the surrounding carrier stream. Also, when the Flow Injection system is to serve merely as a means of reproducible introduction of samples into a detector, e.g., in atomic absorption or flame spectrometry, the conditions of limited dispersion are most suitable.

If, however, one or several chemical reactions resulting in colour formation, change of pH, adjustment of ionic strength, complex formation, etc., are to take place, a medium dispersion of the sample zone is called for. The reason is that the centre of the sample zone must be mixed effectively with the carrier stream and often with several reagents in sequence. A suitable compromise between the requirements of mixing and reaction time on the one hand and maximum acceptable broadening of the sample zone on the other hand must be found, because an increase in the zone width decreases the sampling frequency. Medium dispersion encompasses a very broad area of applications: it can accommodate very fast chemical reactions like those employed in turbidimetry, where the sample is mixed with reagent and measured immediately before the crystals start to cluster from a colloidal precipitate; but it may also be used to promote several reactions in sequence as in the enzymatic analysis of urea measured through the formation of indophenol blue.

If the interfacial concentration profiles between the sample plug and the carrier stream are to be employed, a large dispersion of the sample zone is required so that the resulting "concentration layers" are sufficiently spaced. Thus, in the case of titrations [12], it is the width of the sample zone, measured as it passes through the detector, which is proportional to the titrant consumption. Another application is the multicomponent resolution technique [13] where advantage is taken of the pH gradient created in the interfacial region between the sample and the carrier stream comprizing a suitable colour reagent of fixed pH value. The resulting sequence of colour-forming reactions can be measured as they take place across the dispersed sample zone of a certain pH gradient. For kinetic measurements, the sample—reagent ratio can be varied in a similar way while the reaction time is kept constant. Thus a multitude of measuring points can be obtained from only one flow-through detector which scans the shape of the resulting peak.

It is obvious that the comprehensive theory of the Flow Injection method will eventually combine the theory of mixing of liquids in continuously moving streams with the theory of chemical kinetics. This complex approach is, however, too ambitious at the present stage, when it is desirable rather to

offer understandable guidelines for the design of practical systems. Therefore, the theory presented below represents only a simplified approximation of the theory of mixing which is intended to yield an answer to the question of how to design a Flow Injection system so that it will accommodate the existing batch (or AutoAnalyzer) procedures, and to outline the advantages and limitations of the Flow Injection Analysis.

THEORY*

The design of the flow-system will depend primarily on the type of analysis required, as this will dictate the type of dispersion of the sample zone which should be created. At the same time, in order to obtain maximum sampling frequency (and minimum carryover), the shortest possible residence time of the sample in the system is desirable; this is nearly (but not always) synonymous with the smallest degree of dispersion suitable for the type of measurement to be carried out. The multitude of tools which can be used to vary dispersion and to choose a fitting compromise to fulfil these two contradictory requirements can be divided into two groups: (a) the geometry of flow (type of vessel, "chemical reactor"), and (b) the velocity of flow (flow rate).

The influence of the shape and size of the reaction vessel on the type of flow and the degree of dispersion obtained, is well described in textbooks on chemical reactor engineering (see, e.g., Levenspiel [14]). In a vessel with a stabilized flow, two idealized flow patterns can be visualized: plug flow and mixed flow representing the two extremes (Fig. 4). In reality, however, neither of these patterns is fully developed, and the resulting arbitrary flow contains contributions from both these ideal flow types in different proportions. A knowledge of the residence time distribution (RTD) of the individual molecules (or elements of fluid) within the flow-through reactor is essential for description of the type of flow and leads to a quantitative expression of the dispersion. As each element of fluid takes a different time to pass through the reactor, a certain distribution of residence times can be observed at the exit of the vessel for those elements of fluid which entered the vessel simultaneously. The area under the exit age distribution curve E is for convenience normalized to unity, i.e.,

$$\int_0^\infty E\,dt = 1 \qquad (1)$$

and this function is characteristic for a given type of flow. To measure the E-function in a given flow-through system, the stimulus-response technique has been widely used in chemical reaction engineering. This method is based on addition of a material — either as a step or a pulse signal — which can be quantitatively measured at the exit of the vessel, but which is not adsorbed and does not disturb the flow pattern. Typically, a solution of a dye can be introduced into a colourless stream and measured spectrophotometrically.

*For convenience, the symbols used are listed in Table 1.

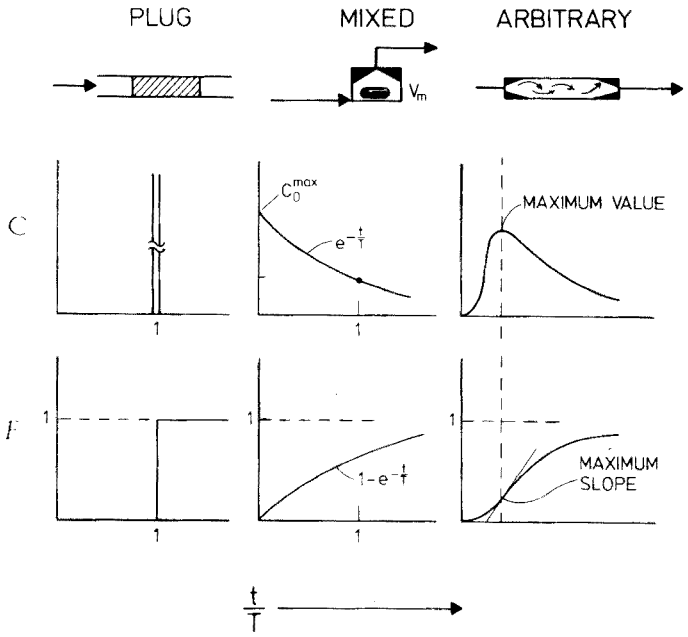

Fig. 4. Different types of flow and the influence of the flow geometry on the shape of the residence time distribution curves [14]. Note that the *C*-curves correspond to those obtained in Flow Injection while the *F*-curves correlate with the "steady-state" mode of operation.

With no tracer initially present, a step input of dye of concentration C_0 can be imposed on the fluid stream entering the vessel, with the result that eventually a gradual increase of colour intensity is observed at the vessel output. If this resulting concentration C is plotted as C/C_0 versus time, a so-called *F*-curve is obtained. The time-span between the introduction of the dye and the inflection point of the curve is the mean residence time T (the reactor holding time, which is V_R/Q where V_R is the reactor volume and Q is the volumetric flow rate), and the slope of the ascending part of the curve is inversely proportional to the dispersion. From an analytical viewpoint, it is noteworthy that the AutoAnalyzer approach to steady-state conditions is in straight-forward relation to the concept of *F*-curves, and much previous confusion on the "origin of the lag phase" [3] could have been avoided if the AutoAnalyzer output curves had been treated simply as *F*-curves [4].

The so-called *C*-curve is obtained by normalizing the response obtained by injecting an instantaneous pulse of a tracer into the stream entering the vessel and measuring the dye intensity at the exit. By measuring C and plotting it versus time, a peaked curve is obtained which is in direct relation to the peaks obtained in the Flow Injection Analysis system (f.i.a.). The time-span between the injection of the dye and the peak maximum is the

TABLE 1

List of symbols

a	distance from the centre of a tube (mm)
C	concentration (mol l^{-1})
C_0^0	concentration of the injected sample (mol l^{-1})
C^{max}	concentration of the element of fluid at peak maximum (at $t = T$) (mol l^{-1})
C_0^{max}	concentration of the element of fluid at peak maximum, extrapolated to $t = 0$ (mol l^{-1})
C-curve	$C = E = dF/dt$
D	dispersion (dimensionless)
D	axial dispersion coefficient ($cm^2\ s^{-1}$)
D_c	molecular diffusion coefficient ($cm^2\ s^{-1}$)
δ	dispersion number (dimensionless)
d	tube diameter (mm)
E-curve	$E = C = dF/dt$
F-curve	time record of exit concentration from a reactor, measured as C/C_0
F	mean linear flow velocity (mm s^{-1})
H	peak height at $t = T$ (mm)
H_0^0	peak height recorded with flow cell filled with solution of concentration C_0^0 (mm)
H_0	peak height extrapolated to $t = 0$ (mm)
L	total length of a line (cm)
l_i	length of a mixing stage (mm)
l_s	length of the sample zone (mm)
$l_{1/2}$	sample zone length corresponding to $S_{1/2}$ (mm)
M	mass of injected material (mol)
N	number of mixing stages (dimensionless)
Q	pumping rate (ml min^{-1})
Re	Reynolds number ($Re = 21.2\ Q/d$) (dimensionless)
r	tube radius (mm)
S_f^{max}	maximum sampling frequency (samples h^{-1})
S	sample volume (μl)
$S_{1/2}$	sample volume necessary to reach 50% of C_0^0 at C^{max} (μl)
σ	variance
T	mean residence time (s)
t	time (s)
t_i	mean residence time in one tank (s)
t_s	sample zone length in time units (s)
$t_{1/2}$	half wash time (s)
V_m	mixing chamber volume (μl)
V_p	volume of the plug flow section of a tube (μl)
V_R	reactor volume (μl)
W	reduced peak width (at $t = T$) (mm)
W_0	reduced peak width extrapolated to $t = 0$ (mm)
W(s)	reduced peak width in time units (s)

mean reactor holding time, T, and the peak width is directly proportional to the dispersion. If the C-curve is normalized, by dividing C by the area under the concentration curve, the relationships between the E-, F- and C-curves are

$$E = C = dF/dt \quad \text{and} \quad F = \int_0^t E dt = \int_0^t C dt \tag{2}$$

Their graphical representation (Fig. 4) gives an idea of the influence of the geometry of the vessel on the RTD. Thus, as the *C*-curve is related to the f.i.a. curve, it can be inferred that the plug type of flow is desirable for methods requiring limited dispersion whereas mixed flow should be used for gradient techniques. The medium dispersion can be obtained by a combination of both types of flow, as produced in longer and thinner, or in shorter and wider tubes (Fig. 5).

Flow velocity

In addition to the degree of dispersion of the sample zone, which will be treated in more detail below, the residence time of the sample in the reactor is of particular interest, as the extent of any chemical conversion (e.g. formation of colour) is proportional to this factor. It is apparent that increasing the size of the reactor is the most suitable way of increasing the residence time, and vice versa, as $T = V_R/Q$. Moreover, increase in the linear flow velocity F (which is related to Q) eventually leads to turbulent flow in tubular reactors and results in a decrease in the dispersion. Thus, if one wishes to increase the intensity of the colour produced by a chemical reaction, one would intuitively increase the length of the coil rather than decrease the pumping rate Q. The correct answer to the question of how the flow velocity influences the dispersion of the sample zone is, however, rather surprising, as it is ostensibly in contradiction to the advice usually provided in chemical reactor engineering.

In a tubular flow reactor the dispersion of the sample plug is the result of redistribution of material through countless repositionings of the elements of fluid, and this process — statistical in nature — is similar to molecular

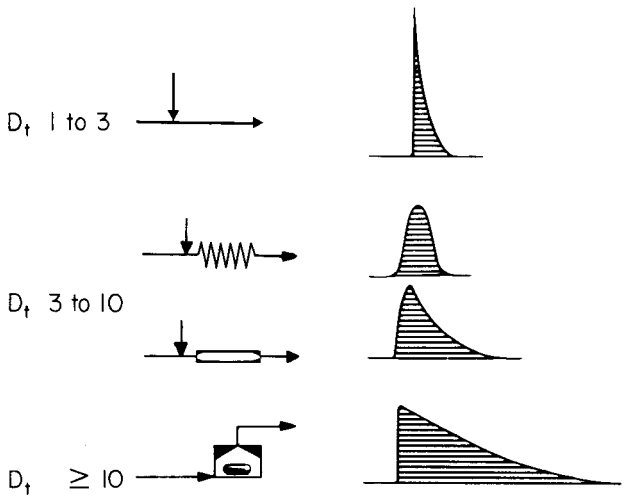

Fig. 5. Limited, medium and large dispersion (D_t), together with the corresponding vessel geometries in which they might be obtained and the resulting peak forms.

diffusion. In analogy with Fick's law, these contributions in the axial direction can be described by the expression

$$\partial C/\partial t = D\,\partial^2 C/\partial x^2 \tag{3}$$

where parameter D is the axial dispersion coefficient. The basic differential equation representing the dispersion plug model is

$$\frac{\partial C}{\partial t/T} = \left(\frac{D}{FL}\right)\frac{\partial^2 C}{\partial z^2} - \frac{\partial C}{\partial z} \tag{4}$$

where $z = x/L$ and $1/T = FL$, L being the tube length and F the mean linear flow velocity. The dimensionless group D/FL is the dispersion number δ. The solution to this equation leads to a symmetrical C-curve for low δ values [14]:

$$C = \frac{1}{2(\pi\delta)^{\frac{1}{2}}}\, e^{-(1 - t/T)^2/4\delta} \tag{5}$$

which is a Gaussian curve in which the variance σ is related to the dispersion number in the following manner:

$$\sigma^2 = 2\delta; \quad C^{max} = \tfrac{1}{2}(\pi\delta)^{\frac{1}{2}}; \quad W_{0.6} = 2(2\delta)^{\frac{1}{2}}; \quad W_B = 4\sigma = 4(2\delta)^{\frac{1}{2}} \tag{6a–d}$$

where W is the peak width (W_B at peak base; $W_{0.6}$ at 60% peak height). Thus the dispersion can be found by computing the variance σ or by measuring the height C^{max}, the width at 0.6 C^{max}, etc. (see Fig. 8). Furthermore, as variances are additive, any number of a series of interconnected vessels can be studied by one-shot impulses as

$$T_{overall} = T_a + T_b + \ldots T_n \tag{7}$$

and

$$\sigma^2_{overall} = \sigma^2_a + \sigma^2_b + \ldots \sigma^2_n \tag{8}$$

This makes it possible to evaluate how the addition of a particular mixing coil, change of a flow-through cell, addition of a stream, etc., contributes to the overall dispersion in the Flow Injection system.

The dispersion number is, however, not independent of the linear flow velocity. This can be understood by considering the interplay between the axial and radial dispersion. In turbulent streams ($Re \geqslant 1000$), the chaotic movement of elements of fluid causes the dispersion in all directions to be similar in magnitude. In the region of laminar flow, however, the axial dispersion is mainly due to velocity gradients, since the liquid at the centre of the tube moves at twice the mean speed of the fluid (F) while the layer close to the wall stands still, i.e.:

$$F_a = F_{max}\,(1 - a^2/r^2) \tag{9}$$

where F_{max} is the velocity of the axial flow, r is the radius of the pipe and a is the distance from the axis. Thus with increasing linear velocity, the concentration gradient in the axial direction will become more pronounced (Fig. 2B) unless this pattern is broken by the onset of turbulence. This is

exactly why turbulent flow (of high F) is recommended in chemical reactor engineering as a means of limiting dispersion. High flow velocities are, however, not suitable for continuous flow analysis, as they can be sustained only at high reagent costs. The other alternative, a decrease in the tube radius (as $Re = 21.2Q/2r$), would require too narrow tubes through which the liquid could be propelled only by high pressure [8] and which could easily become blocked by solid particles.

However, if it is decided to go in the opposite direction and operate at low Q values, radial mixing, which in streamline flow is due to molecular diffusion alone, will start to cancel the formation of the less developed parabolic velocity profiles caused by the forward motion of the liquid. Taylor [15] was the first to explain this process and describe it mathematically, deriving "Taylor's equation", which for tracer input conditions yields a function similar to that of the *C*-curve:

$$C = M \frac{1}{r^2\pi} \left(\frac{1}{2(\pi\delta L^2)^{\frac{1}{2}}} e^{-(L-X)^2/L^2 4\delta} \right) \qquad (10)$$

where C is the concentration at distance X, M is the mass of material injected at point $L = 0$ at time $t = 0$, r is the radius of the tube and the dispersion number is expresses as $\delta = D\ t/L^2$. Comparison of eqns. (5) and (10) reveals the identity of the shape of the *C*-curves they describe and the fact that the dispersion will increase in conditions of laminar flow, with the second power of the tube radius. It also follows from Taylor's work that radial diffusion will start to affect the velocity profiles if the residence time $T = r^2/3.8^2 D_c$, where D_c is the molecular diffusion coefficient. Thus for $D_c = 7 \cdot 10^{-6}$, the minimum time for Taylor's effect to develop is 6.2 s for a tube of 0.5-mm i.d., and 25 s for a tube of 1-mm i.d. This is precisely why the decrease of dispersion with decrease in linear flow velocity cannot be used in chemical reactor design, but is useful in continuous flow analysis, where tubes with bores less than 1 mm can readily be employed. Bearing in mind that the condition of minimum residence time for a given tube radius has to be fulfilled, the relation between the dispersion number and Reynolds number Re can be expressed graphically, according to Taylor and Levenspiel [14, 15], as in Fig. 6, which shows two regions of low dispersion. The Taylor minimum, in the vicinity of $Re = 0.1$, corresponds to the flow rate at which the creation of the velocity profiles is nearly compensated by molecular diffusion in the radial direction. Although such a flow velocity is too slow to allow practical sampling rates, the general tendency is obvious and from it follows the first and most important rule for the design of Flow Injection systems (in which the condition of minimum residence time is fulfilled):

Rule 1: A decrease of the flow rate in narrow tubes will lead to a decrease in the dispersion. This is therefore the most suitable means of increasing the residence time of the sample in the system as it simultaneously results in reduced reagent consumption.

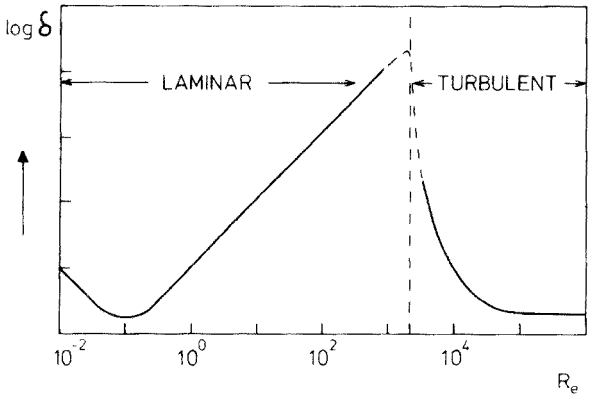

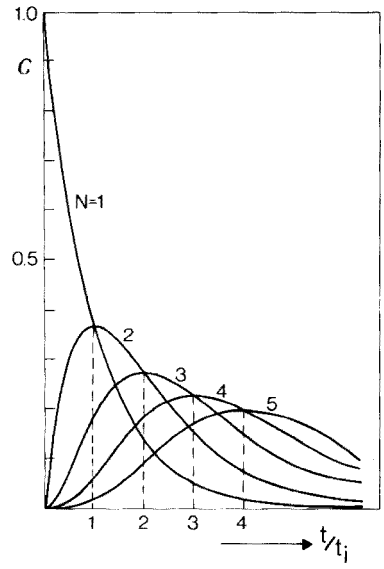

Fig. 6. The dispersion number δ as a function of the Reynolds number (Re) for aqueous solutions in the laminar, transient and turbulent regions of flow [12].

Fig. 7. The C-curves obtained for 1, 2, 3, 4, and 5 tanks in series (eqn. 12).

Flow geometry

The influence of the flow velocity on dispersion in open narrow tubes having been considered, it is appropriate to examine more closely the effect of the flow geometry (type of vessel) on the shape of the C-curve, by an approach different from the dispersion model. The tanks-in-series model is based on the view that a liquid flows through a series of well stirred tanks of equal size. The parameters of this model are N, the number of tanks through which an element of fluid has passed, and t_i, the mean residence time of the element of fluid in one tank. Thus the mixing of two fluids (say, a sample coloured by a dye, and a colourless carrier stream) can be viewed as a repetitive process depending on how many stages the sample plug has passed through. For one tank the normalized C-curve has the form [14]

$$C = (1/t_i)\,e^{-t/t_i} \tag{11}$$

while the G-type statistical function written as the C-curve

$$C = \frac{1}{t_i}\left(\frac{t}{t_i}\right)^{N-1} \frac{1}{(N-1)!}\, e^{-t/t_i} \tag{12}$$

describes the system with any number of tanks (Fig. 7). Thus for large N, the curve approaches a Gaussian shape, while for decreasing N the peak becomes increasingly skewed. The mean residence time of the sample in the system, T, coinciding with the appearance of the maximum of the C-curve at

the exit of the vessel, is related to N through the individual residence times t_i by $T = Nt_i$, while the variance of the curve is:

$$\sigma^2 = Nt_i^2 = T^2/N \qquad (13)$$

For $N \geqslant 10$, where the peak shape can be considered practically symmetrical, it can be shown, by comparing eqns. (6a) and (13), that the dispersion number $\delta = 1/2(T^2/N)$. Thus, for a constant value of T, the dispersion will decrease with increasing N, eventually leading to an approximately plug flow; in contrast, if N is low asymmetrical concentration profiles will be obtained. Therefore, as a short residence time T is preferred, in order to minimize dispersion and to save reagents, the reactor must have a small volume. Yet, it is important to realize that even the same reactor size will yield widely different peak shapes depending on the geometry of flow and the intensity of mixing. Thus:

Rule 2: Symmetrical gradient profiles will be obtained in a long narrow tube which accommodates a large number of identical mixing stages. Shorter or wider tubes of lower N will yield more asymmetrical peaks, while in a one-tank system ($N = 1$) an asymmetrical peak with an exponential rise and fall part will be observed.

Any practical system will always consist of several sections, each of which has individual flow patterns which, through individual contributions, will yield a certain C-curve. As the variances are additive (and related to N), one can establish the contribution of a certain part of a manifold (coil, flow cell, etc.) from the difference in variances of the C-curves with and without the particular component included in the tested circuit.

Dispersion

So far, the approach followed has been based on the concept of normalized C-curves which describe the distribution of residence times of the elements of fluid in a vessel in relation to the mean residence time T which coincides with the maximum of the curve. Except for the gradient techniques, where an exact knowledge of the concentration profile within the sample zone is essential (see ref. [12] and the paragraph on gradient techniques below), it is not necessary to use this rigorous approach for the design and description of the Flow Injection systems where the analytical readout is based on the peak height. This allows the dispersion D for the purpose of f.i.a. to be defined as the *ratio of the concentrations before and after the dispersion process has taken place in those elements of fluid which correspond to the maximum on the dispersion curve (Fig. 8).* By denoting C_0^0 as the original concentration of the injected sample solution and C^{max} as the concentration in the element of fluid corresponding to the peak maximum, the dispersion is related to the peak height H by:

$$D = C_0^0/C^{max} = \text{const.}\ H_0^0/\text{const.}\ H \qquad (14)$$

where const. is a conversion factor between instrument readout and concentration

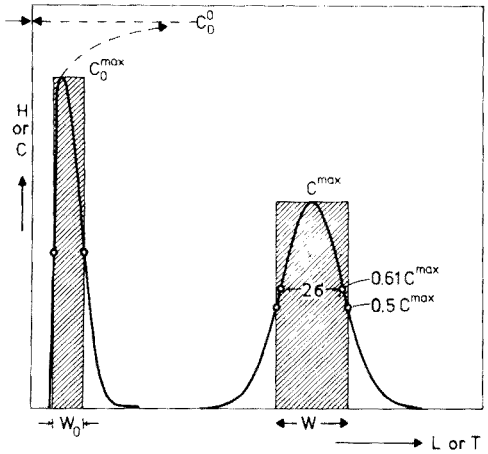

Fig. 8. The key parameters for defining dispersion in the Flow Injection method. Note that for $C = C_0^0$, $D_t = 1$.

obtained by calibration. In colorimetry — provided that the Lambert—Beer law holds for the concentration range chosen — H can be expressed as the recorded peak height (e.g., in mm) and H_0^0 as the distance between the base-line and the signal recorded with the flow cell filled with the dye of the original concentration.

Similarly, if it is necessary to measure the contribution of an individual component in a system, one can take its input condition, e.g. H_n, as a basis. Therefore $D_{n+1} = H_n/H_{n+1}$, and for the total dispersion: $D_t = (H_0^0/H_n) \cdot (H_n/H_{n+1})$, or

$$D_t = D_1 \cdot D_2 \cdot D_3 \ldots D_{n+1} \qquad (15)$$

Thus by injecting, for example, a coloured solution into a colourless stream and by measuring the respective peak heights obtained colorimetrically, the influence of an additional coil, a confluence arrangement, or a mixing chamber can be rapidly estimated.

It is self-evident that the dispersion defined and measured in this manner describes not only the degree of dilution of the original sample at any point along its way from the injection port to the detector, but also the ratio in which the sample has been mixed with the reagent in the carrier stream. For $D = 1$, there is no mixing in the critical volume of fluid, while, e.g., for $D = 5$ the sample volume constitutes 20% of the critical volume.

The next important choice is the parameter to which D should be related, i.e., to line length L or residence time T of the sample in the system. It might appear that the line length is the better choice, as a certain length of tube is easy to associate with a certain degree of dispersion. Moreover, manifolds in continuous flow analysis have been traditionally and most easily described by coil length. Also, residence time T and line length L are related through

the pumping rate Q or linear velocity F:

$$QT = \pi r^2 L = QL/\mathrm{F} = V_R \qquad (16)$$

where V_R is the reactor volume. However, this equation holds only for a manifold of uniform diameter consisting of a single line, i.e., for a flow system infrequently used in practical analysis, when two or several streams often merge and reaction coils of various diameters are used. The residence time T of the sample in the system, however, is easy to measure as it coincides with the appearance of the maximum of the peak in the detector. More importantly, it gives information about the potential rate of sampling for a chosen degree of carryover and about the time available for the chemical reaction to take place. Therefore, the dependence of D on T for various flow rates and flow geometries is more informative and deserves particular attention. Accordingly:

Rule 3: Manifolds for continuous flow analysis, in addition to information on tube length, diameter and pumping rates in individual channels, should be supplemented by the value of residence time T (*and possibly* D_t). The latter data are more informative as they reflect actual flow rates and the influences of coil connectors, flow cell volume, method of sample injection and possible dead volumes.

In order to design systems with low dispersion (D1—3), medium dispersion (D3—10) or large dispersion (D higher than 10), the influence of sample volume S, tube radius r, tube length L, flow rate Q, linear velocity F and reactor volume V_R, have to be considered. It follows from the dispersion and from the tanks-in-series model, that asymmetrical gradient profiles will be obtained immediately after injection (low N), while increasing residence time will result eventually in nearly Gaussian concentration profiles, provided that the equilibration process has repeated itself a sufficient number of times (large N). Because it is perhaps easier to imagine the Flow Injection system as consisting of a number of imaginary tanks, each occupying a certain segment of carrier stream, this model has been chosen. From eqns. (11) and (12) and Fig. 7, as well as Figs. 8 and 13, it is natural to consider that the first portion of the manifold involving the injection port accommodates the volume of liquid corresponding to the first tank, while the whole manifold length L consists of N tanks ($N = L/l_i$). Thus if the same tube diameter is used all along, eqn. (12) can simply be used to compute D. This is, however, not possible in Flow Injection systems when the sample volume, S, is not negligible, but where, for systems with low D, it may correspond to a substantial part of the whole manifold. In fact, the wide range of S-values encountered in f.i.a. complicates the solution of this problem to such an extent that it can be rigorously described only by means of frequency analysis and computer modelling. Therefore, for the present purpose, a further simplification is made: the injection and the dispersion processes are treated separately, although it is clear that they occur within the first portion of the manifold simultaneously. With this approach, according

to eqn. (15), the total dispersion D_t might be considered as

$$D_t = D_i \cdot D_f \cdot D_d \tag{17}$$

where D_i is the dispersion arising from the injection system, D_f is that of the flow arrangement, and D_d is the dispersion ascribed to the detector. When the same flow cell is used throughout, D_d is constant and in the present context, and based on experimental evidence, D_d can be assigned a value of 1, as the detector volume is negligible compared to V_R and S.

If only one mixing stage is involved in the injection process (eqn. 11), the rising part of the peak should be the reversal of the falling part and both should be exponential:

$$\text{rising curve: } C = C_0^0(1 - e^{-kS}) \tag{18}$$

$$\text{and falling curve: } C = C_0^0 e^{-kS} \tag{19}$$

i.e.,

$$S_{1/2} = 0.693/k \tag{20}$$

where $S_{1/2}$ is the volume of sample solution necessary to obtain $C = C^{max} = 50\%$ of C_0^0 corresponding to $D_i = 2$. By sampling for two $S_{1/2}$, 75% of C_0^0 is obtained ($D = 1.33$), etc. For the "flat" portion of the rising curve corresponding to 96.8% of the "steady state", five $S_{1/2}$ volumes have to be injected ($D = 1.03$). As the concept of "steady state" is not required in f.i.a., the maximum sample solution requirement in practice will be of the order of one $S_{1/2}$ volume even for systems with limited dispersion. At the other extreme, injection of a sample volume corresponding to a fraction of $S_{1/2}$ has been shown to be reproducible enough to allow direct analysis of concentrated sample solutions which otherwise would have to be prediluted manually [16]. Thus, for example, $D_i = 4$ or 10 can be obtained by injecting 50% or 20% of $S_{1/2}$, as the first portion of the rising curve can be considered nearly linear.

It is obvious that the choice of sample volume is a powerful means of varying the overall dispersion of the system, and that $S_{1/2}$ is a very important parameter, the magnitude of which should be kept as small as possible, especially in clinical analysis where little sample may be available. This is why eqns. (18) and (19) have been expressed in terms of S rather than l_s or t_s (the length of the sample zone; or the time corresponding to S, by means of eqn. 16), as the sample volume is of primary analytical importance. It is essential to realize the importance of the flow geometry on the D_i value, as the same sample volume ($S = \pi r^2 l_s$) would occupy a four times longer portion of the tube if the radius were halved. Thus, if the dispersion of the flow D_f depends only on the residence time T and not on the tube diameter, which is an acceptable approximation within the range of r 0.2—0.5 mm (see Figs. 15 and 17), $S_{1/2}$ will decrease with the square root of the tube radius as the length of the mixing stage l_i will remain practically constant; therefore, the volume of sample solution

required to reach 50% of C_0^0 ($S_{1/2}$) will be four times smaller. This is why the tube radius should be kept small if low or medium dispersion is required and sample solution is scarce. Additionally, reagent economy is improved when narrow tubes are employed: for the same linear velocity F, the pumping rate Q in a tube of linear radius r is only one quarter of that required for a tube of radius $2r$.

It follows from the foregoing and especially from eqns. (17) and (18) and Fig. 9, that an increase in the sample volume has a gradually decreasing effect on the decrease of the total dispersion in the system, and that regardless of which laws D_f and D_i are governed by, these two values must be kept close to unity if limited dispersion ($D_t \leqslant 3$) is to be obtained in a Flow Injection system. Therefore:

Rule 4: Limited dispersion is obtained by injecting a sample volume corresponding to a minimum of one $S_{1/2}$ into a carrier stream, pumped at the minimum practical flow rate, and by having the shortest possible line length of i.d. 0.4 mm between the injection port and the detector.

For illustration, reference is made to the experimental part (Figs. 10 and 12), from which it appears that $S_{1/2}$ = 28 µl for Q = 0.5 ml min^{-1} and L = 22 cm of 0.4-mm i.d. (D_i = 1.3; D_d = 1). In other words, the sample zone should always pass through less than half its own length in all systems with limited dispersion ($L < l_i < l_s$).

From an analytical viewpoint, systems with medium dispersion are much more interesting as they can accommodate various chemical reactions. To

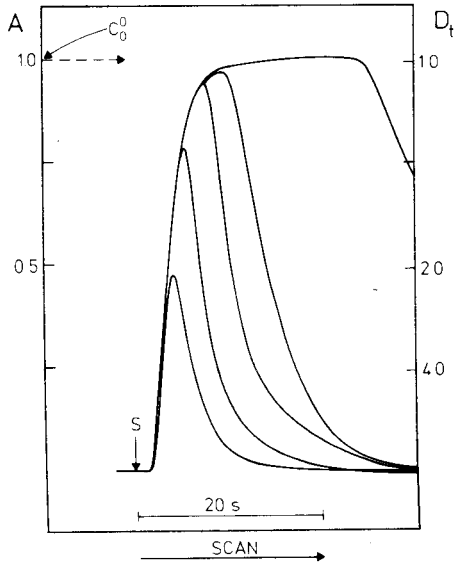

Fig. 9. Flow Injection response curves obtained by injecting 59, 108, 206, 403, and 795 µl, respectively, of a dye solution into a colourless carrier stream. S is the point of injection, while C_0^0 marks the absorbance (A) corresponding to the undiluted dye solution placed in the flow cell under static conditions. See also points (○) in Fig. 10.

estimate the dispersion of the sample zone in such systems, where often two or several streams merge, D_f has to be investigated.

From eqns. (5) and (12) and Fig. 7, as well as from Rule 2, a nearly symmetrical peak is obtained if the sample zone passes through a large number (N) of mixing stages so that the mixing process is repeated many times in the same fashion. Thus the concentration profile in a narrow tube will become nearly Gaussian in shape with a maximum close to the centre of the sample zone. This process can be followed experimentally by placing the flow-through cell at different distances downstream from the injection point, provided that all the tubing is of the same i.d. If all other parameters remain constant (i.e., S, C_0^0, Q, spectrophotometer adjustment and chart speed), the areas under all recorded curves will be identical, as no colour is formed or lost during the dispersion process. With the convention that the peak area is equal to peak height H multiplied by the width W at half height, each curve can be related to a hypothetical "square input" of height H_0 and width W_0 (Fig. 8). Thus the parameter D_f in such a system is described as:

$$D_f = H_0/H = W/W_0 = \text{const. } C_0^{max}/\text{const. } C^{max} \quad (21)$$

For Gaussian curves, the reduced sample zone width is approximately equal to two variances (eqn. 6). Thus $N = (2L/W)^2$ and $l_i = L/N$, from which it follows that

$$D_f = 2\, L^{\frac{1}{2}}\, l_i^{\frac{1}{2}}/W_0 \quad (22)$$

or in terms of the residence time, which might be preferable:

$$D_f = 2\, Q\, T^{\frac{1}{2}}\, t_i^{\frac{1}{2}}/W_0 \pi r^2 \quad (23)$$

When the pumping rate Q is replaced by the linear flow velocity F:

$$D_f = (2/W_0)\ \mathrm{F}\ T^{\frac{1}{2}}\, t_i^{\frac{1}{2}} \quad (24)$$

where l_i or t_i are system constants which describe the mixing intensity in terms of a characteristic tube length or residence time for a given flow rate, viscosity, surface tension between the carrier stream liquid and the wall material, temperature, diffusion coefficient of the dye, etc. Rule 5 summarizes these considerations:

Rule 5: The dispersion of the sample zone during its travel through a narrow tube increases with pumping rate but only with the square root of the travelled distance or of the residence time.

To measure D_f, one could use a series of either W or H values and extrapolate them to the respective W_0 or H_0 values by plotting versus the square root of time. The peak height method was chosen, as it is more directly related to C_0^0 and less subject to experimental errors.

By combining the definition of the dispersion (eqn. 14) with eqns. (17), (18) and (24), it is possible to describe the total dispersion in a manifold consisting of one line of uniform diameter

$$D_t = C_0^0/C^{max} = (2/W_0)\ \mathrm{F}\ T^{\frac{1}{2}}\, t_i^{\frac{1}{2}}(1 - 2^{-n}) \quad (25)$$

where $n = S/S_{1/2}$ and $e^{-n \cdot 0.693} \simeq 2^{-n}$. In this expression, all the parameters are accessible to measurement or can be, as W_0, obtained by extrapolation. It might thus appear that the relation between $S_{1/2}$ ($S_{1/2} = \pi r^2 l_{1/2}$), l_i, l_s and t_i should be straightforward if the concept of a certain length of a liquid representing one tank is correct. However, it should be emphasized that the values H_0 and W_0 do not exist in reality, as the injection and dispersion processes occur at the same time so that any $S_{1/2}$ (or $l_{1/2}$) is influenced by D_t and vice versa. Therefore the experimental values cannot be expected to agree precisely with this coarse model. Yet it is important to realize that even an approximate agreement would confirm the validity of Rules 1 to 5 and the usefulness of D which is always accessible to simple and accurate measurement and which exactly describes those properties of the manifold which are of analytical importance.

A large dispersion system may be desirable for two reasons: if the sample solution is too concentrated to be accommodated by the chemistry or the instrumental readout, or if the sample zone should be stretched along the time coordinate in the form of a well defined concentration gradient. A simple dilution is most effectively and precisely performed by injecting such a small volume of sample solution that it corresponds to a fraction of $S_{1/2}$, i.e., typically of the order of 1—5 μl at a Q value of 1—2 ml min^{-1} with a tubing system of 0.75-mm i.d. (eqns. 18 and 19 and ref. 16). The advantage of this approach is its speed, as the sample is dispersed within seconds after the injection has taken place. For this purpose, the concept of D_t proposed above is appropriate.

Formation of a concentration gradient as used in titrations [12] has quite another purpose, i.e., stretching the sample zone in a well defined manner along the time coordinate because it is the peak width which is the analytical readout and not the peak height, as in all the previously described cases. Therefore it is the shape of the peak, i.e., the type of concentration gradient obtained (exponential, Gaussian, etc.) which has analytical meaning. Accordingly, the use of D, which is related to the peak maximum value, is not of value unless merely the degree of sample dilution is of interest.

Mixing chambers

Several flow systems with manual or coulometric injection of substances, mainly for voltammetric or potentiometric applications, have been proposed in the literature [17—21]. All of these flow systems contain a mixing chamber. The mixing chamber is a simple gradient device, and provided that its volume V_m constitutes a substantial part of the whole system, the concentration gradient obtained will be described by eqn. (11) corresponding to one tank. In the case where S is much smaller than V_m, and the sample is injected as a pulse directly into the chamber and mixed instantaneously with the carrier solution, eqn. (11) can be modified [14]

$$CV_m/C_0^0 S = e^{-t/T} \qquad (26)$$

thus describing the concentration profile which is, of course, purely exponential. For $t = 0$, $C = C^{max}$ and therefore $D_m = V_m/S$ where D_m is the dispersion in the mixing chamber. By expressing T as V_m/Q (cf. eqn. 20) and by defining $t_{1/2}$ as the time span during which any concentration decreases by half:

$$t_{1/2} = 0.693\ V_m/Q \qquad (27)$$

and in analogy with eqn. (19) the baseline will be reached with an error of 4% when $t = 4\ t_{1/2} = 4 \times 0.693\ V_m/Q$.

The use of a mixing device in a continuous flow system should be discouraged if the peak height is the basis for measurements. A mixing device, however small, reduces the peak height significantly and broadens the sample zone so that the sampling frequency is decreased. Thus, if $S = 100\ \mu l$, $V_m = 2500\ \mu l$ and $Q = 5$ ml min^{-1}, then $D_m = 25$; i.e., the signal will be 25 times smaller than in the same system without the mixing chamber (cf. Fig. 18). Moreover, the baseline is approached within 4% error only 2 min after the peak height has been recorded, so that the sampling rate cannot exceed 30 samples per hour. In practice, D would be even larger if the sample were not introduced instantaneously and directly into the chamber but slowly during a certain interval of time through a connecting line. Exact computation of the C-curve for such a case, when the total volume of the reactor V is significantly larger than V_m, should be possible by means of a simple triparameter model, which uses the volume of the plug flow section of the tube, V_p, as the correction parameter (ref. 14, p. 296).

To summarize, the incorporation of any mixing chamber into a continuous flow system is a waste of both reagent solution and time, and results in a signal which is uncomfortably close to the baseline (see Fig. 18). Nothing is gained in terms of reproducibility compared to peak-height measurement, even if the area under the curve is integrated, because the unfavourable ratio between the baseline noise and the recorded signal still remains the same.

The use of an unsuitable flow cell may give rise to similar problems if it has too large a holdup volume, and so itself constitutes a miniature mixing chamber. This danger does not arise, however, if tubular flow cells such as those developed for liquid chromatography [19, 22] are used, because their holdup volume is negligible compared to the total volume of the line.

Too much emphasis should not be placed on the sampling frequency as sampling rates exceeding 150 samples per hour are not really required very often. However, a short residence time of the sample in the system is highly desirable as it makes the analytical readout quickly available. The relations between T, S, D_f, W, V_R, Q and F are critical in designing a system, as these parameters not only influence the sampling frequency, the degree to which chemical reactions can proceed, and the consumption of sample and reagent, but also the time needed to start and close down the system. This topic will be discussed in more detail later, but already at this stage the foregoing part can be summarized as follows:

Rule 6: The dispersion caused by the flow, D_f, should always be kept as low as possible by using the shortest possible lines of small and uniform diameter. Dilution of too concentrated sample material is best achieved by reducing the volume of the injected sample solution.

EXPERIMENTAL

Injection of a dye into a colourless stream and spectrophotometric measurement and recording of the dispersed sample zone were used as a tracer response technique to test the validity of eqn. (25).

Apparatus and solutions

The peristaltic pump (MP 13 GJ-4 Ismatec, Switzerland) was always operated at speed 10, to minimize pulsation of the pumped streams. All pumping rates stated in the experiments described are the nominal ones. For L more than 150 cm, r = 0.5 mm or less and Q more than 1.5 ml min^{-1}, the actual pumping rates were always slightly lower than the nominal ones, because of increased flow resistance.

The spectrophotometer (Beckman DBGT) was operated in the dual-beam mode at 600 nm, with a Hellma tubular flow cell of 10-mm optical path and 18-μl volume (OS 178.12). As the connection to the tubular part of the cell had a diameter of about 1.8 mm, the polyethylene tubes of which the various coils were made (0.4, 0.5 mm, etc.) were always inserted into the cell body so that any additional dead volume was eliminated. The recorder (Servograph 51) was interfaced to the spectrophotometer with a standard REA 112 high-sensitivity unit (Radiometer A/S, Denmark).

The carrier stream consisted of 0.1 M sodium tetraborate in distilled water. The indicator solution contained 0.4% of bromothymol blue in aqueous 20% ethanol solution. This stock solution was further diluted before use with 0.1 M sodium tetraborate in ratios ranging from 1:50 to 1:200, depending on the expected range of sample zone dispersion.

Sample injection

The method of sample injection is described in detail, as it is of primary importance. In the first parts of this Series, injection was done with a syringe into a flap-type valve. When this method was used, an additional volume of liquid, S, was forced into the carrier stream, which caused a momentary increase of the linear flow velocity F, manifested by a typical negative or positive peak on the baseline. This approach, although useful for analysis of large sample volumes in manifolds of relatively large V_R, was later replaced by injection through a rotary valve having a volumetric bore of constant volume. The valve was also furnished with a bypass which had a higher flow resistance than the volumetric bore (Fig. 3) so that the carrier stream could flow continuously through the manifold lines even when the valve was turned for introduction of the sample solution into the bore. This arrangement

avoids surging of the carrier stream and allows precise introduction of microlitre sample volumes and overall miniaturization of the system. For the present purpose, however, the use of a bore of fixed volume was not practical. Instead, the core of the valve was machined in such a way that a piece of tubing of any desired length and diameter could be attached to it thereby serving as a sampling loop of well defined volume and flow geometry. In this method of sample injection, the dye solution entirely filled a known length of a tube and stood still until the valve was turned so that the sample zone was passed into the line and was mixed with the carrier solution.

Sample volume

The influence of S on the peak height and the corresponding dispersion was investigated in two ways: (a) in a system with minimum achievable flow dispersion ($D_f < 2$); and (b) in a system where D_f was gradually increased in a reproducible manner by adding coils of known length between the injection port and the detector. All experiments described in this section were made at a nominal pumping rate Q = 1.5 ml min^{-1}.

The system with limited dispersion was made by simply connecting the injection valve to the tubular flow cell by 22 cm of 0.4-mm i.d. tubing as this was the shortest length of tube which could be employed in the experimental setup used. The sample loop was made of 1-mm i.d. polyethylene tubing of various lengths (6.25—100 cm) so that the injected volumes S (consisting of the loop volume plus the 10-μl valve holdup volume) were: 59, 108, 206, 403 and 795 μl altogether. The resulting curves (Fig. 9) had the form predicted by eqn. (18); when log $(1 - (C^{max}/C_0^0))$ was plotted versus S, a straight line was obtained from which $S_{1/2}$ could be read off (Fig. 10).

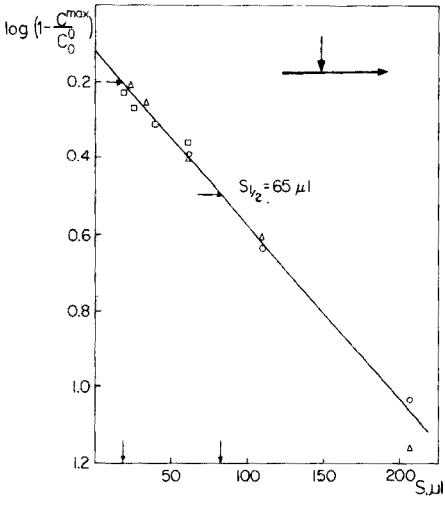

Fig. 10. The influence of the geometry of injection on the $S_{1/2}$ value. No influence is observed within loop tube diameters of 1 mm (○), 0.75 mm (△) and 0.5 mm (□). (Points (○) correspond to the first three curves of Fig. 9.)

The value of C_0^0, corresponding to the concentration of the undiluted dye solution, was determined by filling the flow cell with the pure dye solution and measuring the absorbance and the corresponding recorder pen deflection (H_0^0). Figure 9 indicates that approximately 50 μl are needed to reach D_t = 2, and 75 μl to reach D_t = 1.5, while the "steady state" is reached around S = 250 μl.

The next question is which parameters influence the $S_{1/2}$ value. An (a)-type system was used to study the influence of the geometry of injection by changing the diameter of the sample loop tube from 0.4 to 1 mm. This allowed S values to range from as little as 16 μl (6 μl from the tube and 10 μl from the valve) for the shortest length of the thinnest tube to 210 μl for the largest tube. All the measured C^{max} values, plotted according to eqn. (18), were close to a line with a slope corresponding to $S_{1/2}$ = 65 μl (Fig. 10), which shows — as D_f was kept practically constant in this experiment — that D_i is independent of the geometry of the sample zone prior to injection. Therefore there is no point in constructing valves with external loops as the internal bore may have a diameter of up to 1.0-mm i.d. (and perhaps up to 1.5-mm i.d.) which, with a valve body diameter of 25-mm, could accommodate sample volumes up to 50 μl. For the same linear velocity F, the residence time T is proportional to the length of the system L, which is also true for the relation between the residence time in one mixing stage, t_i, and its length, l_i. From eqn. (16) and Fig. 7 it is seen that a shorter t_i and l_i will result in a steeper curve, and as $S = \pi r^2 l_s$ the ratio of l_i/l_s will decrease and so will $S_{1/2}$, i.e. for lower l_i, the same sample volume will fill a larger number of mixing stages. In contrast, increasing the volume of a mixing stage — in the extreme by using a mixing chamber (eqn. 26) — will also increase $S_{1/2}$.

Therefore, a system with medium dispersion will have a marked influence on $S_{1/2}$. To investigate this parameter, various sample volumes were injected, by means of 0.5-mm i.d. sample loops, into a line of length 50 cm, 100 cm or 200 cm, the i.d. of the manifold tubing being 0.50 mm. The recorded curves are shown in Fig. 11, together with the C_0^0 and D_t values. By plotting log $(1 - C^{max}/C_0^0)$ versus $S_{1/2}$ for any of these three groups of curves, the same $S_{1/2}$ value of 114 μl was found (Fig. 12). When the same experiment was repeated with a tube of 1-mm i.d., an $S_{1/2}$ value of 445 μl was obtained (Fig. 12), which corresponds to a four-fold increase in the $S_{1/2}/l_s$ ratio. Finally, in order to see how small an $S_{1/2}$ value could be obtained with the experimental setup used, r was again minimized by using only 22 cm of 0.4-mm i.d. line, but this time Q was also decreased to 0.5 ml min^{-1} with the aim of decreasing F and thus the intensity of mixing. The resulting log $(1 - C^{max}/C_0^0)$ versus S plot (Fig. 12) yielded $S_{1/2}$ = 28 μl. It is likely that $S_{1/2}$ could be decreased even further if a flow cell with a holdup volume smaller than 18 μl was available; with these small V_R values the volume of the flow cell cannot be neglected.

Line length

The range of D_t values which can be obtained under conditions typical of a Flow Injection system (Q = 1.5 ml min^{-1}, tubes of i.d. 0.5 mm and

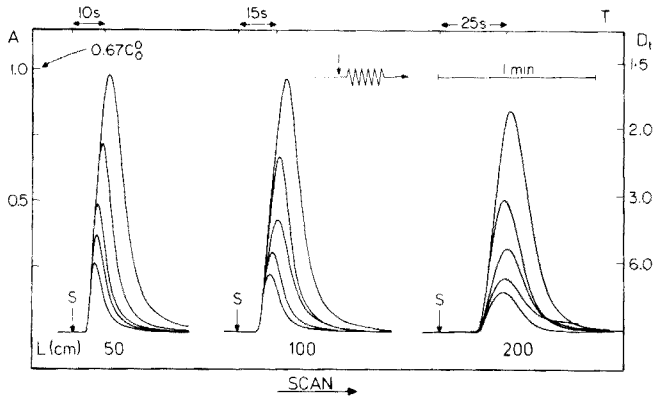

Fig. 11. Response curves obtained by injecting 16, 34, 59, 108, and 206 μl of a dye solution (S) into a carrier stream pumped at a rate of 1.5 ml min^{-1} (Q). The curves were recorded after the sample zone had passed through 50, 100 and 200 cm, respectively, of a tube having 0.5-mm i.d. (See also points (□) in Fig. 12.)

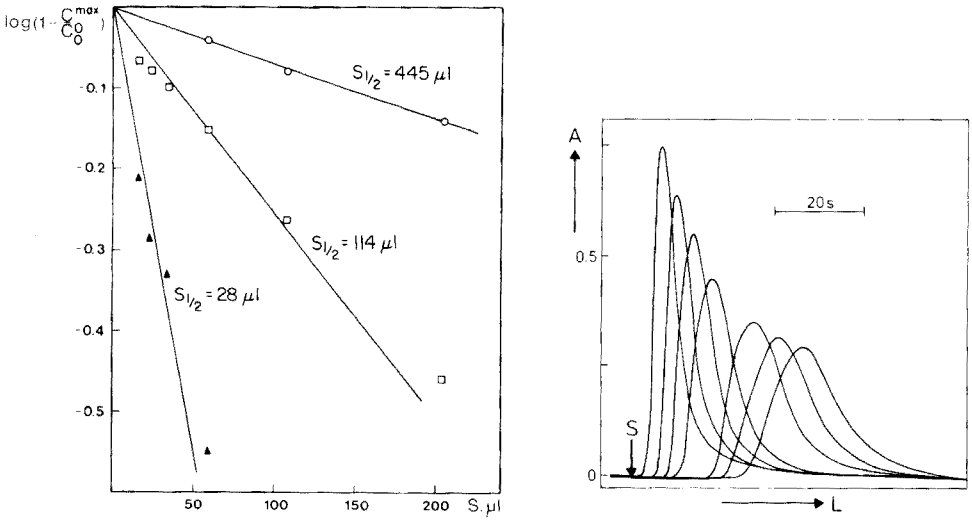

Fig. 12. The dependence of the $S_{1/2}$ value on the flow rate and diameter of the tube carrying the sample to (and through) the detector. (○) 1-mm i.d. tube with measurement at L = 100 cm; (□) 0.5-mm i.d. with measurement at L = 100 cm; (▲) 0.4-mm i.d. with measurement at L = 22 cm. Pumping rate Q for unfilled symbols, 1.5 ml min^{-1}; and for filled symbols 0.5 ml min^{-1}.

Fig. 13. Response curves obtained by injecting 50 μl of a dye solution into a colourless carrier stream pumped at a rate of 1.5 ml min^{-1} through a tube of 0.5-mm i.d. The tube lengths (L) were: 25, 75, 125, 175, 250, 300, and 350 cm, respectively, and the sample was always injected at point S. Compare with the filled circles in curve A of Fig. 14, where measurements at L = 50, 100, 150 and 200 cm are also included.

S = 16—206 μl) varies from 1.6 to 10 within line lengths of 50 to 200 cm with residence times of 10 to 25 s (Fig. 11). This alone shows how flexible the system is in terms of sample/reagent mixing ratio within a very short span of time. It is, however, interesting to determine whether the relation between

L and D_f as predicted by eqn. (22) is correct. For that purpose, a fixed set of values for sample volume (S = 50 μl), dye concentration, tube diameter (0.5 mm) and flow rate (Q = 1.5 ml min^{-1}) was chosen, while L was varied stepwise from 25 to 350 cm (Fig. 13). By plotting C^{max} versus $L^{\frac{1}{2}}$, a straight line was obtained, but it was observed that the residence time T was not in agreement with the nominal Q and F values, as these appeared to vary with increasing length in a peculiar way. An example of this can be seen in Fig. 11, where T for L = 50 is far too long compared with the value calculated from eqn. (16), is closest to the nominal value for L = 100, and is again too long for L = 200. There are two reasons for this apparent discrepancy. First, in a short line the residence time is relatively longer because at the moment of injection the sample zone stands still and has to accelerate to reach the mean flow velocity. Secondly, T marks the appearance of the peak maximum, i.e. of a point which is behind that edge of the sample zone which is in position L = 0 at T = 0. The decrease of F for high L values is a real one, as Q decreases with increasing flow resistance of the line. This problem could be overcome by applying a piston pump rather than the peristaltic pump used, but this would not correspond to the conditions in real Flow Injection systems (which function well with even simpler pumps than the one used here). Accordingly, it should be stressed that the nominal pump rates, however precisely stated by the manufacturers, seldom hold when the pump is attached to lines of higher flow resistance.

A practical means of avoiding these difficulties is to follow Rule 3 and use the residence time T as the main parameter (eqn. 24). Thus by plotting C^{max}, or more conveniently simply peak height H, versus the square root of the time span between the point of injection and the appearance of the peak maximum, a straight line should be observed, which may then be extrapolated to H_0 (or C_0^{max}). Figure 14 shows that this is true; line A corresponds to data from Fig. 13, whereas lines B and C originate from similar experiments with sample volumes of 100 and 25 μl. The D_f values are then obtained from each line by referring the individual points to the extrapolated H_0 value (eqn. 15 and its precursor). Plotting the D_f values thus found against $T^{\frac{1}{2}}$ (Fig. 15) leads to the surprising observation that D_f is practically independent of S within the range 25—100 μl.

Thus, although D_i is dependent on S, tube diameter and flow velocity for medium dispersion, the D_f value is independent of D_i provided that the sample volume used is smaller than $S_{1/2}$. Therefore, the same coil and flow rate would give the same D_f value, regardless of the sample volume (e.g., D_f = 2 or 50% after 16 s for Q = 1.5 ml min^{-1}, tube i.d. 0.5 mm, as in Fig. 15), and it will take a progressively longer time to reduce the peak height even further (another 50% reduction will take an additional 26 s) exactly in the manner predicted by the tank-in-series model (eqn. 12 and Fig. 7).

The influence of flow velocity

Rule 1 states that dispersion of the sample zone should decrease with decrease in the pumping rate, or more correctly, with decrease of the linear flow

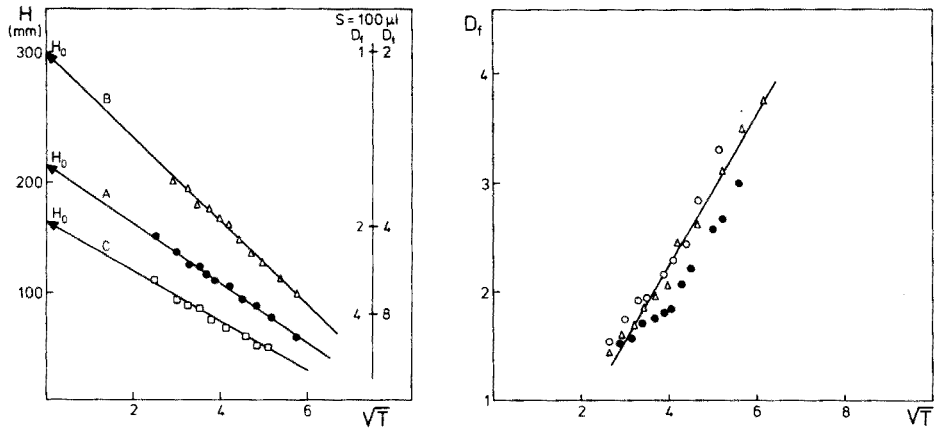

Fig. 14. The relation between peak heights (H), extrapolated peak height (H_0), and residence time T. The D_f and D_t values obtained for curve B corresponding to a sample volume of 100 µl, are shown on the right-hand side. Curve C was obtained for S = 25 µl, while curve A was obtained for S = 50 µl. The actual response curves, corresponding to line A are shown in Fig. 13.

Fig. 15. The dispersion values D_f obtained for the experimental data plotted in Fig. 14 for sample volumes of (○) 25 µl, (△) 50 µl (cf. Fig. 13), and (●) 100 µl.

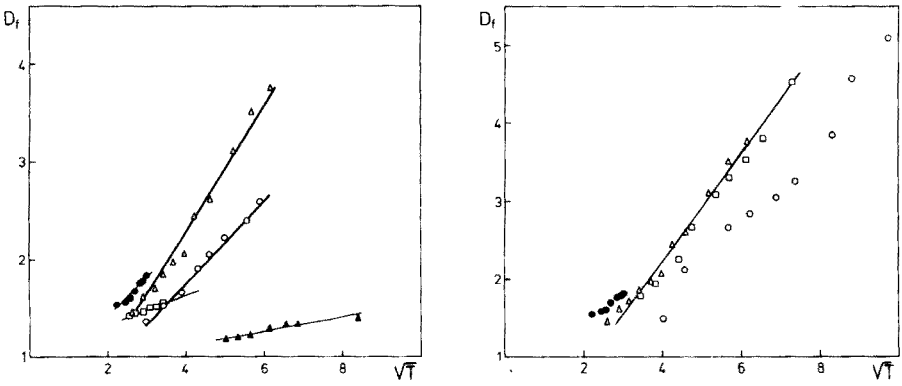

Fig. 16. The influence of flow velocity (expressed as mean residence time T) on the dispersion value D_f. Sample volume, 50 µl. Thin lines relate to a tube diameter of 0.4 mm and pumping rates (Q) of: (●) 1.5 ml min^{-1}, (□) 0.75 ml min^{-1}, and (▲) 0.25 ml min^{-1}. Thick lines relate to a tube diameter of 0.5 mm and pumping rates of: (△) 1.5 ml min^{-1}, and (○) 0.75 ml min^{-1}.

Fig. 17. The influence of tube diameter on the dispersion of the sample zone (S = 50 µl, Q = 1.5 ml min^{-1}). Tube diameter: (●) 0.4 mm; (△) 0.5 mm (cf. Fig. 15); (□) 0.75 mm; (○) 1 mm.

velocity F (eqn. 24). This dependence was investigated by injecting always the same sample volume (50 μl) into 0.5-mm or 0.4-mm i.d. manifold lines at Q values ranging from 1.5 ml min^{-1} to 0.25 ml min^{-1}. For each series of experiments, corresponding values for H and T for gradually increasing L were recorded in the same way as described in connection with Figs. 13—15. From the extrapolated H_0 values, the corresponding D_f values were obtained and are plotted in Fig. 16, where the thin lines correspond to tubes of 0.4-mm i.d. and the thick lines to tubes of 0.5-mm i.d. Clearly, the flow velocity has a profound effect on the dispersion of the sample zone, and thus on the validity of eqns. (24) and (25), and the importance of Rule 1 is confirmed.

The influence of tube radius

Identical sample volumes (25 μl) and pumping rates (1.5 ml min^{-1}) were used in a series of experiments where not only the tube length but also the tube diameter was changed; tube diameters of 0.4, 0.5, 0.75 and 1.0 mm were examined. The resulting D_f values, obtained as described in the two previous experiments, are plotted in Fig. 17. The data obtained for the 0.4-, 0.5- and 0.75-mm i.d. tubes can be grouped — not unreasonably — along a straight line, while points for the 1-mm tube yield a line which is shifted more or less parallelly, and gives lower D_f values. It might thus be concluded that within the range of tube lengths and diameters used in Flow Injection systems, D_f is independent of the tube diameter for the same residence time T.

The confluence of two streams

The confluence of two streams is often used in f.i.a. when an additional reagent is added to the main stream carrying the sample zone. The mixing pattern at the point where two streams meet is therefore very important, not least because it has been doubted that efficient mixing can be accomplished in this way [23, 24]. To study this, a manifold was made of 0.5-mm i.d. tube, and the flow cell was placed at L = 25, 50, 75, 100, 125, 150, 175, 200, and 250 cm from the injection point, so that the peak heights of the sample dye solution (S = 50 μl), passed in the usual way into a carrier stream pumped at a rate of 0.75 ml min^{-1}, could be recorded (Fig. 18). The confluence point, the holdup volume of which was made as small as possible (2—3 μl), was placed after L = 125 cm; at this point, an additional flow of the colourless carrier stream was added at a rate of 0.75 ml min^{-1}. Thus, the pumping rate was 0.75 ml min^{-1} before L = 125 and 1.5 ml min^{-1} afterwards. The D_f values obtained in this way are plotted in Fig. 19 (curve A), together with the results obtained in a similar experiment where a 0.4-mm i.d. line was used with much slower pumping rates in the main line and in the side line joining the main stream at the confluence point (Fig. 19, curve B)

A 1 + 1 confluence would result in a 50% lower peak if the mixing were complete and instantaneous. The change of D_f from 1.94 to 3.1 corresponds, however, only to a peak height change of 63%, and an additional 4 s is required before D_f = 3.88 is reached. This delay is not serious, because in analytical determinations a several-fold excess of a reagent is always used;

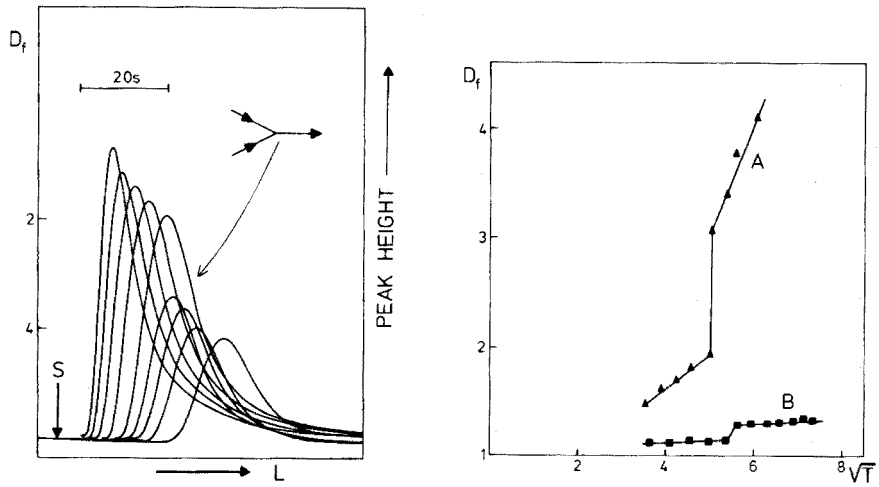

Fig. 18. Response curves obtained by injecting 50 μl of a dye solution at point S into a colourless carrier stream pumped at a rate of 0.75 ml min^{-1}, showing the influence of addition of a second colourless carrier stream also pumped at 0.75 ml min^{-1}. The individual curves (left to right) were recorded at L = 25, 50, 75, 100 and 125 cm; then the second stream was added, and after the confluence point curves for L = 150, 175, 200, and 250 cm were recorded. (Compare also line A, Fig. 19.)

Fig. 19. The dispersion values obtained in a confluence manifold by injecting 50 μl of sample into a system where two streams merge. Curve A corresponds to the curves shown in Fig. 18, while curve B was obtained with tubes of 0.4-mm i.d. and slower pumping rates, i.e. 0.25 ml min^{-1} in the main line and 0.12 ml min^{-1} in the additional line merging with the main stream at the confluence point at T = 30 s.

as long as the mixing process is reproducible, this short delay in complete mixing of merging streams has no practical consequences.

The influence of the pumping rate on the D_f values is profound. First, the slopes of the two dispersion lines (Fig. 19, curve A) before and after the confluence point agree roughly with the slopes of the lines obtained at the respective pumping rates in a simple manifold (Fig. 16). Then, when the pumping rate and the tube diameter are decreased (Fig. 19, curve B), the slope of the dispersion line both before and after the confluence point decreases dramatically, yet the merging streams (1 + 2) are still sufficiently mixed for the purpose of promoting a chemical reaction.

The mixing chamber

The dispersion of the sample zone in a mixing chamber was investigated by injecting 50 μl of the dye solution into a carrier stream pumped at a rate of 0.75 ml min^{-1}, and by recording the peak in the usual manner. Three experiments are shown in Fig. 20. For curve A, the sample zone was carried to the detector through 50 cm of 0.5-mm i.d. tube, so that this experiment corresponds to the third curve shown in the first group of peaks in Fig. 11. For curve B, a mixing chamber (V_m = 1.9 ml) was placed

between the end of the line and the detector. For curve C, the sample zone was passed first through a 50-cm line (0.5-mm i.d.), then mixed in the chamber, and then passed through another 50-cm section of 0.5-mm i.d. line to the detector.

The dramatic influence of the mixing chamber on the peak width and height is obvious. Comparison of the D_f values shows that peak A is 18 times higher than peak B. The D_t values, which were obtained by using the D_i values of Fig. 11 indicate that the peak height of curve B corresponds to only 2.77% of the H_0^0 which would have been obtained if the dye solution of the original concentration C_0^0 had been placed directly in the detector.

The residence time and sampling frequency

There are two basic ways in which the Flow Injection system can be operated: by processing one sample in the line at a time, or by having two (or several) sample zones spaced between the injection port and the detector. The first approach has mainly been used so far, is undoubtedly simpler to execute, and does not require either automated sampling or special sample identification; the operator is in correspondence with the analyser, as one is when using an electronic calculator. The limitation of this approach for slower chemical reactions, is that the time available for chemical reactions is a maximum of 30 s if a sampling frequency, S_f^{max}, of 120 samples per hour is to be maintained. It follows, for example, from Fig. 8 and eqn. (5), that a signal measured at a time $t = T + 1.5\ W$, will be approximately 1% of the C^{max} value (or H) recorded at time T (if the curve is Gaussian), or that a signal measured at a time $t = T + 4 \cdot t_{1/2}$, will be within 4% of the baseline for one tank-in-series (mixing chamber or short line). In routine work, the time span between subsequent injections can be much shorter than either of these t values, provided of course that $T \geqslant 1.5\ W$. This is the manner in which Flow Injection systems have been most frequently operated, and the maximum sampling frequency is then given by $S_f^{max} = 3600/T$ (samples/h).

However, if residence times larger than 30 s are required in order to adapt slow chemical reactions, two or more sample zones must be accommodated in the system at a time. In such cases, it is the sample zone width, observed during its passage through the flow detector, which is the main parameter determining S_f^{max}. If the dwelling time of the sample in the system is sufficiently long so that the peak shape can be considered practically Gaussian, the peak width W (in seconds) will be given, according to the definition of D_t, by:

$$W = D_t W_0^0 = D_t\ S/(Q\ 1000/60) = 0.06\ D_t\ S/Q \qquad (28)$$

where W and W_0^0 are expressed in seconds. Thus, the maximum sampling rate, allowing approximately 1% carryover from one sample to the next, is

$$S_f^{max} = 3600/1.5\ W = 4 \cdot 10^4\ Q/D_t S \text{ (samples/h)} \qquad (29)$$

where the linear flow velocity in the measuring cell is given by $F = Q/\pi\ r^2_{cell}$.

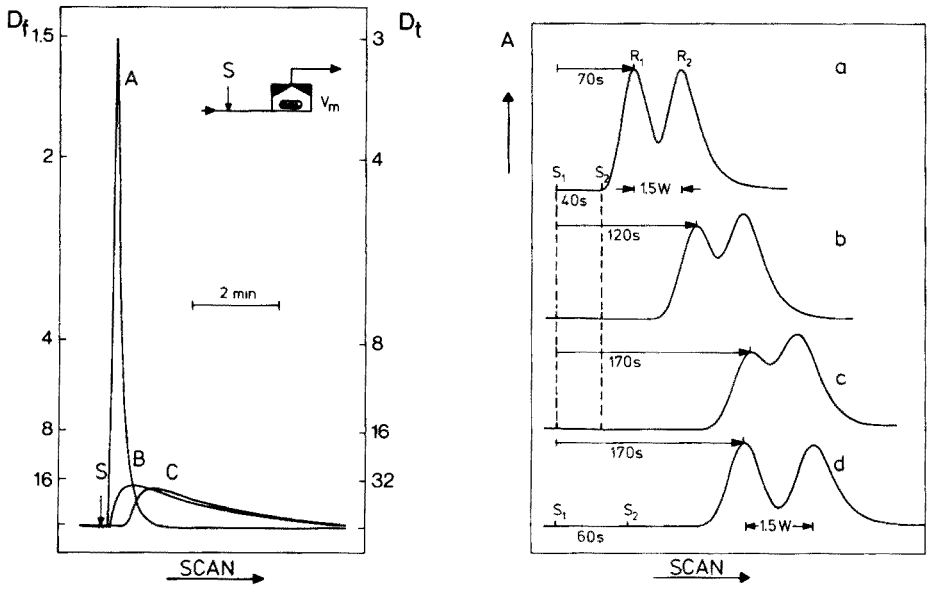

Fig. 20. Response curves obtained without (A) and with (B and C) a mixing chamber placed in a single-line system. Sample volume 50 μl; Q = 0.75 ml min^{-1}; chamber volume V_m = 1.9 ml; tube diameter 0.5 mm; Curve A, L = 50 cm. Curve B, L = 50 cm + mixing chamber. Curve C, L = 50 cm + mixing chamber + 50 cm of 0.5-mm i.d. line.

Fig. 21. Response curves obtained with two samples in a line at the same time. S = 50 μl, tube diameter 0.4 mm, and pumping rate 0.25 ml min^{-1}. The first sample was injected at point S_1 and the next sample at point S_2. While the corresponding readouts R_1 and R_2 show no carryover in cases (a) and (d), considerable carryover is encountered for curves (b) and (c). For peak width W see eqns. (6) and (28) and Fig. 8.

Because W, and therefore D, increases with the square root of T (Rule 5), the sample broadens only relatively slowly with increasing residence time; this can be confirmed from Fig. 21, where S_1 and S_2 are the points of sample zone injection, R_1 and R_2 are the respective readout positions, and T is the time span between S and R. Thus, with one sample in the line at a time and with T = 70 s (Fig. 21, curve a), a maximum sampling rate of S_f^{max} = 51 might be obtained; with several samples in the line, the frequency calculated according to eqn. (29) yields S_f^{max} = 87 samples per hour (where D_t = 2.3). Similarly, the S_f^{max} values in case (d) where T = 170 s, correspond to 21 and 61 samples per hour, respectively (where D_t = 3.3). However, injecting at a higher frequency than 1.5 W leads to significant carryover (cf. Fig. 21, curves b and c). Consequently, with increasing T, and hence W, the maximum sampling frequency will decrease. Thus, increasing T, albeit simultaneously with accommodating several samples in the line, is not really a profitable approach to increasing the sampling rate.

To summarize, the sample zone width (eqn. 28) should be kept at a minimum regardless of whether one wishes to operate with one or several samples in the line at a time:

Rule 7: To obtain maximum sampling frequency, the dispersion D_t should be kept low and the sample volume S *small, while the linear flow velocity in the flow cell should be kept high.* This is best achieved by using a flow cell of small diameter through which the carrier stream is pumped at a moderate flow rate.

The main limitation of the f.i.a. system is thus apparent: the residence time T of the sample in the system can never exceed 30 s if a frequency of analysis of over 100 samples per hour has to be maintained, or 15 s if $S_f^{max} \geqslant 200$.

In addition to most procedures comprizing electrode measurements, there are, fortunately, many colour-forming reactions which yield a readily measurable signal within that short span of time. Moreover, there is a growing interest (e.g., in blood protein chemistry) in differentiating between very fast chemical reactions, the velocities of which differ only slightly from each other. A Flow Injection system designed as a fast analyzer, yielding the result 1—2 s after the sample has been mixed with the reagent, can be readily designed.

Every rule has its exception, and so has the above 30-s limitation for $S_f^{max} \geqslant 100$. An approach which might allow $S_f^{max} \geqslant 100$ even if $T = 1$ min, is described in the paragraph on Future Developments.

DISCUSSION

Although the experimental data obtained agree surprisingly well with the concepts outlined in the theoretical part, it is evident that the model used here is rather crude, because the dispersion D has been defined in the simplest possible way. The main deficiency of this approach is that the H_0 value is not a real entity because both injection and dispersion occur simultaneously and no measurements have been made, owing to the technical difficulties, within the first few seconds after the injection where the interdependence of D_i and D_f should be readily detectable. In this very short span of time the sample zone also accelerates and the peak form is most asymmetrical. Because of these factors, D_f extrapolates to 1 at $T = 4$ s (Figs. 15—17). Yet another difficulty arises from the fact that the dispersion in the flow cell D_d is not negligible for D_f and D_i values close to unity.

Nevertheless, the total dispersion as defined by eqn. (25) is a very useful value, accessible by simple direct measurement. It describes the sample dilution or the sample-reagent ratio at any point of the manifold, and the rules derived from the theory and confirmed by the measurements of D_t, D_i and D_f should prove useful in devising systems for various analytical methods. An example of such an approach may be seen by comparing the experimental conditions in Part II and IV of this series [10, 11] — when the importance of Rule 1 was not realized — with the same chemistries performed in the miniaturized Flow Injection system [25]. In other words, one can design several flow systems of identical D_t and T values by choosing

either large or small values of Q, r, L and S in the appropriate proportions. Although such equivalent manifolds would be capable of performing the same type of chemistry, the miniaturized system with the low pumping velocity will always be more economical in terms of reagent and time consumption. Therefore Rules 1, 6, and 7 are the most important ones to observe.

There are numerous technical solutions to the task of injecting the sample into the carrier stream, of propelling the streams through the system, and of reading out the recorded signal. The techniques used to implement these tasks must, however, not only yield reproducible results, but the components applied must be sufficiently simple so that the whole instrument becomes neither too complex nor too bulky.

Techniques

The components used in the Flow Injection system have — as a result of intensive work carried out over the past two years — undergone an overall miniaturization in both mechanical and electronic aspects, leading to the development of an inexpensive and miniaturized version of this instrument. Thus the Flow Injection Analyzer, designed and constructed in this laboratory and recently demonstrated at the Flow Injection Analysis Workshop organized by the Swedish Chemical Society in Uppsala, is now no larger than a typewriter, yet includes a four-channel peristaltic pump, a water thermostat, an injection valve, a programmable manifold as well as a spectrophotometer with the associated electronics. In this system (Fig. 22) the individual coils are attached to perspex blocks which can be arranged around the injection valve in any sequence, all blocks being interconnected by tubular gaskets, which also assist in aligning the individual components. For operation the whole set of building blocks is then simply clamped together so that any reprogramming of the coils, which are submerged in a small water thermostat, takes only a very short time.

An automated sample changer is undoubtedly very useful for routine analyses, and a sheer necessity even in a research laboratory if one should wish to accommodate several samples at a time in the Flow Injection system. Stewart, Beecher and Hare [23, 24, 26] designed the first sample changer for use with unsegmented flow systems, based on the use of two separate pumps, one for the sampling circuit and one for the high-pressure line which carries the sample to the detector. Although the high-pressure system has now been abandoned, as the same D_t and T values can be obtained by using a short line, the concept of the independent propelling of streams in the sampling and the manifold circuits should preferably be maintained in future designs of fully automated Flow Injection systems. It not only allows better sample economy, but is especially useful in the case of stopped-flow operations (see below).

The readout of any flow-through detector is, of course, best done by continuous recording, because this allows instantaneous as well as ex post detection and possible diagnosis of any malfunction. Provided that the

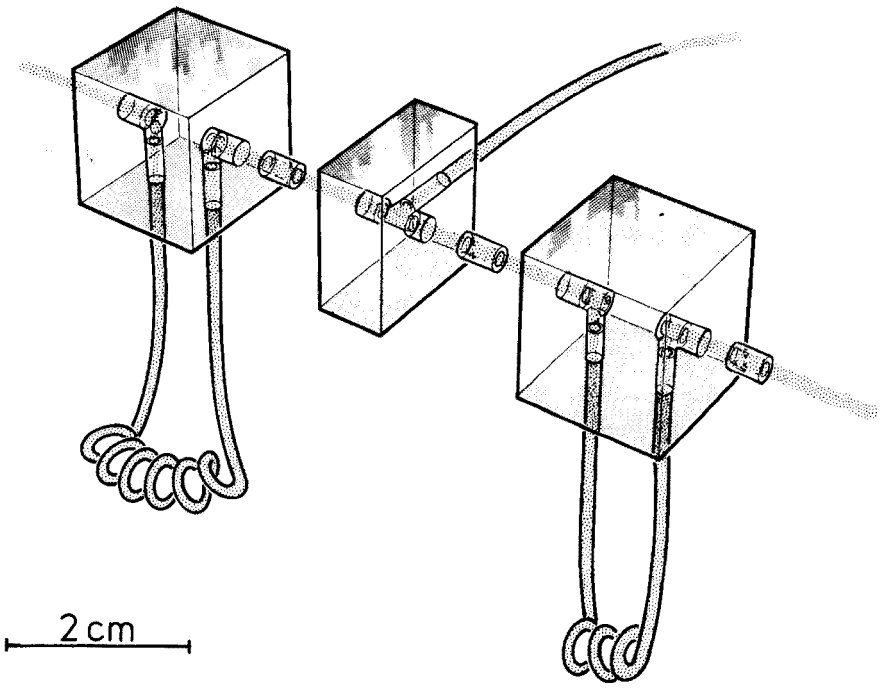

Fig. 22. An exploded view of a part of the miniaturized Flow Injection Analyzer, showing two coils (30 and 15 cm long, 0.5 mm i.d.) and a T-connector. The perspex blocks, to which the coils are attached, have the same modular size as the injection valve and the T-, I- or F-connectors. All manifold components can be arranged in any desired sequence, connected by tubular gaskets and clamped tightly together on the cover plate of the thermostated bath.

baseline is sufficiently stable, the peak height should be preferably measured. A digital electronic readout which automatically retains the maximum readout value on the top of a peak is a most useful device for this purpose. Such a peak maximum sensor was recently developed in this laboratory [27], originally for use with ion-selective electrodes, but later also for spectrophotometric measurements. Such a sensor can not only provide the readout, but might trigger various functions, such as activating the sampling valve of an automated sample changer or, even more importantly, controlling the manifold pump in connection with stopped-flow operation of the system.

FUTURE DEVELOPMENTS

It is tempting to predict the numerous methods that could be compatible with the Flow Injection system, but this might well prove to be an entirely misleading exercise. It would have been impossible to foresee the present developments in 1974 when the work on the Flow Injection method was initiated [9]. Flow Injection Analysis will therefore be related to other

continuous flow methods and then the most recent, still unpublished, results and methods will be briefly mentioned so that the reader may form his own projections.

It is self-evident that unsegmented streams were in use before Skeggs [1] devised the air segmentation method. One may find many examples in the literature on the use of unsegmented streams either in a rudimentary form as in effluent lines from chromatographic systems, or in discrete analyzers. A classical example of such work appears in the papers of Blaedel and Hicks, published in 1962, on the kinetic spectrophotometry of glucose [28] and lactate dehydrogenase [29], and on the determination of glutamic oxaloacetic transaminase [30]. Several years later, voltammetric sensors were used in connection with unsegmented streams [17—21], but with a maximum sampling rate of between 15 and 20 determinations per hour none of these systems could outperform the efficiency of the air-segmented streams. The stumbling block was the choice of method of dispersion of the sample zone: on the one hand, mixing of the sample with the reagent is necessary, and therefore pulsers [28—30] or mixing chambers [17—21] were introduced; on the other hand, the excessive mixing thus produced resulted in carryover and/or decrease in the sampling frequency. Therefore, the sampling frequency of around 300 determinations per hour, with a carryover of less than 1%, achieved with the very simple experimental setup described in the first paper of this series [9], indicated that some breakthrough had been achieved. Further work [10—12, 16, 31—36] simply confirmed that the concept of continuous flow analysis will cease to be synonymous only with that of air-segmented streams. The independent work of Stewart, Beecher and Hare [23, 24, 26], in which a fully automated system was used, also demonstrated the feasibility of high-speed analysis in unsegmented streams; it is interesting that Stewart and his colleagues based their work on their experience from liquid chromatography [23], and therefore used very thin and long tubes (0.25-mm i.d., L = 12 m) through which the carrier stream had to be pumped at pressures of 400—500 p.s.i. This experimental arrangement later provoked criticisms [8] of both Stewart's and the Flow Injection system, which recently resulted in an interesting exchange of views [25]. However, no such scepticism has been show in other laboratories, and a number of new automatic methods were demonstrated at a recent workshop organized by the Swedish Chemical Society. In this laboratory the following new techniques have reached an advanced experimental stage.

Solvent extraction. Solvent extraction automated by the Flow Injection method is perhaps the most fascinating new technique. Originally described by Karlberg and Thelander [37—39], it was developed primarily for pharmaceutical analysis. Up to 100 samples can be extracted and analyzed per hour with a relative precision better than 1% in an extremely simple apparatus which includes an ingenious device for mixing of the organic and the aqueous phases. Caffeine in acetylsalicylic acid preparations [37], codeine [38] and vitamin B_1 [39] have been determined in sample volumes of 12—25 μl at

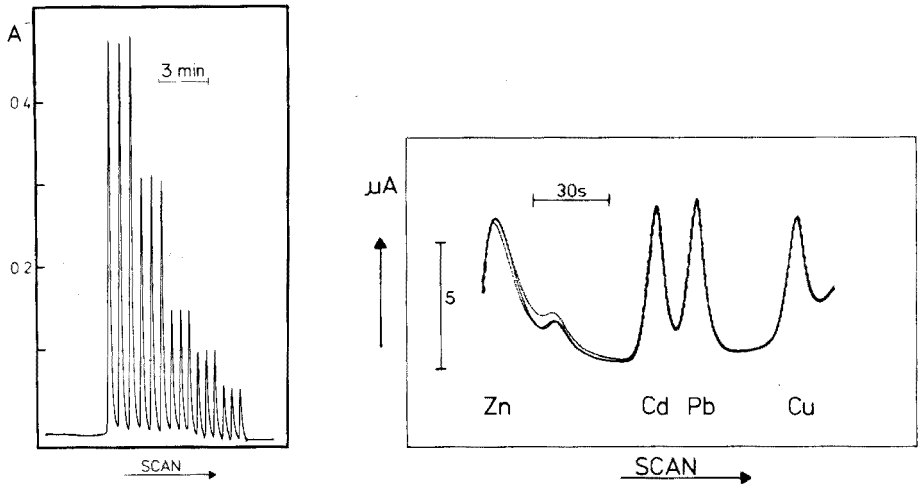

Fig. 23. Solvent extraction of silver ions by dithizone in carbon tetrachloride, measured spectrophotometrically at 500 nm. The sample volume was 30 μl, the compositions of the aqueous samples being from left to right: 3×10^{-4}, 2×10^{-4}, 1×10^{-4}, 7×10^{-5} and 5×10^{-5} M silver nitrate. All solutions were injected in triplicate into an aqueous carrier stream of acetate buffer from which silver was then continuously extracted by 7×10^{-5} M H_2Dz in CCl_4. As the ratio of organic to aqueous phase is 2:1 and D_t in the aqueous stream is about 3, the dithizone is in stoichiometric excess to silver at any point of the response curve even for the most concentrated samples.

Fig. 24. Determination of heavy metals by Flow Injection stripping voltammetry for a 1-ml sample volume containing a mixture of zinc (1×10^{-6} M), cadmium (1.3×10^{-6} M), lead (1×10^{-6} M) and copper (1×10^{-6} M). Three repetitive stripping analyses were made and recorded with a pulse polarograph (pulse height 50 mV; pulse repetition rate 0.5 s; scan rate 10 mV s^{-1}).

such low pumping rates that the consumption of reagents is less than 10% of that required by the manual methods. The technique of Karlberg and Thelander has been used in this laboratory for extraction of metal dithizonates [40]; an example of such measurements is shown in Fig. 23 where silver nitrate in the range 3×10^{-4}—5×10^{-5} M was extracted with 7×10^{-5} M dithizone in carbon tetrachloride (the carrier stream consisting of a 1×10^{-3} M sodium acetate/acetic acid buffer of pH 4.6); the absorbance of the silver dithizonate was measured in the organic phase at 500 nm. Similar experiments with lead, copper and cadmium indicate that optimization of the reaction conditions should allow all these metals to be determined down to 10^{-5} M. To obtain a higher sensitivity for the determination of heavy metals, anodic stripping voltammetry can be considered.

Anodic stripping voltammetry. This method has been automated by the Flow Injection method by Mosbæk and Hansen [41]. The obvious advantage of the unsegmented stream in this application is that stripping is performed into a previously deaerated carrier stream, while the plating itself is done

from injected samples which do not require to be de-oxygenated. Furthermore, as it is easy to switch from one carrier stream to another, plating and stripping can be executed from and into different electrolytes. Thus, many more samples can be analyzed than with the manual method within the same period of time. When 1.0 ml of sample solution is pumped through a flow cell over a 90-s plating period, and the current is measured during a subsequent 140-s stripping period, zinc, cadmium, lead and copper can be determined simultaneously in the range 10^{-5}—10^{-9} M. The reproducibility of this type of determination can be estimated from Fig. 24, which is a photographic reproduction of three stripping curves sequentially recorded by injecting three sample solutions of identical composition.

Voltammetric measurements. Voltammetric measurements of various kinds have been studied by Ramsing [42] for utilization in Flow Injection systems. An example of such f.i.a. measurements is shown in Fig. 25, which is a photographic reproduction of a recording obtained for the determination of ascorbic acid in the range 0.4—10 mmol l^{-1} at a rate of 180 determinations per hour. The potential of a thin-layer carbon-paste electrode, mounted in a flow-through cell similar to that described by Kissinger [22], was kept constant at +700 mV versus SCE while the current was continuously monitored. Iron(II)—iron(III), glucose/glucose oxidase—oxygen systems and other chemistries previously investigated in unsegmented streams in other laboratories [17—21, 43] should therefore be readily accommodated in Flow Injection systems operated at moderate flow rates and conditions of relatively low dispersion.

Potentiometric measurements. Such measurements with ion-selective electrodes have already been reported [9, 16, 35, 36], but none of these measurements was made with the aim of measuring the original ionic activity under conditions of limited dispersion. Measurements of pH serve as an example of such an approach. With 30-μl sample solutions, a 5-cm long 0.4-mm i.d. tube and a flow-through capillary pH electrode (0.5 mm i.d., 5 cm long), pH measurements could be done at a rate of around 150 samples/hour (Fig. 26), when the carrier electrolyte was pumped at a rate of 1.5 ml min^{-1}. For these conditions, T = 2 s and $D_t \approx 1.5$. An interesting aspect of this type of measurement is that by increasing D_t to a medium value and by choosing the carrier stream composition appropriately, not only pH but also the buffering capacity of the injected samples can be determined from the peak-height measurements.

Stopped-flow injection analysis

The theoretical part shows that the dispersion increases with the square root of the residence time, T, but this is, of course, true only if F or Q are constant and larger than zero. Should the carrier stream cease to move, dispersion of the sample zone will stop (except for a negligible contribution caused by radial molecular diffusion) and D will remain constant, i.e., independent of T. In other words, Rule 1 might be applied to the extreme by stopping the flow in order to gain reaction time.

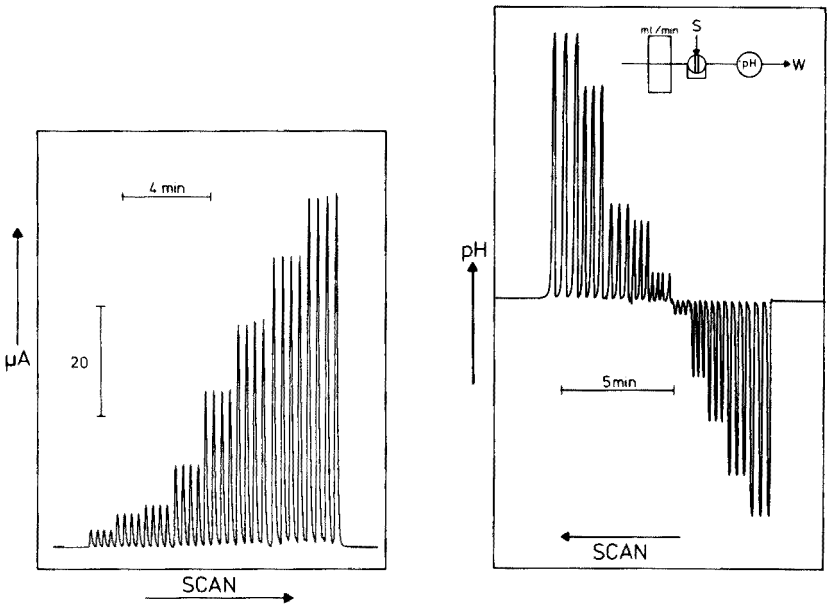

Fig. 25. Calibration record for the voltammetric determination of ascorbic acid at a carbon paste electrode. The samples, (30 μl) containing 0.4, 0.8, 1.0, 2.0, 4.0, 6.0, 8.0, and 10.0 mmol of ascorbic acid per litre, respectively, were injected, in quadruplicate, into a carrier stream of 1 M KCl, pumped at a rate of 1.7 ml min^{-1} (180 samples per hour) through a 100-cm long, 0.5 mm i.d. tube ($D_t \approx 5$; cf. Fig. 11).

Fig. 26. pH measurements under conditions of limited dispersion (L = 5 cm, 0.4-mm i.d., Q = 1.5 ml min^{-1}, S = 30 μl) with a carrier stream of 1 × 10^{-3} M sodium phosphate buffer in 0.14 M NaCl (pH 6.64). All samples were injected in triplicate (except No. 6) and had the following pH-values (from left to right): 9.2, 8.6, 7.6, 7.3, 6,8, 6.5, 5.9, 5.5, 5.0, and 4.6, respectively.

Provided that the movement of the carrier stream can be exactly controlled from the situation of complete standstill to the operational pumping rate used, the sample zone can be allowed to travel through the line until the reagent has been mixed with the sample material to the desired degree (D_t); then the flow can be stopped to allow the reaction to proceed and restarted for measurement and removal of the sample and for introduction of a new sample. In the absence of air, there is no movement of liquid in the conduits of the manifold after the pump has been stopped. This makes it possible to use the concept of stopped flow for two purposes: (1) to increase the sensitivity of a measurement; and (2) to perform kinetic analyses.

Higher sensitivity of a spectrophotometric measurement can be achieved by using a manifold (Fig. 27) in which the sample zone is stopped in the reaction coil for a desired period of time, and then after sufficient colour has developed, the sample is pumped through the flow cell while the peak is recorded in the usual manner. In order to double the sampling frequency, a parallel coil b is attached to the sampling valve which is modified to serve

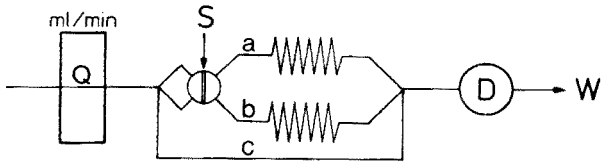

Fig. 27. Manifold for Stopped-Flow Injection Analysis in two parallel reaction coils (a and b). S denotes a two-way injection valve, D the flow-through detector, and W the waste. Line c serves as a shunt which must have a higher hydrodynamic resistance than the sampling valve plus any of the reaction coils.

coils *a* and *b* alternately, so that one can operate with two samples in the system at any one time. The shunt, *c*, of a higher flow resistance than the valve bore plus any of the reaction coils, serves to bypass the coils while the valve is in the fill-position, yet allows the flow-through cell to be continuously rinsed of reaction products. This system was tested on the determination of phosphate in water at the 0.1—1-ppm level, yielding very reproducible results. However, as it is rather difficult to keep track of the individual sequences in manual operation, the system should preferably be controlled by a microprocessor or at least partially automated, with several parallel storage and reaction coils.

In kinetic measurements, when either a substrate or an enzyme is determined, the reaction rate is the basis of the analytical readout. To locate the linear part of the response curve so that its slope can be measured reliably, it is desirable to collect as many measuring points as possible for each individual analysis. In continuous flow analysis, this is difficult to accomplish, and the best that can be achieved is to place several flow cells on the same stream in sequence [32, 44], which is not only expensive, but also rather clumsy. This is why batch analyzers, and recently their most advanced version, the centrifugal analyzers [45, 46], hold a key position in performing many enzymatic analyses, because the signal can be continuously monitored from the moment the reagent and sample solutions are mixed. In the Flow Injection system, however, the sample zone can be allowed to travel through a line until the desired degree of mixing is obtained, and then the dispersed sample zone can be stopped in the flow cell and the chemical reaction monitored continuously. This approach differs from the conventional stopped-flow method [47—49], which is based on forcing two reactant solutions through a mixing chamber to obtain complete and instantaneous mixing, so that monitoring of the chemical reaction in the homogeneous mixture can be started within a few milliseconds. Such fast mixing is, however, not desirable in enzymatic analysis, where an initial lag phase of the order of seconds is often observed. Besides, it can sometimes be advantageous to use the concentration gradients formed by the slow dispersion of the sample zone rather than to work with homogeneous mixtures.

The specific reaction of glucose dehydrogenase with β-D-glucose was used for the kinetic determination of glucose in order to verify the idea of the

stopped-flow injection principle. A commercially available System Glucose enzyme set (Merck, Germany) was used, in which the coenzyme nicotinamide adenine dinucleotide (NADH) serves as a chromogen which can be measured at 340 nm. Details on the reactions and reagent compositions, and some experiences with one- and two-point kinetic measurements have already been reported [32]. The manifold used in the present experiment, and two series of response curves are shown in Fig. 28.

In the first series of experiments, the concentration of glucose in the injected sample (S = 30 μl) was increased from 1 to 20 mmol l^{-1}, and the sample zone was stopped in the flow cell as soon as the recorded curve reached its maximum, i.e. when $t = T$ (Fig. 28b). As the pump was then stopped for 9 s, the measuring cycle consisted of three parts: (1) sample injection, dispersion and transport into the detector (4.5 s); (2) the measuring period with stopped flow (9 s); and (3) the washing period (10 s) at the end of which the next sample was injected. Further details of this method, which allows a multipoint kinetic determination to be performed at a rate of 150 samples/hour, will be published shortly [50].

An interesting aspect of this new approach to kinetic analysis is shown in Fig. 28c, which was obtained when the concentration of glucose in the

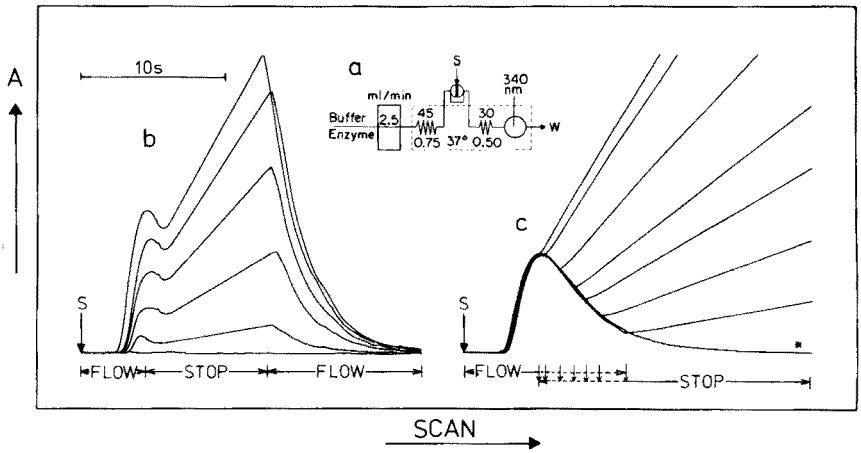

Fig. 28. Stopped-Flow Injection enzymatic analysis. (a) Manifold with injection valve (S), thermostated premixing coil, mixing coil, and flow-through cell. The carrier stream contained 1.76 kU l^{-1} of glucose dehydrogenase, 0.036 kU l^{-1} mutarotase and 0.36 mmol l^{-1} NAD in a 0.04 M ammonium hydrogenphosphate buffer of pH 7.66, containing 150 mmol NaCl l^{-1}. (b) A series of calibration curves obtained by injecting 30 μl of aqueous solutions containing 0.0, 1.0, 5.0, 10.0, 15.0, and 20.0 mmol of glucose per l, respectively. All samples were injected at point S, and each analytical run consisted of a 4.5-s pumping period (FLOW), a 9-s stop (STOP), and a 10-s washout period (FLOW). The slopes of the individual records versus concentration yielded a straight line. (c) A series of curves obtained by injecting 30-μl aliquots of an aqueous solution containing 15.0 mmol glucose per l. The flow was stopped 5.1, 5.5, 6.5, 7.6, 8.4, 9.5, and 11.0 s after the point of injection (S), except for the last experiment (marked *) where the pump was run continuously.

injected samples was kept constant (15 mM), but the flow was stopped at different times. In this way, the kinetics of the chemical reaction were monitored in different sections of the sample zone where — because of concentration gradient profiles — different ratios between sample and reagent solutions were available; consequently, the recorded response curves have different slopes. It is, therefore, important always to perform a kinetic measurement in the same section of the sample zone, as was done in the first series of experiments (Fig. 28b). For this type of analysis, the peak maximum sensor [27], combined with a delay device, will readily allow any section of the dispersed sample zone following the appearance of the peak maximum to be chosen reproducibly.

CONCLUSIONS

The above outline of the theory and the most recent developments in Flow Injection Analysis forms a natural conclusion to this series of ten papers which over the last four years has encompassed the evolution of the method from an initial concept for fast practical application to the design of advanced systems. In this way, a new method of continuous flow analysis has been developed, based on the formation and exploitation of concentration profiles when an injected sample is carried by an unsegmented stream towards a detector.

Although it has been doubted that unsegmented streams could ever become useful in continuous flow analysis, this work does show — as N. G. Anderson once pointed out in a discussion with L. Skeggs [51] — "that there must be some other way to do all that".

The authors express their gratitude to Dr. Oscar Klinghoffer for carrying out a substantial number of the dispersion measurements; to Drs. Gunnar Borch of Chemistry Department A and Michael Michelsen of The Institute for Chemical Engineering of this University for valuable discussions; and to Mr. Georg Møller for conscientious and patient mechanical assistance through all the work of this series of papers. This research was in part supported by grants from the Danish International Development Agency (DANIDA) under Project No. 104.Dan.8/241, and the International Atomic Energy Agency (IAEA) under Research Contract No. 1758/R1/RB, which assistance is greatly appreciated.

REFERENCES

1 L. T. Skeggs, Am. J. Clin. Pathol., 28 (1957) 311.
2 R. E. Thiers, R. R. Cole and W. J. Kirsh, Clin. Chem., 13 (1967) 451.
3 R. E. Thiers, A. H. Reed and K. Delander, Clin. Chem., 17 (1971) 42.
4 R. D. Begg, Anal. Chem., 43 (1971) 854.
5 R. D. Begg, Anal. Chem., 44 (1971) 631.
6 L. R. Snyder and H. J. Adler, Anal. Chem., 48 (1976) 1017, 1022.
7 L. R. Snyder, J. Levine, R. Stoy and A. Conetta, Anal. Chem., 48 (1976) 942 A.

8 M. Margoshes, Anal. Chem., 49 (1977) 17.
9 J. Růžička and E. H. Hansen, Anal. Chim. Acta, 78 (1975) 145. (Danish Patent Application No. 4846/74, Sept., 1974; and subsequent U.S. Patent No. 4,022,575).
10 J. Růžička and J. W. B. Stewart, Anal. Chim. Acta, 79 (1975) 79.
11 J. Růžička, J. W. B. Stewart and E. A. Zagatto, Anal. Chim. Acta, 81 (1976) 387.
12 J. Růžička, E. H. Hansen and H. Mosbæk, Anal. Chim. Acta, 92 (1977) 235.
13 D. Betteridge and B. Fields, Anal. Chem., in press.
14 O. Levenspiel, Chemical Reaction Engineering, 2nd edn., Wiley, New York, 1972.
15 G. Taylor, Proc. R. Soc. London, Ser. A, 219 (1953) 186.
16 E. H. Hansen, F. J. Krug, A. K. Ghose and J. Růžička, Analyst, 102 (1977) 714.
17 G. Nagy, Zs. Feher and E. Pungor, Anal. Chim. Acta, 52 (1970) 47.
18 Zs. Feher, G. Nagy, K. Toth and E. Pungor, Analyst, 99 (1974) 699.
19 E. Pungor, Zs. Feher and G. Nagy, Pure Appl. Chem., 44 (1975) 595.
20 E. Pungor, G. Nagy and Zs. Feher, J. Electroanal. Chem., 75 (1977) 241.
21 E. Pungor, K. Toth and G. Nagy, Hung. Sci. Instrum., 35 (1975) 1.
22 P. T. Kissinger, Anal. Chem., 49 (1977) 446 A.
23 K. K. Stewart, G. R. Beecher and P. E. Hare, Anal. Biochem., 70 (1976) 167.
24 G. R. Beecher and K. K. Stewart, in M. Friedman (Ed.), Proceedings of the Chemical Society Symposium on Chemical and Biological Methods for Protein Quality Evaluation, Part 1, M. Dekker, New York, 1975, p. 411.
25 J. Růžička, E. H. Hansen, H. Mosbæk and F. J. Krug, Anal. Chem., 49 (1977) 1858.
26 K. K. Stewart, G. R. Beecher and P. E. Hare, U.S. Patent No. 4,013,413 (1977).
27 C. E. Foverskov, in preparation.
28 W. J. Blaedel and G. P. Hicks, Anal. Chem., 34 (1962) 388.
29 W. J. Blaedel and G. P. Hicks, Anal. Biochem., 34 (1962) 476.
30 G. P. Hicks and W. J. Blaedel, Anal. Chem., 37 (1965) 354.
31 J. W. B. Stewart, J. Růžička, H. Bergamin Filho and E. A. Zagatto, Anal. Chim. Acta, 81 (1976) 371.
32 E. H. Hansen, J. Růžička and B. Rietz, Anal. Chim. Acta, 89 (1977) 241.
33 J. W. B. Stewart and J. Růžička, Anal. Chim. Acta, 82 (1976) 137.
34 J. Růžička and E. H. Hansen, Anal. Chim. Acta, 87 (1976) 353.
35 J. Růžička, E. H. Hansen and E. A. Zagatto, Anal. Chim. Acta, 88 (1977) 1.
36 E. H. Hansen, A. K. Ghose and J. Růžička, Analyst, 102 (1977) 705.
37 B. Karlberg and S. Thelander, Anal. Chim. Acta, in press.
38 B. Karlberg and S. Thelander, Anal. Chim. Acta, submitted.
39 B. Karlberg and S. Thelander, in preparation.
40 O. Klinghoffer, J. Růžička and E. H. Hansen, in preparation.
41 H. Mosbæk and J. Hansen, in preparation.
42 A. Ramsing, M.Sc. Thesis, The Technical University of Denmark, 1978.
43 Ch. Wolff and H. A. Mottola, Anal. Chem., 50 (1978) 94.
44 S. Morgenstern, R. Rush and D. Lehman, Advances in Automated Analysis, 1972, Techn. Int. Congr. Vol. 1, Mediad 1973, p. 27.
45 N. G. Anderson, Am. J. Clin. Pathol., 53 (1970) 778.
46 C. A. Burtis, J. C. Mailen, W. F. Johnson, C. D. Scott, T. O. Tiffany and N. G. Anderson, Clin. Chem., 18 (1972) 753.
47 E. F. Caldin, Fast Reactions in Solution, Blackwell, Oxford, 1964.
48 A. C. Javier, S. R. Crouch and H. V. Malmstadt, Anal. Chem., 41 (1969) 239.
49 P. M. Beckwith and S. R. Crouch, Anal. Chem., 44 (1972) 221.
50 J. Růžička and E. H. Hansen, in preparation.
51 N. G. Anderson, Clin. Chem., in press.

Analytica Chimica Acta, 99 (1978) 77—88

AN APPROXIMATE METHOD FOR THE SOLUTION OF FICK'S LAW PROBLEMS

STEPHEN G. WEBER and WILLIAM C. PURDY*

Department of Chemistry, McGill University, 801 Sherbrooke St., W. Montreal, Quebec, H3A 2K6 (Canada)

(Received 21st December 1977)

SUMMARY

The simplifying approximation that the concentration of an electroactive species is a linear function of distance into the solution from the electrode surface is used to derive current—time relationships for controlled potential electrolysis. Relationships for thin-layer chronoamperometry, chronoamperometry with a preceding homogeneous reversible reaction and linear-sweep voltammetry are compared with existing relationships to determine the range of applicability of the approximation. The approximation is found to yield qualitatively correct results. To obtain quantitatively or near-quantitatively correct results, it is necessary to incorporate more information about the electrochemical system into the derivation than simply the usual initial and boundary conditions.

The use of electrochemical detectors in continuous-flow analysis and liquid chromatography is currently of widespread interest. It would be advantageous to have an understanding of the theoretical behaviour of such detectors. Unfortunately, the mathematics involved in finding exact equations to describe the current of a potentiostatic electrode in hydrodynamic systems is generally quite difficult, and approximations to make the mathematics more tractable are desirable. Oldham [1] has demonstrated that the approximation that concentration is a linear function of distance from the electrode to a critical distance (equal to the diffusion layer thickness) and thereafter that the concentration equals the bulk concentration (see Fig. 1) may be used to derive useful results. Here is provided a foundation for the expansion of the applicability of this approximation by demonstration of usefulness and shortcomings under conditions not explored by Oldham [1]. Hence, Oldham's results have been rederived in a more useful form, and general expressions for concentration of electroactive species at the electrode surface as a function of time are presented. These equations are used to provide approximate results which are compared with results in the literature for chronoamperometry in thin layers, chronoamperometry with a reversible homogeneous reaction providing the electroactive species, and linear-sweep voltammetry for the reversible case.

DERIVATION OF THE BASIC EQUATIONS

For the assumed concentration profile shown in Fig. 1, the concentration gradient at the electrode surface for the oxidized species is

$$(\bar{C} - C(0,t))/\delta \tag{1}$$

where $\bar{C}$ is the concentration of the oxidized member of the couple in bulk solution, $C(x,t)$ is the concentration of the same species at any distance from the surface of the electrode (x) and at time t, and δ is the diffusion layer thicknesss. Analogously, for the reduced species (indicated by primed quantities), the gradient at the electrode surface may be written

$$(\bar{C}' - C'(0,t))/\delta' \tag{2}$$

From Fick's law, by replacing $(\partial C/\partial x)_{x=0}$ with eqns. (1) and (2), we have

$$J = D\,(\bar{C} - C\,(0,t))/\delta = -D'\,(\bar{C} - C'(0,t))/\delta' \tag{3}$$

where J is the flux of reduced species and is positive for the reduction. The Volmer equation states that

$$J = k_1 C(0,t) - k_{-1} C'(0,t) \tag{4}$$

where the k's are the potential-dependent rate constants. As pointed out by Oldham [1], the areas of the two triangles labelled abc and $a'b'c'$ in Fig. 1 must be equal by Faraday's Law. If these areas be denoted by R, then

$$R = (\bar{C} - C(0,t))\delta/2 = (C'(0,t) - \bar{C}')\delta'/2 \tag{5}$$

From the conservation of mass, the change in area R with time must equal the flux of material to or away from the electrode, thus $\mathrm{d}R/\mathrm{d}t = \pm J$. In case there are other contributions to the change in concentration of some electroactive species (e.g. homogeneous reaction), a source term, r, can be included:

$$\mathrm{d}R/\mathrm{d}t = \pm J + r \tag{6}$$

Both J (eqn. 3) and R (eqn. 5) are equations of $C(0,t)$ and δ (or $C'(0,t)$ and δ') which are unknown functions of time. Furthermore, in a potential controlled experiment J is a function of k_1 and k_{-1} which are known functions of time. Equations (1—5) may be solved together to yield general expressions for $C(0,t)$ and $C'(0,t)$:

$$C(0,t) = \left[\left(\frac{D}{k_1\delta} + \frac{k_{-1}}{k_1}\gamma\right)\bar{C} + \frac{k_{-1}}{k_1}\bar{C}'\right] \Big/ \left[1 + \frac{k_{-1}}{k_1}\gamma + \frac{D}{k_1\delta}\right]$$

$$C'(0,t) = \left[\left(\frac{D'}{k_{-1}\delta'} + \frac{k_1}{k_{-1}}\gamma^{-1}\right)\bar{C}' + \frac{k_1}{k_{-1}}\bar{C}\right] \Big/ \left[1 + \frac{k_1}{k_{-1}}\gamma^{-1} + \frac{D'}{k_{-1}\delta'}\right] \tag{7}$$

where $\gamma = (D/D')^{1/2}$.

Equation (7) can then be used to write R and J as functions of only one unknown, δ or δ'. To recapitulate, eqns. (3) and (5) with eqn. (7) for surface

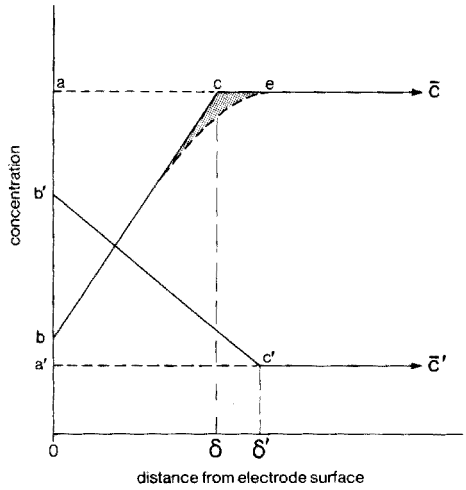

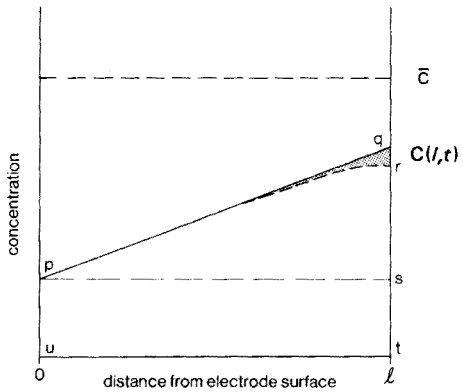

Fig. 1. Line *bce* represents the idealized concentration versus distance plot for a species reacting at the electrode surface. Line *be*, separated from *bce* by the shaded area, represents the actual concentration profile. δ and δ' are diffusion layer thicknesses.

Fig. 2. For the case in which the diffusion is not semi-infinite, line *pq* gives the idealized concentration profile and line *pr* gives the actual concentration profile for a species reacting at the electrode surface.

concentration may be substituted into eqn. (6) to yield a first-order (but not necessarily linear!) differential equation for δ or δ'. The boundary conditions generally applied in electrochemical diffusion problems are contained in eqn. (7). Equation 7 also demonstrates an approximate definition for reversibility. When the reaction velocity k_1 (or k_{-1}) is much larger than the "diffusional velocity" D/δ (or D'/δ'), eqn. (7) reduces to a form derivable from conservation of mass and the Nernst equation, i.e. a reversible reaction.

If the above-mentioned differential equation is solved for $\delta(t)$, and the current $i(t)$ is then determined from eqns. (2) and (7) with $i = nFAJ$, the findings will necessarily be in error because the physical system does not display a linear concentration vs. distance relationship. A solution to this dilemma has been proposed by Oldham [1]. His argument is as follows. In actuality, the area that should be considered is not R, but the slightly larger area *aceb* (Fig. 1). In general, if this area is taken as unity, it can be seen that R is a fraction, f, of this area. It is the change in this area, *aceb*, or R/f which is related to the loss of material by electroreaction. Mass balance then yields

$$(dR/f)/dt = \pm J + r \qquad (6a)$$

instead of eqn. (6). An analogous expression holds for the primed species. Unfortunately, the fraction f is an unknown quantity. It is most generally a function of time, and is strongly dependent upon the shape of the actual

concentration profile. Hence, to determine f one must know the exact solution of $C(x,t)$, a task one is explicitly trying to avoid. For reversible, potentiostatic cases, f may be taken as constant and equal to $\pi/4$ [1]. This value can be used here, but its use leads to quantitative, although not qualitative, errors in the current $i(t)$. Equations (3), (5), (6a) and (7) may then be taken together to yield a differential equation for $\delta(t)$.

The derivation of eqn. (7) tacitly assumes semi-infinite diffusion. If this is not the case, all the above derived equations will not be useful once the diffusion layer thickness, δ, becomes equal to the cell thickness, l. At this point and thereafter, the flux will be given by

$$J = D(C(l,t) - C(0,t))/l \tag{8}$$

and the area *pqrs* in Fig. 2 will be given by

$$S = C(l,t)l/2 \; - C(0,t)l/2 \tag{9}$$

The triangular area below the concentration curve, S, is so designated to differentiate it from the area R above the concentration curve. In fact, the actual area of interest (*prs*, Fig. 2) will be smaller by some factor g than the area *pqrs*. We may then write, analogously to eqn. (6a)

$$\mathrm{d}gS/\mathrm{d}t = \pm J + r \tag{10}$$

where a similar expression holds for the primed species. Solving eqns. (4), (8) and (9) together yields expressions for $C(0,t)$ and $C'(0,t)$.

$$C(0,t) = \left[C(l,t)\left(\frac{D}{lk_1} + \frac{k_{-1}}{k_1}(\gamma - 1)\right) + \frac{k_{-1}}{k_1}(\bar{C} + \bar{C}')\right] \Big/ \left[1 + \frac{D}{lk_1} + \frac{k_{-1}}{k_1}\gamma\right]$$

$$C'(0,t) = \left[C'(l,t)\left(\frac{D'}{lk_{-1}} + \frac{k_1}{k_{-1}}(\gamma^{-1} - 1)\right) + \frac{k_1}{k_{-1}}(\bar{C} + \bar{C}')\right] \Big/ \left[1 + \frac{D'}{lk_{-1}} + \frac{k_1}{k_{-1}}\gamma^{-1}\right] \tag{11}$$

In deriving eqns. (11), the binary expansion to two terms was used to find

$$(D + D')/2D \approx (D'/D)^{1/2} \; ; \; (D + D')/2D' \approx (D/D')^{1/2}$$

and

$$(D' - D)/2D \approx (D'/D)^{1/2} - 1 \; ; \; (D - D')/2D' \approx (D/D')^{1/2} - 1$$

Now eqns. (8) and (9) with eqn. (11) substituted for $C(l,t)$ may be used in eqn. (10) to yield a differential equation in $C(l,t)$. When solved subject to matching conditions from the solution of eqn. (6a) [i.e., the diffusion layer is found from eqn. (6a) up to $\delta = l$, then eqn. (11) is solved to give a complete solution for $i(t)$, $t = 0 \rightarrow \infty$], the value of $C(l,t)$ may be used in eqn. (8) to yield the current.

SPECIFIC EXAMPLES

Thin-layer chronoamperometry, infinite potential pulse

For this case, the Cottrell equation (which may be deduced from the equations given here and in ref. 1) is used at small times, and an equation for long times is derived from eqn. (10).

For an "infinite" potential pulse $C(0,t) = 0$, with no homogeneous reaction $r \to 0$, thus eqn. (10) becomes

$$\mathrm{d}gl\left(-\frac{C(l,t)}{2}\right)\Big/\mathrm{d}t = D\,C(l,t)/l \tag{12}$$

If g is taken as a constant, eqn. (12) may be integrated from an initial time $\bar{t}$ to t to give

$$\ln[C(l,t)/C(l,\bar{t})] = 2D\,(\bar{t}-t)/gl^2 \tag{13}$$

where $\bar{t}$ represents the time at which the Cottrell equation is no longer valid. $C(l,\bar{t})$, g, and $\bar{t}$ may be deduced from the matching conditions: (i) when $t = \bar{t}$, the current calculated from the Cottrell equation must equal the current calculated from eqn. (13); (ii) at $t = \bar{t}$, the derivatives of current with respect to time calculated from the Cottrell equation and eqn. (13) must also be equal, and (iii) the integral of current from $t = 0$ to $t = \infty$ must equal the number of coulombs in the system ($nFV\bar{C}$, V = volume of solution in front of the planar electrode). The situation at $t = \bar{t}$ is represented in Fig. 3.

The Cottrell equation as derived by Oldham [1] is

$$i = nFAD\bar{C}/(4fDt)^{1/2}$$

If f is taken as $\pi/4$ this reduces to the familiar form of this equation. Requirement (i) from above becomes

$\bar{C}/\bar{\delta} = (1+\alpha)\bar{C}/l$ where $(1+\alpha)\bar{C} = C(l,\bar{t})$ (see Fig. 3).

Requirement (ii) becomes

$f/\bar{\delta}^3 = (1+\alpha)/gl^3$ where $\bar{\delta} = (4fD\bar{t})^{1/2}$

Requirement (iii) becomes

$\bar{\delta}/2fl + (1+\alpha)g/2 = 1$

These equations may be solved simultaneously to yield

$$(1+\alpha) = 1/f\,;\ \bar{\delta} = fl\,;\ g = f \tag{14}$$

Because the reaction is diffusion-controlled and potentiostatic, let $f = \pi/4$. Then the final form of the equation for current is:

$$i = nFAD^{1/2}\bar{C}/(\pi t)^{1/2} \quad \text{for } 0 < t < \pi l^2/16D$$

$$i = (4nFAD\bar{C}/\pi l)\exp\tfrac{1}{2}(\exp\{-8Dt/\pi l^2\}) \quad \text{for } \pi l^2/16D < t \tag{15}$$

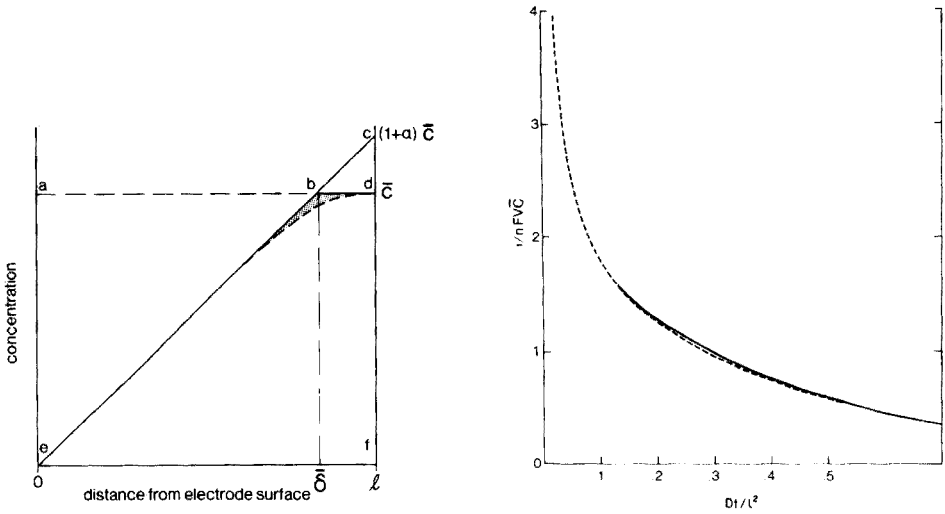

Fig. 3. The idealized concentration versus distance profile at the time when the treatment of the diffusion-layer thickness changes from semi-infinite linear diffusion to non-infinite linear diffusion. $\bar{\delta}$ is the diffusion-layer thickness at this time. Line *ebd* represents the actual concentration profile.

Fig. 4. The solid line shows the approximate equation, eqn. (15). The dotted line shows the rigorously derived equation, eqn. (16), for thin-layer chronoamperometry.

This may be compared with the expression given by Oglesby et al. [2] obtained by solution of the Laplace transformation of Fick's second law for $C(x,t)$ and inverse transformation of the result.

$$i = (2nFADC/l) \sum_{m=1}^{\infty} \exp\{-(2m-1)^2\pi^2 Dt/4l^2\} \qquad (16)$$

The agreement between the two results is more readily appreciated by inspection of Fig. 4.

Chronoamperometry, homogeneous preceding reaction

The case in which there is a homogeneous reaction occurring may be handled in the following fashion. Assume that a substance B is reacting at the electrode surface and is also being produced by the following reaction.

$$A \underset{k_b}{\overset{k_f}{\rightleftharpoons}} B$$

Further assume that it is experimentally feasible to make the concentration of A large enough so that it does not significantly deviate from its equilibrium value, $\bar{A}$. In terms of the present work, one can state that the total change in area of triangle *abc* (Fig. 1) is equal to the separate changes caused by electroreaction and homogeneous reaction. The change in the area per unit time

caused by the homogeneous reaction will be the sum of the reaction products formed per unit time at each x (distance from the electrode) from $x = 0$ to $x = \infty$,

$$(dR/dt)_{\text{reaction}} = \int_0^\infty (\partial [B(x)]/\partial t)\, dx \tag{17}$$

where $[B(x)]$ is the concentration of B as a function of x. Since

$$\partial [B(x)]/\partial t = k_f [A(x)] - k_b [B(x)]$$

and since $[A(x)] = \bar{A}$ and $k_f \bar{A} = k_b \bar{B}$ (from equilibrium considerations),

$$\partial [B(x)]/\partial t = k_b (\bar{B} - [B(x)]) \tag{18}$$

Combining eqns. (17) and (18) yields

$$(dR/dt)_{\text{reaction}} = \int_0^\infty k_b (\bar{B} - [B(x)])dx = k_b R$$

Under potentiostatic conditions for reduction of B ($B(0,t) = 0$) one can then write from eqn. (6a)

$$d(\bar{B}\delta)/dt = \pi D\, (\bar{B}/2\delta) - k_b \bar{B}\delta$$

where f has been taken as $\pi/4$. This equation may be solved (in terms of δ^2) to yield;

$$\delta = [(\pi D/2k_b)\, (1 - \exp\{-2k_b t\})]^{1/2}$$

and thus

$$i = nFA\, (2k_b D/\pi)^{1/2} \bar{B}\, (1 - \exp\{-2k_b t\})^{-1/2} \tag{19}$$

As $k_b \to 0$, the exponential term may be expanded to give

$$(i)_{k_b \to 0} \simeq nFA\, (2k_b D/\pi)^{1/2} \bar{B}\, (1 - (1 - 2k_b t \ldots))^{-1/2} \simeq nFAD^{1/2} \bar{B}/(\pi t)^{1/2}$$

which is the Cottrell equation as expected for chronoamperometry with no homogeneous preceding reaction. Equation (19) may be compared with the exact solution [3] obtained by solution for $B(x,t)$ by Laplace transformation of Fick's second law.

$$i = nFA\, (k_b D)^{1/2} \bar{B}\, (\text{erf}\, (k_b t)^{1/2} + [1/(\pi k_b t)^{1/2}]\, \exp\{-k_b t\}) \tag{20}$$

At steady state, eqn. (19) predicts a current too low by a factor of $(2/\pi)^{1/2}$ (0.798). The relatively large discrepancy is due to the fact that for this system the factor f is not constant. At $t = \infty$, solution of the exact equation for concentration

$$D\, (d^2B/dx^2) = k_b (\bar{B} - B(x))$$

yields $B(x) = \bar{B}\, [1 - \exp\{-(k_b/D)^{1/2}\} x]$.

A comparison of the area of the triangle which has its hypotenuse tangential to $(\partial B/\partial x)_{x=0}$ (i.e. triangle *abc* in Fig. 1) with the area between

$B = \bar{B}$ and $B = B(x)$ from $x = 0$ to $x = \infty$, shows that at $t = \infty$, $f = 1/2$. Thus, even though conditions at the electrode are diffusion-controlled and potentiostatic, the factor f has changed from $\pi/4$ at $t = 0$ to $1/2$ at $t = \infty$. However, general qualitative agreement is obtained, as can be seen in Fig. 5.

Linear-sweep voltammetry, reversible system

For this case, assume $\bar{C}' = 0$, i.e. only the oxidized species is present, and that no homogeneous reactions are present, thus $r = 0$. Then $C'(0,t)$ may be taken from eqn. (7) to yield

$$C'(0,t) = \frac{k_1}{k_{-1}} \bar{C} \Big/ \left[\frac{k_1}{k_{-1}} \gamma^{-1} + 1\right]$$

$$= \bar{C} \Big/ \left[\gamma^{-1} + \frac{k_{-1}}{k_1}\right]$$

k_{-1}/k_1 can be written $\exp(nF/RT)\,(E - E^0)$ where E is the potential at any time t, E^0 is the standard potential, and n, F, R and T have their usual meanings. In linear-sweep voltammetry, the potential is at some initial potential E_i at $t = 0$, and is changed at a rate v V s^{-1}. With the nomenclature of Nicholson and Shain [4]

$$\theta = \exp(nF/RT)\,(E_i - E^0)\ ;\ a = (nF/RT)|v|\ ;\ k_{-1}/k_1 = \theta e^{-at}$$

The negative sign arises from the fact that the potential is scanned in a negative direction for the reduction.

One may then write C' in these terms as

$$C'(0,t) = \bar{C}/(\gamma^{-1} + \theta e^{-at})$$

Equation (6a) becomes

$$d[\bar{C}\delta'/(\gamma^{-1} + \theta e^{-at})]/dt = (\pi/2)D'\,\bar{C}/[\delta'(\gamma^{-1} + \theta e^{-at})] \qquad (21)$$

where f has once again been taken as constant and equal to $\pi/4$. Differentiating the left side of eqn. (21) and putting the resulting equation in terms of $Z = \delta'^2$ one has;

$$\frac{dZ}{dt} = \pi D' - [2a\,\theta e^{-at}/(\gamma^{-1} + \theta e^{-at})]\,Z$$

Since the final equation becomes cumbersome, it is expedient to introduce the following substitution

$$q = (e^{at}/\theta)\,\gamma^{-1}$$

$$= \gamma^{-1} \exp(nF/RT)\,(E^0 - E(t)) \qquad (22)$$

The differential equation in Z becomes

$$dZ/dt = \pi D' - [2a/(q + 1)]\,Z$$

Using the general solution for a linear first-order differential equation [5],

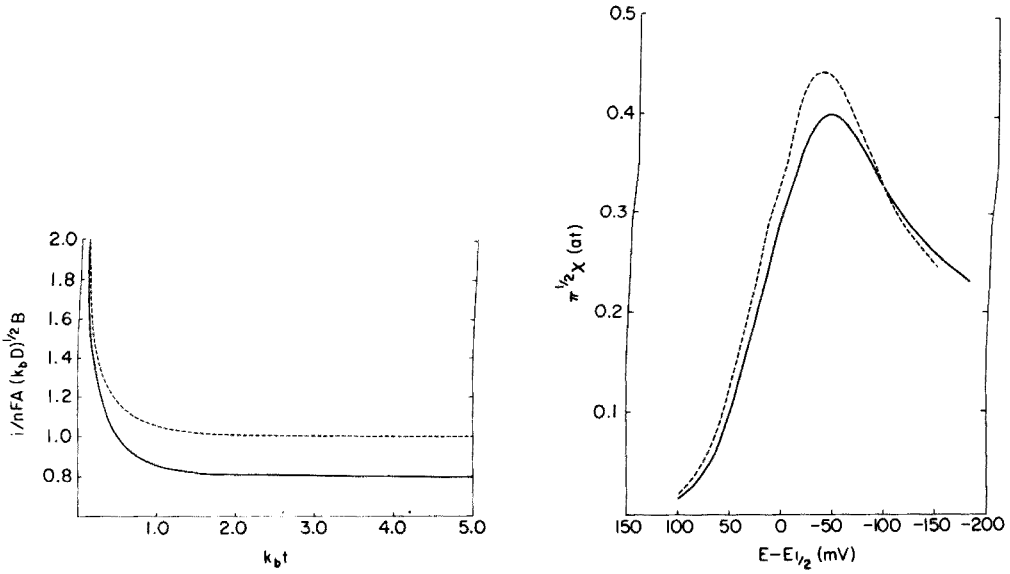

Fig. 5. The solid line shows the approximate equation, eqn. (19). The dotted line shows the rigorously derived equation, eqn. (20), for chronoamperometry with a preceding reversible homogeneous reaction.

Fig. 6. Solid line shows eqn. (23) divided by $[n^{3/2}F^{3/2}A\bar{C}(|v|D)^{1/2}]/RT$. The dotted line shows the comparable numerical data termed $\pi^{1/2}\chi\,(at)$ by Nicholson and Shain [4].

one finds

$$\delta' = (\pi D'/a)^{1/2}\,[\log(1+q) - q/(1+q)]^{1/2}\,[(1+q)/q]$$

In arriving at this final form, θ has been taken as much greater than γ^{-1}. From $i = nFAD'\,C'(0,t)/\delta'$, one arrives at,

$$i = [n^{3/2}F^{3/2}A\bar{C}(|v|D)^{1/2}/(\pi RT)^{1/2}]\,[q/(1+q)]^2\,[\log(1+q) - q/(1+q)]^{-1/2} \qquad (23)$$

At long times $[q/(1+q)]^2 \to 1$, and $[\log(1+q) - q/(1+q)]^{-1/2} \to [(nF/RT)|v|t']^{-1/2}$, thus

$$i_{t\to\infty} = nFA\bar{C}\,D/(\pi t')^{1/2}$$

The variable t' is zero at a time which is $1/a$ seconds after E_0. This confirms the chronoamperometric character of the "tail" of the current–time curve. Equation (23) is compared with Nicholson and Shain's numerically derived data [4] in Fig. 6.

DISCUSSION

The approximation used here is a crude one, and the justification of its use must come from a consideration of the difficulty in deriving a rigorous expression for a particular electrochemical process. The major drawback of the approximation is the uncertainty regarding the factor f. If, in fact, f is known, then this method would yield exact results, because although eqns. (6a) and (10) are differential equations, they are derived from integrated quantities ($\int c(x)\mathrm{d}x$ is related to R). A solution to a differential equation is sought which satisfies the differential equation at all points. The solution to an integral equation must only satisfy requirements at the boundaries (limits of integration) and, on average, satisfy the governing differential equation. Thus even though the approximation made here is crude, the integral-equation-like quality of eqns. (6a) and (10) allows a factor f to be implemented to force the solution *on the average* to agree with the fundamental differential equations, Fick's Laws. The problem, of course, is that in order to know f, $C(x,t)$ must be known. In certain cases, it may be possible to obtain better solutions to diffusion problems by using the exact solutions at $t = \infty$ to determine what f is at that point, and then allow f to vary from $\pi/4$ to this value in some arbitrary fashion. This would undoubtedly make the appropriate equations more difficult to solve.

Oldham [1] has demonstrated the usefulness of this sort of approximate treatment for galvanostatic, potentiostatic and quasipotentiostatic conditions. He determined that the value for f (ν in Oldham's work [1]) always lies between $2/\pi$ and $\pi/4$ for the cases which he considered. Posey and Meyer [6] have demonstrated that the concept is useful for determining chronopotentiometric transients in laminar flow streams. The equations derived by Posey and Meyer [6] are valid for cells which are large (in the same direction as the diffusion flux) with respect to the diffusion-layer thickness.

This laboratory is involved in analytical investigations of thin-channel electrodes for flowing streams. Depending on the application, there may or may not be a homogeneous chemical reaction involving one or both electro-reactants. Expressions relating current to various parameters are needed.

In order to make the mathematics more tractable, an approximation was sought which, while facilitating computation, yielded valid results. The diffusion-layer treatment of Oldham [1] was attractive, but it had not been shown to be valid for any cases but those given above. Hence it seemed necessary to extend the treatment to thin layers and homogeneous reactions and compare the approximate results with exact results to assess the reliability of the treatment. There may be analytical utility in performing linear-sweep voltammetry or cyclic voltammetry during the time when an analyte is passing through a thin-layer channel: thus the diffusion-layer treatment was tested for linear sweep voltammetry.

It seems that the approximation is useful and may lead to fairly accurate results. Excellent agreement between exact and approximate results is obtained in the thin-layer case, indicating that the diffusion-layer approximation is valid here. It is likely that forcing the matching conditions and Faraday's law to be obeyed were responsible for the agreement. For the simple case involving homogeneous reaction, it is clear that the factor f changes with time from $\pi/4 \rightarrow 1/2$. It is worthwhile to note that this falls outside the range given by Oldham [1]. Use of this treatment for circumstances involving homogeneous reactions should only be expected to be semi-quantitative. The same must be said for the linear-sweep case. In this case the results of the approximate derivation yield a wave which is displaced about 7 mV negative (for a reduction) on the $E - E_{1/2}$ axis, and which is about 10% lower at the peak on the current axis. By altering the factor f from $\pi/4$ to $2/\pi$ the quantitative error is removed. Oldham [1] found the factor f (ν in his paper) to be $2/\pi$ under galvanostatic conditions, short-time response to a potentiostatic pulse (irreversible reaction), and response to a quasipotentiostatic pulse (irreversible reaction). In the latter three cases and in the voltage-sweep experiment, the concentration of depolarizer at the electrode surface is a function of time. Under reversible potentiostatic conditions where the concentration of depolarizer at the electrode surface is constant, the factor f has thus far proven to be $\pi/4$. The derivation presented here used $f = \pi/4$ for linear sweep because it was reversible and potential-controlled. Taking the above consideration in mind it might be more reasonable to use the variation of $C(0,t)$ as the criterion in deciding what value to assign f.

Conclusions

A new method for the solution of Fick's Law problems first introduced by Oldham [1] has been reintroduced in a differential form. Extensions of the treatment allow for the inclusion of homogeneous reactions and non-infinite diffusion. To obtain quantitatively correct results, the factor f should be $2/\pi$ if the concentration of depolarizer at the electrode surface is a function of time, and $\pi/4$ if the same concentration is constant. When homogeneous reactions are considered, the factor f depends upon the controlling step in the overall electrochemical reaction. When the surface concentration of depolarizer is constant, f will be $\pi/4$ when the current is diffusion-controlled, and 1/2 when the current is first-order reaction-controlled. The use of this technique to solve complicated problems unassailable by standard methods is anticipated.

The authors are grateful to the National Research Council of Canada for support of this work.

REFERENCES

1 K. B. Oldham, Electrochim. Acta, 11 (1966) 1475.
2 D. M. Oglesby, S. H. Omang and C. N. Reilley, Anal. Chem., 37 (1965) 1312.
3 K. J. Vetter, Electrochemical Kinetics, Theoretical and Experimental Aspects, Academic Press, N.Y., 1967, p. 267.
4 R. S. Nicholson and I. Shain, Anal. Chem., 36 (1964) 706.
5 L. A. Pipes and D. R. Harvill, Applied Mathematics for Engineers and Physicists, 3rd edn., McGraw-Hill, N.Y., 1970.
6 F. A. Posey and R. E. Meyer, J. Electroanal. Chem., 30 (1971) 359.

Analytica Chimica Acta, 99 (1978) 89—98

THE ROTATING DISC ELECTRODE IN FLOWING SYSTEMS
Part I. An Anodic Stripping Monitoring System for Trace Metals in Natural Waters

J. WANG and M. ARIEL*

Department of Chemistry, Technion, I.I.T., Haifa (Israel)

(Received 11th January 1978)

SUMMARY

The rotating disc electrode has been adapted for flow-through cell anodic stripping voltammetry in a flow-through cell. The enhanced sensitivity (compared with that obtained with the solution flowing past a stationary electrode) is the result of higher plating efficiency. During the plating period, mass transfer to the electrode is governed by electrode rotation; peak currents are unaffected by solution flow rate. A continuous deaeration system for solution flow rates up to 100 ml min^{-1} is described. The method is characterized by extreme simplicity, stability and precision, and is suitable for in situ monitoring of heavy metals in aqueous samples.

Electroanalytical flow systems are being increasingly applied to the determination of environmental contaminants [1], the monitoring of chromatographic column effluents [2], and the automated analysis of discrete samples according to the AutoAnalyzer principle [3]. The exploitation of a.s.v. (anodic stripping voltammetry) for the determination of trace heavy metals in natural waters, effected in a discrete samples system, has recently been reviewed [4]. The ever-widening demand for continuous monitoring has triggered recent interest in applying a.s.v. methods to flowing systems [5—11]. The electrodes employed in the flow-through cells include stationary glassy carbon tube or disc electrodes, covered with a thin mercury film [5—9]; forced convection is the mass transfer mode chosen to increase the deposition current. At concentrations in the 0.1—1 ng ml^{-1} range, where the low ratio of peak current to charging current sets the lower sensitivity limit, long (10—20 min) deposition periods combined with solution flow rates exceeding 100 ml min^{-1} are required to ensure a measurable stripping peak current. The demand for faster determinations has led to the development of dual working electrode modes, in which the capacity current is compensated (while still retaining the set-up in which the solution flows past stationary electrodes): a.s.v. with collection [10] and differential a.s.v. [11], which allow fairly rapid and convenient determinations at sub-ppb concentrations.

The adaptation of twin electrode modes for the automated performance required for continuous monitoring is involved: a further improvement in

the sensitivity obtainable in the single electrode mode was therefore attempted.

The rotating disc electrode, well known for the efficient and well-defined mass transfer at its surface [12], has been widely used (covered with a thin mercury film) in a.s.v. in batch processes [13]. In the present work, the rotating mercury film glassy carbon disc electrode has been adapted for a flow-through cell. The efficient mass transfer maintained during the deposition step is combined with the sensitive differential pulse mode during the stripping step, for d.p.a.s.v. at thin film electrodes offers the highest signal to noise ratio of any stripping technique [14]; the required instrumentation is relatively simple.

At this stage of the art, the deaeration of the sample becomes the principal time-consuming step in the determination. Methods published to date describing the continuous deaeration of flowing systems are fairly complicated and effective only for relatively low flow rates [15, 16]. A simple device for the continuous removal of dissolved oxygen from solution streams flowing at rates ranging from 1 to 100 ml min^{-1} is described in this paper. The combined flow system, consisting of a rotating disc electrode detector coupled with this continuous deaeration device is characterized and its performance discussed.

EXPERIMENTAL

Apparatus

The details of the flow system (which may be used with various detectors, together with the continuous deaeration chamber, to be discussed below), have been described [9]; the flow cell (the detector), shown in Fig. 1, was adapted to hold the rotating mercury film glassy carbon disc electrode (hereafter referred to as the disc electrode). The cell consists of an 8-mm i.d. Pyrex glass tube, bent at a right angle to form the working electrode compartment (14-mm i.d.) and widening at the top (about 7 cm above the bend) to accept a Teflon cover through which the working electrode is inserted. The latter is a glassy carbon rod (GC30S, diameter 3 mm; fixed in a glass tube [9]) held in a stainless steel rotation shaft, which doubles as electrical contact. A locally built 4-speed (1350, 1850, 2675, 3600 rev./min) synchronous motor rotates the electrode. The glassy carbon disc face is centered in the working department, 2.5 cm above the bottom. The salt bridges of the reference electrode (Ag/AgCl, $KCl_{sat.}$, against which all potentials were measured) and of the counter electrode (a Pt foil immersed in 0.54 M NaCl) join the working compartment close to the face of the disc electrode. Solution outflow is maintained through an 8 mm i.d. glass tube, branching off the working department at a right angle, 5 cm above its bottom. A variable speed Masterflex pump (Cole Palmer No. 7545), with an "add-on" pump head (No. 7015-20), with its heads placed at the inlet and outlet of the flow cell, maintains solution flow and prevents overflow; the cell is not sealed hermetically.

The deaeration chamber, a 0.5-l bottle (8 cm diameter, 10 cm high; see

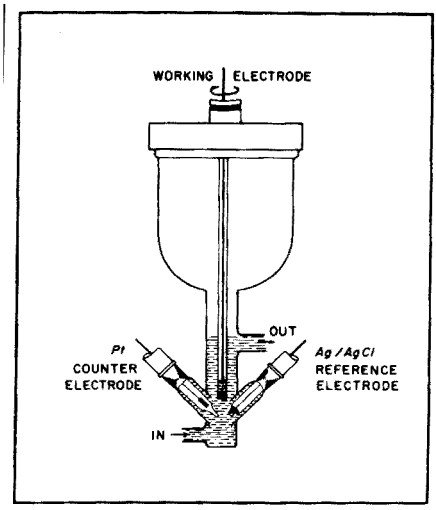

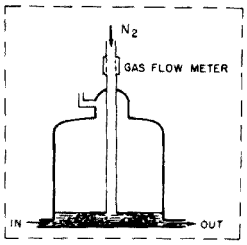

Fig. 1. Flow-through cell for a.s.v. at a rotating disc mercury covered glassy carbon electrode.

Fig. 2. Continuous flow deaeration chamber.

Fig. 2) is placed between the sample bottle and the flow cell, with tygon tubing (7-mm i.d., 15-mm o.d.) connections to each. Two openings, a solution inlet and outlet are placed diametrically opposite in the wall of the bottle, flush with its bottom; another outlet, at the top, allows gases (N_2 and removed O_2) to escape. The N_2 used for sparging is purified by passage through a series of traps containing acidic vanadium(II) solution and water [17]; its flow rate is controlled with a flow-meter. The gas is bubbled through a sintered glass disc (diameter 35 mm; porosity 1), placed about 4 mm above the bottom of the chamber.

The sample flow through the chamber is maintained continuously, except during the stripping process. Positioning the sintered glass disc near the bottom of the chamber allows its complete immersion in a small sample volume (about 25 ml); consequently, the solution is deaerated virtually immediately. The small volume of sample present, at any one time, in the chamber is kept constant by using the two heads of an additional variable speed Masterflex pump, with "add-on" pump head (No. 7015-20), with the heads placed at the inlet and outlet of the chamber.

Current–voltage curves were recorded with a PAR 174 Polarographic Analyzer with a 3077 Yokogawa X-Y recorder.

Reagents and Solutions

Reagents and solutions were prepared as described earlier [9].

Sea-water samples were taken from surface water near the sea shore, at the

Oceanography Institute beach, Haifa, by filling a polyethylene container cleaned with HNO_3 and rinsed with tri-distilled water and sea water. The samples were acidified upon collection, to pH 1.9, with 10 M HCl. The unfiltered samples were analyzed within 2 h of sampling.

Procedure

The sample and 300 ml of the Hg^{2+} solution, to give a final concentration of about 7×10^{-5} M, are introduced into the sample and Hg^{2+} bottles, respectively; 25 ml of the sample is introduced into the deaeration chamber. The mercury solution is purged with purified nitrogen and passed through the flow cell at a rate of 65 ml min^{-1} for 4 min, with a potential of −1.0 V imposed on the working disc electrode (without rotation). The electrode potential is then switched to −0.1 V and held there for 1 min, with the solution flow continuing and the electrode rotating, to dissolve any contaminants which may have codeposited with the mercury film. Stopcock 1 is turned to start the sample flowing through the deaeration chamber to the flow cell at a pre-determined flow rate (equal for both pumps) and the disc electrode rotation is maintained at 2675 rev./min. The sparging gas flow rate is adjusted according to the sample flow rate (see below). The plating potential, chosen appropriately for the ions to be determined, is imposed on the disc electrode for a period depending on their concentration (1—10 min, for concentrations ranging from 10^{-8}—5.10^{-10} M). The electrode rotation and solution flow are then stopped and the metal (metals) stripped from the mercury film by applying a pulse potential ramp (differential pulse mode) with a 5 mV s^{-1} scan rate and 50 mV pulse applied every 0.5 s. The d.p.a.s.v. polarogram is recorded simultaneously. The scan is terminated at −0.1 V; after 30 s, during which the solution flow and electrode rotation are maintained, the system is ready for the next plating—stripping cycle. Throughout the operation, nitrogen is passed over the solution surface to maintain an inert cell atmosphere . Stopcock 2 allows the sample to be conserved by recycling the cell outflow to the sample bottle whenever desired.

RESULTS AND DISCUSSION

Characterization and comparison with stationary disc electrode

Peak currents obtained at the rotating and stationary disc electrodes, at flow rates ranging from 0 to 110 ml min^{-1}, are compared in Table 1. While the peak currents for the rotating electrode are unaffected by flow rate, those for the stationary electrode are proportional to its square root (except for solution flow rates below 20 ml min^{-1} [9]). The independence of the peak currents at the rotating electrode from flow rate indicates that mass transfer to the electrode during the deposition period is governed by the rate of the electrode rotation (via the varying thickness of the diffusion layer). Levich theory [12] is applicable to the system with small deviations caused by the geometries of the electrode and the cell which differ considerably from those

TABLE 1

Comparison of peak currents obtained at stationary and rotating disc electrodes in a flow-through cell for the a.s.v. mode (1.3×10^{-7} M Cd^{2+} in 0.54 M NaCl ; deposition, 2 min at −1.1 V. Electrode rotation, 2675 rev./min. Linear potential scan rate, 100 mV s^{-1}.)

Solution flow rate (ml min^{-1})	i_p (stationary) (μA)	i_p (rotating) (μA)	i_p (stationary)/i_p (rotating)
0	0.13	0.87	0.15
20	0.22	0.88	0.25
60	0.25	0.87	0.28
75	0.29	0.87	0.33
110	0.37	0.88	0.42

quoted by Adams [18]. The lower and upper pump heads transport the solution which is sucked upwards and deflected radially by the rotating disc; this aids in removing the solution from the cell, without appreciably affecting mass transfer to the electrode. The upward streaming of the solution caused by the disc rotation gradually merges with the constant flow rate of the flowing system.

The theoretical correlation between peak current and rate of rotation ($i_p \propto N^{1/2}$) was tested experimentally; the results obtained are shown in Table 2. Quantitative evaluation is based on the linear correlation between peak currents and concentration which holds over a wide concentration range. In the $2 \times 10^{-9} - 2 \times 10^{-8}$ M concentration range (d.p.a.s.v., 6 min deposition) and the $2 \times 10^{-8} - 2 \times 10^{-7}$ M range (a.s.v., 2 min deposition), peak currents increased linearily with concentration, as expected [12, 19]. D.p.a.s.v. voltammograms, obtained after successive standard additions of Pb^{2+} solution to a 0.54 M NaCl solution are shown in Fig. 3. Each addition effects a 2×10^{-9} M increase in Pb^{2+} concentration. The well-defined sharp peaks allow unequivocal quantification at the sub-ppb level. The blank level was 1.9×10^{-9} M Pb^{2+}.

The ratio of the peak currents at the stationary and rotating electrodes ranges from 0.15 to 0.45 for solution flow rates of 0—110 ml min^{-1}, respectively. If the above assumptions continue to hold at higher flow rates, this ratio would reach unity at solution flow rates in the neighbourhood of 400 ml

TABLE 2

Dependence of peak current on rate of electrode rotation, at constant solution flow rate (4×10^{-7} M Pb^{2+} in 0.1 M KCl; deposition, 1 min at −1.0 V. Solution flow rate, 65 ml min^{-1}. Linear scan rate, 100 mV s^{-1}.)

N (rev./min)	i_p (μA)	$i_p/N^{\frac{1}{2}}$
1350	3.15	0.085
1850	3.55	0.083
2675	4.30	0.083
3600	4.84	0.081

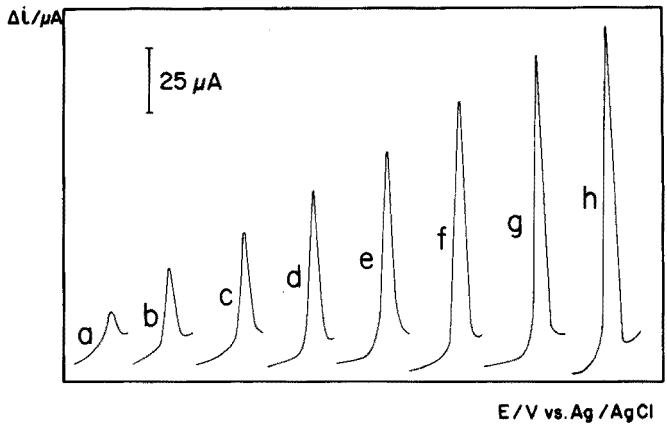

Fig. 3. D.p.a.s. voltammograms obtained after successive standard additions of Pb^{2+} to a 0.54 M NaCl solution. (a) Blank level 1.9×10^{-9} M (0.38 ng ml^{-1}). (b)—(h) Successive concentration increments of 2×10^{-9} M (0.4 ng ml^{-1}). Deposition, 6 min at —1.1 V. Electrode rotation, 2675 rev./min; solution flow rate, 45 ml min^{-1}.

min^{-1}. At the flow rates prevailing in a.s.v. systems (60—100 ml min^{-1}), mass transfer at the rotating electrode is 3—4 times as efficient as at the stationary electrode; this improvement allows a significant curtailment of deposition periods.

The results given in Table 1 indicate the feasibility of using low flow rates without concomitant loss in sensitivity. The solution flow merely serves to bring up the sample to the detector site (working compartment); at stationary electrodes it also determines the height of the current peak and may therefore be adjusted according to the sample volume available, a matter of cardinal importance for low volume samples, as encountered in clinical analysis. The adaptation of the rotating disc electrode as a detector for the automated a.s.v. of discrete samples, following the AutoAnalyzer principle, is the subject of Part II of this series.

Continuous deaeration studies

The efficiency of oxygen removal obtained in this way is demonstrated in Fig. 4, by the polarogram recorded in a 0.1 M KCl solution collected at the outlet of the flow cell into a polarographic cell in which nitrogen is kept flowing over the solution surface. At —0.800 V, the residual current measured in case (b) or (c) is less than 5% of that recorded in (a). Some small traces of oxygen may be left in the continuously deaerated system, because of penetration by diffusion through the tygon tubing; these are of no practical consequence in the a.s.v. determination. The anodic stripping voltammograms with continuous oxygen removal are identical to those obtained after removal of oxygen by bubbling nitrogen through the stagnant sample for 10 min.

The rapidity of deaeration, which efficiently removes oxygen from solution streams flowing at rates up to 100 ml, is the result of the intimate contact

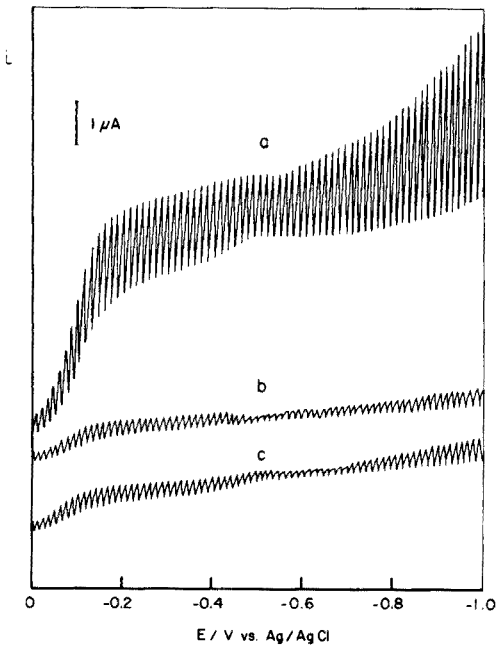

Fig. 4. Polarogram recorded in 0.1 M KCl solution, collected at the outlet of the flow cell operating : (a) without removal of dissolved O_2; (b) (c) with continuous deaeration, at solution flow rates of 30 ml min^{-1} and 80 ml min^{-1} and gas flow rates of 5 l min^{-1} and 8 l min^{-1}, respectively.

between the small sample solution volume and the numerous gas bubbles passed through it by the large sintered glass disc. Larger flow rates obviously require increased sparging gas flow rates; thus solution flow rates of 30, 50, 70, 90 ml min^{-1} require nitrogen flow rates of 5, 6, 7 and 8 l min^{-1} for adequate deaeration. Relatively high nitrogen pressures have also been used in other continuous deaeration devices [15, 16].

Continuous stripping monitoring system

The three S's (Sensitivity, Speed of response and Stability) required for an efficient monitoring system are present in this system exploiting the rotating disc electrode as detector.

Repetitive differential pulse anodic stripping voltammograms of unfiltered sea water, acidified to pH 1.9, recorded in a flow-through cell with the rotating disc electrode, are shown in Fig. 5. Heavy metal ions are present in the untreated entire sample in the free and "acid-exchangeable" form, i.e. that released by acidification from complexing ligands and desorbed from solid particles [20, 21]. Lead and copper are present at the 1 ng ml^{-1} level: 1.5×10^{-8} M Cu^{2+}, 6.5×10^{-9} M Pb^{2+}. The high lead content is most probably due to the exhaust fumes of the numerous motor vehicles passing on the autostrade some 100 m from the sampling site. While deposition periods of

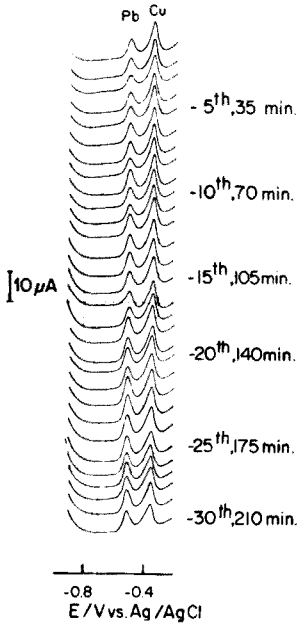

Fig. 5. The performance of the rotating disc electrode under continuous use: 30 successive d.p.a.s. voltammograms for a recycled sea-water sample (pH 1.9) were recorded during a 210-min period. Deposition, 4 min at −1.1 V. Electrode rotation, 2675 rev./min; solution flow rate, 45 ml min^{-1}.

4 min suffice for convenient quantification at the rotated disc electrode, at least 12 min are required at the stationary electrode.

Since the stripping step in the differential pulse mode lasts 2—3 min, the complete plating—stripping cycle ("Speed of Response") takes 6—7 min. Combined with continuous sample deaeration, this allows the performance of 9—10 repetitive analytical cycles per hour, at the 1 ng ml^{-1} concentration level (Fig. 5). At the 10 ng ml^{-1} level, plating periods of 1 min and linear potential scans (5—10 s) are employed, thus shortening the cycle duration to 1.5 min (40 analytical cycles per hour). The limit of detection is identical to that achievable in a discrete sample system [14]; 10—100 ppt (ng l^{-1}) may be conveniently determined by employing 10-min deposition periods and differential pulse mode stripping.

The use of the rotating disc electrode in a flow system for continuously monitoring heavy metal traces requires electrode stability for adequate precision of results. The behavior of the stationary mercury film glassy carbon disc has been discussed previously [9, 11]. In the present system, the high speed of electrode rotation constitutes an additional potential factor, leading to mechanical film deterioration. However, as evidenced by the unchanging base lines and peak currents obtained under repetitive conditions over several hours of use, film stability remains satisfactory (Fig. 5).

The reproducibility of results is indicated by the repetitive determination

of 1.3×10^{-7} M Cd^{2+} in 0.54 M NaCl (deposition at −1.1 V for 1 min; electrode rotation, 2675 rev./min; solution flow rate, 45 ml min^{-1}; linear scan rate, 100 mV s^{-1}); the mean i_p found was 0.434 μA with a range of 0.42–0.45 μA (n = 10). Thus at the 10-ppb level, the relative standard deviation was ±2%.

The chemical pretreatment required for the successful determination of the desired trace metal species in water, as demonstrated for the analysis of discrete samples (see e.g. [22]), may be easily effected in the automated flow system. The determination of total heavy metal content as obtained after subjecting the sample to heating for 5 min at 100°C, pH 0.7 [22], has been carried out [23] by using accessories familiar to AutoAnalyzer users: appropriate mixing of sample and acid are done by adjusting their respective flow rates and by passage through a coil placed in a thermostated bath. Solid fractions may be removed, prior to passage through the system, by employing a flow-through centrifuge.

A multiflow cell arrangement with a number of flow channels will allow the determination of a larger number of ions, with every channel carrying water pretreated as required by the ions to be subsequently determined, e.g. addition of supporting electrolyte, masking agent or complexant.

This paper is part of a thesis to be presented by J. Wang to the Senate of the Technion - I.I.T., in partial fulfilment of the requirements for a D.Sc. degree.

REFERENCES

1 See, e.g., I. H. Suffet, J. V. Radziul and D. R. Goff, in J. W. Scales (Ed.), Water Quality Instrumentation, Vol. 1, Inst. Soc. Am., Pittsburg, 1972, p.11.
2 See, e.g., A. Macdonald and P. D. Duke, J. Chromatogr., 83 (1973) 331.
3 See, e.g., W. Lund and L. Opheim, Anal. Chim. Acta, 79 (1975) 35.
4 H. W. Nurnberg, P. Valenta, L. Mart, B. Raspor and L. Sipos, Fresenius Z. Anal. Chem., 282 (1976) 357.
5 W. R. Seitz, R. Jones, L. N. Klatt and W. D. Mason, Anal. Chem., 45 (1973) 840.
6 S. H. Lieberman and A. Zirino, Anal. Chem., 46 (1974) 20.
7 A. Zirino and S. H. Lieberman, in Analytical Methods in Oceanography, ACS, Washington, 1975, p. 82.
8 R. W. Andrews and D. C. Johnson, Anal. Chem., 48 (1976) 1056.
9 J. Wang and M. Ariel, J. Electroanal. Chem., 83 (1977) 217.
10 G. W. Schieffer and W. J. Blaedel, Anal. Chem., 49 (1977) 49.
11 J. Wang and M. Ariel, J. Electroanal. Chem., 85 (1977) 289.
12 V. G. Levich, Physico-Chemical Hydrodynamics, Prentice-Hall, Englewood Cliffs, N.J., 1962.
13 T. M. Florence, J. Electroanal. Chem., 27 (1970) 273.
14 T. R. Copeland and R. K. Skogerboe, Anal. Chem., 46 (1974) 1257A.
15 W. J. Blaedel and D. Todd, Anal. Chem., 30 (1958) 1821.
16 C. Yarnitzky and E. Ouziel, Anal. Chem., 48 (1976) 2024.
17 L. Meites, Polarographic Techniques, 2nd edn., Interscience, New York, 1965, p. 89.
18 R. N. Adams, Electrochemistry at Solid Electrodes, Dekker, New York, 1969.
19 W. T. de Vries and E. van Dalen, J. Electroanal. Chem., 14 (1967) 315.

20 W. R. Matson, H. E. Allen and P. Rekshon, Am. Chem. Soc., Div. Water, Air, Waste Chem. Gen. Pap., Minneapolis, 1969, p. 164.
21 M. I. Abdullah, O. A. El-Rayis and J. P. Riley, Anal. Chim. Acta, 84 (1976) 363.
22 G. M. Batley and T. M. Florence, Anal. Lett., 9 (1976) 379.
23 J. Wang, Ph.D. Thesis, to be presented, Technion — I.I.T., Haifa, 1978.

Analytica Chimica Acta, 99 (1978) 99—104

DETERMINATION OF SULFITE AND SULFUR DIOXIDE BY ZERO-CURRENT CHRONOPOTENTIOMETRY

IVAN SEKERKA* and JOSEF F. LECHNER

Canada Centre for Inland Waters, Burlington, Ontario L7R 4A6 (Canada)

(Received 14th November 1977)

SUMMARY

The determination of SO_2, SO_3^{2-} and HSO_3^- by zero-current chronopotentiometry is described. The method utilizes a silver(I)-selective electrode with a gas-permeable membrane to monitor decreasing concentration of silver(I). The redox reaction of sulfite with bromate generates bromide, which precipitates silver(I) in the internal solution of the sensor. The speed of the potential change is related to the concentration of the sulfite in the sample. The elimination of the interfering effects of nitrogen oxides, sulfide and cyanide is described. Data on the accuracy, reproducibility and sensitivity are given.

A zero-current chronopotentiometric technique with ion-selective electrodes has already been described [1]. The method utilizes sensors and gas-permeable membranes for measurements under non-equilibrium conditions, i.e. where the speed of the potential change of the sensing electrode is related to the concentration of the ion or species of interest in the sample. This technique is capable of determining various species, provided that a system can be designed where a chemical reaction leads primarily to the formation of a gaseous species, then to reaction of the gaseous species with ions of the internal solution of the sensor, and finally to a change in potential of the ion-selective electrode. Such a system for the determination of sulfur dioxide, sulfite, and hydrogensulfite, with elimination of interfering substances, is described in this paper.

Background of the method

The dissociation constant of the reaction $SO_2 + H_2O = H^+ + HSO_3^-$ ($k \approx 2$) gives 50% conversion to SO_2 in solutions of pH 2. For practically total conversion, the sample must be acidified to below pH 1. Sulfite reacts with many oxidizing agents. The reaction with oxygen introduces problems for storage of samples and preparation and calibration of standard solutions; therefore, precautions must be taken to prevent losses of sulfite by atmospheric oxidation. However, the reducing properties of sulfite can be utilized for the selection of reactions in the internal solution of the sensor and the choice of ion-selective electrodes. An example of a redox reaction of sulfite with an oxidizing agent, producing an ion for which an ion-selective electrode

is available, is the reaction with bromate in acidic solution

$$SO_3^{2-} + BrO_3^- + 4H^+ = Br^- + SO_4^{2-} + 2H_2O \quad (1)$$

The bromide generated can be sensed by a bromide-sensitive electrode. (A similar reaction can be obtained with iodate to form iodide.) In the present example, a bromide electrode is immersed in a solution with a zero or very low concentration of bromide; the increase in the electrode potential caused by the increasing concentration of bromide which is generated from bromate by the reaction of SO_2 diffusing through the gas-permeable membrane is related to the SO_2 concentration. To obviate the slow response time of the electrode to extremely low levels of bromide, the system can be modified by adding silver ion to the internal solution and by operating the bromide electrode as a silver(I) electrode. In this case, the electrode is immersed in a solution containing a relatively high concentration of silver ion (e.g. 10^{-3} M), so that bromide generated by the process described above precipitates silver(I), and allows the speed of the potential change ($\Delta E/t$) to be related to the original concentration of SO_3^{2-} in the sample. This reaction can be utilized for quantitative measurements, as the sensing silver electrode is always exposed to a high concentration of silver ion (10^{-3}—10^{-5} M) where the response time is fast. These conditions create fast re-establishment of the starting potential after each rejuvenation of the film of internal solution on the active surface of the sensing element. The internal electrolyte, however, must be well buffered to prevent possible changes of pH caused by the reactions or by interfering species.

Volatile weak acids (gases) that react with water in acidic solution and are converted to dissociated forms, are possible interferences. Procedures for limiting these interferences as well as for preventing sulfur dioxide from being oxidized by oxygen, are described below.

EXPERIMENTAL

The sensor and measuring technique have been described [1]. An Ionel SL-02A bromide-selective electrode and a capillary silver/silver chloride gel reference electrode [2] were used as the electrode system. A Corning 101 millivoltmeter and a Hewlett-Packard 7004 B recorder were used for measuring and recording the electrode response and for potentiometric titrations.

All chemicals used were of analytical-reagent grade. The stock solutions, prepared by weight, were standardized by appropriate standard analytical methods.

The internal electrolyte contained a known concentration of $AgNO_3$ (1×10^{-3}—1×10^{-5} M) in 1×10^{-2} M $KBrO_3$. The pH of the solution was adjusted to 3.4 with 0.2 M acetic acid and 0.2 M sodium acetate.

The pH of the sample was adjusted with H_2SO_4 to less than 1.0.

RESULTS AND DISCUSSION

Basic function

To verify the initial assumptions, 10.0 ml of 1×10^{-3} M Ag^+ solution in the presence of 1×10^{-2} M potassium bromate, acidified with acetic acid, was titrated with 1×10^{-3} M Na_2SO_3 solution. The titration was monitored by a silver (bromide) electrode. The course of the titration when the titrant was added in 0.01-ml increments at constant time intervals of 40 s is shown in Fig. 1 (curve A). Titrations with increasing speeds of titrant delivery are presented in Fig. 1, curves B, C, D and E. The standard deviation ($s < 0.05$ mg) and coefficient of variation ($s_r < 5\%$) achieved show that the proposed reaction system is sufficiently precise and reproducible. The response of the electrode in the area convenient for the calibration — from start to equivalence point — is about 200 mV and sufficiently fast. All these factors support the application of the system in zero-current chronopotentiometry. Similar experiments with iodate ion in combination with silver(I), Hg(I) or Hg(II) ions were unsuccessful.

Calibration

Measurements of different concentrations of sulfite ion are given in Fig. 2, where change of potential ΔE (mV) is plotted against concentration (ppm) of SO_3^{2-}. The internal filling solution contained 100 ppm Ag^+ and the time interval for ΔE was 30 s. Under the given experimental conditions, the method was applicable to concentrations higher than 10^{-5} M. At concentrations below 10^{-5} M SO_3^{2-}, the potential changed at the beginning of the measurement (after the injection of SO_3^{2-}) but became constant after several seconds. Repeated measurements did not show any potential change in time, indicating the disappearance of SO_2 from the solution during the

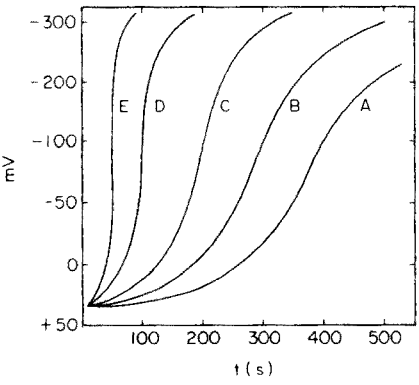

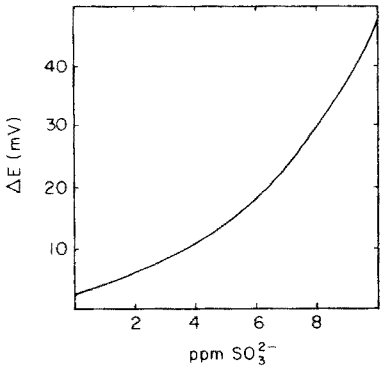

Fig. 1. The course of the potentiometric titration of 10^{-3} M Ag^+ in the presence of 10^{-2} M BrO_3^- with 10^{-3} M SO_3^{2-} at different speeds of titrant delivery. (A) 0.01 ml/40 s. (B) 0.01 ml/30 s. (C) 0.01 ml/20 s. (D) 0.01 ml/10 s. (E) 0.01 ml/5 s.

Fig. 2. Calibration curve for the SO_3^{2-} determination in the range 0.1—10 ppm.

measurement. Two reasons for this were considered: the SO_2 may have been consumed by the reaction in the sensor; or SO_2 may have been oxidized by dissolved oxygen in the water. Approximate calculations in which the given geometry of the system was considered showed that 2.5% of the SO_2 from 100 ml of 10^{-7} M SO_3^{2-} solution reacted in the titration of the Ag^+ content in the surface film of the electrode (for a 10^{-4} M Ag^+ internal solution). Therefore, the disappearance of SO_2 from the sample cannot be related to depletion by the sensor.

An attempt to inhibit the oxidation of SO_2 by dissolved oxygen by the addition of glycine and other recommended organic compounds [3] was unsuccessful. The addition of 1 ml of 1 M ascorbic acid to the sample lowered the detectable level of SO_2 to 10^{-6} M. Finally, deaeration of the sample with extra-pure nitrogen gas at neutral pH decreased the detection limit to the 10^{-7} M SO_2 level.

The determination of sulfite at concentrations lower than 5×10^{-5} M requires either the addition of ascorbic acid or the deaeration of the sample with inert gas, depending on the expected level. It is obvious that under normal aerobic conditions, the existence of low levels ($<10^{-5}$) of sulfite ion in samples of natural waters is not probable. Therefore, the detection limit of the method is governed more by the existence of the ion of interest than by the capability of the sensor. Under anaerobic conditions, practically useful values of ΔE ($\Delta E > 2$ mV) were obtained down to 5×10^{-7} M sulfite

Different concentrations of sulfite were determined after the oxygen had been removed by passing nitrogen at neutral pH or in the presence of an antioxidant. The results are shown in Table 1.

Interferences

The proposed method suffers direct interferences only from dissolved gaseous species (or species which are converted to gas by acidification) in the sample, that can produce a change in the concentration of the silver ion in the internal electrolyte.

TABLE 1

Precision of sulfite determination

SO_3^{2-} taken (ppm)	Ag^+ in internal solution (ppm)	Mean ($n = 5$) SO_3^{2-} found (ppm)	s (ppm)	s_r (%)
0.008	10	0.007	0.002	33
0.040	10	0.04	0.004	10
0.080	10	0.07	0.004	5
0.40	100	0.39	0.02	5
0.80	100	0.79	0.05	5
4.00	100	4.2	0.16	4
8.00	1000	7.8	0.35	5
40.0	1000	38.0	0.50	4
80.0	1000	76.8	3.0	6

Cyanide, sulfide, and partially nitrite are converted to gases at pH 4.5; theoretically they should be removed together with dissolved oxygen by bubbling through an inert gas. Sulfite ion remains in ionic form and should not be expelled. Such sample treatment gave unsatisfactory results, mainly because of the long time necessary to achieve complete removal of the gaseous species and the resulting losses of sulfite. Attempts to eliminate cyanide interference by the addition of chloralhydrate, formaldehyde [4], or masking with Cu(II) or Cd(II) ions did not give satisfactory results. Cyanide complexes of silver or mercury cannot be used because of the redox reaction with sulfite; only the Co(II) cyanide complex, formed in ammoniacal solution, remains stable below pH 1 and can be used to mask cyanide ion. Sulfide and thio compounds (i.e. thiourea, sodium mercaptoacetate, potassium ethyl xanthate, ammonium pyrrolidinedithiocarbamate) up to 1 ppm can be successfully masked by the addition of Bi(III) [5]. The precipitation by other cations which form sparingly soluble sulfides [6, 7] is inadequate below pH 1; Ag(I) and Hg(II) cannot be used. The addition of hydrazine hydrate [3] did not remove the interference by nitrite. This was successfully achieved by adding the sulfamic acid [5] before the addition of ascorbic and sulfuric acids.

Addition to the sample of 0.1 ml of 10^{-2} M sulfamic acid, 0.1 ml of 10^{-2} M $Bi(NO_3)_3$, 0.1 ml of 10^{-2} M $Co(NO_3)_2$, sufficient ammonia solution to give (pH 8—9) and finally enough H_2SO_4 to give pH < 1, eliminates all the mentioned interfering ions. This procedure is adequate for sulfite levels above 10^{-5} M. Samples containing less than 10^{-5} M sulfite require an additional deaeration with pure nitrogen (prior to the acidification with H_2SO_4), or the addition of 1 ml of 1 M ascorbic acid. Satisfactory results for sulfite determinations in the presence of interfering ions, with the preliminary sample treatment described, are summarized in Table 2.

TABLE 2

Determination of 4.0 ppm sulfite in the presence of interferences

Interference added (ppm)			Mean SO_3^{2-} found (n = 5) (ppm)	s (ppm)	s_r (%)
NO_2^-	S^{2-}	CN^-			
0.5			4.0	0.14	3.6
5.0			3.9	0.18	4.6
50.0			3.7	0.27	7.3
	0.3		3.9	0.22	5.5
	3.0		3.9	0.17	4.2
	30.0		3.9	0.16	4.1
		0.25	3.9	0.19	4.9
		2.5	3.8	0.19	5.1
		25.0	4.3	0.11	2.6
5.0	3.0	2.5	3.8	0.21	6.0
50.0	30.0	25.0	3.6	0.34	9.0

TABLE 3

Analysis of water samples by the proposed method and by a standard titration method

Sample No.	Origin	SO_2 found (ppm)	
		Proposed method	Titration
1	Municipal waste	3.3	3.0
2	Municipal waste	1.4	1.5
3	Industrial waste	2.3	3.5
4	Industrial waste	6.8	7.0
5	Harbour	0.05	not detectable
6	Harbour	0.06	not detectable
7	Harbour Channel	0.02	not detectable
8	Harbour Channel	0.02	not detectable
9	Lake Ontario	not detectable	not detectable
10	Lake Ontario	not detectable	not detectable

The determination of sulfite is of great interest in the food and petrochemical industries. Sulfite is commonly found in boiler and boiler feed waters to which it has been applied to reduce oxygen and prevent corrosion. Industrial wastes, polluted waters, and air are other examples of sulfite occurrences.

As an example, several samples of polluted and waste waters from Hamilton Harbour area were analyzed by the proposed as well as by a standard method [9]. Ten representative results, given in Table 3, show acceptable correlation of both procedures in the case of the samples containing high levels of sulfite. The proposed method however, is capable of measuring levels of sulfite well below the detection limit of the standard method.

REFERENCES

1 I. Sekerka and J. F. Lechner, Anal. Chim. Acta, 93 (1977) 129.
2 I. Sekerka and J. F. Lechner, Anal. Lett., 8 (1975) 769.
3 Orion Research Inc., Industrial Manual 95-64 Sulfur Dioxide Electrode, Cambridge, Mass.
4 D. D. Perrin, Masking and Demasking of Chemical Reactions, Wiley-Interscience, New York, U.S.A., 1970.
5 I. Sekerka and J. F. Lechner, Water Res., 10 (1976) 479.
6 J. H. Riseman, Am. Lab., 4 (1972) 63.
7 M. S. Frant, J. W. Ross and J. H. Riseman, Anal. Chem., 44 (1972) 2227.
8 D. W. W. Andrews, Analyst, 89 (1964) 730.
9 Standard Methods for the Examination of Water and Waste Water, 13th edn., Am. Public Health Association, Washington, D.C., 1974.

Analytica Chimica Acta, 99 (1978) 105—113

ANALYTICAL APPLICATIONS OF TRIETHYLENETETRAMINEHEXAACETIC ACID

Part I. The Influence of TTHA on the Polarographic Reduction of some Metal Ions

STANISLAW RUBEL and MAREK WOJCIECHOWSKI*

Institute of Fundamental Problems in Chemistry, University of Warsaw, 02-093 Warszawa (Poland)

(Received 16th January 1978)

SUMMARY

The influence of triethylenetetraminehexaacetic acid (TTHA) on the d.c. and square-wave polarographic curves of Cu(II), Pb(II), Cd(II), Ni(II), Co(II), Zn(II), Fe(III), Bi(III), Sb(III), As(III) and In(III) has been investigated in several supporting electrolytes over the pH range 1—13. The $E_{1/2}$ and E_p values with and without a 10-fold excess of TTHA are compared. Some analytical applications are suggested.

The neutral molecule of triethylenetetraminehexaacetic acid (TTHA) occurs in aqueous solutions in tautomeric forms, with protons attached to carboxylic oxygens or to amine nitrogens. The protonation constants and stability constants of several metal complexes with TTHA have been summarized [1]. The molecule of TTHA has ten donor atoms and has stronger complexing properties than many other polyaminopolycarboxylic acids. It forms very stable mononuclear complexes with tri- and tetra-valent metal ions and can form polynuclear complexes (M_2L), primarily with divalent metal ions. This last property distinguishes TTHA from the whole group of polyaminopolycarboxylic acids and has produced some interesting analytical applications.

Polarographic investigations of the reduction of metal complexes with TTHA were first made by Conradi and Kopanica [2], who listed the $E_{1/2}$ values for the reduction waves of metal complexes with TTHA. The $E_{1/2}$ values were established for three supporting electrolytes of pH 1.9, 4.7 and 9.2. Since then, many papers describing the polarographic properties of metal complexes with TTHA have been published. The reduction of the complexes with Cd(II) [3], Cu(II) [4], Fe(II) and Fe(III) [5, 6], In(III) [7], Ga(III) [8] and Cr(III) [9] has been studied. Kopanica et al. investigated polarographically the substitution reactions between metal complexes with TTHA and other metal ions [10—13]. A detailed bibliography of studies on TTHA and its applications in analytical chemistry has been compiled [14].

Some of the most interesting problems in the application of polarography

to the determination of metals are connected with the advantages that may be obtained by the use of a given complexing reagent. For this purpose, the influence of the ligand on the polarographic curves of metal ions, i.e. on the half-wave potentials of the reduction waves as well as on the shape and separation of the waves, must be known. Because such information is not directly available from previous work, the results of a systematic investigation carried out on solutions of several metal ions over a wide pH range [14] are presented here.

The widespread application of square-wave polarography stimulated similar investigations with this technique, for which there are few literature data on TTHA complexes [6, 9].

EXPERIMENTAL

Apparatus

The d.c. polarographs used were the Radiometer PO3 and the Laboratorni Pristroje LP60a. The square-wave polarograph was a Radelkis OH-104 model. The dropping mercury electrode (d.m.e.) had the following characteristics: m = 2.98 mg Hg s^{-1}, t = 3.2 s in 0.1 M KCl solution at zero potential for h = 70 cm. For d.c. polarography, a saturated calomel electrode (s.c.e.) served as reference electrode. For square-wave polarography, an s.c.e. and a platinum auxiliary electrode were used.

Reagents

Triethylenetetraminehexaacetic acid (Fluka AG) was used as a 1.0×10^{-2} M solution [2]. The metal ion solutions (1×10^{-3} M) as nitrates contained nitric acid to prevent hydrolysis. Antimony solution was prepared as the tartrate and arsenic solutions as arsenite.

Perchloric acid (d = 1.54; Riedel AG) was used as 1.0 M and 0.1 M solutions. Sodium hydroxide was used as 5.0 M solution. The buffers were: citrate buffer pH 3.3 from sodium citrate and perchloric acid; acetate buffer pH 4.1; ammonium buffer pH 10.1 ($NH_4Cl + NH_3$).

All reagents were of analytical grade (POCh—Poland if not otherwise indicated). Water was thrice-distilled from quartz apparatus.

Measurements

The influence of an excess of TTHA on the polarographic behaviour of metal ions was investigated by determining the $E_{1/2}$ or E_p values of the waves or peaks in several supporting electrolytes. Investigations of a particular metal ion in a given supporting electrolyte were based on recording the polarographic curves (after deaeration) from a 1.0×10^{-4} M metal solution in the electrolyte, and from a similar solution containing 1.0×10^{-3} M TTHA.

The absence of a significant wave or peak was decided on the basis of curves recorded at the highest polarographic sensitivity. $E_{1/2}$ and E_p values, determined graphically from the polarographic curves for supporting electrolytes with and without TTHA, are presented in Tables 1 and 2.

D.c. polarography. The influence of TTHA (1×10^{-3} M) on the $E_{1/2}$ values (V) of the reduction (or oxidation) waves of metal ions (1×10^{-4} M) in solutions of several supporting electrolytes

Electrolyte	0.1 M $HClO_4$ pH 1.0		0.01 M $HClO_4$ pH 2.0		0.1 M citrate buffer pH 3.3		1.0 M acetate buffer pH 4.1		0.1 M ammonium buffer pH 10.1		1.0 M NaOH	
Metal	Alone	+TTHA	Alone	+TTHA	Alone	+TTHA	Alone	+TTHA	Alone	+TTHA	Alone	+TTHA
Cu(II)	+0.01	−0.03	+0.025[a]	−0.085	−0.09[a,b]	−0.15[b]	−0.005	−0.205	−0.15 −0.405	−0.475	−0.40	−0.45
Pb(II)	−0.39	−0.39	−0.37	−0.435	−0.40	−0.49	−0.43	−0.52 −0.64 −0.74	$Pb(OH)_2\downarrow$	−1.13[a]	−0.71	−0.75
Cd(II)	−0.585	−0.585	−0.57	−0.59	−0.57	−0.665 −0.81	−0.59	−0.91	−0.74	n.d.[c]	−0.80	n.d
Ni(II)	−1.02	n.d.	−0.935	n.d.	−1.00	n.d.	−1.025	n.d.	−0.94	n.d.	$Ni(OH)_2\downarrow$	n.d.
Zn(II)							−1.05[d]	n.d.	−1.28[a]	n.d.	−1.495	−1.505
Co(II)	n.d.	n.d.	−1.12	n.d.	−1.21	n.d.	−1.25	n.d.	−1.19[a]	n.d.	−1.43	n.d.
Fe(III)	n.d.	n.d.	n.d.	+0.035	n.d.	−0.07[e]	+0.055[e] −1.31	−0.135		$Fe(OH)_3\downarrow$		$Fe(OH)_3\downarrow$
Bi(III)	+0.035	−0.305	+0.05[e]	−0.375 −0.635	−0.105	−0.455 −0.71	−0.16	−0.86 −1.06		−1.39		−0.63
Sb(III)	−0.18 −0.27	−0.28	−0.24 −0.35[a]	−0.38	−0.48	−0.49	−0.36[a] −0.45	−0.36 −0.48	−0.83	−0.82	−0.415[f] −1.14	−0.39[f] −1.15
As(III)	−0.56 −0.70[a]	−0.70	−0.61 −0.75[a]	−0.75	−0.60[g]	−0.60[g]	−0.70[g]	−0.70[g]	n.d.	n.d.	−0.25[f]	n.d.
In(III)	−0.98	−0.55[g]	−0.56[a]	n.d.	−0.595	n.d.	−0.65	n.d.	n.d.	n.d.		n.d.

[a]Wave with a maximum on the limiting current. [b]pH 2.6. [c]No wave was detected in the potential range investigated. [d]pH 4.6. [e]Part of the wave falls below the zero line. [f]Anodic wave. [g]Potential at which depolarization of the d.m.e. by the metal ion starts; the shape of the wave made it impossible to determine the $E_{1/2}$ value.

TABLE 2
Square-wave polarography. The influence of TTHA on E_p (V) of s.w. peaks of metal ions reduction in solutions of several supporting electrolytes

Electrolyte	0.1 M $HClO_4$ pH 1.0		0.01 M $HClO_4$ pH 2.0		0.1 M citrate buffer pH 3.3		1.0 M acetate buffer pH 4.1		0.1 M ammonium buffer pH 10.1		1.0 M NaOH	
Metal	Alone	+TTHA	Alone	+TTHA	Alone	+TTHA	Alone	+TTHA	Alone	+TTHA	Alone	+TTHA
Cu(II)	+0.01	−0.05	0.00	−0.09	−0.16[a]	−0.19[a]	−0.04	−0.235	−0.155 −0.425	−0.505	−0.39 −0.455	−0.47
Pb(II)	−0.41	−0.41	−0.41	−0.465	−0.44	−0.52	−0.46	n.d.[b]	$Pb(OH)_2\downarrow$	−1.22	−0.76	−0.78
Cd(II)	−0.60	−0.60	−0.62	−0.635	−0.62	−0.67 −0.86	−0.635	−0.97	−0.76	n.d.	−0.82	n.d.
Ni(II)	−1.08	n.d.	−1.08	n.d.	−1.09	n.d.	−1.095	n.d.	−1.00	n.d.	$Ni(OH)_2\downarrow$	n.d.
Zn(II)							−1.055[c]	n.d.	−1.33	n.d.	−1.55	−1.55
Co(II)	n.d.	n.d.	n.d.	n.d.	n.d.	n.d.	n.d.	n.d.	−1.24 −1.41	n.d.	−1.47	n.d.
Fe(III)	n.d.	−0.04 −0.21	n.d.	n.d.	n.d.	−0.08	n.d.	−0.125		$Fe(OH)_3\downarrow$		$Fe(OH)_3\downarrow$
Bi(III)	+0.01	n.d.	−0.34	−0.21	−0.125	n.d.	−0.175	n.d.		−1.54		−0.685
Sb(III)	−0.185 −0.28	−0.31	−0.39	n.d.	−0.525	−0.535	−0.40 −0.49	−0.38 −0.52 −0.63	−0.91	−0.90	−0.41 −1.23	−0.38 −1.24
As(III)	−0.72	−0.31 −0.72 −0.84	−0.78 −1.365	n.d.	n.d.	n.d	n.d.	n.d.	n.d.	n.d.	n.d.	n.d.
In(III)	−1.02	−0.78	−0.55	n.d.	−0.615	n.d.	−0.66	n.d.	n.d.	n.d,		n.d.

[a]pH 2.6. [b]The notation n.d. for solutions without TTHA indicates the absence of a peak at maximum sensitivity. For solutions

RESULTS

Copper(II)

Addition of TTHA to acidic supporting electrolytes improves the shapes of the d.c. wave and the s.w. peak corresponding to reduction of copper(II). This is connected with a shift of $E_{1/2}$ and E_p to more negative potentials (0.1 M $HClO_4$, 0.01 M $HClO_4$, acetate buffer) or with more reversible reduction of the Cu—TTHA complex (citrate buffer).

Lead(II)

In addition to the influence of TTHA connected with complexation (shift of $E_{1/2}$ and E_p), TTHA also decreased the limiting current. For example, in 1.0 M NaOH solution, the addition of a 10-fold excess of TTHA causes a 2-fold decrease in the d.c. wave and a 10-fold decrease in the s.w. peak. Increasing the TTHA concentration causes further decreases in limiting current. This effect can be utilized in the polarographic determination of metals in the presence of lead(II) for suppressing the reduction current of lead(II).

In acetate buffer containing TTHA, three overlapping waves appear (Fig. 1); the total height of these waves equals the height of the Pb—TTHA

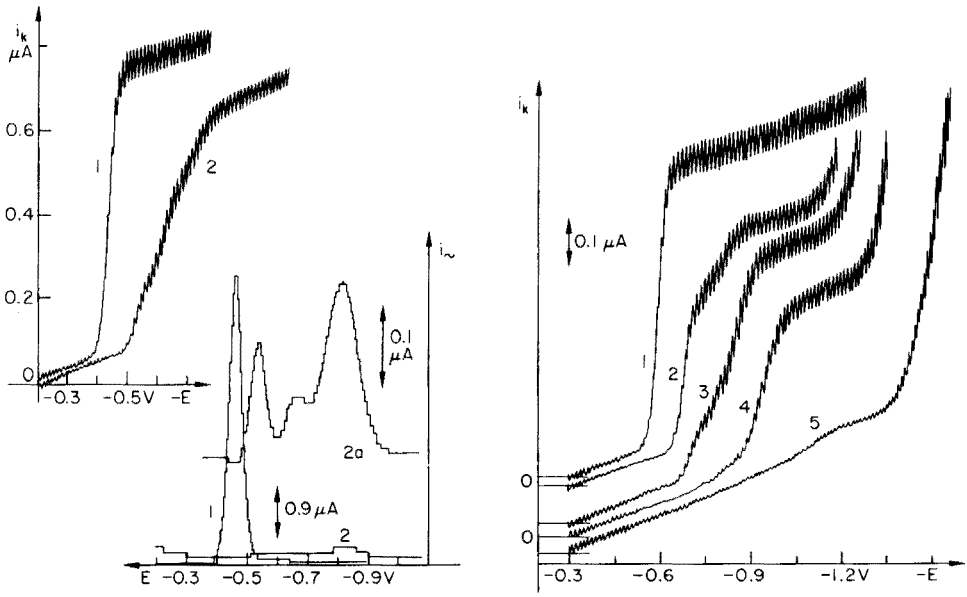

Fig. 1. The d.c. and s.w. curves for 1×10^{-4} M lead(II) recorded from 1.0 M acetate buffer. Curves 1 are without TTHA, and curves 2 and 2a are with 1×10^{-3} M TTHA.

Fig. 2. The influence of pH on the d.c. wave of 1×10^{-4} M cadmium(II) in 0.1 M $NaClO_4$. Curve 1 is without TTHA and curves 2—5 are with 1×10^{-3} M TTHA. Curves 1 and 2, pH 3.00; curve 3, pH 3.47; curve 4, pH 4.05; curve 5, pH 5.20.

wave in a solution at pH 3.3. Higher ligand concentrations decrease the first two waves and increase the third wave. Further study of the effects of pH and TTHA concentration indicated that the waves mentioned correspond to the reduction of three differently protonated Pb—TTHA complexes.

As with acetate buffer, the use of ammonium buffer in the presence of TTHA spoils the shapes of the d.c. and s.w. curves.

Cadmium(II)

The polarographic curves of Cd(II), recorded from solutions at pH 3.3 containing TTHA, show two waves. As the ligand concentration is increased, the first wave decreases whereas the second increases. A comparison of the conditional stability constants of the Cd—TTHA and Cd_2—TTHA complexes suggests that the mononuclear Cd—TTHA complex predominates at this pH. It seems that, as in the case of Pb(II) in acetate buffer, these waves correspond to the reduction of two differently protonated Cd—TTHA complexes. To confirm this statement, experiments were carried out on series of solutions containing a fixed Cd:TTHA ratio of 1:10 at fixed ionic strength (0.1 M $NaClO_4$) and at pH values varying from 3 to 5. Above pH 3, the first wave decreased and the second increased. At pH 4.0, only the second wave remained; this wave decreased as the pH was increased, and disappeared above pH 5 (Fig. 2). The results of experiments and calculation of the contribution of protonated forms of the Cd—TTHA complexes (as a function of pH) indicate that the first wave corresponds to reduction of the CdH_2-$(TTHA)^{2-}$ complex, whereas the second wave corresponds to $CdH(TTHA)^{3-}$. Below pH 5.0, the unprotonated $Cd(TTHA)^{4-}$ complex predominates; this is not polarographically reducible in the accessible potential range. This was confirmed by the complete elimination of the d.c. wave and s.w. peak of cadmium(II) after the addition of TTHA in ammoniacal buffer and in 1.0 M NaOH media.

Nickel(II), cobalt(II) and zinc(II)

Complexes of Ni(II), Co(II) and Zn(II) with TTHA are not reduced at the d.m.e. within the accessible potential range in any of the supporting electrolytes studied. The reduction of these complexes in acidic supporting electrolytes becomes difficult because of the shift of the supporting electrolyte decomposition wave towards positive potentials (Fig. 3). Further experiments suggest that the catalytic influence of TTHA (similarly to EDTA) on the reduction of H_3O^+ ions at the d.m.e. is responsible for this phenomenon.

Iron(III)

The reduction wave of the Fe—TTHA complex appears in solutions of pH above 2.0. The wave shape is best in buffer of pH 3—3.5. Because of irreversible Fe(III) and Fe—TTHA reduction, as well as the proximity of the reduction current of mercury, the s.w. curves do not show peaks corresponding to Fe(III) reduction, and the peaks corresponding to the Fe—TTHA complex are badly shaped.

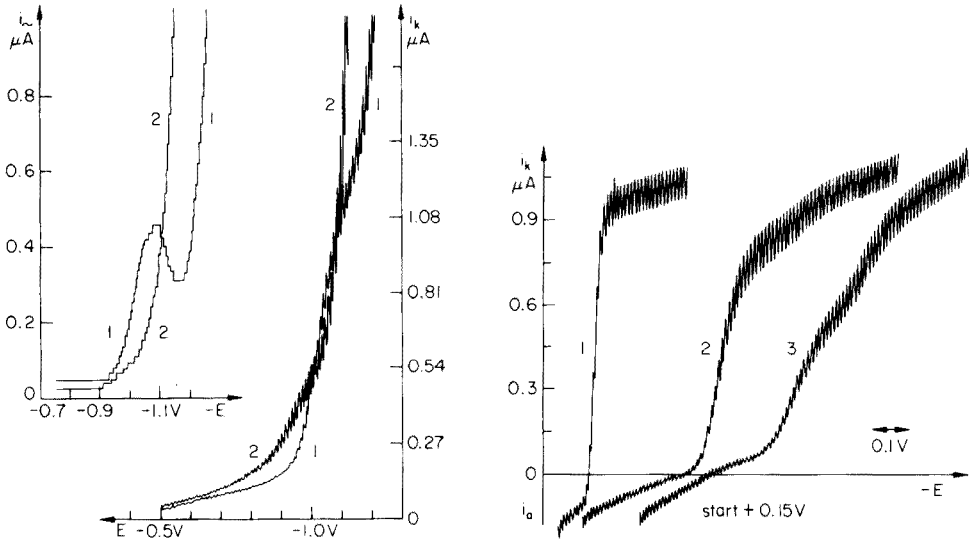

Fig. 3. The d.c. and s.w. curves for 1×10^{-4} M nickel(II) in 0.1 M $HClO_4$. Curves 1 are without TTHA; curves 2 are with 1×10^{-3} M TTHA.

Fig. 4. The d.c. curves for 1×10^{-4} M bismuth(III) in 0.1 M $HClO_4$. Curve 1, no TTHA; curve 2, 1×10^{-3} M TTHA; curve 3, 5×10^{-3} M TTHA.

Bismuth(III)

In 0.1 M $HClO_4$ solution, bismuth(III) is reversibly reduced, giving a well shaped d.c. wave (Fig. 4) and s.w. peak. The wave recorded in the presence of TTHA (10-fold excess) is less well shaped, and a very small second wave appears at its limiting current. Increase in the ligand concentration causes a decrease in the first wave and an increase in the second wave, but the total height of the two waves is constant (Fig. 4). The s.w. curve in the presence of excess of TTHA exhibits three badly shaped peaks with E_p values of −0.3 V, −0.6 V and −1.0 V at very high sensitivity. With other supporting electrolytes, the addition of TTHA again has a very disadvantageous effect on the shapes of waves and peaks. Only in 1.0 M NaOH solution is a well shaped reduction peak formed for the Bi(III) complex.

Antimony(III)

In 0.1 M $HClO_4$, antimony(III) is reduced at the d.m.e., giving two waves of nearly equal height. Addition of TTHA decreases the first wave and increases the second wave. In 0.01 M $HClO_4$ medium, TTHA completely eliminates the first wave and improves the shape of the second. The d.c. curve recorded from ammoniacal buffer shows a well shaped wave corresponding to the irreversible s.w. peak. Neither wave nor peak changes significantly when an excess of TTHA is added, because the solution contains the stable antimony(III) tartrate complex from the initial metal salt.

In 1.0 M NaOH solution, Sb(III) is oxidized at the d.m.e. to Sb(V). The d.c. curve shows anodic and cathodic waves. In the presence of TTHA, the anodic wave shifts towards positive potentials whereas the cathodic wave shifts to more negative potentials.

Arsenic(III)

In each of the supporting electrolytes tested, arsenic(III) is reduced in two stages, giving two closely adjacent waves. Above pH 3.0, these waves are badly shaped and their $E_{1/2}$ values differ so insignificantly that the limiting current of the first wave is scarcely visible. The addition of TTHA does not improve matters. In 1.0 M NaOH, arsenic(III) like antimony(III) is oxidized at the d.m.e. to As(V), giving a well shaped anodic wave which disappears in the presence of an excess of TTHA.

Indium(III)

In acidic electrolytes of pH above 2.0 ($HClO_4$, citrate buffer, acetate buffer), indium(III) is reduced reversibly, giving a well shaped wave and s.w. peak. However, in the alkaline electrolytes (ammoniacal buffer, NaOH solution) indium(III) is not reduced in the accessible potential range. The In—TTHA complex is not polarographically active above pH 2.0.

DISCUSSION

The influence of TTHA on the polarographic curves of metal ion reduction is variable. It depends on the stability of the particular TTHA complex, on pH and on the composition of supporting electrolyte, as well as on the technique of recording the polarographic curve. On the basis of the above data, the following conclusions can be drawn.

TTHA improves the shapes of the d.c. waves and s.w. peaks for some metal ions, e.g. Cu(II) and Fe(III) in acidic supporting electrolytes, Sb(III) in 0.01 M $HClO_4$, and As(III) in 0.1 M and 0.01 M $HClO_4$. However, an excess of TTHA suppresses the reduction processes of several metal ions at the d.m.e. The d.c. waves, and especially s.w. peaks, corresponding to the reduction of complexes are generally lower than the waves and peaks corresponding to reduction of simple ions. This may be explained, at least partly, by differences in the diffusion coefficients of simple and complex ions, and by the greater irreversibility of complex reduction compared to that of simple ions.

With some metal ions, e.g. Pb(II) and Cd(II), the peak height corresponding to complex reduction decreases with increasing TTHA concentration. At some excess of the ligand, the peak is completely suppressed. This phenomenon can be explained by adsorption of TTHA on the d.m.e.

The complexes of Cd(II) above pH 5.0, of In(III) above pH 2.0, of As(III) in 1.0 M NaOH, and of Ni(II), Co(II) and Zn(II) with TTHA, are not reduced at the d.m.e. in the accessible potential range.

In the presence of TTHA, the following polarographic determinations should be possible:
(1) Cu(II) and Bi(III) in 0.1 M $HClO_4$;
(2) Sb(III) in the presence of In(III) in 0.1 M citrate buffer pH 3.3;
(3) Cd(II) in the presence of In(III) in 1.0 M acetate buffer pH 4.1;
(4) Sb(III) in the presence of Ni(II) in 0.1 M ammoniacal buffer pH 10.1;
(5) Pb(II) in the presence of Cd(II), and Zn(II) in the presence of Co(II), in 1.0 M NaOH medium.

The above-mentioned metal systems in the absence of TTHA give waves or peaks of similar $E_{1/2}$ or E_p values.

REFERENCES

1 A. E. Martell and R. M. Smith, Critical Stability Constants, Plenum Press, New York, 1974.
2 G. Conradi and M. Kopanica, Collect. Czech. Chem. Commun., 28 (1963) 1600.
3 G. Conradi, M. Kopanica and J. Koryta, Collect. Czech. Chem. Commun., 30 (1965) 2029.
4 K. S. Klausen, G. O. Kalland and E. Jacobsen, Anal. Chim. Acta, 33 (1965) 67.
5 K. N. Schröder, Acta Chem. Scand., 19 (1965) 1797.
6 E. Jacobsen, W. Lund and T. Rojahn, Anal. Chim. Acta, 63 (1973) 147.
7 T. Ch. Huyen and M. Kopanica, Collect. Czech. Chem. Commun., 36 (1971) 3244.
8 T. Ch. Huyen and M. Kopanica, Collect. Czech. Chem. Commun., 37 (1972) 2874.
9 V. Stara and M. Kopanica, J. Electroanal. Chem., 47 (1973) 343.
10 M. Kopanica, Talanta, 15 (1968) 1457.
11 L. Neubauer and M. Kopanica, Collect. Czech. Chem. Commun., 36 (1971) 1121.
12 M. S. Haque and M. Kopanica, Bull. Chem. Soc. Jpn., 46 (1973) 3072.
13 V. Stara and M. Kopanica, Collect. Czech. Chem. Commun., 40 (1975) 3153.
14 M. Wojciechowski, Ph.D. Thesis, University of Warsaw, 1977.

Analytica Chimica Acta, 99 (1978) 115—124

AN ANALYTICAL STUDY OF METAL—THIOBARBITURIC ACID COMPLEXES

R. J. MURPHY and G. SVEHLA*

Department of Analytical Chemistry, The Queen's University, Belfast (U.K.)

(Received 21st February 1978)

SUMMARY

Polarography shows the formation of 2:1 and 4:1 copper(II)—thiobarbituric acid complexes. The formation of two further 1:1 and 1:2 copper(II)—2-thiobarbituric acid complexes in alkaline solution is indicated by amperometric titrations. The 1:2 complex has been confirmed by Job's Plots; co-ordinate bonding involving the sulphur atom of the 2-thiobarbituric acid has been shown by infra-red spectroscopy. Copper(II) can be determined by amperometric titration with 2-thiobarbituric acid. The reaction of nickel(II) with 2-thiobarbituric acid was examined polarographically; the existence of 2:1, 1:1, 1:2, and 1:6 nickel(II)—thiobarbituric acid complexes was suggested. A detailed study of 2-thiobarbituric acid complexes with cobalt and lead was not possible by polarographic methods; polarographic evidence of complex formation between zinc or cadmium and 2-thiobarbituric acid was not found. The effect of complex formation on the polarographic behaviour of 2-thiobarbituric acid has been examined.

Until the discovery [1—3] of the hypnotic properties of 5,5′-diethyl-barbituric acid little interest had been shown in barbiturates following the synthesis [4, 5] of barbituric acid in 1864. Similarly thiobarbituric acid and its derivatives were used as intermediates for the synthesis of 5,5′-dialkyl-barbituric acids until the anaesthetic properties of some thiobarbituric acids were discovered [6—8].

The anodic polarographic waves [9] shown by thiobarbiturates correspond to the formation of slightly soluble mercury compounds. Detailed polarographic and spectral investigations have been made of substituted thiobarbiturates [10], thiobarbiturates with substituents on the sulphur atom [11], and some amino and imino derivatives [12]. 2-Thiobarbituric acid dissociates in two steps; the first may be attributed to protonation of a nitrogen and the second to the formation of a carbanion-enolate or thiolate form [11]. The cathodic wave may be used for the determination of some substituted thiobarbiturates but anodic waves are necessary for the determination of unsubstituted 2-thiobarbituric acid and its 5-monoalkyl derivatives [10].

The reaction between divalent metal ions and unsubstituted 2-thiobarbituric acid was studied by polarographic and spectrophotometric methods. Details of the polarographic waves of these metal ions and the supporting electrolytes are shown in Table 1.

TABLE 1

Polarographic waves for the metal ions examined (2e reduction)

Depolarizer	Supporting electrolyte	$E_{\frac{1}{2}}$ vs. SCE (V)	Remarks[a]
Cu^{2+}	M Sodium acetate	—0.055	W, Rev.
Ni^{2+}	0.1 M Potassium chloride	—1.075	W, Irr.
Co^{2+}	0.1 M Potassium chloride	—1.20	W, Irr.
Pb^{2+}	M Ammonium chloride	—0.46	W, Irr.
Zn^{2+}	M Sodium acetate	—1.04	W, Irr.
Cd^{2+}	0.1 M Potassium chloride	—0.615	W, Irr.

[a]W = Well-defined. Rev = Reversible. Irr = Irreversible.

EXPERIMENTAL

Reagents

The 2-thiobarbituric acid, metal salts, and chemicals for supporting electrolytes were all of analytical grade.

Apparatus

The polarographic curves were recorded with a Polariter PO4 polarograph (Radiometer, Copenhagen) and drop-life timer. The dropping mercury electrode had the following characteristics: outflow velocity m = 2.62 mg s^{-1}; drop time t_1 = 1.0 s at the potential of the saturated calomel electrode; mercury pressure h = 50 cm. For amperometric studies, the facility for disconnecting the synchronization between the movement of the chart recorder and the potentiometer drum was used. This enabled the chart paper to be moved manually while applying a constant e.m.f.

An instrument similar in design to that described by Bezman and McKinney [13] was constructed and used in conjunction with a Hewlett-Packard 3310B Function Generator for cyclic voltammetric studies. A Hewlett-Packard 7035B X-Y recorder was used to record the cyclic voltammograms at low scan rates and a Hewlett-Packard 1201B Storage Oscilloscope at fast scan rates. A three-electrode, single-compartment cell (Metrohm) was fitted with a platinum foil auxiliary electrode, a saturated calomel reference electrode, and a micrometer-type hanging mercury drop electrode (all Radiometer).

For spectrophotometric studies the visible spectra were recorded with a Unicam SP 800 recording spectrophotometer; absorbance measurements for the method of continuous variations were made with a Coleman Model 55 u.v.—visible spectrophotometer. Infra-red studies were made with a Perkin-Elmer Model 700 spectrophotometer.

Experimental techniques

Polarographic studies. The appropriate supporting electrolyte (20 ml) and 2 drops of 0.4% Triton X-100 were de-aerated with nitrogen. An aliquot of

metal ion solution (usually 0.2 ml) was added and, after a brief flush with nitrogen, the *i*—*E* curves were recorded at a slow rate of scanning (100 mV min^{-1}) to reduce the effects of hysteresis of the recording instrument. Minimum damping was used and 70% blanking of the drop life to minimize the condenser current. Polarographic studies were carried out within the pH range 3—10.

Amperometric titrations. The polarograph was used in the mode already described. Aliquots (20 ml) of the metal ion in supporting electrolyte, adjusted to the required pH, were de-aerated with nitrogen and titrated with 2-thiobarbituric acid at a constant applied potential. To minimize dilution effects, the concentration of the 2-thiobarbituric acid was 20 times that of the metal ion. The titrant was added in either 0.025-ml or 0.05-ml increments from a 1-ml microburette. After each addition, the solution was well mixed by a stream of nitrogen and the chart turned manually so that 1 cm chart corresponded to 0.05 ml of titrant. The readings from the recorder chart were later plotted on a current—titrant volume graph.

U.v.—visible spectra. Spectra of the metal ion, 2-thiobarbituric acid, and the metal—thiobarbiturate complex were recorded at pH 8.0 to find the wavelength of maximum absorbance of the complex. Metal—thiobarbituric acid solutions of varying composition but of constant total concentration were prepared in 1 M sodium acetate and adjusted to pH 8.0. The maximum absorbance of the solutions was measured, usually within one minute after the addition of the metal ion solution. Care had to be taken to ensure that the absorbance of the more intensely coloured solutions was recorded before the formation of a finely divided blue precipitate which appeared rapidly in these solutions. After reaching a maximum, the absorbance of the weakly coloured solutions rapidly decreased. Job's method of continuous variations [14, 15] was applied to the results.

Infra-red spectra. The metal—thiobarbiturate complex, which formed as a finely divided precipitate at pH 8.0, was separated by centrifuging at 3000 rpm. It was washed with small volumes of distilled water and centrifuged after each washing. Finally the complex was vacuum-dried overnight at 30°C over silica gel. The i.r. spectra of the complex and 2-thiobarbituric acid were obtained by standard Nujol mull and potassium disc techniques (pressure, 12 tons; Beckmann-RIIC 25 ton hydraulic press).

RESULTS

Polarographic Studies

Copper(II) in 1 M sodium acetate solution gives a single well-defined reduction wave throughout the pH range investigated. The addition of 2-thiobarbituric acid gives no separate complex wave; the half-wave potential of the copper wave remains unchanged, but the wave decreases in size and becomes less well-defined (Fig. 1) as the thiobarbituric acid concentration is increased. The copper wave appears to reach a minimum and becomes too

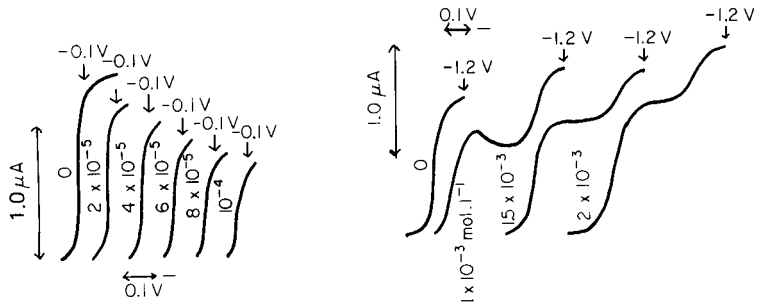

Fig. 1. The effect of increasing TBA concentration on the copper(II) wave. (2×10^{-4} mol l^{-1} Cu^{2+}; 1 M sodium acetate, pH 4.4.) The numbers on the curves indicate the TBA molarity.

Fig. 2. The effect of increasing TBA concentration on the polarographic waves of nickel(II) solutions. (2×10^{-4} mol l^{-1} Ni^{2+}; 0.1 M KCl, pH 9.) The numbers on the curves indicate the TBA molarity.

small and ill-defined to be measured accurately when the concentration of thiobarbituric acid is half that of copper. From plots of log $i/(i_d - i)$ against the applied potential, the copper waves were reversible throughout the pH range, alone and in the presence of increasing thiobarbituric acid concentration. The curves obtained from plots of i_d (Cu) against thiobarbituric acid concentration indicated the formation of one or more complexes; when log i_d (Cu) was plotted, segmented linear graphs were obtained. The results of the polarographic study of copper—thiobarbituric acid complexes are shown in Table 2.

In solutions of 0.1 M potassium chloride, nickel(II) produces a well-defined 2e reduction wave, which is irreversible throughout the pH range 3—10 (Table 2). On the addition of 2-thiobarbituric acid, a separate complex wave forms at ca. —0.60 V. This wave, also well-defined, increases as the nickel(II) wave height decreases (Fig. 2). The rate of growth of the complex wave depends on pH. The rate of increase in wave height of the complex is greater at high pH than at low pH with increasing thiobarbituric acid concentration. A rounded maximum, which quickly returned to the correct current level, was observed on the complex wave. Below pH 5.0 the complex wave is irreversible and the irreversibility increases with increasing thiobarbituric acid concentration. Above pH 5.0 the complex wave is reversible throughout the ligand concentration range. The half-wave potentials of the complex waves are shifted to more negative potentials with increasing ligand concentration. The measured half-wave potentials throughout the pH and thiobarbituric acid concentration range are shown in Table 3. The method of Lingane [16] was used to find the metal—ligand ratios (Table 2) throughout the pH range from this shift in $E_{\frac{1}{2}}$ value of the complex wave.

Cobalt(II) gives a single well-defined 2e reduction wave at —1.20 V in 0.1 M potassium chloride at pH 7.0. On the addition of 2-thiobarbituric acid, a

TABLE 2

Polarographic properties of copper(II) and nickel(II) in the presence of TBA

Metal	pH	$E_{\frac{1}{2}}$ metal (V)	$\frac{dE}{d \log [i/(i_d - i)]}$	Formation of metal: TBA complex indicated[a]				
				4:1	2:1	1:1	1:2	1:6
Cu(II)	4.4	−0.052	0.036	W	W	—	—	—
	4.8	−0.0535	0.031	W	W	—	—	—
	5.8	−0.0565	0.033	W	W	—	—	—
	6.5	−0.050	0.031	W	W	—	—	—
	7.0	−0.0535	0.031	W	W	—	—	—
	8.0	−0.061	0.031	W	W	—	—	—
	9.0	−0.0[illegible]	0.032	W	W	—	—	—
Ni(II)	3.0	−1.042	0.077	—	—	—	W	—
	4.0	−1.075	0.065	—	—	I	W	W
	5.0	−1.072	0.062	—	I	W	—	—
	6.0	−1.073	0.075	—	—	W	W	W
	7.0	−1.077	0.071	—	I	W	—	—
	8.0	−1.080	0.072	—	I	W	—	—
	9.0	−1.066	0.079	—	—	W	I	—
	10.0	−1.062	0.070	—	—	W	W	—

[a]W indicates a well-defined break and I an ill-defined break on the various plots.

TABLE 3

Variation of the half-wave potential (in V) of the Ni—TBA complex wave with pH at different TBA concentrations[a]

[TBA] ($\times 10^3$ mol l^{-1})	pH							
	3	4	5	6	7	8	9	10
0.05	—	−0.595	—	−0.653	−0.620	−0.650	−0.635	—
0.1	—	−0.622	−0.623	−0.622	−0.625	−0.632	−0.619	—
0.2	−0.532	—	−0.622	−0.623	−0.628	−0.640	−0.622	−0.640
0.5	−0.568	−0.652	−0.630	−0.634	−0.640	−0.637	−0.635	−0.635
0.75	−0.585	−0.651	−0.641	−0.637	−0.639	—	−0.638	−0.635
1.0	−0.582	−0.655	−0.642	−0.641	−0.647	−0.641	−0.645	−0.645
1.5	−0.603	−0.657	−0.649	−0.648	−0.645	−0.650	−0.647	−0.650
2.0	−0.605	−0.672	−0.650	−0.651	−0.653	−0.652	−0.650	−0.650
3.0	−0.619	−0.685	+	−0.653	−0.658	−0.651	−0.654	−0.657
4.0	−0.624	−0.697	+	−0.658	−0.667	−0.666	−0.655	−0.665
5.0	−0.632	−0.703	+	−0.663	−0.657	−0.668	−0.661	−0.664
6.0	−0.640	−0.714	+	−0.672	−0.670	−0.670	−0.670	−0.673
8.0	−0.647	−0.732	+	−0.688	+	−0.677	−0.665	−0.674
10.0	—	−0.755	+	−0.699	+	+	−0.672	−0.680
12.0	—	−0.765	—	—	—	—	−0.674	−0.683
14.0	—	−0.779	—	—	—	—	−0.682	−0.677

[a] — Half-wave potential not measurable. + Wave splits into two.

separate complex wave forms at —0.96 V at low ligand concentration. As the concentration of the ligand is increased, the height of the complex wave increases as the cobalt(II) wave diminishes.

The half-wave potential of the complex wave shifts to more negative potentials and quickly merges with the cobalt(II) wave, making accurate measurements of half-wave potentials and diffusion currents impossible.

In 1 M ammonium chloride, lead(II) gives a well-defined wave at —0.46 V; in 0.1 M sodium nitrate the half-wave potential of the metal is —0.39 V. In both cases, when the concentration of thiobarbituric acid was increased, the ligand wave, forming at about —0.3 V, became more negative with increasing concentration and quickly merged with the metal wave. Precipitation occurred in both supporting electrolytes when the ligand concentration was 4—8 times the metal concentration, depending on the pH.

Zinc gives a single well-defined irreversible wave with a half-wave potential of —1.04 V in 1 M sodium acetate solution. In 0.1 M potassium chloride, the wave produced by cadmium has a half-wave potential of —0.615 V. Under the experimental conditions used, there was no polarographic evidence of complex formation between these metals and 2-thiobarbituric acid.

2-Thiobarbituric acid also gives a single wave with a half-wave potential between —0.3 V and —0.5 V in 0.1 M potassium chloride and two waves at low concentrations with half-wave potentials between —0.2 V and —0.5 V in 1 M sodium acetate. The half-wave potential becomes more negative with increasing concentration. This tendency was noted also in the presence of metal ions (Fig. 3).

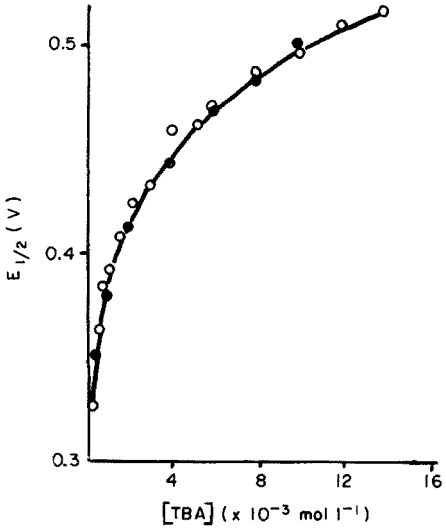

Fig. 3. Variation of the half-wave potential of TBA with concentration. (•) TBA alone; (○) TBA in complex with Ni^{2+}. pH 4 in both cases.

Study of complex formation by amperometric titrations

Amperometric titrations were carried out to gain further information about the rapid decrease in the copper(II) wave in the presence of low concentrations of 2-thiobarbituric acid. Current measurements were made at —0.10 V and current—titrant volume graphs were plotted. Aliquots (20 ml) of 0.0005 M Cu(II) were titrated with 0.01 M thiobarbituric acid throughout the range pH 3—10. The end-points were obtained as the points of intersection of the linear portions of the graphs. All current measurements were corrected for dilution. Figure 4 shows a typical amperometric titration curve.

The results in Table 4 show that only polynuclear complexes exist in acid solution whereas the mononuclear and 1:2 Cu(II)—TBA complexes predominate in alkaline solutions. The formation of the single binuclear complex at pH 3.0 provides the basis for a method of determining copper(II) (see below).

Spectrophotometric studies

Spectrophotometric studies showed that the copper(II)—TBA complex absorbs in the entire visible range with a very broad maximum at 690 nm. A mixture of 4×10^{-4} mol l^{-1} copper(II) and 6×10^{-4} mol l^{-1} TBA at pH 8 displays an absorbance of ca. 0.8 with 1-cm cells at 690 nm. Under similar conditions the absorbance of 10^{-3} mol l^{-1} copper(II) and 10^{-3} mol l^{-1} TBA solutions alone is negligible. These complex formation reactions were therefore studied by the method of continuous variations. A typical Job's plot is shown in Fig. 5. Results obtained at other concentration levels are summarized

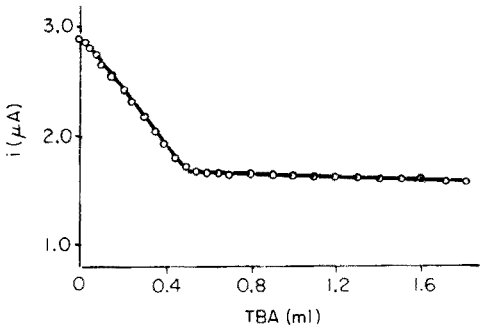

Fig. 4. Amperometric titration curve of 20 ml of 5×10^{-4} mol l^{-1} copper(II) sulphate with 10^{-2} mol l^{-1} TBA solution at pH 3 and —0.1 V vs. SCE.

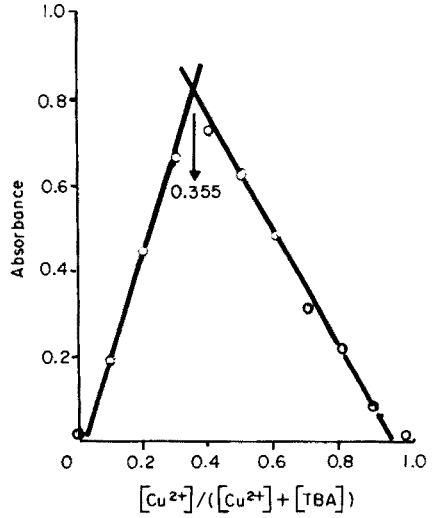

Fig. 5. Job's plots from spectrophotometric data. The absorbance of the Cu—TBA complex was measured in 1-cm cells at 690 nm, at pH 9. The total concentration of copper and TBA is 10^{-3} mol l^{-1}.

TABLE 4

Cu(II)—TBA complexes found by amperometric titrations (W, Well-defined; I, ill-defined; —, absent).

pH	Composition of the complexes[a] (Cu(II): TBA)			
	4:1	2:1	1:1	1:2
3.0	—	W	—	—
4.0	W	W	—	—
5.0	W	W	—	—
6.0	W	W	—	—
7.0	W	I	I	W
8.0	W	I	W	W
8.5	—	W	W	W
9.0	—	—	W	W
9.5	Readings		W	W
10.0	unsteady		W	W

[a] 4:1 complex corresponds to 0.25 ml 0.01 M TBA at end-point; 1:2 complex corresponds to 2.00 ml 0.01 M TBA at end-point.

in Table 5, confirming the existence of the 1:2 complex suggested by the results of amperometric titration. The results obtained at wavelengths other than 690 nm (Table 6) indicate that this is the only coloured complex present in the solution.

The most conspicuous difference between the infra-red spectra of TBA and the complex is displayed in the 1160—1170 cm^{-1} region (Table 7). TBA alone absorbs strongly here, but the absorption band virtually disappears from the spectrum of the complex. The bands near 1100 cm^{-1} in the TBA spectrum can be assigned as C=S stretching frequencies; their disappearance is obviously due to the coordination of copper to the sulphur atom. Yamaguchi et al. [17] found a similar effect with i.r. spectra of thiourea complexes and attributed it partly to the change in the nature of the C—N bonds because of the coordination to the nitrogen atom. This interpretation has been applied in a study of substituted thiobarbiturates [18].

TABLE 5

Summary of results obtained from Job's plots

$c_{Cu^{2+}} + c_{TBA}$ (mol l^{-1})	$c_{Cu^{2+}}/(c_{Cu^{2+}} + c_{TBA})$ at maximum	Mole ratio Cu: TBA in complex
6×10^{-4}	0.36	1:1.78
10^{-3}	0.355	1:1.82
1.5×10^{-3}	0.35	1:1.86
2×10^{-3} (P)[a]	0.38(P)	(1:1.63)

[a] Precipitation occurs rapidly in the intensely coloured solution at this concentration.

TABLE 6

Results obtained from Job's plots at different wavelengths for $[Cu^{2+}] + [TBA] = 10^{-3}$ mol l^{-1}

Wavelength (nm)	$c_{Cu^{2+}}/(c_{Cu^{2+}} + c_{TBA})$ at maximum	Mole ratio Cu: TBA in complex
670	0.355	1:1.82
690	0.355	1:1.82
710	0.36	1:1.78

TABLE 7

Absorption maxima (in cm^{-1}) of thiobarbituric acid and the copper(II)—thiobarbituric acid complex (KBr disc)
(S Strong; M medium; W weak; VW very weak; SH shoulder; B broad.)

TBA	Cu(II)—TBA	TBA	Cu(II)—TBA	TBA	Cu(II)—TBA	TBA	Cu(II)—TBA
3450 WB	3400 SB	1620 W	—	1360 M	1370 M	1030 SH	1030 M
3130 M	3150 SH	1575 M	1570 M	1305 W	1310 W	940 M	980 W
2900 M	—	1440 W	1430 W	1280 W	1270 SH	830 M	820 SH
1750 M	—	1410 VW	—	1250 M	1235 W	780 SH	790 W
1655 M	1635 M	1390 W	1390 SH	1170 S	—	725 W	710 SH

Determination of copper with TBA as amperometric titrant

The sharp and stoichiometric end-point obtainable by amperometric titrations can be used as a basis for the determination of 2—20 μmol (0.1—1 mg) of copper. The test solution is mixed with an equal volume (but at least 5 ml) of 1 M sodium acetate, the pH is adjusted to ca. 3 with 2 M hydrochloric acid, 2 drops of 0.4% Triton X-100 are added and the solution is titrated with aqueous 0.01 M TBA solution; the diffusion current is monitored at —1.0 V DME potential. The end-point is marked by a sharp break in the titration curve (cf. Fig. 4); 1 ml of 0.01 M TBA corresponds to 1.2708 mg copper. The titrant can be standardized against analytical-grade copper sulphate.

TABLE 8

Determination of copper by amperometric titration with TBA

Copper taken (mg)	0.01 M TBA consumed (ml)	Copper found (mg)	Error (%)
0.127	0.053	0.135	+6.2
0.318	0.132	0.335	+5.3
0.477	0.188	0.478	+0.2
0.635	0.255	0.648	+2.0
0.953	0.376	0.956	+0.3
1.271	0.498	1.266	—0.4

The results are accurate for this concentration level (Table 8). Interference studies showed that equal amounts of nickel, cobalt(II), lead(II), zinc, barium and iron(II) do not interfere with the determination at the 10-μmol level, but manganese(II) and cadmium cause serious distortions in the titration curves.

REFERENCES

1 E. Fischer and J. von Mering, Ther. Gegenwart, 44 (1903) 97.
2 E. Fischer and J. von Mering, Ther. Gegenwart, 45 (1904) 145.
3 K. Hoesch, Emil Fischer sein Leben und sein Werk, Ber. (Sonderheft), 54 (1921) 241.
4 A. Baeyer, Ann. Chem., 127 (1863) 199.
5 A. Baeyer, Ann. Chem., 130 (1864) 129.
6 E. Miller, J. C. Munch and F. S. Crossley, Science, 81 (1935) 616.
7 D. L. Tabern and E. H. Volwiler, J. Am. Chem. Soc., 57 (1935) 1961.
8 E. Miller, J. C. Munch, F. S. Crossley and W. H. Hartung, J. Am. Chem. Soc., 58 (1936) 1090.
9 P. Zuman, Collect. Czech. Chem. Commun., 20 (1955) 649, 876, 883.
10 W. F. Smyth, G. Svehla and P. Zuman, Anal. Chim. Acta, 52 (1970) 463.
11 W. F. Smyth, G. Svehla and P. Zuman, Anal. Chim. Acta, 52 (1970) 129.
12 W. F. Smyth, P. Zuman and G. Svehla, J. Electroanal. Chem., 30 (1971) 101.
13 R. Bezman and P. S. McKinney, Anal. Chem., 41 (1969) 1560.
14 I. Ostromisslensky, Chem. Ber., 44 (1911) 268.
15 P. Job, Ann. Chim. (Paris), 9 (1928) 113; 6 (1936) 97.
16 J. J. Lingane, Chem. Rev., 29 (1941) 1.
17 A. Yamaguchi, R. B. Penland, S. Mizushima, T. J. Lane, C. Curran and J. V. Quaghano, J. Am. Chem. Soc., 80 (1958) 527.
18 V. Nikolasev, J. Szabo and J. Morvay, Glas. Hem. Drus., Beograd, 36 (1971) 161.

Analytica Chimica Acta, 99 (1978) 125—132

INFLUENCE DE L'OXYGENE EN SPECTROMETRIE D'ABSORPTION ATOMIQUE AVEC UTILISATION D'UN FILAMENT DE GRAPHITE ET MISE EN EVIDENCE A L'AIDE D'UNE CELLULE A DOUBLE FLUX GAZEUX

G. GUIOCHON

Ecole Polytechnique, Laboratoire de Chimie Analytique Physique, Route de Saclay, 91120 Palaiseau (France)

B. HIRCQ* et C. TAILLAND

Commissariat à l'Energie Atomique, B.P. 561, 92542 Montrouge Cedex (France)

(Reçu le 16 janvier 1978)

RÉSUMÉ

Après description d'une cellule d'absorption atomique avec utilisation d'un filament de graphite, l'influence, sur le signal d'absorption, de la distance du filament au faisceau de mesure est étudiée dans le cas du zinc et du cuivre. La concentration en oxygène est ensuite évaluée en fonction de cette distance et du débit d'argon, et l'influence de l'oxygène est mise en évidence à l'aide d'une cellule à double flux gazeux. L'introduction d'un flux externe crée une barrière de diffusion pour l'oxygène ce qui permet de diminuer le phénomène d'oxydation et d'obtenir un gain de sensibilité en fonction du débit extérieur.

SUMMARY

The influence of oxygen in graphite-rod atomic absorption spectrometry. A study with a double argon-flow cell

An atomic absorption cell with a graphite filament is described. The influence on the absorption signal of the distance of the filament from the optical beam is studied with zinc and copper. The oxygen concentration is then evaluated as a function of this distance and of the argon flow. The influence of oxygen is proved with a double argon flow cell; the external flow forms a diffusion barrier for oxygen and a sensitivity gain is observed as a function of that flow.

Parmi les nombreux systèmes sans flamme utilisés en spectrophotométrie d'absorption atomique, nous nous sommes orientés vers un procédé permettant de réaliser l'atomisation à l'aide d'un filament métallique ou en graphite [1—3], comme d'autres auteurs [4—8]. Dans un premier temps, ces procédés ont seulement permis de constater les effets de l'atomisation sans définir dans l'espace le "nuage atomique" responsable de l'absorption d'énergie. Depuis, certains auteurs [9—15] ont élaboré un modèle théorique définissant le processus de transfert des atomes en fonction du temps. Dans notre cas [3], nous avons étudié la répartition de concentration et les dimensions du

nuage atomique en fonction des différents paramètres expérimentaux: volume de solution déposée, prise d'essai pondérale, distance du générateur d'atomes au faisceau de mesure (h), température d'atomisation et débit d'argon. En particulier, la cellule utilisée nous a permis de constater et d'évaluer les effets de la diffusion atomique dans l'espace, ce qui entraîne une perte de sensibilité.

Afin de mieux comprendre certains phénomènes, il nous a paru intéressant, d'une part, d'évaluer la diffusion de l'oxygène de l'air ambiant en fonction du débit d'argon et de la distance h et d'autre part, de mettre en évidence son influence à l'aide d'une cellule à double flux gazeux.

PARTIE EXPERIMENTALE

Description de l'appareillage

Nous ne rappelons que le schéma de principe (Fig. 1) de l'installation décrite précédemment [3]. Le spectrophotomètre utilisé est un appareil Perkin-Elmer modèle 303 légèrement modifié afin d'obtenir un faisceau lumineux plus étroit et une meilleure focalisation. Le générateur d'atomes constitué d'un filament de graphite (charbon spectroscopique qualité RWO) ayant un diamètre de 1 mm et une longueur de 10 mm, est tenu par deux tiges de tungstène. Le chauffage par effet Joule est réalisé à l'aide d'une alimentation basse-tension permettant d'imposer trois paliers thermiques.

Mode opératoire

Toutes les prises d'essai sont de 1 μl en milieu nitrique et elles sont déposées sur le centre du filament à l'aide d'une microseringue. Après une période de séchage de 10 s à environ 100°C, suit une période de préchauffage à 600°C environ pendant 5 s, puis la période d'atomisation: la vapeur atomique est entrainée par un courant d'argon sur le trajet optique du spectrophotomètre, et il en résulte une absorption d'énergie qui se traduit sous la forme d'un pic par enregistrement en fonction de temps.

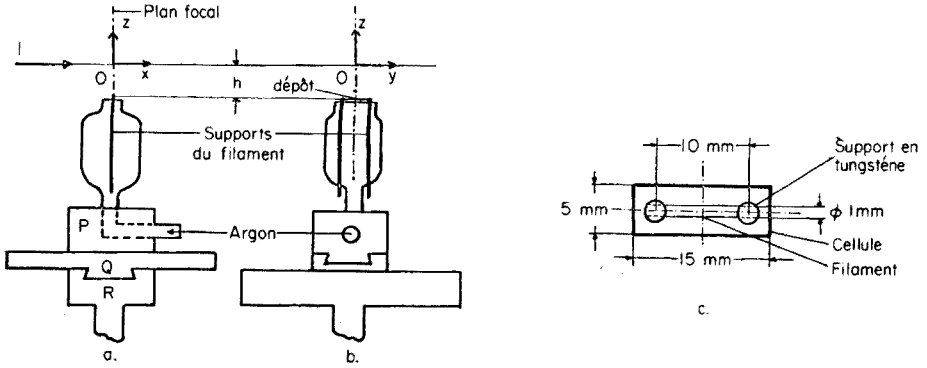

Fig. 1. Schéma du générateur d'atomes et de son support permettant de fixer les coordonnées du dépôt par rapport au faisceau lumineux par l'intermédiaire des pièces P, Q et R. Système vu de face (a), de profil (b), détail du générateur d'atomes vu de dessus (c).

Dans tous les cas, le plan vertical contenant le faisceau de mesure est perpendiculaire au filament et passe par le centre du dépôt.

Les longueurs d'onde respectivement utilisées pour le zinc, le cuivre et le chrome sont de 213,9; 324,7 et 357,9 nm.

RESULTATS ET DISCUSSION

Influence de la distance h *du filament au faisceau de mesure sur le signal*

Les mesures ont été effectuées avec 0,5 ng de zinc en utilisant 4 conditions de débit d'argon—température d'atomisation: 1. 140 ml min^{-1}, 1500°C; 2. 740 ml min^{-1}, 1500°C; 3. 140 ml min^{-1}, 2000°C; 4. 740 ml min^{-1}, 2000°C.

Chaque point des courbes de la Fig. 2 représente la moyenne de 8 mesures donnant un écart-type relatif inférieur à 5%.

Nous constatons dans tous les cas que le signal décroit en fonction de *h*. Cette décroissance est en partie justifiée par une dilution du nuage que nous avons précédemment mise en évidence[3]. Le signal optimum est obtenu lorsque *h* tend vers une valeur nulle et il est supérieur lorsque le débit est plus faible, pour une même température. Nous avons, en outre, comparé cette décroissance du signal en fonction de *h* pour deux éléments différents, à savoir le cuivre et le zinc. Les quantités de zinc et de cuivre respectivement déposées sont de 0,1 et 5 ng de façon à obtenir un signal optimum comparable. Les valeurs du débit d'argon et de la température d'atomisation sont de 740 ml min^{-1} et de 2000°C environ pour les deux éléments.

Nous constatons sur la Fig. 3 qu'en fonction de *h*, le signal décroit plus fortement dans le cas du cuivre: en particulier, les rapports des signaux

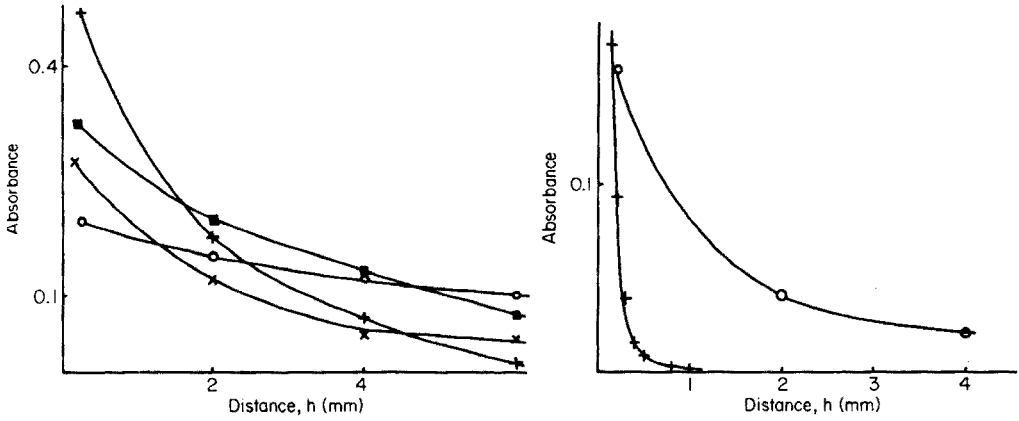

Fig. 2. Variation de l'absorbance en fonction de la distance *h* du filament au faisceau de mesure avec un dépôt de 0,5 ng de Zn, pour différentes valeurs du débit d'argon et de la température d'atomisation: 140 ml min^{-1}, 1500°C (+); 740 ml min^{-1}, 1500°C (▪); 140 ml min^{-1}, 2000°C (×); 740 ml min^{-1}, 2000°C (○).

Fig. 3. Variation de l'absorbance en fonction de la distance *h* du filament au faisceau de mesure: avec un dépôt de 0,1 ng de Zn (○), avec un dépôt de 5 ng de Cu (+). .

obtenus pour des valeurs de h de 0,5 et 0,2 cm sont respectivement de 0,10 et 0,75 pour le cuivre et le zinc. La décroissance du signal ne peut donc être totalement justifiée par un phénomène de dilution qui serait beaucoup plus important dans le cas du cuivre: en effet, les différences de dimensions du nuage observées [3] en fonction de la prise d'essai pondérale (seul paramètre qui diffère dans notre cas), ne justifient pas le phénomène observé. La différence entre les décroissances est donc liée aux propriétés de l'élément et en particulier, la cinétique d'oxydation du cuivre étant plus favorable, il est logique de penser qu'à la dilution atomique se superpose une oxydation par diffusion de l'oxygène de l'air dans la veine d'argon.

Mise en évidence de l'influence de l'oxygène à l'aide d'une cellule à double flux gazeux

La cellule à double flux (Fig. 4) comporte une partie intérieure analogue dans le principe à la cellule décrite précédemment et elle permet de créer un flux gazeux externe entourant le flux interne d'argon. Ce flux externe peut ainsi constituer un film protecteur servant de barrière à la diffusion de l'air, à condition d'avoir une vitesse assez grande tout en restant en écoulement laminaire.

Dans un premier temps, nous avons évalué la concentration en oxygène dans la veine d'argon sans faire intervenir un flux externe (ce qui nous place dans des conditions analytiques comparables à celles utilisées auparavant) qui nous permettra ensuite de mettre en évidence l'influence de l'oxygène.

Evaluation de la concentration en oxygène en fonction du débit interne d'argon D. Nous l'avons évaluée en dosant d'abord le gaz carbonique par coulométrie. Ensuite, connaissant le rapport des concentrations en oxygène et gaz carbonique, nous en avons déduit la concentration en oxygène.

Le prélèvement gazeux effectué dans la veine d'argon à l'aide d'une aiguille de 1 mm de diamètre intérieur placée verticalement et reliée à l'aide d'un tube souple à la cellule de coulométrie par l'intermédiaire d'une pompe péristaltique, correspond à un volume de 120 ml. Les mesures ont été effectuées avec un coulomètre Strohlein "Coulomat 7000". Le point de

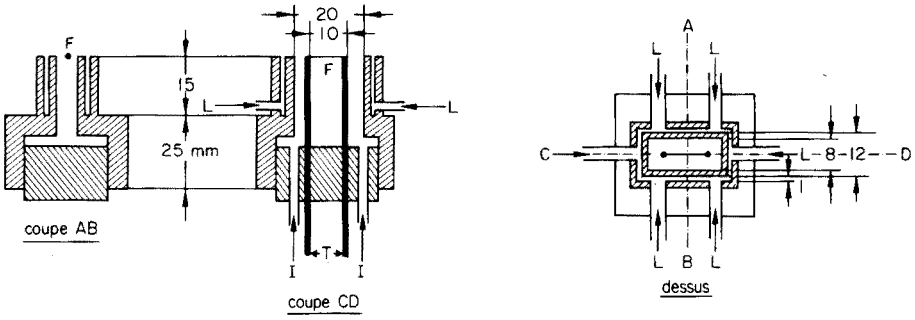

Fig. 4. Schéma de la cellule à double flux. Filament de graphite (F), tiges de support 3 mm (T), arrivées latérales du gaz (L), arrivées internes d'argon (I).

prélèvement est situé à 1 mm au dessus du point correspondant au dépôt sur le filament (x et $y = 0$, $h = 1$ mm). Dans ces conditions, nous avons fait varier D de 600 à 3000 ml min^{-1}.

Conjointement, une analyse par chromatographie en phase gazeuse a été effectuée sur une éprouvette incluse dans le circuit de prélèvement et correspondant à un débit de 160 ml min^{-1}. Le rapport des concentrations pondérales O_2/CO_2 ainsi déterminé est de 350. Nous avons évalué la concentration en O_2 à partir de ce rapport, en négligeant la variation du rapport des coefficients de diffusion de O_2 et CO_2 en fonction de la composition de la veine d'argon.

Les résultats récapitulés sur le Tableau 1 nous montrent que la teneur en O_2 est considérable pour des débits inférieurs à 1 l min^{-1}. Ceci nous explique en partie, la nécessité d'opérer avec un débit plus important afin d'obtenir le maximum de sensibilité avec les éléments dont les oxydes sont difficilement réductibles et pourquoi l'oxydation de l'échantillon peut être très rapide malgré les précautions prises.

Evaluation de la concentration en oxygène en fonction de la distance h. Les mesures ont été effectuées dans les mêmes conditions (x et $y = 0$) avec un débit D de 1 l min^{-1}, en faisant varier h de 0 à 10 mm.

Nous observons sur le Tableau 2 une augmentation importante de la concentration en oxygène en fonction de h. D'autre part, nous avons observé que la concentration augmentait plus, toutes proportions gardées, en fonction de h pour les débits d'argon faibles: c'est pourquoi, la décroissance du signal est moins importante en fonction de h pour les débits d'argon plus élevés (Fig. 2).

Influence du débit extérieur sur la concentration en oxygène au niveau de mesure. Les mesures ont été effectuées dans les mêmes conditions (x et $y = 0$) avec un débit interne d'argon de 1 l min^{-1} (soit une vitesse moyenne de 10 cm s^{-1} à la sortie de la cellule), un débit d'argon externe variant de 0 à 15 l min^{-1} pour 2 distances h de 0 et 5 mm.

Dans les deux cas, nous observons sur le Tableau 3 une forte diminution de la concentration en oxygène pour un débit externe supérieur à 2 l min^{-1},

TABLEAU 1

Influence du débit d'argon D sur la concentration C en oxygène au niveau de mesure

D (ml min^{-1})	600	720	1000	1400	2000	3000
C (μg ml^{-1})	26	20	9	7	4	4

TABLEAU 2

Etude de la concentration C en oxygène en fonction de la distance h du filament au niveau de mesure avec un débit d'argon D de 1 l min^{-1}

h (mm)	0	5	7	10
C (μg ml^{-1})	10	33	66	103

TABLEAU 3

Influence de débit extérieur D_e sur la concentration C en oxygène pour 2 valeurs de la distance h du filament au niveau de mesure

D_e (l min^{-1})	0	1	2	3—7	10	12	15
C (μg ml^{-1})	10	3	<2	<2	10	20	33
h = 0							
C (μg ml^{-1})	33	16	3	<2	21	35	53
h = 5 mm							

ce qui représente une vitesse moyenne de 44 cm s^{-1} du film extérieur à la sortie de la cellule. Nous observons, en outre, que la diminution de la concentration en oxygène est plus importante, toutes proportions gardées, pour une valeur de h plus élevée.

Par contre, pour des débits externes supérieurs à 8 l min^{-1} (soit une vitesse moyenne de 175 cm s^{-1}), nous observons une augmentation de la concentration en oxygène qui correspond à l'apparition d'un régime de turbulence, supprimant ainsi la barrière de diffusion.

Mise en évidence de l'influence de l'oxygène. Afin de confirmer l'hypothèse d'une corrélation entre la décroissance du signal et la présence d'oxygène, des essais ont été réalisés avec la cellule à double flux, dans le cas du chrome, avec lequel le signal d'absorption disparait lorsque la distance h est supérieure à 3 mm, sans film extérieur. Les conditions opératoires sont les suivantes: débit d'argon intérieur 1,8 l min^{-1}; température d'atomisation 2500°C environ; h 1 mm; longueur d'onde 357,9 nm; prise d'essai 0,5 ng (1 μl).

Nous observons sur la Fig. 5, qu'en fonction du débit extérieur qui varie de 0 à 8 l min^{-1}, le signal augmente en passant par un optimum pour un débit extérieur de 3,5 l min^{-1} environ et qui correspond à un gain d'un facteur 2,5. Pour les débits plus importants, nous observons une décroissance et un manque de reproductibilité qui sont liés à l'apparition du régime de

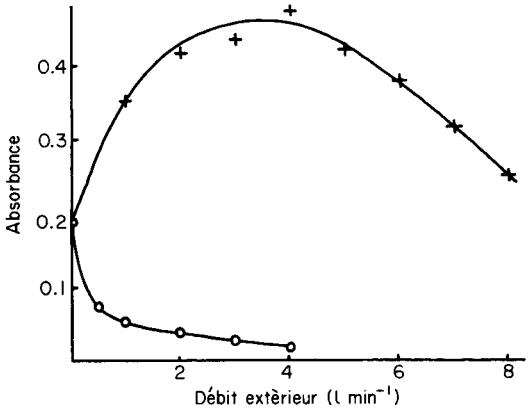

Fig. 5. Variation de l'absorbance en fonction du débit extérieur avec 0,5 ng de Cr avec un débit extérieur d'argon (+), avec un débit extérieur d'oxygène (○).

turbulence qui entraine des apports en oxygène et perturbe la géométrie du nuage atomique. Globalement, nous observons donc une corrélation entre la concentration en oxygène et le signal d'absorption. D'autres essais ont été effectués pour des distances h supérieures et pour lesquelles, sans débit extérieur, nous n'observons aucun signal ($3 < h < 6$ mm). L'introduction d'un débit extérieur permet alors de "recréer" un signal.

D'autre part, afin de vérifier que ce gain de sensibilité n'était pas dû seulement à une diminution de la dilution du nuage atomique sous l'influence du flux externe, nous avons remplacé l'argon du film externe par de l'oxygène. Nous observons sur la Fig. 5 que le signal décroît alors rapidement lorsque le débit externe d'oxygène augmente, ce qui confirme l'hypothèse.

Des essais comparables ont été effectués dans le cas du cuivre et nous avons noté les mêmes phénomènes, mais avec des gains de sensibilité moins importants pour une même valeur de h. Ceci signifie que la concentration en oxygène est dans ce cas un facteur moins critique.

La présence d'oxygène entraîne au niveau du filament, une formation d'oxyde de carbone. Ce dernier peut jouer un rôle de réducteur dans la mesure où la distance h est faible, c'est à dire si l'élément ne peut être réoxydé avant la mesure. En fait, nous observons la somme des deux phénomènes antagonistes de réduction et d'oxydation, qui pour une distance h, est certainement fonction du rapport des concentrations en oxygène et en oxyde de carbone. Dès que h croît, il est certain que la réaction de réduction doit être relativement négligeable par rapport à l'oxydation par l'oxygène provenant de la diffusion.

Sur un plan général, ce type de cellule à double flux permet un gain de sensibilité qui est certainement perfectible en fonction de la position et de l'axe de déplacement du flux externe. En effet, dans la mesure où il est correctement orienté, il doit pouvoir contribuer à diminuer les dimensions du nuage et donc la dilution atomique. Il possède, en outre, l'avantage par rapport à un système isolant avec faces de quartz, de ne pas absorber d'énergie lumineuse et d'éviter les phénomènes de condensation. Ce modèle de cellule est aussi intéressant pour le dosage des éléments dont la longueur d'onde d'absorption se situe dans le domaine du visible et pour lesquels il est nécessaire de travailler avec des valeurs de h plus importantes.

BIBLIOGRAPHIE

1 B. Hircq, 3ème Cong. Int. de Spectrométrie d'Absorption et Fluorescence Atomique, Paris 1971 (CISAFA), résumés des communications N° 209, Gams, Paris, 1971.
2 B. Hircq, Spectrochim. Acta Part B, 31 (1976) 153.
3 B. Hircq, Spectrochim. Acta Part B, 31 (1976) 317.
4 J. Aggett et T. S. West, Anal. Chim. Acta, 55 (1971) 349.
5 T. S. West et X. K. Williams, Anal. Chim. Acta, 45 (1969) 27.
6 J. F. Alder et T. S. West, Anal. Chim. Acta, 51 (1970) 365.
7 M. D. Amos, P. A. Bennett, K. G. Brodie, P. W. Y. Lung et J. P. Matousek, Anal. Chem., 43 (1971) 211.
8 M. Williams et E. H. Piepmeier, Anal. Chem., 44 (1972) 1342.

9 G. Tessari et G. Torsi, Anal. Chem., 46 (1974) 1032.
10 G. Tessari et G. Torsi, Anal. Chem., 47 (1975) 842.
11 C. Fuller, Analyst, 99 (1974) 739.
12 C. Fuller, Analyst, 100 (1975) 229.
13 D. J. Johnson, B. L. Sharp et T. S. West, Anal. Chem., 47 (1975) 1234.
14 G. Torsi et G. Tessari, Anal. Chem., 47 (1975) 839.
15 G. Torsi et G. Tessari, Anal. Chem., 48 (1976) 1318.

Analytica Chimica Acta, 99 (1978) 133—141

MULTIELEMENT ANALYSIS OF LAKE SEDIMENTS BY NEUTRON ACTIVATION ANALYSIS

R. A. NADKARNI and G. H. MORRISON*

Department of Chemistry, Cornell University, Ithaca, N.Y. 14853 (U.S.A.)

(Received 1st February 1978)

SUMMARY

By combining instrumental and radiochemical neutron activation analysis, up to 47 elements including major, minor, and trace elements, have been determined in lake sediment samples. Instrumental neutron activation involving both short and long irradiations is used to determine 40 elements including most of the environmentally important ones. A radiochemical separation procedure allows the determination of 7 noble metals. The accuracy and precision of the method are 5—10%.

A knowledge of naturally occurring metals in the environment is necessary for the evaluation of Man's impact on the environment. Exploration and environmental geochemists both investigate the same types of areas but with different motivations. Lake sediments act as major sinks for the incoming materials and provide an excellent source for obtaining information for both groups of investigators.

If the rate of deposition of sediments is known, it is possible from sediment core samples to differentiate between natural or background levels and anthropogenic deposition levels. Among the contributors to the metal composition of lake sediments are large-scale mining and minerals processing, domestic and industrial sewage effluents, algicides, herbicides, fertilizers, domestic detergents overflow, and airborne particulate fallout from power plants and automobile exhaust [1].

Thus, the problem of metal pollution in lakes is primarily concerned with complex interactions between particulate matter and water. By analyzing lake sediments it is possible to determine the source, distribution, and possible hazards of metal contamination. The accumulation of some trace elements has been studied by analyzing sediment cores from lakes in Wisconsin [2, 3], Lake Michigan [4], Lake Superior [5], Western Michigan lakes [6], Lake Peoria, Illinois [7], Lake Ontario [8], Lake Erie [9], Lake Huron [10], Lake Washington [11, 12], Lake George [13], and Chautaugua, N.Y. [14]. Sediments from rivers and coastal areas have also been studied and these include the Northern Adriatic Sea [15], Southampton Water [16], the Mediterranean Sea [17], Canadian rivers [18], Puget Sound, Wash. [19], the Rhine delta in the Netherlands [20], the Ems delta in Germany [20],

the Chao Phya delta in Thailand [20], the Isar River in Bavaria [21], and the Saronikos Gulf in Greece [22].

The analytical techniques used in the above studies were confined to either atomic absorption spectrometry (a.a.s.) [3, 9, 11, 16—18] or neutron activation analysis (n.a.a.) [5, 14, 15, 19—23], with only one study based on x-ray fluorescence spectrometry [9]. The technique of a.a.s. is amenable to only single-element determination so that these studies have been limited to the total determination of no more than 9 elements sequentially. In addition, the sediment samples must be brought into solution for analysis.

Neutron activation analysis is ideally suited for multielement analysis of sediment samples. Instrumental neutron activation analysis (i.n.a.a.) without any chemical separations is the choice of most analysts, although limited work on n.a.a. of sediments together with radiochemical separations has been performed [24]. Thermal neutron activation in a reactor is the preferred irradiation source; however, 14-MeV neutrons from a Cockcroft—Walton accelerator [25] and a ^{252}Cf isotopic source for in situ analysis [26] have also been used. These latter two sources suffer from the limited number of elements that can be determined. The i.n.a.a. methods published so far have involved the determination of 10—20 elements in various sediment samples [5, 14, 15, 19—23].

This study presents an i.n.a.a. method for the determination of up to 40 elements including 7 major elements, 11 rare earth elements (REE) and 22 other trace elements in sediments. In addition, a radiochemical n.a.a. method is presented which provides information on 7 noble metals in sediment samples. Over 24 sediment samples have been analyzed by this method.

Similar i.n.a.a. methods have been developed in this laboratory in the past to determine trace elements in biological materials [27], sludges [28], and human blood serum [29]. The radiochemical method has been used to determine noble metals in rocks [30, 31]. The sediment samples analyzed in this investigation were from lakes in two areas in Northeastern U.S.: the Adirondack Mountains in northern New York State and the Hubbard Brook Experimental Forest in the White Mountains in the State of New Hampshire. Both of these areas are remote from population centers and are well suited for long-term in-depth studies of hydrology, biogeochemistry, and ecology [32].

EXPERIMENTAL

Samples and standards

The sediment samples were dried at 100°C overnight and powdered in an agate mortar before analysis. For irradiation, 100—400 mg of samples were sealed in high-purity polyethylene (for short irradiation) or quartz (for longer irradiation) containers. U.S. Geological Survey standard diabase rock W-1 was used as the irradiation elemental standard. Where concentrations of elements in W-1 are not well characterized, such as As, Br, and Zn, synthetic

standards were prepared by drying aliquots of standard solutions on "Specpure" SiO_2. Similar synthetic standards were used for the determination of the noble metals.

Irradiation

The irradiations were performed at the Cornell TRIGA Mark II nuclear reactor in a thermal neutron flux of $1-3 \times 10^{12}$ n cm^{-2} s^{-1}. Samples were irradiated for 2 min in the pneumatic rabbit tube first and counted immediately after the end of the irradiation up to 2—3 h. Another aliquot of sample was irradiated for 8 h in the central thimble facility. This set was allowed to decay overnight and then sequentially counted from 2 to 30 days at flexible intervals.

Radiochemical separation

After overnight decay of the 8-h irradiated samples, they were dissolved by alkali peroxide fusion in the presence of noble metals carriers. The solutions, adjusted to pH 1.5, were passed through ion-exchange columns of Srafion NMRR resin, which were washed with 0.05 M HCl. The resin phase was used for noble metals measurement. Further details of the radiochemical separation are published elsewhere [30, 31].

Data processing

All the samples were counted with a coaxial 56-cm^3 Ge(Li) detector and a 4096-channel pulse-height analyzer. The system resolution was 1.96 keV (FWHM), with a peak-to-Compton ratio of 37:1, and a counting efficiency of 13%, all compared to the 1.332-MeV photopeak of ^{60}Co. The data from the analyzer were stored on a 9-track magnetic tape and later processed on a PDP 11/20 computer. The final output was in the form of digital tables of input data, peak locations, and calculated peak areas corrected for background. The peaks of interest were then corrected for decay when necessary. The identification of the isotopes was based on the observed γ-peaks, peak energy, relative intensity of associated peaks, and where feasible, the half-lives.

RESULTS AND DISCUSSION

With the i.n.a.a. method, it was possible to determine at least 40 elements in the sediment samples. These include 7 majors, 11 REE, and 22 other trace elements, comprising elements of environmental interest such as Al, As, Ba, Br, Cl, Co, Cr, Cu, Fe, Mn, Ni, Sb, Se, Th, Ti, U, V, and Zn. Table 1 gives the nuclear data for the elements determined in the sediments. All of the isotopes listed in Table 1 were not necessarily found in all of the sediments. This is a function of the concentration of elements of interest and the γ-ray activity produced from highly activated elements present in the sediment such as Al, Mg, Mn, Na, K, Br, Sm, and Sc. The footnotes to Table 1 include various interfering nuclear reactions and corrections that had to be made for these interferences.

TABLE 1

Nuclear data for elements determined in sediments

Isotope	Half-life	Best γ-ray for measurement, keV	Best time for measurement
2-min irradiation			
^{28}Al[a]	2.3 m	1778	2—10 m
^{52}V	3.75 m	1434	
^{66}Cu[b]	5.2 m	1039	
^{51}Ti	5.76 m	320	
^{82m}Br[b]	6.05 m	777	
^{29}Al[b,c]	6.6 m	1280	10—20 m
^{27}Mg[d]	9.5 m	1013	
^{101}Mo[b]	14.6 m	307	
^{80}Br[b]	16.8 m	616, 666	
^{88}Rb	17.8 m	1836	
^{70}Ga[b]	21.1 m	1039, 1051	
^{155}Sm	21.9 m	104	30 m
^{233}Th	22 m	312	
^{239}U	23.5 m	74.7	
^{128}I[b]	25 m	443	
^{38}Cl	37.3 m	1642, 2170	
^{111m}Cd[b]	49 m	247	1 h
^{139}Ba	85 m	166, 1430	
^{116m}In	54 m	1085	
^{149}Nd[b]	1.8 h	211, 270	
^{165}Dy	2.3 h	95, 716	
^{65}Ni[b,e]	2.52 h	1481	1 h
^{56}Mn[f]	2.56 h	847, 1811	
^{87m}Sr	2.8 h	388	
^{152m}Eu	9.35 h	122	2 h
^{42}K[g]	12.4 h	1524	
^{64}Cu	12.8 h	1348	
8-h irradiation			
^{152m}Eu	9.35 h	122	1 d
^{42}K[g]	12.4 h	1524	
^{64}Cu	12.8 h	1348	
^{69m}Zn	13.8 h	439	
^{72}Ga[b]	14.1 h	630, 835	
^{24}Na[h]	15 h	1369, 1732	
^{76}As	24 h	657, 559	
^{239}Np[i]	2.35 d	278, 106	4 d
^{122}Sb	2.8 d	566, 686	
^{143}Ce	33.4 h	293	
^{82}Br	35.3 h	777, 555	
^{140}La	40.2 h	1596, 328, 487	
^{153}Sm	47 h	103	
^{115}Cd, ^{115m}In[b]	53 h	528, 337, 493	
^{198}Au	65 h	412	7 d
^{99}Mo	67 h	140, 740	
^{197}Hg	65 h	78, 69	
^{47}Sc[j]	3.4 d	160, 808	
^{174}Yb	4.21 d	396, 283	
^{177}Lu	6.7 d	208	15 d
^{147}Nd	11.1 d	531, 91	
^{131}Ba	12 d	496, 373	
^{86}Rb	18.7 d	1077	
^{233}Pa[k]	27 d	312	20—30 d
^{51}Cr	27.8	320	
^{169}Yb	32 d	177, 198	
^{141}Ce[l]	32 d	145	

8-h irradiation: radiochemistry			
^{194}Ir	17.4 h	328	1—2 d
^{197}Pt	19 h	77	
^{109}Pd	13.5 h	88	
^{193}Os	31.5 h	139, 460	3—4 d
^{97}Ru	69.1 h	216	
^{198}Au	64.8 h	412	
^{199}Au[q]	75.6 h	158	
^{191}Os	15 d	129	15 d
^{192}Ir	74 d	317, 468	
^{103}Ru	39.5 d	497	
^{110m}Ag	253 d	658, 885	
^{59}Fe	45 d	1291, 1100	20—30 d
^{54}Mn[m]	291 d	835	
^{203}Hg[n]	46.6 d	280	
^{124}Sb	60 d	1691	
^{85}Sr	65 d	514	
^{95}Zr, ^{95}Nb	65 d + 35.3 d	757, 766	
^{58}Co[o]	71.4 d	810, 865	
^{160}Tb	72.1 d	299	
^{46}Sc	83.9 d	899, 1120	
^{182}Ta	115 d	1222	
^{75}Se	120 d	265, 401, 136	
^{170}Tm	130 d	84	
^{153}Gd	242 d	97, 103	
^{65}Zn[p]	243 d	1115	
^{134}Cs	2.05 y	796	
^{60}Co	5.26 y	1332, 1173	
^{152}Eu	12 y	1408, 122, 779	
^{154}Eu	16 y	1277	

[a]Correct for ^{28}Si(n,p)^{28}Al and ^{31}P(n,α)^{28}Al. [b]Usually cannot be detected because of high intensity γ-rays of other nuclides, unless present in high concentrations. [c]Used for determination of Si. [d]Correct for ^{27}Al(n,p)^{27}Mg and ^{30}Si(n,α)^{27}Mg. [e]Corrections for ^{65}Cu(n,p)^{65}Ni and ^{68}Zn(n,α)^{65}Ni are negligible. [f]Corrections for ^{56}Fe(n,p)^{56}Mn and ^{59}Co(n,α)^{56}Mn are negligible. [g]Corrections for ^{42}Ca(n,p)^{42}K and ^{45}Sc(n,α)^{42}K are negligible. [h]Correct for ^{24}Mg(n,p)^{24}Na and ^{27}Al(n,α)^{24}Na. [i]Used for determination of U. [j]Used for determination of Ca. [k]Used for determination of Th. [l]^{59}Fe has a γ-ray at 143 keV close to ^{141}Ce. [m]Used for determination of Fe. [n]^{75}Se has γ-ray also at 280 keV; thus, the ^{75}Se contribution has to be subtracted from ^{203}Hg peak. [o]Used for determination of Ni. [p]^{46}Sc has a peak at 1120 keV close to ^{65}Zn. [q]Used for determination of Pt.

Interference-free γ-ray energies are also given in Table 1. In only two cases — ^{203}Hg and ^{65}Zn, both of which have only one γ peak — interferences were observed from ^{75}Se and ^{46}Sc, respectively, which have almost identical γ-rays as ^{203}Hg and ^{65}Zn. Corrections for contributions from ^{75}Se and ^{46}Sc to the peaks at 280 and 1114 keV, respectively, can be computed from their other associated peaks and subtracted before the Hg and Zn concentrations are calculated.

Except in the cases of As, Br, and Zn, the U.S.G.S. standard rock W-1 was used as the irradiation elemental standard in i.n.a.a. The use of standard reference materials as irradiation standards has been proposed recently [33]. This considerably simplifies the operation and eliminates the errors inherent in the preparation of a large number of synthetic standards at trace levels. Since no rock standard is available containing noble metals known with a great degree of certainty, multielement synthetic standards had to be used in this case.

Table 2 gives the data on the determination of 47 elements in sediment samples. Instead of individual data for the 24 sediment samples, only the ranges and average values are given for these materials. For most elements there is considerable variation from sample to sample. The environmental aspects of this study will be discussed elsewhere [34].

Also included in Table 2 are the results of an intercomparison analysis of sediment SL-1 prepared by the International Atomic Energy Agency, Vienna (IAEA). This lake sediment was collected from the Sardis Reservoir, Mississippi. We have analyzed 4 to 8 replicates of this material and the results in Table 2 represent the mean and standard deviation values of these replicates. The accepted mean values are not yet available from IAEA. However, the precision of the results is seen to vary between 0.1 and 12% with a few results around 20%. Most of the results show a precision of better than 5%.

Although the accuracy of the method cannot be evaluated in the absence of a standard sediment, past experience in this laboratory with similar i.n.a.a. and r.n.a.a. methods on standard rocks, biological materials, and coal and coal fly ash standards, leads to the conclusion that the accuracy of the sediment results is better than 10%. Complete results can be obtained within about three weeks after the first irradiation. Since the i.n.a.a. method is essentially non-destructive, after the counting is finished, the samples can be used for the determination of other environmentally interesting elements, such as lead, by different analytical techniques.

Until the present study, there have been no published results for the determination of the noble metals in sediments. This is because they are normally present in such low concentrations that previous methods have been ineffective. The proposed radiochemical method is capable of providing the necessary sensitivity. The levels of the noble metals in sediments could provide information on anthropogenic contribution to watersheds. In those cases where their levels are high in both background and dated sediment cores, it could reveal mineral deposits of considerable economic interest.

TABLE 2

Multielement analysis of sediments

Element	Range	Mean	IAEA Sediment SL-1
Majors (%)			
Al	2.62—6.38	4.38	10.4 ± 0.5
Ti	0.08—0.38	0.28	0.45 ± 0.04
Mg	0.59—1.68	1.10	2.98 ± 0.17
Na	0.30—0.92	0.61	0.17 ± 0.01
K	0.50—2.29	1.13	1.67 ± 0.36
Ca	1.23—4.00	2.69	4.34 ± 0.02
Fe	1.47—3.06	2.24	6.51 ± 0.08
Rare earths (ppm)			
La	28—73	37	44 ± 0.6
Ce	53—160	85	153 ± 1
Nd	15—137	52	64 ± 5
Sm	7.86—28	13	8.41 ± 2.0
Eu	0.77—1.94	1.28	1.86 ± 0.24
Gd	6.37—22	11	—
Tb	0.95—2.39	1.52	1.90 ± 0.02
Dy	5.26—15	8.76	5.89 ± 0.63
Tm	0.19—0.74	0.52	—
Yb	2.34—9.34	4.46	3.46 ± 0.07
Lu	0.52—1.20	0.72	0.75 ± 0.06
Noble metals (ppm unless specified otherwise)			
Ag	<0.1—1.04	0.42	0.082 ± 0.015
Au[a]	0.25—19	3.55	1.59 ± 0.09
Ru[a]	45—500	160	140 ± 30
Pd[a]	<20—180	70	<30
Os	<1—4.49	—	—
Ir[a]	0.52—48	13	8.41 ± 1.08
Pt	0.30—8.11	2.45	0.36 ± 0.06
Trace elements (ppm unless specified otherwise)			
As	1.86—26	13	—
Ba	163—375	287	452 ± 49
Br	23—96	44	8.02 ± 0.01
Cl	<20—609	249	—
Co	3.91—16	7.31	19.7 ± 0.3
Cr	16—50	27	99 ± 2
Cs	0.56—14	2.93	8.32 ± 0.09
Hf	1.67—12	7.05	4.52 ± 0.09
In[a]	5.3—19	12	200 ± 10
Mn	214—4500	684	3300 ± 200
Ni	<1—218	38	49 ± 2
Rb	19—49	35	183 ± 3
Sb	<0.01—2.9	1.56	1.11 ± 0.04
Sc	3.30—9.16	5.70	16.1 ± 0.2
Se	0.03—1.01	0.39	—
Sr	<10—242	90	—
Ta	0.41—1.44	0.87	1.45 ± 0.03

(continued)

TABLE 2 (continued)

Element	Range	Mean	IAEA Sediment SL-1
Th	4.02—9.38	6.39	13.5 ± 0.2
U	0.78—4.35	2.25	4.05 ± 0.11
V	28—68	46	166 ± 9
Zn	<10—450	278	—
Zr	54—488	263	399 ± 16

[a]Results are given as ppb.

The sediment samples analyzed by the proposed method are part of a comprehensive environmental study of the Adirondack and Hubbard Brook Experimental Forest regions being conducted by Drs. G. E. Likens and J. N. Galloway of Cornell University.

REFERENCES

1 U. Forstner, Naturwissenschaften, 63 (1976) 465.
2 G. C. Bortleson and G. F. Lee, Environ. Sci. Technol., 6 (1972) 799.
3 I. K. Iskandar and D. R. Keeney, Environ. Sci. Technol., 8 (1974) 165.
4 J. C. Fry and N. F. Shimp, Illinois Geol. Surv. Environ. Geol. Notes, 37 (1970).
5 P. A. Helmke, R. D. Koons, P. J. Schomberg, and I. K. Iskandar, Environ. Sci. Technol., 11 (1977) 984.
6 R. Wheeler and C. Dunning, Geol. Soc. Am. Abstr. 7 (1975) 880.
7 C. Collinson and N. F. Shimp, Environ. Geol. Notes, 56 (1972).
8 R. L. Thomas, Can. J. Earth Sci., 9 (1972) 636.
9 A. L. W. Kemp, R. L. Thomas, C. I. Dell, and J. M. Jaquet, J. Fish. Res. Board Can., 33 (1976) 440.
10 A. L. W. Kemp and R. L. Thomas, Geol. Soc. Am. Abstr., 7 (1975) 795.
11 E. A. Crecelius and D. Z. Piper, Environ. Sci. Technol., 7 (1973) 1053.
12 E. A. Crecelius, Limnol. Oceanogr., 20 (1975) 441.
13 M. Schoettle and G. M. Friedman, Sedimentology, 21 (1974) 478.
14 P. K. Hopke, D. F. Ruppert, P. R. Clute, W. J. Metzger, and D. J. Crowley, J. Radioanal. Chem., 29 (1976) 39.
15 G. Grancini, M. B. Stievano, F. Girardi, G. Guzzi, and R. Pietra, J. Radioanal. Chem., 34 (1976) 65.
16 H. Armannson, Anal. Chim. Acta, 88 (1977) 89.
17 I. Roth and H. Hornung, Environ. Sci. Technol., 11 (1977) 265.
18 B. G. Oliver, Environ. Sci. Technol., 7 (1973) 135.
19 E. A. Crecelius, M. H. Bothner, and R. Carpenter, Environ. Sci. Technol., 9 (1975) 325. 64
20 A. J. deGroot, K. H. Zschuppe, M. de Bruin, J. P. W. Houtman, and P. A. Singgih, Proc. Conf., NBS (publisher), Modern Trends in Activation Analysis, Gaithersburg, Md., 1 (1968) 62.
21 E. A. Uken, P. Hahn-Weinheimer, and H. Stark, J. Radioanal. Chem., 37 (1977) 741.
22 A. P. Grimanis, M. Vassilaki-Grimani, and G. B. Griggs, J. Radioanal. Chem., 37 (1977) 761.
23 R. V. Moore, EPA-R2-73-009 (1973).
24 O. Landstrom, K. Samsahl, and C. G. Wenner, Modern Trends in Activation Analysis, Proc. Conf., NBS (publisher), Gaithersburg, Md., 1 (1968) 353.
25 W. E. Kuykendall, Jr., B. W. Hoffman, and R. E. Wainerdi, in A. O. Brunfelt and E. Steinnes (Eds.), Activation Analysis in Geochemistry and Cosmochemistry, Universitetsforlaget, Oslo, 1971, 321.

26 N. A. Wogman, H. G. Rieck, Jr., J. R. Kosorok, and R. W. Perkins, J. Radioanal. Chem., 15 (1973) 591.
27 R. A. Nadkarni and G. H. Morrison, Anal. Chem., 45 (1973) 1957.
28 R. A. Nadkarni and G. H. Morrison, Environ. Lett., 6 (1974) 273.
29 R. A. Nadkarni and G. H. Morrison, Radiochem. Radioanal. Lett., 24 (1976) 103.
30 R. A. Nadkarni and G. H. Morrison, Anal. Chem., 46 (1974) 232.
31 R. A. Nadkarni and G. H. Morrison, J. Radioanal. Chem., 38 (1977) 435.
32 G. E. Likens, Chem. Eng. News, 55 (Nov. 22, 1976) 29.
33 R. A. Nadkarni and G. H. Morrison, J. Radioanal. Chem., 43 (1978) 345.
34 G. E. Likens and J. N. Galloway, unpublished results.

Analytica Chimica Acta, 99 (1978) 143—150

FRACTIONATION OF CIGARETTE SMOKE CONDENSATE FOR CHEMICAL AND BIOLOGICAL TESTING

D. B. WALTERS*, W. J. CHAMBERLAIN, F. J. AKIN, M. E. SNOOK and O. T. CHORTYK

Tobacco Laboratory, Agricultural Research Service, U.S. Department of Agriculture, P.O. Box 5677, Athens, Georgia 30604 (U.S.A.)

(Received 2nd February 1978)

SUMMARY

Large-scale fractionation of cigarette smoke condensate (CSC) was carried out by gel filtration and silicic acid column chromatography, and selected fractions and their subfractions were tested for tumorigenicity by mouse-skin bioassay. The weak-acid fraction was separated into four subfractions, the polynuclear aromatic hydrocarbon (PAH) fraction into two subfractions, and the polar neutral lipid fraction into three subfractions. Also, combinations of subfractions were examined for synergic effects and portions of all active material were subjected to chemical analyses by gel filtration, column, thin-layer and gas chromatography, and ultraviolet and mass spectrometry. A weak-acid subfraction (F-63) in which catechol was concentrated, and which comprized 3.27% CSC was shown to be tumorigenic, as were combinations of this subfraction with the active PAH (F-67) subfraction and a polar, neutral lipid (F-70) subfraction, representing 0.01 and 0.05% CSC, respectively. The results indicated that catechol may be a potent cocarcinogen and that the PAH in CSC interact with other components to exert a tumorigenic effect.

The biological effects of cigarette smoking have been widely studied and presented in numerous reports, including nine by the U.S. Department of Health, Education and Welfare [1]. In this laboratory efforts have been concentrated on the fractionation of cigarette smoke condensate (CSC) for bioassay and identification studies [2—6]. Large-scale fractionations of CSC have been done and bioassays have indicated that three fractions account for most of the tumorigenicity of CSC [7—9].

This paper describes the fractionation methods used to separate further the ether-soluble, weak-acid fraction (F-8), the polycyclic aromatic hydrocarbon (PAH) fraction (F-55), and a polar, neutral lipid fraction (F-25 + 26) of CSC (Figs. 1 and 2). Data obtained from recombined subfractions are also presented. The object of the study was to concentrate active fractions into subfractions of minimum weight without loss of biological activity so that they could readily be used both for bioassay and chemical identification studies. Some chemical identifications are given for general characterization of the subfractions.

*National Institute of Environmental Health Sciences (USDHEW), Environmental Biology and Chemistry Branch, P.O. Box 12233, Research Triangle Park, North Carolina 27709, U.S.A.

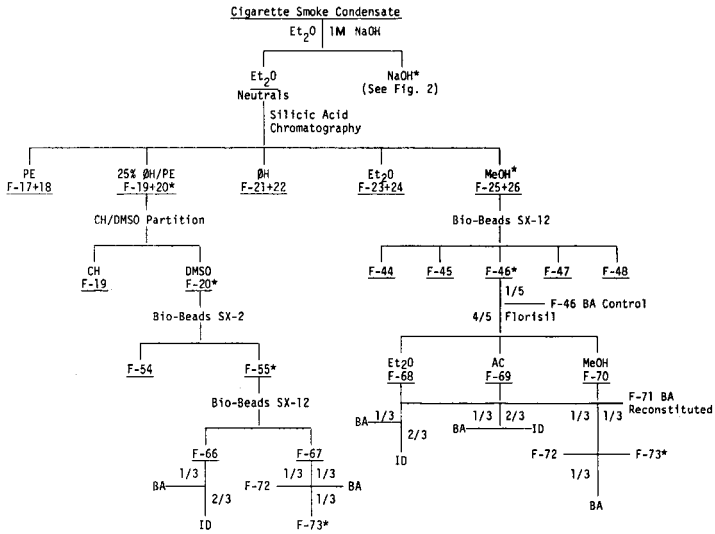

Fig. 1. Modified fractionation scheme. Et_2O, diethyl ether; PE, petroleum ether; ØH, benzene; CH, cyclohexane; DMSO, dimethylsulfoxide; AC, acetone; MeOH, methanol; (ID), portion for chemical identifications; *, tumorigenic fraction; (BA), portion for bioassay.

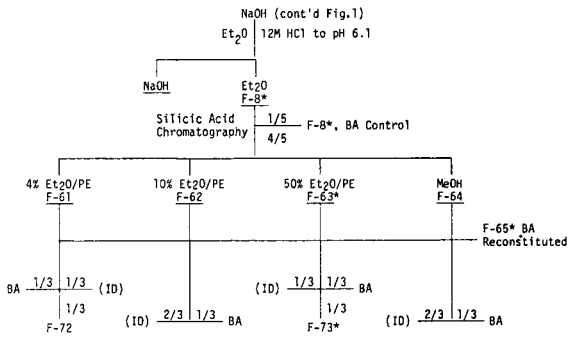

Fig. 2. Weak acid fractionation scheme (continued from Fig. 1).

EXPERIMENTAL

CSC in kilogram quantities was prepared at the Roswell Park Memorial Institute and shipped as previously described [2]. A total of 10 kg was fractionated in 1-kg portions for this study with only solvents purified by "distillation in glass". Preparation of fractions F-8, F-55, F-25 + 26 has been described previously [2, 5, 6].

Subfractionation procedures

Before subfractionation, 20% of F-8 was removed as a bioassay control (Fig. 2). The remainder was mixed with 200 g of activated silicic acid [3] and the solvent was removed. The powdered silicic acid—sample mixture was placed onto a 8.5 × 107.0-cm glass column containing activated silicic acid (silicic acid used in a ratio of 15:1 to F-8). A 13-l fraction, designated F-61, was eluted by a solvent mixture of 4% diethyl ether in petroleum ether. Similarly, F-62, F-63, and F-64 were eluted with 10 l of 10% ether in petroleum ether, 10 l of 50% ether in petroleum ether, and 4 l of methanol, respectively. The reconstituted fraction, F-65, was prepared by recombining 25% aliquots of each of the fractions F-61, F-62, F-63 and F-64. The remaining amounts of F-61 and F-63 were divided into three portions each, one for chemical identification, one for bioassay, and one to make up part of the combination bioassay fractions F-72 and F-73 [F-72 = 1/3 (F-61 + F-67 + F-70); F-73 = 1/3 (F-63 + F-67 + F-70)]. One-third portions of fractions F-62 and F-64 were used for bioassay, and the remainders for chemical identification.

Preparation of the PAH-containing fraction, F-55, has been reported previously [6]. F-55 was further fractionated by gel filtration chromatography on Bio-Beads SX-12 (Bio-Rad Laboratories, Richmond, California) with benzene. Four 1.25 × 109.0-cm glass columns connected in series, were packed with Bio-Beads and were eluted with benzene, by a constant flow pumping system described elsewhere [8], to yield F-66 and F-67. Fraction F-66 was divided into two parts, one-third for bioassay and two-thirds for chemical identification; F-67 was divided into three equal parts, for bioassay, for F-73, and for preparation of F-72.

F-25 + 26 was further fractionated on three 3.0 × 200.0-cm glass columns packed with Bio-Beads SX-2 in a 155:1 ratio of substrate to sample. Elution with 200, 110, 60, 40, 100, and 150 ml of benzene yielded the 200-ml void volume and fractions F-44, F-45, F-46, F-47, and F-48, respectively. Previous data indicated that F-46 is moderately active as a tumor promoter [7]. After removal of a 20% portion of F-46 for bioassay control, the remainder was chromatographed on 100-120 mesh Florisil in a 6.0 × 56.0-cm glass column with a 1.5:400 ratio of F-46. The Florisil was prewashed with ether, acetone, methanol and water, and activated at 150°C overnight. Elution of F-46 on Florisil with 3 l of ether, 4 l of acetone, and 3 l of methanol yielded F-68, F-69, and F-70, respectively. The reconstituted fraction, F-71, was prepared from equivalent aliquots of each of these three fractions. The remaining quantities of fractions F-68 and F-69 were each divided into a bioassay portion (1/3) and an identification portion (2/3). Fraction F-70 was divided into three equal parts for bioassay and addition to F-72 and F-73.

Bioassay procedures

Methods used for mouse-skin bioassay are reported elsewhere [9]. Fractionation of 1 kg of CSC produced enough material for 6 weeks of bioassay. To inhibit possible decomposition, the samples were divided into six equal parts, the solvent was removed with a flash evaporator, and the samples were stored in the dark, under nitrogen, at −23°C. Solutions for skin painting were prepared weekly by appropriate dilution with acetone and quantitatively transferred to Teflon-stoppered brown glass bottles. After each treatment the bottle was flushed with nitrogen and stored in darkness at −23°C.

Identification procedures

The subfractions obtained from F-8 by column chromatography on silicic acid were monitored by thin-layer chromatography (t.l.c.). Fatty acids were detected by t.l.c. on 20 × 20-cm silica gel plates, 0.1-mm thick, developed with 90:10:1 petroleum ether:ether:acetic acid, and sprayed with methyl red. Phenolic and higher-molecular-weight material were monitored on 15 × 15-cm micro-polyamide plates (Schleicher and Schuell, Keene, New Hampshire), developed with 45:8:4 benzene:methanol:acetic acid, and sprayed with diazotized benzidine [10]. (Benzidine is a complete carcinogen and must be used with extreme care.) The R_F values for the polyamide plates were compared with knowns, which were spotted concurrently, and with t.l.c. results obtained with the above Brinkmann plates but by the development with 20:80:2, benzene:ethyl acetate:acetic acid and spraying with *p*-nitroaniline.

Details of the methods used for the analysis of fractions F-67 and F-25 + 26 have been reported [8, 11].

RESULTS AND DISCUSSION

The object of this study was to develop fractionation schemes so that the active constituents in the biologically active fractions F-8, F-55, and F-25 + 26 could be readily bioassayed and identified. Subfractions were assayed in the same relative concentrations as present in CSC. Chamberlain et al. [6] fractionated F-8 by solvent partitioning but were unable to concentrate its biological activity into any one subfraction. Because of the partition coefficients, catechol, for example, was detected in all subfractions. Accordingly, in the present work, silicic acid column chromatography was used to effect a better separation of the F-8 constituents. F-8 was separated into various subfractions containing fatty acids, phenols, polyphenols, phenolic acids, and other higher-molecular-weight materials. Moreover, most of the catechol, reported to be a potent cocarcinogen [12], was concentrated into one fraction, F-63.

The PAH-containing fraction, F-55, was separated by gel filtration chromatography into two subfractions, F-66 and F-67. The latter contained essentially

pure PAH, and represented 0.01% by weight of CSC, whereas F-66 contained the remaining constituents of F-55. The PAH of CSC have been completely characterized by use of gel filtration and by gas and high-pressure liquid chromatography in conjunction with u.v. and mass spectrometry [8].

The use of solvent partitioning to separate the polar, neutral lipid fraction, F-25 + 26, as described previously [6], was also re-evaluated. Partitioning of this fraction between petroleum ether and methanol only resulted in a 10% and 90% weight distribution, respectively. Better separation of the biologically active constituents was obtained when the whole (F-25 + 26) fraction was subjected to gel filtration and column chromatography: three new subfractions — F-68, F-69, and F-70 — were obtained which were shown to contain glycolipids, sterol glucosides and other high-molecular-weight materials [11].

The fractions, subfractions, their respective controls, and combination fractions were submitted for testing by mouse-skin painting and preliminary bioassay results have been reported [9].

Average yields for weak-acid and neutral subfractions, as obtained by the large-scale fractionation schemes (Figs. 1 and 2), are given in Tables 1 and 2. All data were normalized to 1000 g CSC; details of the statistical methods used have been described elsewhere [2, 3]. In agreement with Bock et al. [7], it was found that yield variability of some fractions was often high; therefore, the mean weights presented do not represent the exact percentage of the fraction in CSC. Variation of fractionation techniques for the preparation of different batches of CSC during the 60-week experiment account, in part, for the discrepancies. The active F-8 fraction represents 11.15% of CSC, before removal of 20% for control. When subfractionated, it yielded F-61 to F-64, constituting 1.82, 1.75, 3.27, and 3.43 % of CSC, respectively. F-65 was the reconstituted fraction. This represented a mean recovery of about 94%.

The fractionation procedure used here has several advantages over the previously described solvent-partitioning procedure [6]. Besides concentrating the biological activity in subfractions containing significantly smaller

TABLE 1

Average yield of weak-acid subfractions[a]

Fraction	% CSC	Range		Mean (g)	Standard deviation[b]
		Min.	Max.		
F-8 (total)	11.15	106.63	120.81	113.79	5.43
F-8 (control)	—	21.32	25.39	22.76	1.37
F-61 (total)	1.82	9.19	20.82	15.52	3.48
F-62 (total)	1.75	10.37	18.86	13.90	3.03
F-63 (total)	3.27	25.69	29.07	27.85	1.07
F-64 (total)	3.43	24.68	38.73	29.20	4.14
F-65 (reconstituted)	—	20.65	24.68	22.06	1.53

[a]Based on 1000 g of CSC. [b]$n = 10$.

TABLE 2

Average yields of neutral and combined subfractions[a]

Fraction	% CSC	Range		Mean (g)	Standard deviation[b]
		Min.	Max.		
F-66	0.01	0.03	0.12	0.06	0.03
F-67	0.01	0.03	0.09	0.07	0.02
F-46 (total)	0.19	1.44	2.74	2.17	0.45
F-46 (control)	—	0.33	0.63	0.44	0.10
F-68 (total)	0.04	0.10	0.60	0.30	0.15
F-69 (total)	0.15	0.84	1.61	1.26	0.26
F-70 (total)	0.05	0.25	0.68	0.46	0.14
F-71 (reconstituted)	—	0.33	0.63	0.48	0.11
F-72 = 1/3 (F-61 + 67 + 70)	—	2.72	5.38	4.11	0.79
F-73 = 1/3 (F-63 + 67 + 70)	—	6.46	7.40	7.13	0.30

[a]Based on 1000 g CSC. [b]n = 10.

percentages of initial CSC weight, the method also concentrated various groups of compounds (e.g., fatty acids, phenols, polyphenols, phenolic acids, etc.) into individual subfractions, facilitating mean chemical and biological analyses. For example, monitoring of the silicic acid column effluent by t.l.c. indicated that: F-61 contained mainly fatty acids and some simple phenols; F-62 contained relatively simple phenols such as phenol, eugenol, and guiacol; F-63 contained phenols such as catechol and some phenolic acids; and F-64 contained phenolic acids, polyphenols, and miscellaneous material of high molecular weight. T.l.c. on silica gel and micropolyamide plates and spraying with *p*-nitroaniline and diazotized benzidine, respectively, yielded characteristic spots for the various phenolic compounds. Particular attention was given to monitoring catechol in the subfractions because of the report by Van Duuren et al. [12] on its cocarcinogenicity. Catechol produced a purplish-yellow spot with an R_F value of 0.45 on micro-polyamide and a dark gray spot on silica gel (R_F = 0.53). It was estimated, by semi-quantitative t.l.c., that 95% of the catechol in F-8 was concentrated in F-63. Analogously, t.l.c. indicated that fatty acids were present only in F-61.

The biologically active, PAH-containing fraction, F-55, constituted 0.02% of CSC and was subfractionated into F-66 and F-67, each representing 0.01% CSC. Their recovery from F-55 was 97% (Table 2). Analyses of F-66 and F-67 by gas chromatography and u.v. spectroscopy indicated that, except for trace amounts, all of the PAH of F-20 are present in F-67, and that F-66 contains polymeric material of high molecular weight (>400) which is not g.c.-volatile [9]. Several hundred PAH in F-67 have been positively identified [8].

Fraction F-25 + 26, representing 2.08% CSC, was chromatographed by gel filtration on Bio-Beads SX-2, to produce the active fraction F-46 (0.20% CSC) [6]. Column chromatography of this fraction on Florisil produced

TABLE 3

Final tumor yield (60 weeks) of smoke fractions

Fraction	Final tumor yield			
	At risk	Number of tumor bearers	% tumor bearers	Total number of tumors
F-8	45	22	48.5[a]	25
F-61	33	8	24.2	12
F-62	37	6	16.2	6
F-63	39	12	30.7	20
F-64	39	4	10.2	4
F-65	35	17	48.5[a]	22
F-66	36	5	13.8	5
F-67	36	2	5.5	2
F-46	39	9	23.0	10
F-68	40	8	20.0	8
F-69	45	3	6.6	3
F-70	35	6	17.1	10
F-71	43	8	18.6	9
F-72	39	6	15.3	8
F-73	33	21	57.5[a]	27
DMBA/AC[b]	58	12	20.6	12
TPA[c]	—	—	50.0[a]	—
Untreated	17	0	0	0

[a]Significantly different from concurrent DMBA/AC controls ($P < 0.01$).
[b]DMBA/AC (7,12-dimethylbenzanthracene/acetone) group started with 75 mice; untreated group started with 25 mice; all other groups started with 50 mice.
[c]TPA (12,*O*-tetradecanoylphorbyl-13-acetate) treatment discontinued when 50% of the mice developed tumors.

fractions F-68 to F-70, corresponding to 0.04, 0.15, and 0.05% CSC, respectively (Table 2). These fractions were analyzed, as described by Chamberlain [11], by column, thin-layer, gel filtration, and gas chromatography and found to contain small amounts of sterol glucosides and glycolipid material as well as uncharacterized miscellaneous compounds of high molecular weight.

Bioassay results (at 60% relative CSC concentration) for the tested fractions are given in Table 3. The weak-acid fractions F-8 and F-65 (reconstituted F-8) showed significant tumor-promoting activity (48.5% tumor bearers each). The catechol-containing subfraction, F-63, showed a tendency to promote tumor formation (30.7% tumor bearers). Although the PAH fraction, F-55, has consistently shown tumorigenic activity [5, 6, 9], the F-66 and PAH-containing F-67 showed no activity. Similarly, F-46, F-71 (reconstituted F-46), and F-68 to F-70 were not active, although previous testing showed F-46 [7] to be marginally active.

Of particular interest are the results from F-72 and F-73. Earlier bioassays showed that CSC fatty acids were marginally active [7] and that catechol was a potent cocarcinogen [12]. Therefore, tests were made on two combination fractions, both containing equal amounts (relative to CSC) of the PAH fraction F-67, the polar neutral lipid fraction, F-70 and (a) the fatty acid-containing fraction F-46, to yield F-72, and (b) the catechol-rich fraction, F-63, to yield F-73. Results indicated no significant activity for F-72 (15.3% tumor bearers). However, F-73 exhibited significant activity (57.5% tumor bearers); hence, a synergic tumorigenic effect was indicated.

REFERENCES

1 The Health Consequences of Smoking, 1975, DHEW Publication (CDC) 76-8704 and references therein and previous reports.
2 A. P. Swain, J. E. Cooper, R. L. Stedman, and F. G. Bock, Cancer Res., 29 (1969) 579.
3 A. P. Swain, J. E. Cooper, R. L. Stedman, and F. G. Bock, Beitr. Tabakforsch., 5 (1969) 109.
4 W. J. Chamberlain and R. L. Stedman, in I. Schmeltz (Ed.), The Chemistry of Tobacco and Tobacco Smoke, Plenum Press, New York, 1971, p. 99.
5 A. P. Swain, F. G. Bock, J. E. Cooper, W. J. Chamberlain, E. D. Strange, L. Lakritz, R. L. Stedman, and I. Schmeltz, Beitr. Tabakforsch., 7 (1973) 1.
6 W. J. Chamberlain, D. B. Walters, M. E. Snook, O. T. Chortyk, and F. J. Akin, Beitr. Tabakforsch., 8 (1975) 133.
7 F. G. Bock, A. P. Swain and R. L. Stedman, J. Natl. Cancer Res., 49 (1972) 477.
8 M. E. Snook, R. F. Severson, H. C. Higman, R. F. Arrendale, and O. T. Chortyk, Beitr. Tabakforsch., 8 (1976) 250.
9 F. J. Akin, M. E. Snook, R. F. Severson, W. J. Chamberlain, and D. B. Walters, J. Natl. Cancer Inst., 57 (1976) 191.
10 J. Sherma and L. V. S. Hood, J. Chromatogr., 17 (1965) 307.
11 W. J. Chamberlain, Tob. Sci., (1976) 168.
12 B. L. Van Duuren, C. Katz, and B. M. Goldschmidt, J. Natl. Cancer Inst., 51 (1973) 703.

Analytica Chimica Acta, 99 (1978) 151—156

SELECTIVE DETERMINATION OF TARTARIC ACID IN AQUEOUS SOLUTION WITH 2-[1-(*o*-DIHYDROXYBORYLPHENYL)-2-PHENYLETHYL]-2-IMIDAZOLINE

JOUKO J. KANKARE* and JUHANI VARHIALA

Department of Chemistry, University of Turku, SF-20500 Turku 50 (Finland)

(Received 4th January 1978)

SUMMARY

An organoboron reagent, 2-[1-*o*-dihydroxyborylphenyl)-2-phenylethyl]-2-imidazoline hydrochloride, is used for the determination of tartaric acid in aqueous solution. The complex of tartaric acid with the organoboron reagent can be extracted into an organic solvent and determined spectrophotometrically in the concentration range 10^{-5}—10^{-4} M, with a relative standard deviation of ca. 5%. Alternatively, the complex can be determined turbidimetrically in the concentration range 2×10^{-4}—10^{-3} M with approximately the same precision.

Boric acid [1] and its organic derivatives [2] form complexes with α-hydroxy carboxylic acids:

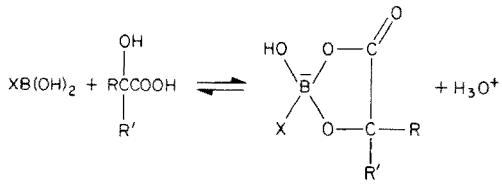

(1)

This equilibrium differs from the well-known reaction between polyols and boric acid in that it lies considerably towards the right-hand side even at rather low pH values. For instance, when X = Ph, R = CH_3 and R′ = H, the equilibrium constant for the reaction (1) is 3.7×10^{-3} [2]. In principle, the reaction could be utilized for the analysis of either boric acid or its organic derivatives or for α-hydroxy carboxylic acids. However, the reaction has analytical significance only if it induces some easily measurable changes. The most accurate quantitative method for boric acid is based on the analogous reaction between mannitol and boric acid. In this case, the hydroxonium ion released is easily titrated since neither boric acid nor mannitol dissociates appreciably at the pH levels used. The determination of α-hydroxy carboxylic acids based on the amount of hydroxonium ion released in reaction (1) is much more difficult because the acids themselves dissociate and, in comparison, the pH change induced by reaction (1) is too low to be of analytical significance. Hence, other means should be sought if a practical method for the determination of α-hydroxy carboxylic acids based on equilibrium (1) is

to be devised; a feasible way is to find a suitable substituent X such that the resulting cyclic ester is sparingly soluble and/or easily extractable into an organic solvent.

Aromatic boronic acids with a neighboring nitrogen group form an interesting class of compounds. Apart from catalytic effects on certain solvolytic reactions [3, 4], the compounds exhibit considerable aqueous solubility and the ability to preserve the tetrahedral coordination of boron even at rather low pH. Letsinger and MacLean [5] found that these compounds form sparingly soluble derivatives with pyrocatechol. In a previous paper [6] it was shown that compound (I), (N^3-*B*)-2-[1-(*o*-dihydroxyborylphenyl)-2-phenylethyl]-2-imidazoline, forms sparingly soluble cyclic esters with α-hydroxy carboxylic acids. Qualitative tests showed that the ester of tartaric acid was the most sparingly soluble of these derivatives.

Many of the numerous methods devised for the determination of tartaric acid are not adaptable to very low concentrations. Except for the chromatographic methods, the known colorimetric or titrimetric methods also lack selectivity. The low solubility of the tartrate ester of compound (I), both in the absolute sense and in comparison with closely related hydroxy acids, indicated a possibility of developing a sensitive and selective analytical method for the assay of tartaric acid. There are three possible methods based on the low solubility of a derivative: (1) filtration and subsequent assay of the precipitate by gravimetric or other means, (2) turbidimetry or nephelometry, and (3) extraction of the precipitate into a suitable organic solvent.

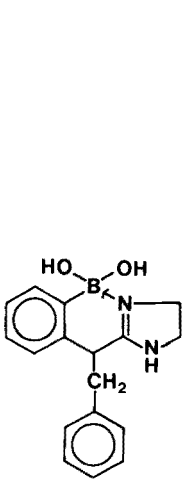

I

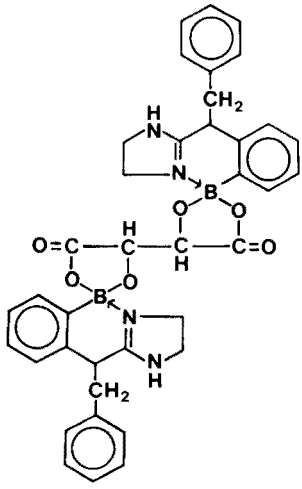

II

EXPERIMENTAL

Reagents

The 0.01 M and 0.075 M stock solutions of 2-[1-(*o*-dihydroxyborylphenyl)-2-phenylethyl]-2-imidazoline hydrochloride (hydrochloride of compound (I))

[6] were prepared by grinding the compound in a vibration ball mill and dissolving in water. The solutions should be used within 2 days because of slow decomposition.

Isobutyronitrile (Fluka AG., reagent grade) was purified by the method of Teter and Merwin [7].

Formate buffer was prepared from sodium hydroxide and formic acid by adjusting the pH to 3.2 and ionic strength to ca. 2.

The other reagents, of analytical grade, were used without further purification.

Characterization of the tartrate derivative

A solution of 793.8 mg (2.4 mmol) of 2-[1-(*o*-dihydroxyborylphenyl)-2-phenylethyl]-2-imidazoline hydrochloride in 50 ml of water was prepared, and a solution of 151.3 mg (1.01 mmol) of (+)-tartaric acid in 10 ml of water was added. After 2h, the precipitate was filtered on a crucible, washed with water, dried in a vacuum desiccator overnight and at 80°C for 45 min. The yield was 667.0 mg (99.1%, assuming that the boronic acid: tartaric acid complex is 2:1, or 161.3% on the basis of a 1:1 complex).

The boron content of the complex was found by the modified method of Rittner and Culmo [4, 8] to be 3.19%. The calculated values are 3.24% (2:1 complex) and 2.64% (1:1 complex).

The u.v. spectra of compound (I) and its tartrate derivative(II) were rather similar (Fig. 1).

Determination of the solubility of the tartrate derivative

The solubility of the tartrate derivative of compound (I) in ten buffer solutions with pH values between 1.55 and 8.09 was determined by shaking 30-mg portions with 100 ml of each buffer at 25°C. After equilibration for 4 days in a thermostated shaking machine, 25-ml aliquots were drawn from the supernatant liquid, 2 ml of 1 M sodium hydroxide was added, and the

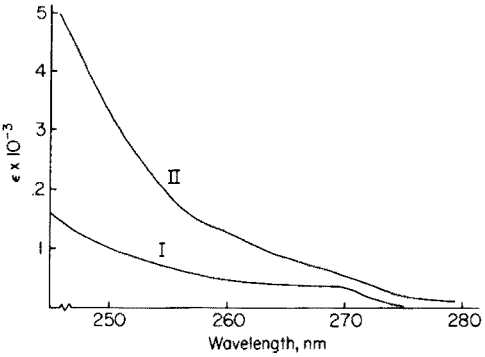

Fig. 1. U.v. absorption spectra of (N^3-*B*)-2-[1-(*o*-dihydroxyborylphenyl)-2-phenylethyl]-2-imidazoline (I) in phosphate buffer (pH 7) and its tartrate complex (II) in isooctane—isobutyronitrile (1:1).

absorbance was recorded at 262 nm against the same buffer solution with a Beckman DU spectrophotometer. The molar absorptivity of tartaric acid at this wavelength is negligible compared with that of compound (I).

Analytical procedures

Extraction method. A 20-ml portion of sample solution containing 1.5—15 $\mu g\ ml^{-1}$ of tartaric acid is pipetted into a graduated cylinder; 2 ml of 0.075 M solution of compound (I) and 2 ml of formate buffer are added. A 10-ml aliquot of 1:1 (v/v) isooctane—isobutyronitrile mixture is pipetted into the cylinder, the mixture is shaken vigorously for 5 min, and the layers are allowed to separate. The absorbance of the organic layer is measured at 259 nm against the same mixture but without tartaric acid. The concentration of the unknown is read from the calibration curve.

Turbidimetric method. A 1-ml sample containing 30—150 $\mu g\ ml^{-1}$ of tartaric acid is pipetted into a 1-cm spectrophotometric cuvette; 1 ml of formate buffer and 2 ml of a 0.01 M solution of compound (I) are added. The cuvette is stoppered and shaken vigorously for 15 s. After standing for 3 min the cuvette is turned gently up and down for 2 min and the absorbance at 500 nm is recorded immediately. This is not by any means the only procedure, but strict adherence to the same procedure is essential in order to obtain reproducible results.

RESULTS AND DISCUSSION

The quantitative analyses show unambiguously that the complex is formed from two molecules of boronic acid and one molecule of tartaric acid. The ultraviolet spectrum of the complex (Fig. 1) implies the lack of conjugation other than the benzene rings. Hence structure (II) is quite plausible.

The low solubility of compound (II) in water can be understood on the basis of the high molecular weight, symmetry, and lack of hydrogen-bonding groups. Figure 2 shows the solubility of the complex as a function of pH; the shallow minimum at ca. pH 3 is as expected on the basis of the ionization constant (10^{-3}) of the hydrochloride of compound (I) [6] and the first ionization constant ($10^{-2.9}$) of tartaric acid. The minimum solubility is ca. 10^{-4} mol dm^{-3}. Although the solubility is reasonably slight, the gravimetric finish for the tartaric acid analysis was not pursued further because of the fluffy nature of the precipitate, high consumption of the expensive reagent, and inherent inconvenience of the gravimetric assay. However, the solubility of the complex in polar organic solvents made analysis by extraction possible. The u.v. spectrum of compound (II) limits severely the number of solvents if a spectrophotometric method is to be used for the assay of the compound. Hydrocarbon solvents do not extract measurable quantities from aqueous solutions. Higher alcohols extract large quantities of the boronic acid reagent; chlorinated hydrocarbons are too opaque below 270 nm. Aliphatic nitriles possess sufficient polarity and transparency in the spectral region in question,

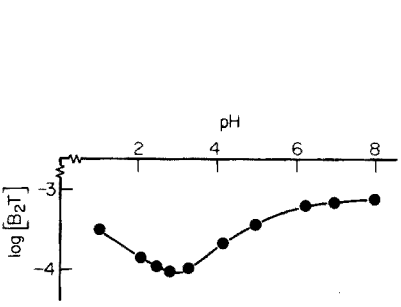

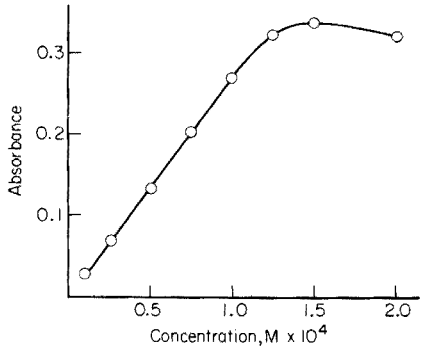

Fig. 2. Influence of pH on the solubility of compound (II). Buffers: pH 1.55 and 2.19, KCl + HCl; pH 2.54 and 2.79, chloroacetate; pH 3.20 and 4.10, formate; pH 5.14, acetate; pH 6.20, 7.21, and 8.09, phosphate.

Fig. 3. Calibration curve for the determination of tartaric acid by the extraction method.

but the lowest member, acetonitrile, is too water-soluble. Isobutyronitrile was chosen, but the polarity of this solvent had to be lowered by adding an equal volume of isooctane to suppress the extraction of the boronic acid reagent into the organic phase.

Figure 3 shows the calibration curve for the determination of tartaric acid by the extraction method. The curvature above 1.5×10^{-4} mol dm^{-3} arises from the precipitation of the complex. The calibration curve does not reveal the precision of the determination but repeated measurements showed that the relative standard deviation is well below 5% in the region from ca. 2×10^{-5} mol dm^{-3} to ca. 1.3×10^{-4} mol dm^{-3}.

In a previous paper [6] it was shown that a large number of α-hydroxy carboxylic acids form sparingly soluble complexes with compound (I). Hence these compounds would be expected to interfere with the analysis of tartaric acid. Citric and malic acid are the most probable constituents of samples to be analyzed for tartaric acid; their influence on the accuracy can be seen in Table 1. The interference could not be removed by lowering the polarity of the extraction solvent nor by changing the pH.

TABLE 1

Influence of citric and malic acids on the determination of tartaric acid by the extraction method
(All concentrations are given as $x \times 10^{-5}$ mol dm^{-3})

Tartaric acid added	—	—	7.5	7.5	7.5	7.5	7.5
Citric acid	7.5	—	7.5	—	7.5	75	—
Malic acid	—	7.5	—	7.5	7.5	—	75
Tartaric acid found	—	—	7.7	8.0	8.2	9.5	13.3
Error (%)	—	—	2.7	6.7	9.3	27	77

In preliminary experiments it was observed that although citric and malic acids interfere at the concentration level of ca. 10^{-4} M, their complexes are soluble and no precipitate is formed. In the search for a more selective method for tartaric acid a turbidimetric assay was investigated. Turbidimetric methods are known to be generally irreproducible in character. However, when many samples are to be analyzed by a standardized procedure, turbidimetry has the merit, at least, of instrumental simplicity. A linear calibration was obtained with the procedure reported above; tartaric acid can be determined with fair precision in the narrow range from 2×10^{-4}—1×10^{-3} M. From 5 determinations for a solution containing 6×10^{-4} mol dm^{-3} of tartaric acid and 6×10^{-3} mol dm^{-3} of both citric and malic acids, the value found was $(6.0 \pm 0.3) \times 10^{-4}$ mol dm^{-3} of tartaric acid (range, 5.66—6.36 $\times 10^{-4}$ mol dm^{-3}). Unfortunately, the lower limit of the turbidimetric method is about an order of magnitude higher than that of the spectrophotometric finish.

Conclusion

In the past the assay of involatile and water-soluble tartaric acid at low concentrations has not been without considerable difficulties. Specific color reactions have not been presented and the chromatographic procedures have tended to be tedious and inaccurate. The two methods reported here have a reasonably high degree of selectivity, employ easily accessible instruments, and give sufficient precision for most practical problems. Unfortunately the organoboron reagent is not available commercially but its synthesis is straightforward with a reasonable yield [6].

REFERENCES

1 N. Vermaas, Rec. Trav. Chim. Pays-Bas, 51 (1932) 955.
2 S. Friedman, B. Pace and R. Pizer, J. Am. Chem. Soc., 96 (1974) 5381.
3 R. L. Letsinger, Adv. Chem. Ser., 42 (1964) 1.
4 J. J. Kankare, Ann. Acad. Sci. Fenn. Ser. A 2, 160 (1971).
5 R. L. Letsinger and D. B. MacLean, J. Am. Chem. Soc., 85 (1963) 2230.
6 J. J. Kankare and J. Varhiala, Acta Chem. Scand. Ser. B, 31 (1977) 914.
7 J. W. Teter and W. J. Merwin, U.S. 2,411,346 (1946); Chem. Abstr., 41 (1947) 983i.
8 R. C. Rittner and R. Culmo, Anal. Chem., 35 (1963) 1268.

Analytica Chimica Acta, 99 (1978) 157—166

NUCLEAR MAGNETIC RELAXATION RATE AS INDICATOR IN COMPLEXIMETRIC TITRATIONS

A. SCHLÜTER and ALARICH WEISS*

Institut für Physikalische Chemie, Physikalische Chemie III, Technische Hochschule Darmstadt, Petersenstrasse 20, D-6100 Darmstadt (Federal Republic of Germany)

(Received 24th January 1978)

SUMMARY

Nuclear magnetic relaxation titration was applied for determinations of transition metal ions in aqueous solutions through complex formation. With EDTA, Co^{2+}, Cu^{2+}, Mn^{2+}, Fe^{3+} and Ni^{2+} were titrated; the simultaneous determination of Cu^{2+} and Mn^{2+} is possible. With NTA, single ion solutions, e.g. Mn^{2+}, and multiple ion solutions can be analysed. The influence of kinetic effects is shown and the possibility of determining ratios of equilibrium constants is discussed.

The nuclear magnetic relaxation rate can be used in chemical analysis as shown by Nothnagel and Weiss [1] and by Schlüter and Weiss [2, 3] (nuclear magnetic relaxation titration, n.m.r.t.). The nuclear magnetic relaxation times T_1 and T_2 of ^1H depend linearly on the concentration of paramagnetic ions in aqueous solutions. Furthermore, T_1 and T_2 are functions of the magnetic moment μ_{eff} of the paramagnetic ions in the solution, and of the gyromagnetic ratio of the protons, γ_H, and they are also properties of the solutions involved [1—3]. Restricting the experiments to measurements of T_1, which is measured more conveniently than T_2, the paramagnetic relaxation rate $(1/T_1)_p$ is given by

$$(1/T_1)_p = \sum_i a_i C_i \qquad (1)$$

where C_i are the concentrations of the different paramagnetic ions in the solution and a_i the magnetic coefficients, $a_i = f(\mu_{eff}, \gamma_H, \ldots)$. In investigations of complexes in solutions, the concentration of the paramagnetic ions is constant and a correction for dilution effects has to be applied [3]. However, the complexing reagent changes the magnetic coefficients a_i of the ion considered to some extent. For example, the formation of $[Ni(CN)_4]^{2-}$ is accompanied by a strong change in μ_{eff} and thus by a large change in $(1/T_1)_p$ [1]. Much smaller but measurable changes of a_i were observed in complexiometric titrations with EDTA and NTA. Some single ion determinations are reported here and the use of n.m.r.t. in the simultaneous complexiometric determination of two different ions is discussed.

THEORY

Discussion is restricted to 1:1 complexes, Me + L ⇌ MeL, and it is assumed that the magnetic coefficient a (complexed ion) ≠ a (uncomplexed ion). Then it follows from eqn. (1):

$$(1/T_1)_p = \sum_i a_i C_i = a_{Me}\,[Me] + a_{MeL}\,[MeL] \tag{2}$$

Taking the mass balance $[Me]_0 = [Me] + [MeL]$ into account,

$$(1/T_1)_p = a_{MeL}\,[Me]_0 + (a_{Me} - a_{MeL})\,[Me] = a_{Me}\,[Me]_0 + (a_{MeL} - a_{Me})\,[MeL] \tag{3}$$

Equation (3) shows that $(1/T_1)_p$ of the protons in the solution changes if the difference in the magnetic coefficients is not zero: $a_{Me} \neq a_{MeL}$. Generally, the relaxation rate $(1/T_1)_p$ depends on both the aquo ions $Me(H_2O)_n$ and the complex ions MeL (for simplification the electric charge is neglected); eqn. (1) has to be written in the form:

$$(1/T_1)_p = \sum_i a_i C_i = \sum_{q=1}^{k} a_q C_{Me}^{(q)} + \sum_{r=1}^{m} a_r C_{MeL}^{(r)} \tag{4}$$

For the practical application of n.m.r.t. in complexometry, a linear change in $(1/T_1)_p$ as a function of the added ligand concentration [L] is wanted for both regions $[L] < [L]_{eq}$ (reaction line) and $[L] > [L]_{eq}$ (excess line), where eq denotes the equivalence point. This condition is fulfilled if the effective complex formation constant is sufficiently large. For mass balance, before the equivalence point is reached

$$[L] \approx 0; \quad [MeL] = [L]_0 \left(\frac{V_L}{V_{tot}}\right); \quad [Me] = [Me]_0 \left(\frac{V_0}{V_{tot}}\right) - [L]_0 \left(\frac{V_L}{V_{tot}}\right) \tag{5}$$

where V_0 is the initial volume containing $[Me]_0$, $[L]_0$ is the concentration of L in the standard solution, V_L the volume of the standard solution added, and $V_{tot} = V_0 + V_L$ the total volume of the reaction mixture. In this range the paramagnetic relaxation rate is then:

$$\left(\frac{1}{T_1}\right)_p = a_{Me}\,[Me]_0 \left(\frac{V_0}{V_{tot}}\right) + (a_{MeL} - a_{Me})\,[L]_0 \left(\frac{V_L}{V_{tot}}\right) = \left(\frac{1}{T_1}\right)_{p,o} \left(\frac{V_0}{V_{tot}}\right) + (a_{MeL} - a_{Me})\,[L]_0 \left(\frac{V_L}{V_{tot}}\right) \tag{6}$$

where $(1/T_1)_{p,o}$ is the initial paramagnetic relaxation rate in the paramagnetic solution. Above the equivalence point, $(1/T_1)_p$ stays constant as long as the ligand L is diamagnetic and the experimentally measured paramagnetic relaxation rate is corrected for dilution effects. Finally, for one kind of paramagnetic ion, after correcting the dilution effect,

$$\frac{V_{tot}}{V_0}\left(\frac{1}{T_1}\right)_p = a_{Me}\,[Me]_0 + (a_{MeL} - a_{Me})\,[L]_0\,V_L/V_0 \tag{7}$$

This equation shows linear dependence of the corrected relaxation rate $(V_{tot}/V_0)\ (1/T_1)_p$ on the added volume V_L of the titrant.

RESULTS AND DISCUSSION

*Titrations with ethylenediamine-*N,N,N',N'*-tetraacetic acid (EDTA)*

The determination of cations by titration with EDTA is based on the formation of soluble but undissociated chelate complexes. The equivalence point of the reaction is observed with an indicator which forms colored complexes with the metal ion that are less stable than the metal complexes with EDTA. During the formation of the complexes, protons are released and the conditions for the reaction (e.g. pH value) have to be chosen carefully. When the nuclear magnetic relaxation rate is the indicating method, the external conditions for the reaction are probably less critical if the effective constant of complex formation is sufficiently large.

Figure 1 shows the titration curves for Co^{2+}, Mn^{2+}, Fe^{3+}, and Ni^{2+} with the disodium salt of EDTA. The corrected and normalized paramagnetic relaxation rate, $(V_{tot}/V_0)\ (T_{1,0}/T_1)_p$, is plotted as a function of the ratio of the mol number of the organic ligand to the initial mol number of para-

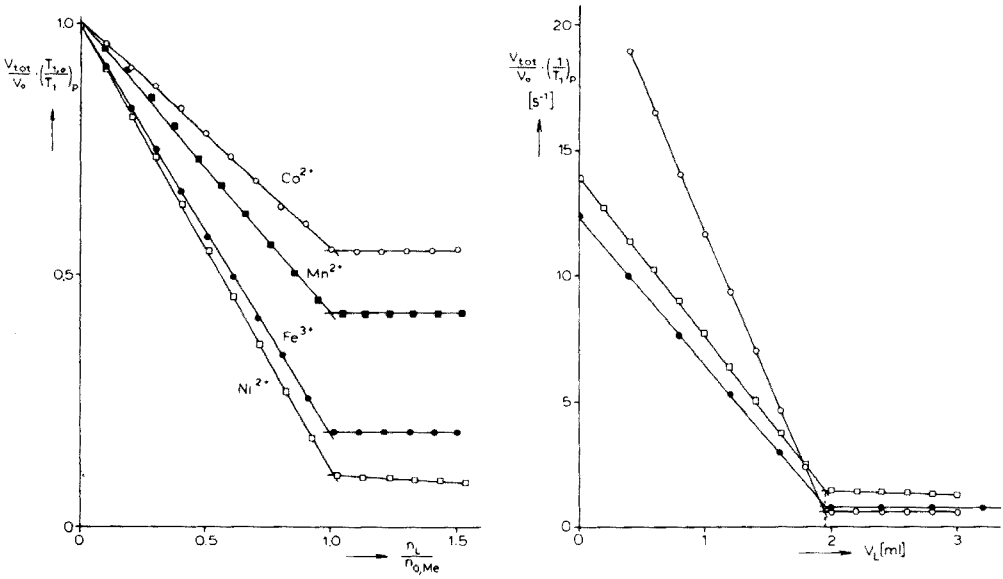

Fig. 1. N.m.r.t. of different transition metal ions with EDTA (disodium salt). The corrected and normalized proton relaxation rate, $(V_{tot}/V_0)\ (T_{1,0}/T_1)_p$, is plotted as a function of the ratio of the mol number of the ligand to the mol number of the transition metal ion in solution.

Fig. 2. N.m.r.t. of Ni^{2+} with EDTA in different media. The corrected relaxation rate of the protons, $(V_{tot}/V_0)\ (1/T_1)_p$, is plotted as a function of the volume of titrant (0.1 M EDTA, disodium salt). V_0 = 10.0 ml, $[Ni^{2+}]_0$ = 0.0196 M. ○ Ammoniacal solution; □ neutral solution; • acetate buffer.

magnetic ions in the solution. This diagram shows the usefulness of n.m.r.t. in complexiметric titrations.

Titration of Ni^{2+} with EDTA. Details of the titration of Ni^{2+} with EDTA are shown in Fig. 2, where the corrected relaxation rate, $(V_{tot}/V_0)\,(1/T_1)_p$, is plotted as a function of the added volume V_L of 0.1 M EDTA solution, disodium salt. The influence of the medium (e.g. pH) on the n.m.r.t. of Ni^{2+} with EDTA was studied in ammoniacal solution, neutral solution, and acetate-buffered solution.

Independent of the particular pH, the volume-corrected relaxation rate changes linearly with the added volume of EDTA solution. In the three cases, 10.0 ml of 0.0196 M $NiSO_4$ were titrated with 0.1 M EDTA (Titriplex III, E. Merck, Darmstadt); the equivalence point was found at V_{eq} = (1.96 ± 0.01) ml which was the same as obtained in a control titration with murexide as indicator. Figure 2 shows that the pH of the solution is only of minor importance in determining V_{eq} by n.m.r.t., in contrast to the classical indicator method. The slopes of both the reaction line and the excess line, however, depend on the particular conditions chosen for the reaction. The sensitivity of the slope of the reaction line to the reaction conditions is probably due to the medium-dependent formation of different Ni^{2+} complexes (different magnetic factors a_i, see eqn. 1). For n.m.r.t. of Ni^{2+} with EDTA, an ammoniacal solution is the most useful.

N.m.r.t. of Cu^{2+} with EDTA. The n.m.r.t. of Cu^{2+} with EDTA is similar to the determination of Ni^{2+} by this method. In Fig. 3 the titration of

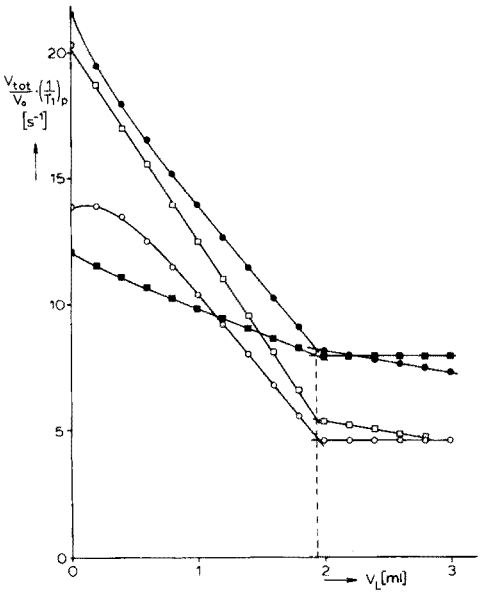

Fig. 3. N.m.r.t. of V_0 = 10.0 ml of 0.0195 M Cu^{2+} with the disodium salt of EDTA (0.1 M) in different media. • Neutral solution, □ neutral solution + K_2SO_4; ○ acetate buffer; ▪ ammoniacal solution.

10.0 ml of 0.0195 M $CuSO_4$ with 0.1 M EDTA is shown for different reaction conditions. The equivalence point, independent of external conditions, was (1.95 ± 0.01) ml. However, in contrast to the titration of Ni^{2+}, deviations from linearity are found at the start of the titration. This is probably due to the formation of H^+ during the titration whereby the equilibria may be influenced. Another interesting point is that, depending on the conditions, different relaxation rates are found at the equivalence point. During the reaction not only the complex $Cu(EDTA)^{2-}$ but also other complexes are formed, particularly protonated complexes. This was proved by studying the proton spin lattice relaxation time T_1 in aqueous solution of $Cu(EDTA)^{2-}$ as a function of the H^+ concentration. At high proton concentrations (pH = 0 ... 1) the relaxation rate is about 9.0 s^{-1}. With increasing pH, $1/T_1$ decreases to about 4.5 s^{-1} (pH ≈ 6). Above pH 10, $1/T_1$ increases.

N.m.r.t. of Fe^{3+} with EDTA. Fe^{3+} forms very stable complexes with EDTA. A pH value of 2.5 and sulfosalicylic acid, tiron, or xylenol orange as indicator are common in classical complexiметry. N.m.r. titrations of 0.0196 M $Fe(NO_3)_3$ (10.0 ml) with 0.1 M EDTA were done in neutral solutions and in solutions acidified with 0.10 ml of 2 M HNO_3, or buffered with acetate. The results are given in Fig. 4. Again, the reaction medium is important. In the acidified solution, $(V_{tot}/V_0)\ (1/T_1)_p$ decreases by a factor of about 5 until the equivalence point is reached. However, in the buffered

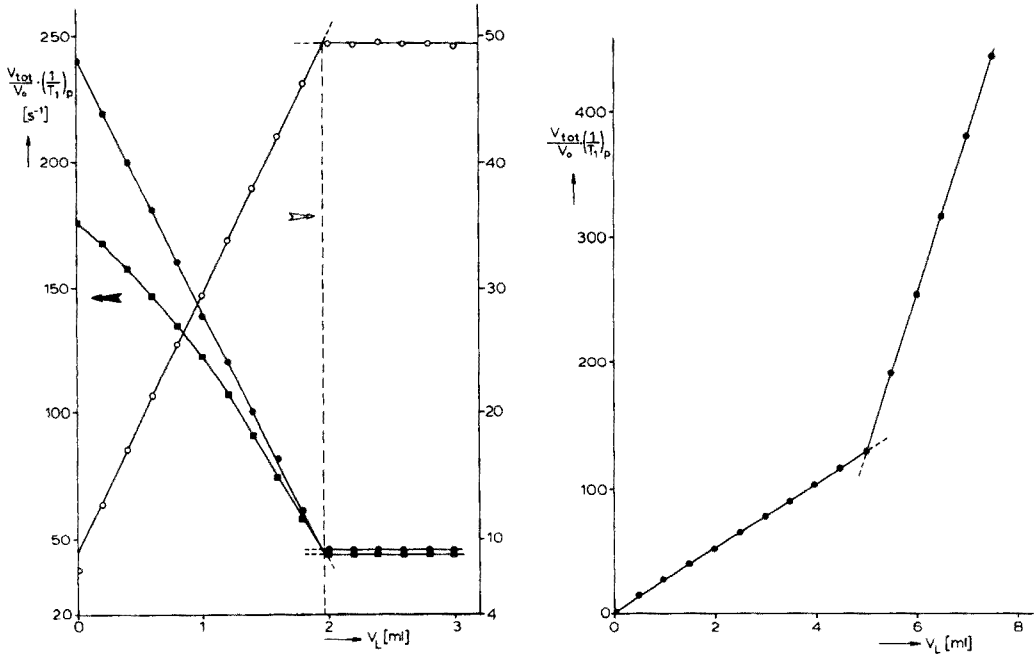

Fig. 4. N.m.r.t. of V_0 = 10.0 ml of 0.0198 M Fe^{3+} with the disodium salt of EDTA (0.1 M) in different media. • Acidified solution; ▪ neutral solution; ○ acetate buffer.

Fig. 5. N.m.r.t. of EDTA with Fe^{3+} solution (0.1 M $Fe(NO_3)_3$. V_0 = 10.0 ml of 0.05 M EDTA.

solution (V_{tot}/V_0) $(1/T_1)_p$ increases until the equivalence point is reached. In both cases the relaxation rate at the equivalence point is about the same (compare the two ordinates in Fig. 4). The large decrease of $(1/T_1)_{p,o}$ on the addition of a buffer solution is due to the formation of the complex $Fe_3(CH_3COO)_6O^+$. The almost identical excess lines are determined mainly by the influence of the Fe(EDTA) complex on the relaxation rate of the protons; therefore the pH is of minor importance. The n.m.r.t. curve for a pure $Fe(NO_3)_3$ solution is slightly bent, as the solution is partially hydrolysed. Protons produced during the titration shift the hydrolysis equilibrium. This explains the slight curvature of the reaction line. The reverse procedure — titration of an EDTA solution with an appropriate ionic solution — is also possible, as shown in Fig. 5. In this case, the effect is particularly pronounced because of the high effective magnetic moment of Fe^{3+}.

N.m.r.t. of Mn^{2+} with EDTA. The disodium salt of EDTA produces unreliable results because the protons released during titration prevent the complete formation of complexes at the equivalence point. With the tetrasodium salt good results were obtained.

N.m.r.t. of Co^{2+} with EDTA. The titration of Co^{2+} is similar to the Mn^{2+} titration, i.e. the tetrasodium salt of EDTA is required. The results are shown in Fig. 1. The complexation of Co^{2+} produces a smaller change in $(1/T_1)_p$ than Ni^{2+}, Fe^{3+}, or Mn^{2+}.

Simultaneous determination of several cations by n.m.r.t. with EDTA

EDTA forms very stable complexes with many polyvalent cations, so that it is not a selective reagent, although the selectivity can be increased by masking, pH control etc. As far as n.m.r.t. is concerned, the possibility of determining several cations directly without masking reagents, auxiliary complex-forming reagents, or variable pH, should be possible when the complex formation constants for the different cations in the solution differ by a factor of ca. 10^3, in the same way as for other instrumental methods. Also, the complex equilibria have to be reached quickly.

In mixtures of Cu^{2+} + Mn^{2+}, or Ni^{2+} + Mn^{2+}, the complexes Cu(EDTA) and Ni(EDTA) are formed before Mn^{2+} reacts with the chelating ligand EDTA. The magnetic coefficient a_i (see eqn. 1) for Mn^{2+} is quite different from the coefficients $a(Cu^{2+})$ and $a(Ni^{2+})$. N.m.r.t. of Cu^{2+} + Mn^{2+} and of Ni^{2+} + Mn^{2+} is possible; the results are shown in Fig. 6. At the beginning of the formation of Cu(EDTA) and Ni(EDTA), $(1/T_1)_p$ changes slowly. After complete complexation of Cu^{2+} in the mixture of Cu^{2+} + Mn^{2+}, the slope of the curve $(1/T_1)_p = f(V_L)$ changes abruptly and is quite steep in the range where Mn(EDTA) is formed. In the mixture Ni^{2+} + Mn^{2+}, the two steps are not so sharply separated, probably because of kinetic effects. The end of the complex formation of both (Ni^{2+} + Mn^{2+})—EDTA and (Cu^{2+} + Mn^{2+})—EDTA is marked by a very sharp change of $(1/T_1)_p = f(V_L)$. Further addition of EDTA changes the relaxation rate very little (the magnetic coefficients remain almost constant).

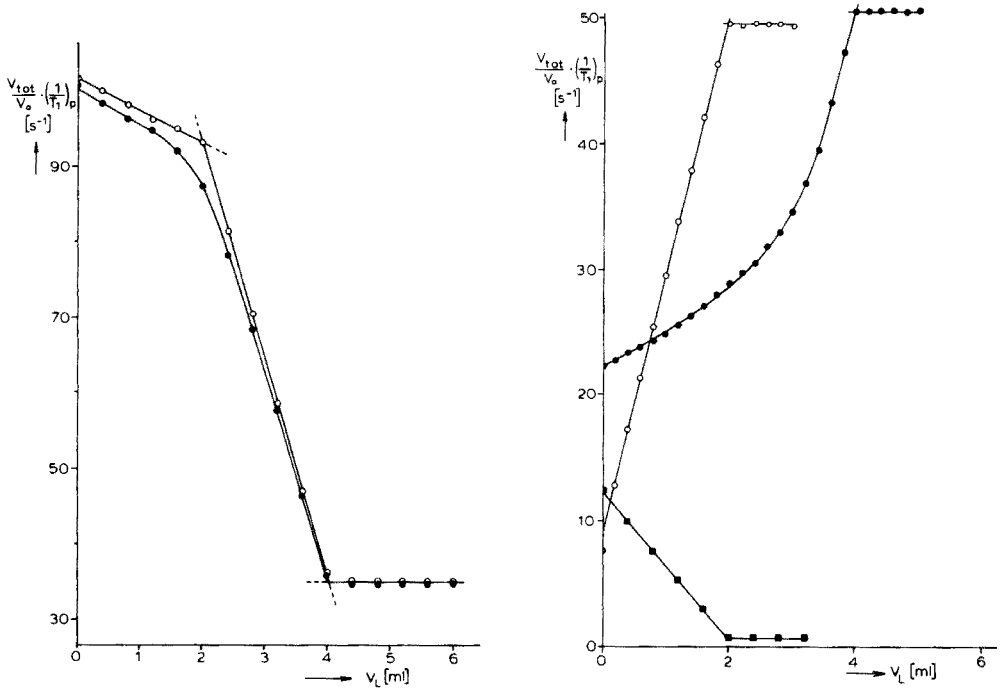

Fig. 6. Simultaneous titration of (Ni^{2+} + Mn^{2+}) and (Cu^{2+} + Mn^{2+}) with 0.05 M EDTA (tetrasodium salt). Initial volume: V_0 = 10.0 ml. ○ Cu^{2+} + Mn^{2+}, $[Cu^{2+}]_0 = [Mn^{2+}]_0$ = 0.01 M; ● Ni^{2+} + Mn^{2+}, $[Ni^{2+}]_0 = [Mn^{2+}]_0$ = 0.01 M.

Fig. 7. Simultaneous and individual titrations of Fe^{3+} + Ni^{2+} with 0.1 M EDTA (disodium salt) in acetate buffer solution. Initial volume: V_0 = 10.0 ml. ○ $[Fe^{3+}]_0$ = 0.02 M; ▪ $[Ni^{2+}]_0$ = 0.02 M; ● $[Fe^{3+}]_0 = [Ni^{2+}]_0$ = 0.02 M.

Another example of a simultaneous n.m.r.t. is the determination of Ni^{2+} and Fe^{3+} in acetate-buffered solution of pH 4.62. The titration curve is shown in Fig. 7 together with those for the individual ions Ni^{2+} and Fe^{3+}. The titration curve of the mixture is the sum of the two individual titration curves.

N.m.r.t. with nitrilotriacetic acid (NTA)

NTA and its salts may be applied in complexiметric n.m.r.t., and complexes of the type MeL as well as MeL_2 are to be expected. In Fig. 8 the n.m.r.t. of Mn^{2+} with NTA is shown. Curve (a) was found with the disodium salt of NTA; complex formation is not complete and it is impossible to find the respective equivalence point. Satisfactory results were obtained with the trisodium salt of nitrilotriacetic acid. The hydrolysis equilibrium makes a solution of $N(CH_2COONa)_3$ strongly alkaline: $NTA^{3-} + H_2O = HNTA^{2-} + OH^-$. In the formation of metal complexes $Mn^{2+} + HNTA^{2-} = Mn(NTA)^- + H^+$, the H^+ ions formed are neutralized and the Mn^{2+} solution titrated is practically

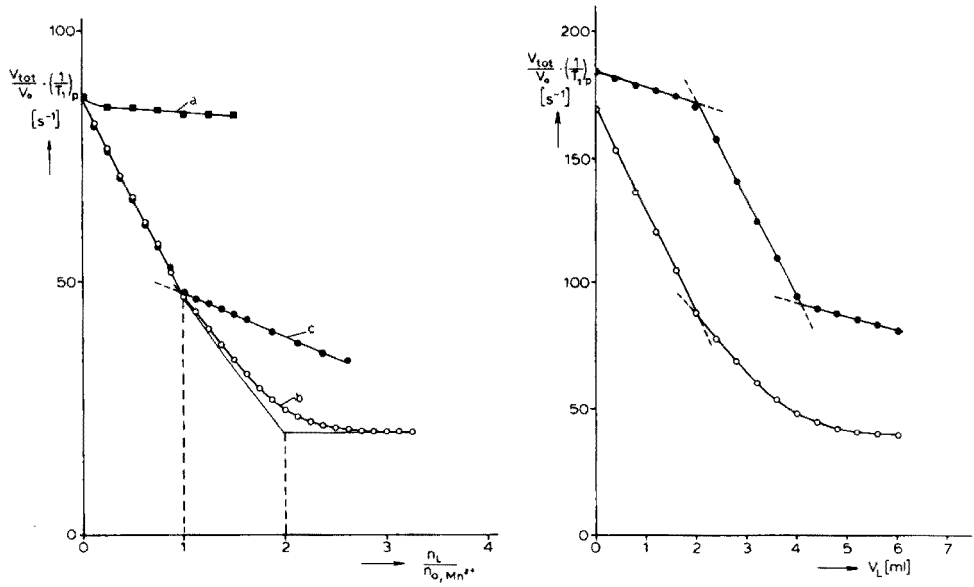

Fig. 8. N.m.r.t. of Mn^{2+} with nitrilotriacetic acid (NTA). Initial concentration of Mn^{2+}: 0.01 M. Initial volume of the solution: 10.0 ml. ▪ Titration with disodium salt of NTA (0.1 M) (a); ○ titration with trisodium salt of NTA (0.1 M) (b); • titration with trisodium salt of NTA (0.1 M) at pH 7.5 (borate) (c).

Fig. 9. Simultaneous titration of Ni^{2+} and Mn^{2+} with the trisodium salt of NTA (0.1 M). Initial volume: V_0 = 10.0 ml. • Mn^{2+} + Ni^{2+}, $[Ni^{2+}]_0 = [Mn^{2+}]_0$ = 0.02 M; ○ Mn^{2+} alone, $[Mn^{2+}]_0$ = 0.02 M.

neutral until the complex formation is completed (a self-buffering system). Curve (b) in Fig. 8 shows the titration of Mn^{2+} with $N(CH_2COONa)_3$. The spin lattice relaxation rate of the protons decreases linearly with increasing concentration of the complex formed until the first equivalence point at $n_L/n_{o,Mn^{2+}} = 1$ is reached. Beyond this point, $Mn(NTA)^-$ reacts with a second ligand and forms the complex ion $Mn(NTA)_2^{4-}$. This reaction is not completed at the second equivalence point; the titration curve bends gently in this region.

The complex formation constant $K_2 = [MnL_2]/([MnL]\ [L])$ is clearly smaller than 10^6 l mol^{-1}. This limit is estimated because of the deviations of $(V_{tot}/V_0)\ (1/T_1)_p = f(n_L/n_{0,Me})$ from a straight line. A quantitative investigation of the curvature of the titration function $1/T_1 = f(n_L)$ should allow a calculation of K_2. To do so, the pH of the solution containing MnL^- was kept constant at 9.3 with a borate buffer, and $\log K_2 = 3.02 \pm 0.02$ (T = 25°C) was found. Dividing this value by the activity coefficient α_H of NTA, which takes the proton equilibria into account, gave $\log K_2 = 3.60 \pm 0.02$, in good agreement with the value $\log K_2 = 3.7 \pm 0.2$ determined by Schwarzenbach and Beidermann [4]. In a third experiment Mn^{2+} was titrated with $N(CH_2COONa)_3$ at pH 7.5 (borate buffer). The results are shown in curve (c) of

Fig. 8; the curvature of $(1/T_1) = f(n_L/n_0)$ beyond $n_L/n_0 = 1$ is not visible in practice. This experiment reveals the importance of the proton concentration for the formation of $Mn(NTA)_2^{4-}$.

The trisodium salt of NTA can also be used for simultaneous titrations, e.g. for a solution of ($NiSO_4$ + $MnSO_4$). At first, the complex $Ni(NTA)^-$, which is more stable than $Mn(NTA)^-$, is formed. Then $Mn(NTA)^-$ is formed before $Ni(NTA)^-$ reacts with NTA^{3-} to give $Ni(NTA)_2^{4-}$. These consecutive steps are indicated by the two breaks in the upper titration curve in Fig. 9. The lower curve represents the n.m.r.t. of Mn^{2+} alone with $N(CH_2COONa)_3$. First, the formation of $Mn(NTA)^-$ occurs (compare the slopes of the upper and lower curves). The second stage $Mn(NTA)^- + NTA \rightarrow Mn(NTA)_2^{4-}$ is represented by the bent part of the titration curve. The rather low equilibrium constant is responsible for this non-linear behavior (see above).

As a final example, the simultaneous titration of ($CaCl_2$ + $MnCl_2$) with NTA was studied. There is only a small difference in the equilibrium constants of Ca^{2+} and Mn^{2+} with regard to the first and second complexing step. As expected, the individual equivalence points are no longer intercepts of straight lines but bent titration curves. From these curves ratios of equilibrium constants may be determined: $K_1(Mn(NTA)^-)/K_1(Ca(NTA)^-)$ and $K_2(Mn(NTA)_2^{4-})/K_2(Ca(NTA)_2^{4-})$. From the titration curve shown in Fig. 10, the deviations from the straight lines yield the equilibrium constants (T = 25°C): $K = K_1(Mn(NTA)^-)/K_1(Ca(NTA)^-) = 14.2$; $\log K = 1.15$; $K' = K_2(Mn(NTA)_2^{4-})/K_2(Ca(NTA)_2^{4-}) = 3.60$; $\log K' = 0.56$. These values are in good agreement with literature data: Mn^{2+}: $\log K_1 = 7.44$ [5], $\log K_2 = 3.7 \pm 0.2$ [4]. Ca^{2+}: $\log K_1 = 6.33$ [6], $\log K_2 = 3.43$ [7]. The values $\log K = 1.11$ and $\log K' = 0.27$ follow from these data.

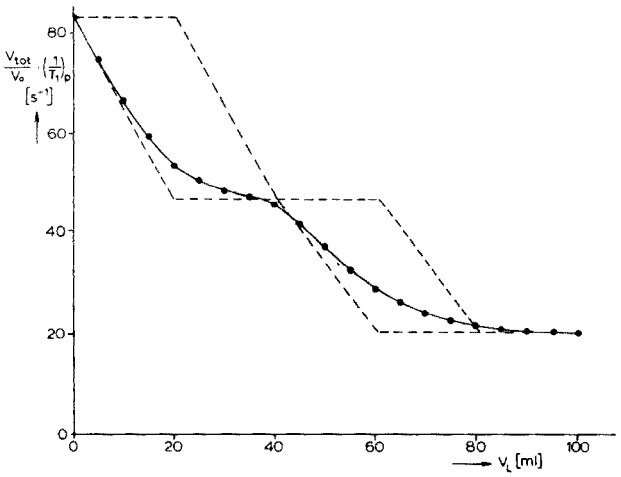

Fig. 10. Simultaneous titration of Mn^{2+} and Ca^{2+} with 0.05 M NTA (trisodium salt). Initial volume: V_0 = 100.0 ml. Initial concentrations: $[Mn^{2+}]_0 = [Ca^{2+}]_0 = 0.01$ M.

Support of this work by the "Deutsche Forschungsgemeinschaft" and the "Fonds der Chemischen Industrie" is gratefully acknowledged.

REFERENCES

1 K. H. Nothnagel and A. Weiss, Ber. Bunsenges. Phys. Chem., 74 (1970) 599.
2 A. Schlüter and A. Weiss, Fresenius, Z. Anal. Chem., 266 (1973) 177.
3 A. Schlüter and A. Weiss, Anal. Chim. Acta, 97 (1978) 93.
4 G. Schwarzenbach and W. Beidermann, Helv. Chim. Acta, 31 (1948) 331.
5 G. Schwarzenbach and E. Freitag, Helv. Chim. Acta, 34 (1951) 1492.
6 T. H. Bohigian and A. E. Martell, Prog. Report. US Atomic Energy Commission, Contract No. AT (30-1)-1823, 1960.
7 G. Schwarzenbach, E. Kampitsch and R. Steiner, Helv. Chim. Acta, 28 (1945) 828.

Analytica Chimica Acta, 99 (1978) 167—175

CHELATE FORMATION OF ZIRCONIUM WITH XYLENOL ORANGE AND SEMI-XYLENOL ORANGE

HISAKUNI SATO*, YUKIO YOKOYAMA, and KOZO MOMOKI

Laboratory of Analytical Chemistry, Faculty of Engineering, Yokohama National University, Ooka 2-31-1, Minami-ku, Yokohama (Japan)

(Received 31st January 1978)

SUMMARY

The composition, formation constants, and molar absorptivities of the chelates of zirconium ion wtih xylenol orange and semi-xylenol orange are investigated spectrophotometrically in strong acid medium at ionic strength 3.0 ($NaClO_4$ and $HClO_4$). The data obtained were processed with a newly-constructed computer program and with LETAGROP/SPEFO. In the zirconium—xylenol orange system, $Zr \cdot H_3L$, $Zr \cdot H_4L$, and $Zr_2 \cdot L$ are present with logarithmic overall formation constants of 37.80, 38.68, 43.47, and molar absorptivities of 3.10×10^4 (485 nm), 5.98×10^4 (528 nm), 9.50×10^4 (551 nm) l mol^{-1} cm^{-1}, respectively. The chelates $Zr \cdot L$ and $Zr \cdot HL$ were found in the zirconium—semi-xylenol orange system with logarithmic overall formation constants of 26.25 and 27.56, and molar absorptivities of 5.70×10^4 (532 nm) and 8.30×10^4 (535 nm) l mol^{-1} cm^{-1}, respectively. Semi-xylenol orange is more sensitive and reliable than xylenol orange as a spectrophotometric reagent for zirconium.

The many investigations [1—6] of the chelate formation of zirconium ion with xylenol orange differ [7] in terms of the composition of the chelates formed, the wavelength of maximum absorption, the molar absorptivities, etc. These differences are caused mainly by the use of impure reagents and by the innate properties of the zirconium ion [8] in aqueous solution. Nevertheless, xylenol orange is often used empirically as a sensitive reagent for the spectrophotometric determination of zirconium. Olson and Margerum [9] separated xylenol orange from semi-xylenol orange, and pointed out that the latter is the more sensitive reagent for zirconium ion. However, the method of purification was inadequate [10], and the results are inconclusive.

In the present work, the chelate formation of zirconium ion with xylenol orange and semi-xylenol orange was studied spectrophotometrically with purified reagents. Because the chelate formation is very slow at room temperature, approximate values of the formation constants can only be obtained under definite conditions; here, visible spectra were measured at room temperature after the solutions of zirconium ion, depolymerized beforehand, were mixed with the reagent and heated at 80°C for 30 min. Ionic strength was adjusted to 3.0 with sodium perchlorate and perchloric acid; the acid concentration range was 0.1—1.0 M.

EXPERIMENTAL

Reagents

Xylenol orange and semi-xylenol orange were purified by ion-exchange chromatography with DEAE—cellulose [11]. The hydrochloric acid salts were dissolved in water (10^{-3} M). Sodium perchlorate was recrystallized from aqueous solution. Other reagents were of guaranteed grade. Zr(IV) solution (10^{-3} M) was prepared by dissolving zirconium oxychloride, $ZrOCl_2 \cdot 8H_2O$, in 0.1 M $HClO_4$ solution. The zirconium concentration was determined by titration with EDTA and xylenol orange.

Apparatus

Visible spectra were measured (Simazu UV-200) in 1.00-cm quartz cells. A Beckman Expandomatic pH meter with glass and calomel electrodes was used. For data processing, the HITAC 8700/8800 system (Computer Center, University of Tokyo) was used.

Procedure

An aliquot of 10^{-3} M Zr(IV) solution and a suitable amount of 5 M $HClO_4$ solution were placed in a 50-ml volumetric flask, and diluted with water to adjust the acid concentration to about 2 M. The mixed solution was heated in a water bath (80°C) to depolymerize zirconium ion, and cooled to room temperature. Suitable amounts of xylenol orange or semi-xylenol orange solution and 5 M $NaClO_4$ solution were added, and the solution was diluted to 50.0 ml with water (μ = 3.0) and heated to 80°C in a water bath for reaction to take place, before cooling to room temperature. The absorption spectrum of this solution was recorded over the range 650—350 nm. The heating times necessary for depolymerization and chelate formation will be mentioned later.

The acid formation constants of xylenol orange were evaluated from the curve obtained by titration of xylenol orange solution (30.12 mM, 10.0 ml) with 1 M NaOH (carbonate-free) at 28°C (1 M KNO_3).

Data processing

The transmittance values of the m solutions, in which the concentrations of zirconium ion (C_M), ligand (C_L), and $HClO_4$ (C_H) were varied, were obtained from 600 to 410 nm at intervals of 10 nm. From the experimental data (T_{ij}, C_{Mj}, C_{Lj}, C_{Hj}; i = 1—20, j = 1—m), the molar ratios of the chelates formed ($p:q:r$), overall formation constants (β_{pqr}), and molar absorptivities (ϵ_{pqr}) were evaluated as follows.

Initially, the molar ratios ($p:r$) and conditional formation constants (β_{pr}*) of the chelates formed at constant $HClO_4$ concentration were estimated roughly with a preparatory, newly constructed computer program in which the second moment matrix, R, is calculated [12] from the absorbance matrix:

$$[R_{kl}] = [\sum_{j=1}^{m} A_{kj} A_{lj}] \quad (k, l = 1, 2, \ldots, 20) \tag{1}$$

From the eigenvalues of this matrix, the rank of the absorbance matrix, $[A_{ij}]$, can be estimated. This rank indicates the number of independent absorption patterns in a group of absorption spectra, and so, the number of independent absorbing species, though these are not always equal. Next, the sum of the squares of the differences between the calculated and the measured absorbance values is calculated with systematic variations of two conditional formation constants, β_1^* and β_2^*, for the limited cases in which two types of chelate are formed. If necessary, the absorbance data are used partially. Absorbances can be represented as $[A_{ij}] = [\epsilon_{ik}][C_{kj}]$, where ϵ_{ik} is the molar absorptivity of the kth absorbing species at the ith wavelength, and C_{kj} is the concentration of the kth species in the jth solution: $C_{kj} = \beta_{pr}^*[M^*]_j^p [L^*]_j^r$. The equilibrium concentrations are calculated with the revised sub-routine, COGSNER [13]:

$$[\epsilon_{ik}]^{calc} = [[A_{ij}][C_{kj}]^T][[C_{kj}][C_{kj}]^T]^{-1} \tag{2}$$

where T denotes transform. Then, absorbance values can be calculated for the assumed values of β_1^* and β_2^* from

$$[A_{ij}]^{calc} = [\epsilon_{ik}]^{calc}[C_{kj}] \tag{3}$$

with $s = \Sigma_{i,j} (A_{ij}^{calc} - A_{ij}^{meas})^2$ and $\sigma^2 = s/20\ m_l$

If the values of σ^2 are properly graded as $<10^{-6}$, $10^{-6} \sim 10^{-5}$, $10^{-5} \sim 10^{-4}$, and so on, a contour map of σ^2 can be obtained roughly in a $\log \beta_1^* - \log \beta_2^*$ plane. Thus, the change of σ^2 with the changes in β_1^* and β_2^* can be obtained. The assumed molar ratio, $p:r$, can be confirmed as appropriate or not.

The program LETAGROP/SPEFO [14] refines the conditional formation constants for each step of the acid concentration (Typ = 1 calculation).

The proton number (q) and the approximate values of the overall formation constants (β_{pqr}) are evaluated from the molar ratios ($p:r$), the conditional formation constants estimated above, the acid formation constants of the ligand, and the formation constants of the hydroxo complexes of the zirconium ion. The resulting overall formation constants are refined with LETAGROP/SPEFO (Typ = 2 calculation). The molar absorptivities for each chelate formed are obtained simultaneously.

Acid formation constants of xylenol orange and semi-xylenol orange

Murakami et al. [10] have reported the acid formation constants of xylenol orange and semi-xylenol orange, but $\log k_6$ for xylenol orange and $\log k_4$ for semi-xylenol orange are quoted as "<1.5"; $\log k_7$, k_8, k_9 for xylenol orange and $\log k_5$, k_6 for semi-xylenol orange are doubtful as they were obtained by means of Hammett's acidity function (H_0) which should be used for one-step protonation to the neutral base.

Accordingly, k_1—k_7 for xylenol orange were estimated by means of the pH titration at relatively high concentration. A similar titration of

semi-xylenol orange could not be performed because of its low solubility at ca. pH 2. The values of k_1—k_3 for semi-xylenol orange taken were inevitably those obtained in dilute solution (μ = 0.1); the value of log k_4 was assumed to be 1.50. Values for k_8 (xylenol orange) and k_5 (semi-xylenol orange) were estimated from the spectra data for ionic strength 3.0.

The acid formation constants observed are shown in Table 1.

Formation constants of the hydroxo complexes of zirconium ion

Zirconium ions form hydroxo complexes, even in strong acid solution, and polymerize [8]. To calculate the overall formation constants for zirconium—xylenol orange and zirconium—semi-xylenol orange, these hydrolysis and polymerization constants are necessary. Many different values [15] have been reported and selection of the best value is difficult. Solovkin's hydrolysis constants [16] were adopted because of the similarity of the experimental conditions; polymerization reactions were neglected in data processing.

RESULTS AND DISCUSSION

Examination of the experimental conditions for chelate formation

Zirconium ion must be depolymerized [8] before reaction with the ligand in suitable experimental conditions, otherwise long reaction times would be needed, even at high temperature, to attain equilibrium. The heating times at 80°C necessary for the depolymerization of zirconium, and for chelate formation with xylenol orange or semi-xylenol orange, were therefore examined. The stock solution of zirconium ion was prepared several months before use, so that the polymerization reaction referred to an equilibrium state.

Heating for 20 min was sufficient for depolymerization when the acid concentration was adjusted to 2 M or higher with $HClO_4$. After the xylenol orange or semi-xylenol orange solution was added and the solution was adjusted to 50 ml (ionic strength, 3.0), heating for more than 20 min was needed to achieve equilibrium chelate formation for a final acid concentration of 0.1 M. The solutions were therefore heated for 30 min at 80°C.

Zirconium—xylenol orange system. Solutions (44) were prepared, in which the $HClO_4$ concentration was changed in four steps (0.1, 0.2, 0.5 and

TABLE 1

Logarithmic acid formation constants for xylenol orange and semi-xylenol orange

Constant	k_1	k_2	k_3	k_4	k_5	k_6	k_7	k_8
Xylenol orange	10.58[a]	9.34[a]	6.09[a]	2.56[a]	2.24[a]	1.45[a]	1.43[a]	−1.24[b]
Semi-xylenol orange	10.76[c]	7.46[c]	2.37[c]	1.50[d]	0.11[b]	—	—	—

[a]pH titration, 1 M KNO_3. [b]Spectrophotometric method, μ = 3.0. [c]pH titration, 0.1 M KNO_3. [d]Assumed.

1.0 M), the xylenol orange concentration was 9.95×10^{-6} or 1.990×10^{-5} M, and the zirconium ion concentration was varied between 0 and 10^{-4} M. Some spectra for 0.1 M $HClO_4$ media (Fig. 1) indicate that more than one type of chelate is formed. For higher acid concentrations, a similar tendency is observed. Irrespective of the change in acid concentration, the spectra tend towards a common pattern when C_M/C_L increases.

The number of independent spectrum patterns was presumed to be three for all four groups with the same acid concentration, for initial data processing purposes. The formation of two types of chelate, in which the molar ratios (p: r) are 1:1 and 2:1, was indicated.

Figure 2 shows a contour map of σ^2 for the data group of 1.0 M $HClO_4$; 1:1 and 2:1 chelates were assumed to form. The contour lines show clearly the presence of a minimum. When the acid concentration decreases, the contour lines in similar maps are increasingly distorted to give a more elliptic form, resulting in shallower minima. This means that there is a positive correlation between log β_1* and log β_2*. The correlation, which is thought to appear because both of these constants are too large, causes low precision in the determination of each constant.

Table 2 gives the data processing results. The conditional formation constants obtained for each acid concentration are shown at the left side of the Table. From these constants, the formation of three types of chelate, $Zr \cdot H_3L$, $Zr \cdot H_4L$, and $Zr_2 \cdot L$, was deduced after numerous calculations involving trial and error. The overall formation constants were estimated (see center column) and from these the conditional constants,

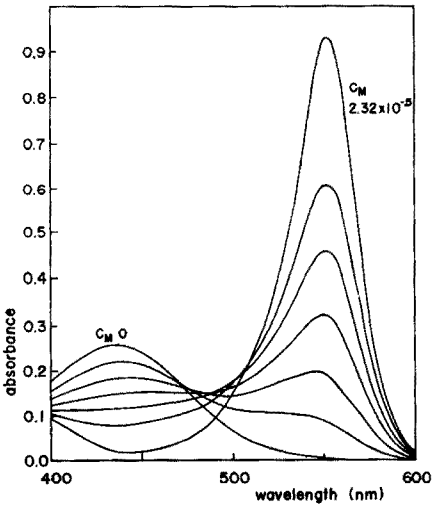

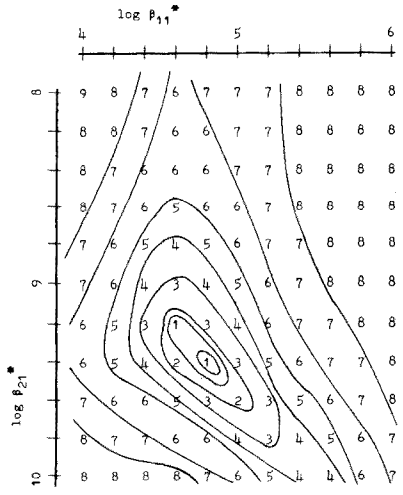

Fig. 1. Absorption spectra of zirconium—xylenol orange. 0.10 M $HClO_4$, $C_L = 9.95 \times 10^{-6}$ M, $C_M = 0$—2.32×10^{-5} M.

Fig. 2. Contour map of σ^2 for zirconium—xylenol orange (1.0 M $HClO_4$).

TABLE 2

Logarithmic formation constants for the zirconium—xylenol orange system

Typ = 1 calculation			Typ = 2 calculation		Re-calculation	
Conditional formation constant			Overall formation constant		Conditional formation constant	
Acid concn. (M)	$Zr \cdot L^*$	$Zr_2 \cdot L^*$			$Zr \cdot L^*$	$Zr_2 \cdot L^*$
0.10	8.07	15.90	$Zr \cdot H_3L$	37.80	6.98	14.18
0.20	6.88	13.91	$Zr \cdot H_4L$	38.68	6.51	13.17
0.50	5.54	11.20	$Zr_2 \cdot L$	43.47	5.63	11.20
1.00	4.81	9.36			4.83	9.40

of practical use, were re-calculated. Table 2 shows that the latter values agree more closely with the values evaluated directly when the acid concentration increases. Although the differences are attributed mainly to the low precision in the determination of each conditional constant, there may be the possibility of formation of other types of chelate.

Figure 3 shows the calculated molar absorptivity curves for the chelates formed. The spectrum of $Zr \cdot H_3L$ is broad and its maximum is small in comparison with that of $Zr \cdot H_4L$. The present experiment could not distinguish whether, for example, $Zr \cdot H_3L$ or $Zr(OH)H_4L$ is actually formed. The hydroxo complex may be the origin of such a broad absorption curve.

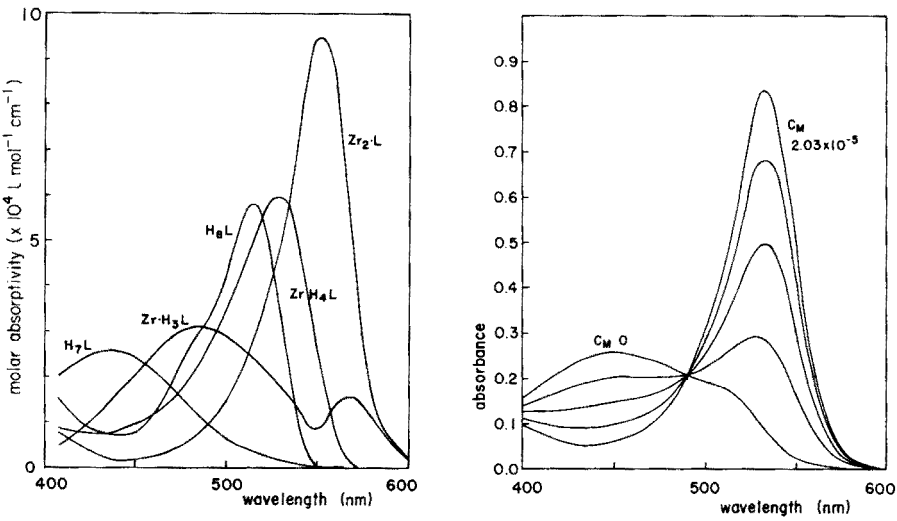

Fig. 3. Molar absorptivity curves for zirconium—xylenol orange.

Fig. 4. Absorption spectra of zirconium—semi-xylenol orange. 0.10 M $HClO_4$, C_L = 1.14 x 10^{-5} M, C_M = 0—2.03 x 10^{-5} M.

Zirconium—semi-xylenol orange system. The spectra for 25 solutions, in which C_L was kept constant and C_M was varied from 0 to 2.90×10^{-5} M for three $HClO_4$ concentrations (0.10, 0.20 and 0.50 M), were measured. Some absorption curves for 0.10 M $HClO_4$ are shown in Fig. 4. Similar curves were obtained for other acid concentrations. Isosbestic points were observed at 489, 492, and 500 nm for 0.1, 0.2, and 0.5 M $HClO_4$, respectively.

For preparatory data processing purposes, the number of independent absorbing patterns was presumed to be two for all groups with the same acid concentration; the formation of a 1:1 chelate was indicated. When the acid concentration is 0.10 M and C_L is larger than C_M, the 1:2 chelate may form to a slight extent but as its stability might not be high, and the spectral difference between the 1:1 and 1:2 chelates might not be large, it was difficult to determine its formation constant. Therefore, the formation of only the 1:1 chelate was assumed in the calculation of the spectral data, from which those of $C_L > C_M$ at 0.1 M $HClO_4$ were eliminated.

Table 3 shows that the best results were obtained when the formation of Zr · L and Zr · HL was assumed. Molar absorptivity curves for these chelates are shown in Fig. 5.

The conditional formation constants and the molar absorptivities of zirconium—semi-xylenol orange chelates are larger than those of 1:1 chelates with zirconium—xylenol orange. The spectral patterns of two zirconium—semi-xylenol orange chelates are similar, but the molar absorptivities of Zr · HL are larger than those of Zr · L. In these two chelates, all four possible sites in the ligand are thought to coordinate with the zirconium ion, because of the high absorptivities. It is interesting that the protonation of Zr · L results in increased absorptivities.

The spectrophotometric determination of zirconium ion

For zirconium—xylenol orange, the relation between absorbance and zirconium concentration is linear at 540 nm, and the molar absorptivity is 3.43×10^4 l mol^{-1} cm^{-1} for 0.2 M $HClO_4$ and ionic strength 3.0. When $NaClO_4$ was not added and xylenol orange was present in considerable excess, as is

TABLE 3

Logarithmic formation constants for zirconium—semi-xylenol orange system

Typ = 1 calculation		Typ = 2 calculation		Re-calculation
Conditional formation constant		Overall formation constant		Conditional formation constant
Acid concn. (M)	Zr · L*			Zr · L*
0.10	7.64	Zr · L	26.25	7.37
0.20	6.84	Zr · HL	27.56	6.86
0.50	6.05			5.88

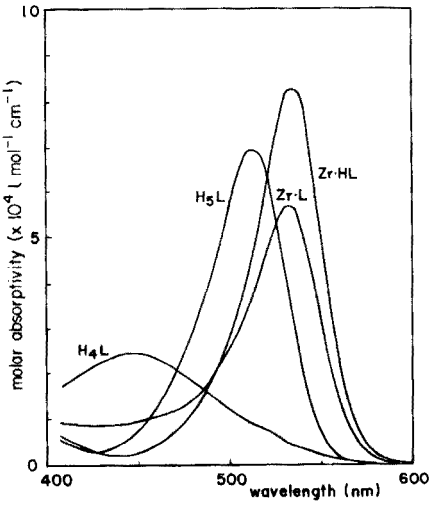

Fig. 5. Molar absorptivity curves for zirconium—semi-xylenol orange.

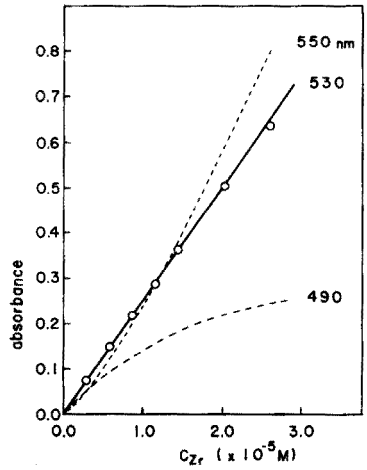

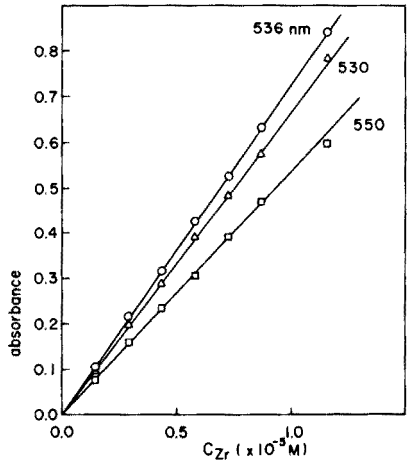

Fig. 6. Calibration curves with xylenol orange. 0.20 M $HClO_4$, $C_L = 4.98 \times 10^{-5}$ M.

Fig. 7. Calibration curves with semi-xylenol orange. 0.20 M $HClO_4$, $C_L = 3.42 \times 10^{-5}$ M.

usual in spectrophotometric work, a linear relationship was obtained at 530 nm (Fig. 6); the molar absorptivity was 2.52×10^4 l mol^{-1} cm^{-1}. Ionic strength influences the equilibrium state seriously. Semi-xylenol orange forms mainly 1:1 chelates in 0.2 M $HClO_4$; the molar absorptivity is high as indicated by Olson and Margerum [9]. Figure 7 shows the calibration curves for different wavelengths without the addition of $NaClO_4$. The linearity at each wavelength is good; the molar absorptivity at 536 nm is 7.24×10^4 l mol^{-1} cm^{-1}, about three times larger than that given by xylenol orange.

If the xylenol orange reagent contains semi-xylenol orange, a linear calibration curve can be obtained at 530 nm when the concentration of $HClO_4$ is 0.2 M and the ionic strength is ca. 0.2, but the slope of the line varies with the amount of semi-xylenol orange present. The use of xylenol orange, commercial or purified, may therefore be undesirable. Semi-xylenol orange gives more sensitive and reliable results; although this reagent is not available commercially, its synthesis [10] and purification [11] are simple.

REFERENCES

1 K. L. Cheng, Talanta, 2 (1959) 61.
2 A. K. Babko and M. I. Shtokalo, Ukr. Khim. Zh., 27 (1961) 566.
3 A. K. Babko and G. I. Gridchina, Zh. Neorg. Khim., 7 (1962) 889.
4 K. L. Cheng, Anal. Chim. Acta, 28 (1963) 41.
5 B. Budesinsky, Collect. Czech. Chem. Commun., 28 (1963) 1858.
6 P. M. Champion, P. Crowther, and D. M. Kemp, Anal. Chim. Acta, 36 (1966) 413.
7 R. Pribil, Analytical Applications of EDTA and Related Compounds, Pergamon Press, Oxford, 1972.
8 P. Pakalns, Anal. Chim. Acta, 44 (1969) 73.
9 D. C. Olson and D. W. Margerum, Anal. Chem., 34 (1962) 1299.
10 M. Murakami, T. Yoshino, and S. Harasawa, Talanta, 14 (1967) 1293.
11 H. Sato, Y. Yokoyama, and K. Momoki, Anal. Chim. Acta, 94 (1977) 217.
12 J. J. Kankare, Anal. Chem., 42 (1970) 1322.
13 I. G. Sayce, Talanta, 15 (1968) 1397.
14 L. G. Sillén and B. Warnqvist, Ark. Kemi., 31 (1968) 377.
15 L. G. Sillén and A. E. Martell (Eds.), Stability Constants of Metal-ion Complexes, The Chemical Society, London, 1964.
16 A. S. Solovkin, Zh. Neorg. Khim., 2 (1957) 611.

Analytica Chimica Acta, 99 (1978) 177—182

Short Communication

THE CURRENT—POTENTIAL RELATIONSHIP FOR DIFFERENTIAL PULSE POLAROGRAPHY

I. RUZIC[§] and M. SLUYTERS-REHBACH*

Laboratory of Analytical Chemistry, Rijksuniversiteit, Utrecht (The Netherlands)

(Received 12th December 1977)

The growing importance of differential pulse polarography (d.p.p.) as a precise and sensitive method in analytical chemistry has naturally evoked growing interest in the exact theoretical representation of the differential pulse polarogram. One of the aspects is to account for both the "d.c. current" from the continuously applied linear voltage ramp and the "pulse current" arising from the applied pulse. In other words, the fairly simple equation, usually quoted from Parry and Osteryoung [1], but deriving from Barker and Gardner [2, 3], is apt to be corrected for uncompensated current arising from d.c. polarization, as has been discussed by Christie and Osteryoung [4] and, more recently, by Heyne and v.d. Linden [5].

When references [1], [4] and [5] are read, a rather confusing impression is obtained of what might be the correct theory, the conceptual work of Barker and Gardner being almost disregarded. Therefore, a short discussion of the topic seems in order.

Normal, derivative and differential pulse polarography

In modern literature, the concept "*differential* pulse mode" indicates the application of a programmed potentiostatic excitation as shown in Fig. 1b, in contrast to the older literature [1—3] where the technique is called "*derivative* pulse polarography". The adjective "derivative" is now in use to indicate an already abandoned technique which measures the difference between two successive current samples obtained in "normal" pulse polarography (cf. Fig. 1a). This classification seems logical and will be maintained in the following. However, along the historical line the confusion is obvious.

Theories for reversible electrode processes

From the notations and conventions used in the papers to be compared, we choose the following:

[§] On leave from Center for Marine Research, Institute "Rudjer Boskovic", Zagreb, Yugoslavia.

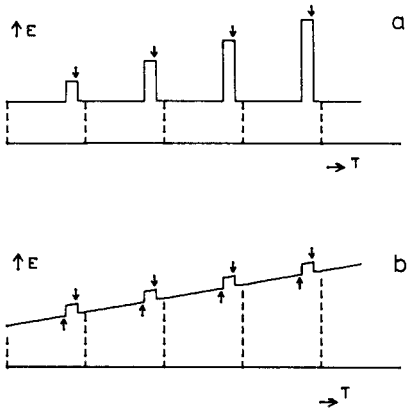

Fig. 1. Potential programming in (a) normal pulse polarography, (b) differential pulse polarography. The dashed vertical lines indicate drop fall. The arrows indicate the moments of current sampling.

(i) surface concentrations, $C(0,t)$; bulk concentration of Ox, C_0^*; bulk concentration of Red, zero. For the reversible process,

$$C_0(0,t) = C_0^* P/(P+1) \tag{1}$$

$$D_R^{1/2} C_R(0,t) = D_0^{1/2} C_0^* P/(P+1) \tag{2}$$

$$P = \exp[(nF/RT)(E - E_{1/2}^r)] \tag{3}$$

where $E_{1/2}^r$ is the reversible half-wave potential.
(ii) time variables: t = time elapsed since start of the drop; t_0 = moment of pulse application; $t^* = t - t_0$; δ = value of t^* where the current is measured; $A(t)$ = surface area;
(iii) for processes initiated at t_0, the dropping mercury electrode (DME) can be treated as a stationary planar electrode, provided that $t^* < 0.02\ t_0$ [6]. This means that the additional flux resulting from a change in surface concentration at $t = t_0$ is

$$\Delta\Phi = -[C(0,t^*) - C(0,t^* = 0)]\ (D/\pi t^*)^{1/2} \tag{4}$$

Pointing to the close connection with earlier studies on square-wave polarography [6], Barker and Gardner [2] give for the current initiated at $t = t_0$, the "pulse current":

$$i_p = -A(t)nFC_0^* \left(\frac{D_0}{\pi t^*}\right)^{1/2} \left[\frac{P_1}{1+P_1} - \frac{P_2}{1+P_2}\right] \tag{5}$$

where P_1 refers to the initial potential E_1, and P_2 refers to the potential after pulse application, following eqn. (3). Equation (5), which follows immediately from eqns. (1) and (4), was assigned to the normal pulse polarogram, whereas for the differential pulse polarogram only the limiting expression for small ΔE ($\Delta E \ll RT/nF$) was presented:

$$i_p = A(t)\frac{n^2F^2}{RT} C_0^* \left(\frac{D_0}{\pi\delta}\right)^{1/2} \frac{\sigma P_1}{(1+\sigma P_1)^2}\ \Delta E \tag{6}$$

where

$$\sigma = \exp\left[(nF/RT)\,(\Delta E/2)\right] \tag{7}$$

Equation (6) is incorrectly quoted by Parry and Osteryoung [1], who suggested that it was obtained by differentiating the reversible current—potential relation for a stationary planar electrode. However, this could never lead to eqn. (6), but to the equation given by Parry and Osteryoung, i.e. with P_1 instead of σP_1. The most important difference is that the maximum current would be found at $E^{\mathrm{I}}_{1/2}$ instead of $E^{\mathrm{I}}_{1/2} - \Delta E/2$.

Similarly, in order to obtain a general expression, Parry and Osteryoung replace this differentiation by a simple subtraction of two currents, seemingly pertaining to two different potentials, but to the same electrolysis time. This mathematical exercise has been criticized rightly by Heyne and v.d. Linden [5] as being an unsound basis for the derivation of the *differential* pulse polarogram, where the time scales of the two currents to be subtracted are different. In fact, it is merely the derivation of the *derivative* pulse polarogram, as follows clearly from Fig. 1.

However, it is easily recognized — but overlooked by both Christie and Osteryoung [4] and Heyne and v.d. Linden [5] — that eqn. (5) is completely general both for the normal and the differential pulse polarogram (without restriction of pulse amplitude). In the former case, E_1 is constant and so far positive with respect to $E_{1/2}$ so that $P_1/(1 + P_1) \approx 1$. In the case of d.p.p., E_1 varies and $E_2 = E_1 + \Delta E$, i.e. $P_2 = \sigma^2 P_1$. Consequently, the general equation for the *differential* pulse polarogram is

$$i_{\mathrm{p}} = A(t)nFC_0^*\left(\frac{D_0}{\pi\delta}\right)^{1/2} \frac{P_1(1-\sigma^2)}{(1+P_1)\,(1+\sigma^2 P_1)} \tag{8}$$

which is mathematically identical to the equation of Parry and Osteryoung.

D.c. current effect

The total current flowing is related to the total flux, because of the change in surface concentration already caused by the ramp potential, E_1, and because of the additional change in surface concentration by pulse excitation. In other words, the faradaic current must be composed of two contributions, which can be distinguished as "d.c. current", i_{dc}, and "pulse current", i_{p}. This was clearly explained by Barker and Gardner [2, 3], who — in view of the electronics available in 1958 — built an ingenious apparatus which largely compensated for the d.c. current.

A "modern" differential pulse polarograph samples the current i_1 just before the pulse ($t = t_0$) and the current i_2 at $t = t_0 + \delta$ and simply subtracts these currents without such compensation. When the difference $\Delta i = i_2 - i_1$ is identified as i_{p}, one neglects the difference in i_{dc} at the two moments t_0 and $t_0 + \delta$.

The effect of this has been calculated by Christie and Osteryoung [4], who expressed the d.c. component by the Heyrovsky—Ilkovic equation. They

obtain the following expression for Δi:

$$\Delta i = i_p + \Delta i_{dc} = nFC_0^* (D_0/\pi)^{1/2}$$

$$\times \left\{ \frac{A(t_0 + \delta)}{\delta^{1/2}} \frac{P_1(1 - \sigma^2)}{(1 + P_1)(1 + \sigma^2 P_1)} + \left[\frac{A(t_0 + \delta)}{(t_0 + \delta)^{1/2}} - \frac{A(t_0)}{t_0^{1/2}} \right] \frac{(7/3)^{1/2}}{1 + P_1} \right\} \quad (9)$$

The d.c. effect is shown [4] to manifest itself as an increase in peak current of ca. 0.3% and an increase in the baseline at the cathodic side of ca. 1% of the peak height. This hardly seems important, but it should be noted that the second effect is rather unfavourable for the determination of a small amount of a reducible species in the presence of an excess of a species reduced at a more positive potential.

An almost identical expression for the d.p.p. has been proposed by Heyne and v.d. Linden [5]:

$$\Delta i = i(t_0 + \delta) - i(t_0) = nFC_0^* (D_0/\pi)^{1/2}$$

$$\times \left\{ \frac{A(t_0 + \delta)}{\delta^{1/2}} \frac{P_1(1 - \sigma^2)}{(1 + P_1)(1 + \sigma^2 P_1)} + \left[\frac{A(t_0 + \delta) - A(t_0)}{t_0^{1/2}} \right] \frac{(7/3)^{1/2}}{1 + P_1} \right\} \quad (10)$$

The essential claim of the authors is that it is more correct to perform a straightforward derivation of $i_1 = i(t_0)$ and $i_2 = i(t_0 + \delta)$ instead of what is called an "artificial separation of the faradaic current into a d.c. contribution and a contribution because of the pulse". (Although the actual result, eqn. (10), reveals such a separation explicitly.) Unfortunately, the impression is given that this is the only way of arriving at the general expression, since it is suggested that Christie and Osteryoung proposed only eqn. (8). The existence of eqn. (9) is thus ignored, whereas the close similarity between eqns. (9) and (10) should have provoked an examination of the peculiar difference, viz. the occurrence of $t_0^{1/2}$ instead of $(t_0 + \delta)^{1/2}$ underneath $A(t_0 + \delta)$.

The straightforward approach

When the mathematics in the treatment of Heyne and v.d. Linden [5] are inspected, the following conclusions can be drawn.

(i) The expression for $i(t_0)$ [eqn. 9 in ref. 5] is the Heyrovsky—Ilkovic equation, i.e. the same as used in ref. 4. (Of course, this is known from the literature [7].)

(ii) Similarly, the expressions (13) and (14), or the simplified ones (15) and (16) of ref. 5, for the surface concentrations at $t = t_0$, are familiar in terms of the expanding plane model for a DME, and are therefore correct.

(iii) The first term in the expression for $i(t_0 + \delta)$ equals the "pulse current" i_p, of our eqn. (8). However, the second term is not equal to what is defined by Christie and Osteryoung as the d.c. component in $i(t_0 + \delta)$.

To put it differently, $i(t_0 + \delta)$ [eqn. (19) in ref. 5] does not reduce to a "normal" Heyrovsky—Ilkovic current when the pulse height is made zero, which is the opposite to what would be expected. In fact, for zero pulse

height ($\Delta E = 0$), the residue of $i(t_0 + \delta)$ is not time-dependent, except for the time-dependency of the surface area. Also, for a zero pulse height the concentrations in the diffusion layer, $C(r_x, t^*)$ [eqns. (17) and (18), ref. 5], are not time-dependent, but equal to the concentrations $C(r_x, t_0)$, i.e. the "initial concentrations" at $t^* = 0$.

Study of the derivation of these equations indicated that this illogical phenomenon must be the result of the transition from the "d.c. variable" t to the "pulse variable" t^* for the total concentration. Although it is possible to formulate Fick's law for the new time variable, it is very risky (or even not allowed) to solve it by Laplace transform. It is easily shown that the function expected, viz. $f(t^*) = g(t_0 + t^*) = g(t)$, has to be found by inverse transformation of

$$\mathcal{L}\{f(t^*)\} = \exp(st_0) \cdot \mathcal{L}\{g(t) \cdot u(t - t_0)\} \tag{11}$$

where $u(t - t_0)$ is the unit step function. Clearly, the information contained in the time domain $t = 0$ to $t = t_0$ is rejected this way (see, e.g., [8]). It can be shown quite generally that with a linear function for $C(r_x, 0)$ in r_x as an initial condition, the Laplace transform method leads inevitably to the solution $C(r_x, t^*) = C(r_x, 0)$ when the potential is not changed at $t^* = 0$ (i.e. zero pulse height). A finite pulse height merely adds a term to this solution.

Equation (11) suggests the proper approach to the problem: put the total concentration $C(r, t)$ equal to the sum of a "d.c. component" $C_{dc}(r, t)$ and a "pulse component" $C_p(r, t)$, the latter related to the potential jump ΔE (artificially or not). Because $C_p(r, t) = 0$ up to $t = t_0$, no information is rejected when it is replaced by the function $C_p(r, t^*)$ with the boundary condition $C_p(r_x, 0) = 0$. Therefore:

$$C(r, t) = C_{dc}(r, t) + C_p(r, t^*) \tag{12}$$

Both $C_{dc}(r, t)$ and $C_p(r, t^*)$ are solutions of Fick's law, the former with t and the latter with t^* as the time variable. To keep it general, the expanding plane model should be taken, but following Barker's arguments [9], the stationary plane model will suffice for the pulse part. It will be clear from the foregoing that this results in eqn. (9), which therefore is the correct equation.

Conclusions

By using eqn. (10) instead of eqn. (9), Heyne and v.d. Linden largely overestimated the effect of the d.c. component: levels for the cathodic base line up to 10% or even 20% of the peak height are reported, whereas they should be 2—4%. Experimentally, indeed, a less dramatic effect is found, although in the example of 5×10^{-4} M Tl(I) in 0.1 M KNO_3, it seems to be higher than would be expected from eqn. (9). However, two remarks can be made. First, no attention was paid to the capacitive effect, also described correctly by Christie and Osteryoung [4]. This effect causes the baseline to

be closely connected with the double-layer capacity of the electrode; consequently the levels of the anodic and cathodic baselines need not be the same. Secondly, it is known that Tl(I) is specifically adsorbed at the mercury electrode [10]. The behaviour of the system may be complicated by this. The authors mention that a few drops of 0.2% Triton X-100 were necessary in order to obtain a base-line shift at all. Since it is not clear what the function of a maximum suppressor in differential pulse polarography could be, the whole experiment is somewhat questionable.

Finally, one should be careful in applying d.p.p. to the determination of stability constants, not only because of the instrumental artefacts mentioned [5, 11], but also because of the possibility that the electrode reaction may be irreversible. In the latter case, the theory discussed above does not hold, and should be replaced by a more general theory recently published [12].

REFERENCES

1 E. P. Parry and R. A. Osteryoung, Anal. Chem., 37 (1965) 1634.
2 G. C. Barker and A. W. Gardner, Atomic Energy Res. Establ. Harwell C/R 2297 (1958).
3 G. C. Barker and A. W. Gardner, Fresenius Z. Anal. Chem., 173 (1960) 79.
4 J. H. Christie and R. A. Osteryoung, J. Electroanal. Chem., 49 (1974) 301.
5 G. J. M. Heyne and W. E. v.d. Linden, Anal. Chim. Acta, 82 (1976) 231.
6 G. C. Barker, R. L. Faircloth and A. W. Gardner, Atomic Energy Res. Establ. Harwell C/R 1786 (1956).
7 J. Heyrovsky and D. Ilkovic, Collect. Czech. Chem. Commun., 7 (1935) 198.
8 W. D. Day, Introduction to Laplace Transforms, Cliffe, London, 1960, pp. 86—87.
9 G. C. Barker, Atomic Energy Res. Establ. Harwell C/R 1553 (1954).
10 M. Sluyters-Rehbach and J. H. Sluyters, Rec. Trav. Chim. Pays Bas, 82 (1963) 553.
11 J. H. Christie, J. Osteryoung and R. A. Osteryoung, Anal. Chem., 45 (1973) 210.
12 I. Ružić, J. Electroanal. Chem., 75 (1977) 25.

Analytica Chimica Acta, 99 (1978) 183—187

Short Communication

THE CURRENT—POTENTIAL RELATIONSHIP IN DIFFERENTIAL PULSE POLAROGRAPHY: A REVISION

G. J. M. HEIJNE and W. E. VAN DER LINDEN*

Laboratory for Analytical Chemistry, University of Amsterdam, Nieuwe Achtergracht 166, Amsterdam (The Netherlands)

(Received 16th January 1978)

Ružić and Sluyters-Rehbach [1] have correctly shown that the equation resulting from our derivation of the current—voltage relationship in differential pulse polarography (d.p.p.) [2] shows a discontinuity at zero pulse height. A similar objection on this point has recently been made by Kies [3]. On second thoughts we must agree that the result presented by Christie and Osteryoung [4] is more correct. However, we maintain our preference for a derivation via a straightforward evaluation of the concentration profile.

The discontinuity in our derivation is caused by the suggestion that after application of the pulse the initial condition no longer contains the variable parameter t.

A revision of our approach on this point leads to a simple derivation with the additional advantage that the same diffusion model with the same assumptions can be used throughout the whole mathematical derivation [see Appendix]. A new function $V(x,y)$ is introduced which is obtained by subtracting the value $U(x,y\ (t < t_0))$ from the general function $U(x,y)$, where $U(x,y) = C^0 - C_{OX}(x,y)$. Introduction of this new function in the basic differential equation as well as in the initial and boundary conditions yields after transformations $t^* = t - t_0$ and $y^* = y - y\ (t = t_0)$ a set of equations which is exactly similar to the set of equations in U, which is valid before the application of the pulse. This implies that a comparable solution is obtained provided that θ_1 has to be replaced by θ_2 and y by y^*.

In this way C_{OX} can be expressed as a function of y and y^*. Differentiation of the concentration with respect to the distance in order to obtain the concentration gradient gives some difficulties. By means of a series expansion in δ/t_0 according to Barker [5—7], and by disregarding second and higher terms, finally the correct current after pulse application is obtained. Subtraction of the current just before the pulse yields:

$$i_{d.p.p.} = nFkm^{2/3}\left(\frac{D_{OX}}{\pi}\right)^{1/2} C^0\left[\left(\frac{(t_0+\delta)^{2/3}}{\delta^{1/2}}\right)\left(\frac{\epsilon_1(1-\sigma^2)}{(1+\epsilon_1)(1+\sigma^2\epsilon)}\right)\right.$$

$$\left. + \{(t_0+\delta)^{1/6} - t_0^{1/6}\}\left(\frac{7}{3}\right)^{1/2}\ \frac{1}{1+\epsilon_1}\right]$$

TABLE 1

Values of X and Y for corrected d.p.p. eqn. for PAR 174[a]

Drop time τ(s)	0.5	1.0	2.0
X	2.843	4.541	7.230
Y	0.028	0.015	0.008

[a] $X = (t_0 + \delta)^{2/3}/\delta^{1/2}$; $Y = ((t_0 + \delta)^{1/6} - t_0^{1/6})\,(7/3)^{1/2}$.

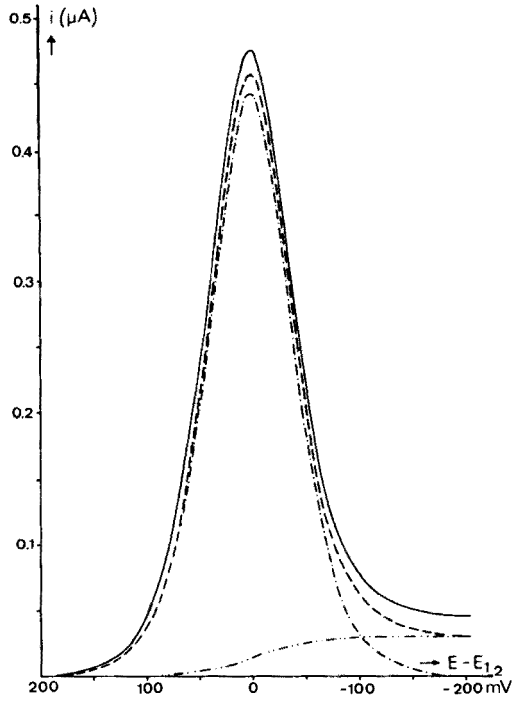

Fig. 1. Differential pulse polarogram of 5×10^{-4} M Tl(I) in 0.1 M KNO_3. Pulse amplitude ΔE = 5 mV; drop time τ = 1 s. Theoretical curves: —·— first term of right-hand side of $i_{d.p.p.}$; —··— second term; ——— total current. Experimental curve ———.

It is obvious that because of this revised equation, Tables 1 and 3 as well as Fig. 1 of ref. [12] have also to be revised. Because of the experimental conditions and the instrumental parameters of the PAR 174, the cathodic base line can be more than the 2—4% of the peak height suggested by Ružić and Sluyters-Rehbach. Figure 1 shows that the difference between experimental and theoretical curves has diminished but is still appreciable. This might be at least partially caused by the effects mentioned by these authors. Another factor is the fact that disregarding the second term in the series expansion mentioned above causes a theoretical peak height which is 2% too low.

TABLE 3

Values of $\Delta i_{base\text{-}line}/i_{peak}$ for PAR 174

$n\Delta E$	Theoretical drop time τ(s)			Experimental τ = 1 s	
	0.5	1.0	2.0	Tl	Cd
5	0.185	0.066	0.023	0.095	
10	0.097	0.034	0.012	0.050	0.049
15	0.066	0.023	0.008		
20	0.050	0.017	0.006		0.025
25	0.041	0.014	0.005	0.019	
30	0.034	0.012	0.004		
50	0.022	0.007	0.003	0.009	0.010
75	0.016	0.005	0.002		
100	0.013	0.004	0.002	0.000	0.004
150	0.011	0.004	0.001		
200	0.010	0.003	0.001		0.000
300	0.010	0.003	0.001		

The authors gratefully acknowledge valuable discussions with T. M. T. Coolen about the mathematics of the problem.

APPENDIX

The notation is the same as used in ref. [2]. In Appendix 1 of that paper the solutions of $U(x,y)$ and $C_R(x,y)$ were found for $C_{OX}(0,y)/C_R(0,y) = \theta_1$:

$$U(x,y) = C^0 - C_{OX}(x,y) = \frac{C^0}{1 + \theta_1\xi} \operatorname{erfc}\left[\frac{x}{2(m_{OX}y)^{1/2}}\right] = k_1 \cdot \operatorname{erfc}\left[\frac{x}{2(m_{OX}y)^{1/2}}\right] \tag{1}$$

$$C_R(x,y) = \frac{C^0\xi}{1 + \theta_1\xi} \operatorname{erfc}\left[\frac{x}{2(m_R y)^{1/2}}\right] = k_2 \cdot \operatorname{erfc}\left[\frac{x}{2(m_R y)^{1/2}}\right] \tag{2}$$

At $t = t_0$ the potential is changed and $C_{OX}(0,y)/(C_R(0,y) = \theta_2$.

If we consider again the expanding sphere model, the diffusion equations (1.5) and (1.6) of ref. [2] can be used with this new boundary condition. If the solutions (1) and (2), found for $y < y_0$, and so for $t < t_0$, are written as $p(x,y)$ and $q(x,y)$ respectively, new functions can be defined:

$$V_{OX}(x,y) = U(x,y) - p(x,y) \tag{3}$$

$$V_R(x,y) = C_R(x,y) - q(x,y) \tag{4}$$

Since $U(x,y)$, $p(x,y)$ and $C_R(x,y)$, $q(x,y)$ satisfy the respective differential equations and initial and boundary conditions of Appendix 1 of ref. [2] — except the one reflecting the potential change — we obtain a new set of equations for $y_0 < y < \infty$ and $0 < x < \infty$:

$$m_{OX} \frac{\partial^2 V_{OX}(x,y)}{\partial x^2} - \frac{\partial V_{OX}(x,y)}{\partial y} = 0$$

$$m_R \frac{\partial^2 V_R(x,y)}{\partial x^2} - \frac{\partial V_R(x,y)}{\partial y} = 0$$

$$V_{OX}(x,y_0) = 0 \text{ and } V_R(x,y_0) = 0$$

$$D_{OX}\left(\frac{\partial V_{OX}(x,y)}{\partial x}\right)_{x=0} - D_R\left(\frac{\partial V_R(x,y)}{\partial x}\right)_{x=0} = 0$$

and since $p(0,y) = k_1$ and $q(0,y) = k_2$, $C_{OX}(0,y)/C_R(0,y) = \theta_2$ can be written as $K - V_{OX}(0,y) = \theta_2 V_R(0,y)$ with $K = C^0 - k_1 - \theta_2 k_2$.

After the translation $y^* = y - y_0$, the solutions can be found in the same way as in Appendix 1, but with the constants K and θ_2 replacing C^0 and θ_1 respectively. Thus:

$$V_{OX}(x,y) = \frac{K}{1+\theta_2\xi}\ \text{erfc}\left[\frac{x}{2(m_{OX}(y-y_0))^{1/2}}\right]$$

$$V_R(x,y) = \frac{K\xi}{1+\theta_2\xi}\ \text{erfc}\left[\frac{x}{2(m_R(y-y_0))^{1/2}}\right]$$

By substitution of $C_{OX}(x,y) = C^0 - U(x,y) = C^0 - V_{OX}(x,y) - p(x,y)$, and of K, k_1 and k_2, and after transformation of x and y to r and t respectively, we find for $C_{OX}(r,t)$:

$$C_{OX}(r,t) = C^0 - \frac{C^0\xi(\theta_1-\theta_2)}{(1+\theta_1\xi)(1+\theta_2\xi)}\ \text{erfc}\left[\frac{r^3-r_0{}^3}{2(m_{OX}(t^{7/3}-t_0{}^{7/3}))^{1/2}}\right]$$

$$-\frac{C^0}{1+\theta_1\xi}\ \text{erfc}\left[\frac{r^3-r_0{}^3}{2(m_{OX}t^{7/3})^{1/2}}\right]$$

The same can be done for $C_R(r,t)$.

In order to obtain the current, we have to determine the flux at the surface:

$$\left(\frac{\partial C_{OX}(r,t)}{\partial r}\right)_{r=r_0} = \frac{C^0\xi(\theta_1-\theta_2)}{(1+\theta_1\xi)(1+\theta_2\xi)} \times \frac{2}{\pi^{1/2}} \times \frac{3r_0{}^2}{2(m_{OX}(t^{7/3}-t_0{}^{7/3}))^{1/2}}$$

$$+\frac{C^0}{(1+\theta_1\xi)} \times \frac{2}{\pi^{1/2}} \times \frac{3r_0{}^2}{2(m_{OX}t^{7/3})^{1/2}}$$

Since $m_{OX} = (27/7)\,\gamma^{4/3} D_{OX}$ and $r_0{}^3 = \gamma t$,

$$\left(\frac{\partial C_{OX}(r,t)}{\partial r}\right)_{r=r_0} = \frac{C^0\xi(\theta_1-\theta_2)}{(1+\theta_1\xi)(1+\theta_2\xi)} \times \frac{1}{(\pi D_{OX})^{1/2}} \times \frac{t^{2/3}}{(3/7(t^{7/3}-t_0{}^{7/3}))^{1/2}}$$

$$+\frac{C^0}{(1+\theta_1\xi)} \times \frac{1}{(\pi D_{OX}t)^{1/2}} \times \left(\frac{7}{3}\right)^{1/2}$$

With

$$\frac{t^{2/3}}{(3/7(t^{7/3}-t_0{}^{7/3}))^{1/2}} = \frac{1}{\left(\delta\left(1-\frac{2}{3}\frac{\delta}{t_0}+\frac{20}{27}\left(\frac{\delta}{t_0}\right)^2\cdots\right)\right)^{1/2}}$$

where $\delta = t - t_0$ (see e.g. ref. [7]) and disregarding terms with δ/t_0,

$$i(t_0 + \delta) = nFA(t_0 + \delta)C^0 \left\{ \left(\frac{D_{ox}}{\pi\delta}\right)^{1/2} \times \frac{\xi(\theta_1 - \theta_2)}{(1 + \theta_1\xi)(1 + \theta_2\xi)} + \left(\frac{D_{ox}}{\pi t}\right)^{1/2} \times \left(\frac{7}{3}\right)^{1/2} \times \frac{1}{(1 + \theta_1\xi)} \right\}$$

from which the correct d.p.p. current equation can be obtained.

REFERENCES

1 I. Ružić and M. Sluyters-Rehbach, Anal. Chim. Acta, 99 (1978) 177.
2 G. J. M. Heijne and W. E. van der Linden, Anal. Chim. Acta, 82 (1976) 231.
3 H. L. Kies, private communication, September 1977.
4 J. H. Christie and R. A. Osteryoung, J. Electroanal. Chem., 49 (1974) 301.
5 G. C. Barker, R. L. Faircloth and A. W. Gardner, Atomic Energy Res. Establ. Harwell, C/R 1786 (1956).
6 G. C. Barker and A. W. Gardner, Atomic Energy Res. Establ. Harwell, C/R 2297 (1958).
7 G. C. Barker, Atomic Energy Res. Establ. Harwell, C/R 1553 (1954) p. 9.

Analytica Chimica Acta, 99 (1978) 189—192

Short Communication

DATA TRANSMISSION BY FREQUENCY MODULATION IN AN AUTOMATED GAS CHROMATOGRAPHIC SYSTEM

E. BECHGAARD, J. A. CHRISTENSEN, O. CHRISTENSEN and J. LUND*
Research Laboratories of A/S Ferrosan, 1-5 Sydmarken, DK-2860 Soeborg (Denmark)
(Received 6th January 1978)

Automated gas chromatography has been commonly used in the last few years, and commercial equipment is now available. Liquid as well as solid injection techniques have been used [1, 2]. Unless the gas chromatograph and the calculating unit have been combined in one instrument, transmission of data and control orders must be transmitted between the two units, in many cases over a distance of more than a hundred metres. Transmission of analog signals is not attractive in an industrial environment because of high levels of electromagnetic interference. Digital transmission has been used frequently [3], but demands expensive equipment for analog/digital conversion or for parallel-to-serial and serial-to-parallel conversion.

To overcome these difficulties, a new transmission system has been constructed based on frequency modulation for transmission of data. It is possible to use a calculator for the control of the gas chromatograph and for data treatment.

Experimental

G.l.c. system. The gas chromatograph was a Packard 419 with automatic solid sampling (ASS, model 770), nitrogen detector (type 413), and flame ionization detector (type 706). The column of silanized glass was packed with 1.5% SP 2250 on Chromosorb G-AW-DMCS (80-100 mesh). Operating conditions were: column 275°C, injection unit 280°C, detector 285°C; flow-rates of nitrogen, hydrogen and air, ca. 25, 25, and 280 ml min^{-1}, respectively.

The chromatographic equipment was modified in several ways. The ASS was modified to take 48 sample containers (spiral springs) instead of 24, and the first part of the column was changed to serve as a reservoir for up to 100 sample containers. Further, the chromatograph was equipped with a fan to cool the ASS, and the outflow from the nitrogen detector was vented to another room with a steady pressure.

Transmission system. The data transmission system is outlined in Fig. 1. The analog signal from the gas chromatograph (taken prior to the attenuator) is converted to a corresponding frequency in the Front End (FE) and

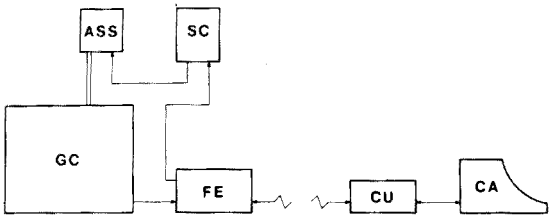

Fig. 1. Configuration of the system. GC, gas chromatograph; FE, front end; CU, control unit; CA, calculator; SC, signal converter; ASS, automatic solid sampling system.

transmitted to the Control Unit (CU). The frequency is converted in the CU to a digital signal and fed into a Hewlett-Packard 9830 A calculator. The ASS is operated by a Packard 762 Signal Converter (SC) controlled by the calculator via the CU and FE.

The main function of the FE (Fig. 2), placed near the chromatograph, is conversion of the voltage signal from the gas chromatograph to a square wave with frequency proportional to voltage (20 Hz—20 kHz). Before the conversion, the signal can be inverted and/or logarithmically transformed by the FE.

The CU (Fig. 2) is situated near the calculator, up to 100 m from the FE. It contains a real-time clock for precise control of sampling. The frequency from the FE is counted for 0.5 s, and the result (four decimal digits) is transmitted as ASCII characters followed by a LINE-FEED to the calculator. The sampling interval was usually 1 s but could be varied between 1 and 32 s. This sampling frequency (one per s) in the CU was determined on the assumption that a g.l.c. peak is gaussian to fulfil Nyquist's sampling theorem [4]. The calculator (with a HP 11202 A 8 bit parallel interface) is programmed to collect the data in the relevant period after an injection.

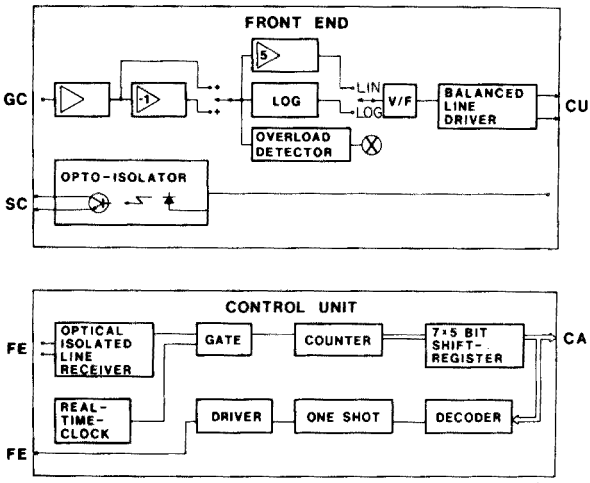

Fig. 2. Block diagrams of the front end and the control unit.

After a preset time, the calculator issues an injection command via the CU and FE to the SC (usually 4 min).

Details and diagrams of the two interface units are not given but are available from the authors upon request.

Calculations. Usually 600 data points were collected per chromatogram and stored on magnetic tape for later processing, but the processing could also be performed during the data collection. Data processing was done in the following steps: (1) location of chromatographic peaks (combination of "tangent skim" and slope); (2) base-line corrections and calculation of peak areas and peak heights; (3) location of peaks corresponding to test substance and internal standard, and calculation of the ratio of the two peak areas or peak heights.

When all chromatograms had been calculated, the standards were used to calculate a standard curve for calculation of the individual results.

Results and discussion

The system described was tested with the nitrogen detector as well as the flame ionization detector for urine and plasma samples to which femoxetine hydrochloride (FG 4963) had been added in the range 0—100 ng ml^{-1}. The sensitivity, accuracy and precision were the same as those found with an earlier method [5] where manual liquid injection was used. No carry-over effect was observed in the range investigated; flame ionization gave fewer problems than the nitrogen detector.

Smoothing of curves has been discussed by Enke and Nieman [6]. In the present case, it was found that the method used for data collection (the mean of 0.5 s per second) gave sufficient smoothing. In agreement with Janik [7], calculations based on peak heights and peak areas yielded identical results.

The system has now been used without troubles for more than two years. The normal procedure is to prepare samples for gas chromatography during the day and carry out the chromatography and data logging during the night.

The A/D converter and the analog circuitry are stable after a warm-up time of a few hours, and the base-line drift is negligible compared to the gas chromatographic drift. The analog circuitry was built with "discrete" (IC) operational amplifiers, etc., and adjustment was therefore tedious. If the system were to be built today, a better choice for the analog circuitry would be complete log amplifier and V/F converter modules.

We thank Mrs. Ulla Laursen and Mr. Ole Wassmann for valuable and skilful technical assistance, and Mr. G. Bak-Rasmussen, Packard Instruments, for assistance with the ASS modification.

REFERENCES

1 A. Kuksis, J. J. Myher, L. Marai and K. Geher, J. Chromatogr. Sci., 13 (1975) 423.
2 A. Morrone and E. Beretta, J. Chromatogr., 128 (1976) 27.
3 G. E. Nelson and D. W. Ricci, Hewlett-Packard Journal, 24, no. 2 (1972) 2.
4 P. C. Kelly and G. Horlick, Anal. Chem., 45 (1973) 518.
5 E. Bechgaard and J. Lund, J. Chromatogr., 133 (1977) 147.
6 C. G. Enke and T. A. Nieman, Anal. Chem., 48 (1976) 705A.
7 A. Janik, J. Chromatogr. Sci., 13 (1975) 93.

Analytica Chimica Acta, 99 (1978) 193—195

Short Communication

THE DETERMINATION OF SMALL AMOUNTS OF ALUMINIUM AND SILICON IN STABILIZED ZIRCONIA CERAMICS

H. KRUIDHOF

Twente University of Technology, Department of Chemical Engineering, Laboratory of Inorganic Chemistry and Materials Science, Enschede (The Netherlands)

(Received 31st January 1978)

Zirconias, stabilized by the oxides of rare earths, calcium, and yttrium, are applied as solid electrolytes in high-temperature fuel cells, devices for hydrogen production from steam, exhaust control systems and electrode materials. The assay of aluminium and silicon is important because of their influence on the electrical conductivity, but their determination in stabilized zirconias has not been described in the literature; the present communication reports colorimetric methods for their determination in small amounts. Solutions of samples can be obtained by fusion with a mixture of borax, boric acid, and lithium hydroxide, followed by dissolution in dilute acid. Zirconium and rare earth ions interfere with the determination of aluminium; these constituents are removed by cation exchange and aluminium is determined with chromazurol S. Silicon is measured as molybdenum blue, after the reduction of molybdosilicate.

Experimental

Reagents and standard solutions. Redistilled water was used for reagent preparation. All chemicals were of analytical grade. The flux was prepared by mixing 45 parts of borax, 16 parts of boric acid, and 7 parts of lithium hydroxide. The buffer solution was prepared by dissolving 27.5 g of ammonium acetate and 0.5 ml of glacial acetic acid in 50 ml of water, with dilution to 100 ml.

The standard silicon solution was obtained by fusing pure silicon dioxide with anhydrous sodium carbonate. The melt was dissolved in water; after suitable dilution, a solution containing 1 μg Si ml^{-1} was prepared. The standard aluminium solution was prepared by dissolving pure aluminium in 6 M hydrochloric acid; this solution was diluted to give 1 μg Al ml^{-1}. The standard solutions can be stored for several weeks in plastic containers.

Preparation of the cation-exchange column. A strong acid cation exchanger (Dowex 50W-X8, 100-200 mesh) was used. The resin was slurried with a few ml of 6 M hydrochloric acid and, after 10 min, was poured into an ion-exchange column (height, ca. 15 cm; diameter, 1 cm) filled with the same acid. The resin was pretreated as described below.

Dissolution of samples. Accurately weigh ca. 50 mg of powdered sample into a Pt—5% Au crucible and add 500 mg of flux. Mix carefully with a spatula and fuse at 900°C for about 10 min.

Procedure for aluminium. Add 5 ml of 6.5 M hydrochloric acid to the melt described above. Heat to ca. 60°C until the melt is released from the crucible. Transfer melt and liquid to a graduated beaker, and reheat to 60°C until the melt has completely dissolved. Cool and dilute to 20 ml with 6.5 M hydrochloric acid. Add 20 ml of ethanol and mix. Pass the mixture through the ion-exchange column (pretreated with 60 ml of 6 M hydrochloric acid, 40 ml of water and 50 ml of 3 M hydrochloric acid in 50% ethanol) at a flow-rate of ca. 0.5 ml min^{-1}. Subsequently wash the resin bed with 150 ml of 3 M hydrochloric acid in 50% ethanol and combine this effluent in a 250-ml volumetric flask with the effluent obtained from the sample solution. Dilute the solution to the mark. Transfer a 25-ml aliquot to a 50-ml beaker, add three drops of concentrated sulphuric acid and evaporate to dryness on a steam-bath. Add 5 ml of water and neutralize the solution. Transfer the solution to a 50-ml volumetric flask and add 2 ml of ascorbic acid solution (50 mg ml^{-1}) and 10 ml of buffer solution, followed by 2 ml of chromazurol S reagent (0.2% solution in 25% ethanol) [1]. Dilute the solution to the mark, shake well, and wait for 15 min. Measure the absorbance in 4-cm cells at 540 nm against a blank containing all reagents used. To calibrate the method, transfer aliquots up to 10 ml of standard aluminium solution to 50-ml volumetric flasks and treat in the way described above.

Procedure for silicon. Add 8 ml of 3 M hydrochloric acid to the melt obtained after fusion. Heat to ca. 60°C until the melt is released from the crucible. Transfer melt and liquid to a plastic beaker and reheat until the melt has dissolved completely. Cool, and transfer the solution to a 50-ml volumetric flask; dilute to the mark. Transfer a 25-ml aliquot to a dry beaker, add 10.0 ml of ammonium molybdate reagent (50 mg ml^{-1} in water), and mix. Wait for 20 min and add 10.0 ml of oxalic acid solution (40 mg ml^{-1} in water). Mix until the sediment has disappeared and immediately add 5.0 ml of ammonium iron(II) sulphate solution (60 mg ml^{-1} in 0.02 M sulphuric acid). Wait for at least 25 min and measure the absorbance in 4-cm cells, at 815 nm, against a blank containing all the reagents used. For calibrating the method, transfer aliquots up to 25 ml of standard silicon solution to 50-ml volumetric flasks; add 6.5 ml of 3 M hydrochloric acid, and dilute the solutions to the mark. Transfer 25-ml aliquots to dry beakers and treat in the way described above.

Results and discussion

To test the removal of the interfering constituents by cation exchange [2], various zirconias were dissolved, aluminium was added, and the solutions were passed through the column. The aluminium was always present in the first 180 ml of effluent, in which none of the other constituents was present.

TABLE 1

Recovery of aluminium added to hydrochloric acid solutions containing flux

Flux present (μg)	—	—	100	100	250	250
Al^{3+} added (μg)	5	10	5	10	2	5
Al^{3+} found (μg)	4.95	10.05	5.15	9.7	1.95	5.2

TABLE 2

Recovery of aluminium and silicon added to a sample of stabilized zirconia

Si	added, %	0.008	0.016	0.020	0.024	0.030	0.036
Si	found, %	0.0081	0.0157	0.0205	0.023	0.027	0.037
Al	added, %	0.20	0.40	0.10	0.05	0.02	—
Al	found, %	0.22	0.38	0.09	0.05	0.02	0.001

The cation exchanger can be regenerated with 6 M hydrochloric acid. The flux does not interfere with the method, but hydrochloric acid must be removed. Sulphuric acid prevents the loss of aluminium chloride. To test the colorimetric procedure, hydrochloric acid and different amounts of flux were added to various solutions of aluminium. These solutions, analysed as described under the procedure for aluminium, gave the results in Table 1. This determination is adapted from a method used for silicon in steel [3]. All glassware must be cleaned with 6 M hydrochloric acid rinsed in distilled water. Amounts greater than 0.05% Si are measured in 1-cm cells.

To test both methods, stabilized zirconias, free from both elements, were taken. Known amounts of aluminium and silicon were added; the materials were analysed according to the Procedures. The results are shown in Table 2. It can be concluded that the methods described are reliable with an accuracy acceptable for the materials described. They may also be applicable to allied materials.

The author thanks Dr. K. J. de Vries and Professor A. J. Burggraaf for their stimulating interest.

REFERENCES

1 J. Fries, Spurenanalyse, E. Merck, Darmstadt, 1971, p. 6.
2 J. Marinsky and Y. Marcus, Ion Exchange and Solvent Extraction, M. Dekker, New York, Vol. 5, 1973, p. 169.
3 T. R. Andrew and C. H. R. Gentry, Analyst, 81 (1956) 339.

Analytica Chimica Acta, 99 (1978) 197—201

Short Communication

SPECTROPHOTOMETRIC DETERMINATION OF CYANIDE WITH SODIUM ISONICOTINATE AND SODIUM BARBITURATE

SHIGERU NAGASHIMA

Department of Chemistry, Tokyo Metropolitan Industrial Technical Institute, Nishigaoka, Kita-ku, Tokyo (Japan)

(Received 20th October 1977)

The spectrophotometric methods for the determination of cyanide based on the König reaction [1], such as the pyridine–pyrazolone method [2], the pyridine—barbituric acid method [3] and the γ-picoline—barbituric acid method [4] are very sensitive; the latter two methods have the particular advantage that maximum absorbance is achieved within 5 min. However, pyridine, used in these methods, is unpleasant and noxious in routine work. Ishii et al. [5] proposed a method with an isonicotinic acid—pyrazolone reagent; this odorless reagent was prepared by dissolving isonicotinic acid and pyrazolone in dimethylformamide—water mixed solvent. But the sensitivity of this method is about half as much as that of the above methods [2—4], and requires a heating time (30 min at 40°C). Recently, Watanabe et al. [6] modified the method of Ishii et al. by using sodium isonicotinate instead of isonicotinic acid to enhance the sensitivity.

The present communication reports a method for the determination of cyanide with a sodium isonicotinate—sodium barbiturate reagent. The sensitivity of this method is almost the same as that of the above methods [2—4, 6]. The method has the advantages that the reagent can be prepared by dissolving in water without dimethylformamide, and is stable for at least 2 weeks when stored at room temperature (about 25°C), while the Watanabe reagent has to be stored at below 10°C.

Experimental

Apparatus and reagents. These were almost the same as those previously used [4], except for the following solution and reagent.

Buffer solution (pH 5.2). Dissolve 68.0 g of potassium dihydrogenphosphate and 3.0 g of disodium hydrogenphosphate in water and dilute to 1 l.

Sodium isonicotinate–sodium barbiturate reagent. Dissolve 1.0 g of sodium isonicotinate and 1.0 g of sodium barbiturate in 100 ml of water at 60—70°C with stirring. After cooling, dilute the mixture to 100 ml with water. The reagent obtained is colorless and its pH is about 6.5.

Preparation of sodium isonicotinate. In an evaporating dish, dissolve 10.0 g of isonicotinic acid (pyridine-4-carboxylic acid) in 200 ml of sodium hydroxide solution (3.3 g NaOH/200 ml). After evaporating on a water bath, dry the residue at 110°C or under reduced pressure.

Preparation of sodium barbiturate. In a beaker, place 200 ml of sodium hydroxide solution (3.1 g NaOH/200 ml) and 10.0 g of barbituric acid. Stir until the acid dissolves; a white precipitate forms immediately. Transfer the contents to an evaporating dish and evaporate on a water bath. Dry the residue under reduced pressure. The sodium barbiturate residue should not be dried at 110°C, because it is then difficult to dissolve in water. The x-ray powder diffraction spectra of these two sodium barbiturates showed no distinct differences. The x-ray data obtained for the starting material, barbituric acid, were in very good agreement with those of Clark [7].

Procedure. In a dried reaction tube, place 10.0 ml of sample solution containing less than 5 μg of cyanide, and free from sulfide and thiocyanate ions. Add 3.0 ml of buffer solution and 0.2 ml of 1% (w/v) chloramine-T solution, stopper the tube and shake gently. After 1—2 min, add 5.0 ml of sodium isonicotinate—sodium barbiturate reagent, stopper the tube again, mix, and keep the mixture at 20—25°C for 30 min. Measure the absorbance at 600 nm against a reagent blank.

Results and discussion

When the reagent used for color development was prepared by dissolving isonicotinic acid and barbituric acid in aqueous dimethylformamide, a violet-blue product was also formed; but after a day, this reagent changed from light-yellow to deep-yellow, and the final colored solution obtained was tinged with yellow. Water was examined as solvent. Maximum absorbance was then found at around pH 5.7 for the final reaction solution (see below). The nearly neutral reagent solution was most satisfactory. As both isonicotinic acid and barbituric acid are difficult to dissolve in water, sodium isonicotinate and sodium barbiturate were prepared.

Figure 1 shows the absorption spectra obtained by the proposed method with the sodium isonicotinate—sodium barbiturate reagent. The wavelength of maximum absorption lies at ca. 600 nm.

The effects of temperature and time on color development were examined at 20, 25 and 30°C by varying the standing time after the addition of the mixed reagent. At 20 and 25°C, maximum absorbance was achieved in 30 min; the absorbance then remained constant for about 30 min, but decreased by about 2.5% after 60 min, and by about 5% after 90 min. At 30°C, maximum absorbance was reached within 30 min, but the absorbance decreased by about 3% after 30 min. These tests were made with 1.0—5.0 μg CN^-/10 ml. The reaction time was thus established as 30 min at 20—25°C.

Stability of the reagent. Calibration curves obtained with a reagent which had been stored for 2 weeks at room temperature (about 25°C) agreed (within 2%) with curves prepared with fresh reagent. The absorbance of the

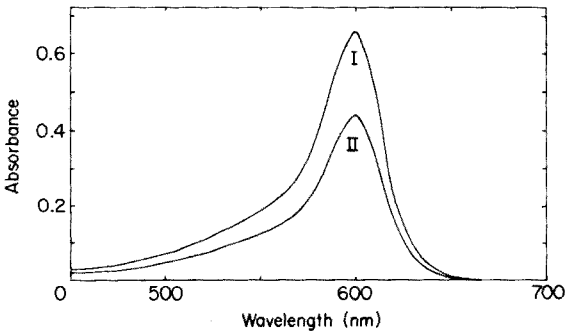

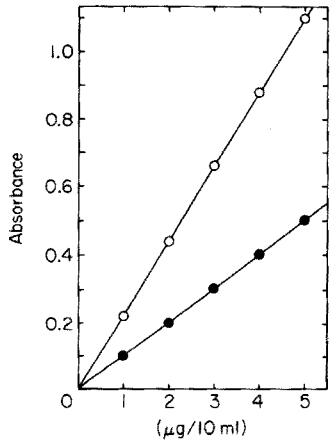

Fig. 1. Absorption spectra of the solution obtained by the proposed procedure. (I) 3.0 μg CN^-/10 ml; (II) 2.0 μg CN^-/10 ml. Reference: reagent blank.

Fig. 2. Calibration curves. (○) Cyanide, (●) thiocyanate. Reference: reagent blank.

reagent blank was almost the same as that of water, and did not increase with time. In this procedure, reagent blanks were used as reference for the sake of security.

Effect of experimental variables. According to Asmus and Garschagen [3], the amount of chloramine-T solution affects significantly the results of the pyridine—barbituric acid method. Thus, the effect of varying the amount of the chloramine-T solution (0—1.0 ml) on the present procedure was examined. For 1.0—5.0 μg CN^-/10 ml, constant absorbance was obtained with 0.1—0.3 ml of the chloramine-T solution, but the absorbance decreased slightly when more than 0.5 ml was added. The amount of chloramine-T solution was therefore chosen as 0.2 ml. With the 0.2 ml of chloramine-T solution, repeated experiments were performed at five steps in the range 1.0—5.0 μg CN^-/10 ml; the results obtained showed a relative standard deviation below 2%.

The effect of standing time after the addition of the chloramine-T solution (0.2 ml) was tested. The absorbance did not change for standing times of 1—10 min.

The effect of the pH on the solution before the addition of chloramine-T and the mixed reagent was examined by varying the buffer solution. Buffer solutions were prepared by mixing various ratios of 0.25 M potassium dihydrogenphosphate solution and 0.25 M disodium hydrogenphosphate solution. The absorbance was constant in the pH range 4.5—6.0, and the pH of the final solution was around 5.7. The absorbance decreased gradually outside the specified range. Since the pH range was thus narrow, a concentrated phosphate buffer solution (pH 5.2) was selected.

Recovery of cyanide using a distillation technique. In the determination of "total cyanide" consisting of free and complex cyanides, distillation

techniques are usually employed, and these techniques normally require an alkaline absorbent. As the present method involves a more concentrated buffer solution than usual, the effect on recovery of cyanide from a distillation technique was examined. For 0.1—0.5 mg CN^- l^{-1}, distillation was done by the method of Kruse and Mellon [8] with phosphoric acid, and the receiving solution was analyzed by the proposed method. When sodium acetate solution (2%) was used as absorbent, cyanide was almost completely recovered (above 98%); when sodium hydroxide solution (2%) was used as absorbent and the receiving solution was neutralized with acetic acid, recoveries were 95—98%. The latter slightly lower recovery is considered to be due to partial evaporation of cyanide during neutralization and not to the concentrated buffer solution, because almost the same results were obtained when the buffer solution was diluted (1 + 1) with water.

Effect of diverse ions. The effect of diverse ions was examined by using solutions containing 2.0 μg CN^- and various diverse ions. The results are shown in Table 1. A large amount of sulfide led to a negative error; 1 mg of sulfide caused a white turbidity, which made it impossible to measure the absorbance. Therefore, when much sulfide is present in a sample solution, suitable pretreatment is necessary for the removal of sulfide. Thiocyanate caused a significant positive error. Distillation tests made with thiocyanate and cyanide solutions and with mixtures, showed that the interference could be avoided in this way. However, when oxidants are present in the sample, thiocyanate might decompose to cyanide during distillation, so that care is needed.

TABLE 1

Effect of diverse ions on the determination of 2.0 μg CN^-/10 ml

Ion	Added as	Amount added (μg/10 ml)	CN^- found (μg)	Error (μg)
Cl^-	NaCl	1000	2.0	0.0
NO_2^-	$NaNO_2$	1000	1.9	−0.1
NO_3^-	KNO_3	1000	2.0	0.0
SO_3^{2-}	Na_2SO_3	1000	2.1	+0.1
SO_4^{2-}	Na_2SO_4	1000	2.0	0.0
CH_3COO^-	$CH_3COONa \cdot 3\ H_2O$	1000	2.0	0.0
OCN^-	KOCN	1000	2.0	0.0
S^{2-}	$Na_2S \cdot 9\ H_2O$	1	2.0	0.0
		10	2.0	0.0
		100	1.1	−0.9
		1000	—	—
SCN^-	KSCN	2	2.9	+0.9
		5	4.3	+2.3
Fe^{3+}	$FeCl_3$	100	2.0	0.0
$Fe(CN)_6^{4-}$	$K_4[Fe(CN)_6] \cdot 3\ H_2O$	100	2.1	+0.1
$Fe(CN)_6^{3-}$	$K_3[Fe(CN)_6]$	100	2.1	+0.1

Calibration curves. Thiocyanate caused a large positive error, which suggested that thiocyanate can be determined by the present method. Figure 2 shows the calibration curves obtained for thiocyanate and cyanide solutions. Both show a good linear relationship.

REFERENCES

1 W. König, J. Prakt. Chem., 69 (1904) 105.
2 J. Epstein, Anal. Chem., 19 (1947) 272.
3 E. Asmus and H. Garschagen, Fresenius Z. Anal. Chem., 138 (1953) 414.
4 S. Nagashima, Anal. Chim. Acta, 91 (1977) 303.
5 K. Ishii, T. Iwamoto and K. Yamanishi, Jpn. Anal., 22 (1973) 448.
6 A. Watanabe, I. Ito and A. Hirakoba, Jpn. Anal., 26 (1977) 505.
7 C. C. Clark, Thesis, Columbia University, New York, N.Y. (1950). Cited in X-ray Powder Data File, Organic Vol., Sets 6—10, ASTM, 1967, p. 94.
8 J. M. Kruse and M. G. Mellon, Anal. Chem., 25 (1953) 446.

Analytica Chimica Acta, 99 (1978) 203—208

Book Reviews

N. Lakshminarayanaiah, *Membrane Electrodes*, Academic Press, New York, 1976, x + 368 pp., price £20.00.

P. L. Bailey, *Analysis with Ion-Selective Electrodes*, Heyden, London, 1976, xii + 228 pp., price £6.80 ($13.50).

G. E. Baiulescu and V. V. Coşofret, *Applications of Ion-Selective Membrane Electrodes in Organic Analysis*, Ellis Horwood, Chichester, 1977, 235 pp., price £16.00, $30.40.

Ion-selective electrodes are certainly one of the most exciting developments in analytical chemistry over the past twenty years. These electrodes offer possibilities not only of fast and relatively cheap precise methods for the determination of ionic activities and concentrations at low levels, but of easy automation for routine applications. Although a few ion-selective electrodes, other than glass electrodes, had been described earlier — the work of Tendeloo and Kolthoff and their co-workers in the 1930s should not be forgotten in any historical context — it was not until the publications of Pungor and his co-workers in the early 1960s that ion-selective electrodes could be seen as a viable proposition for routine chemical analysis. Thereafter, the work of Ross on fluoride and calcium(II) electrodes exploded the scene, and within a very few years many different practical electrodes and sensors for many different inorganic and organic species were described in the literature and became available commercially.

For some years, workers and teachers in the field of ion-selective electrodes have been crying for an up-to-date book to which newcomers and students could be directed. Now three texts have appeared within a short period of time. Each has its strengths and weaknesses.

Professor Lakshminarayanaiah provides a thorough background of relevant theoretical electrochemistry as well as a full discussion of the principles underlying the behaviour of membrane electrodes. Theory provides almost a third of the book. This is followed by a chapter on organic ion exchangers, which contains an odd collection of miscellaneous information. Thereafter there are chapters on electrodes for halides, other anions and cations, and on liquid membrane electrodes, glass electrodes, gas sensors, and enzyme electrodes. Overall, even in these chapters, theory tends to be stressed rather than practice. The arrangement of the material in alphabetical order in some chapters obscures the essential similarity of certain electrodes such as the cadmium-, copper-, and lead-selective electrodes based on silver sulphide. Practical and theoretical aspects are also considerably confused by treating electrodes based on liquid ion exchangers in different parts of the book depending on whether the exchanger is used as a "liquid membrane", as in

the Orion electrode construction, or is incorporated into a PVC or other membrane. Very little practical detail is given about any of the electrodes, although applications are reviewed with numerous references; it is to be hoped that the misspelling of authors' names will not be perpetuated in the literature.

In contrast, Dr. Bailey's book is essentially a practical text. After a short historical introduction, and discussions of cells, reference electrodes and electrode performance, the chapters deal with glass electrodes, electrodes based on inorganic salts, ion exchangers and neutral carriers, gas sensors, and miscellaneous sensors such as enzyme electrodes and surfactant electrodes. The penultimate chapter covers practical procedures. Most praiseworthy and unusual of all, in view of the increasing costs of commercial electrodes, the manufacture of electrodes is discussed in the final chapter, with sufficient detail for laboratory use. This book is commendably free of typographical errors (but see Fig. 5.7!), and is clearly written and well organized.

Professor Baiulescu and Dr. Coşofret deal with applications of i.s.e. in organic analysis. Their initial description of the theoretical background to i.s.e. is rather peculiar but mercifully short; the analytical techniques available with i.s.e. are then discussed, as well as electrode behaviour in non-aqueous media. The subsequent twelve chapters cover the applications, and include direct potentiometric measurements and all types of titrations in which i.s.e. have been involved, whether a compound is determined directly or is first decomposed to yield a determinable component. Examples of the coverage are the determination of fluorine after various sorts of decomposition process, of alcohol with an enzyme electrode, of vicinal glycols with a perchlorate electrode, of maleic acid with a crystal violet ion-pair electrode. The authors seem to have done an admirably comprehensive job on the literature, but there is a good deal of padding in this book, and the referencing is not always accurate.

Comparisons are generally held to be odious; fortunately, these three books offer essentially different things despite their basic theme of ion-selective electrodes. Thus for organic analysts, Baiulescu and Coşofret's book will be of interest, though it is clear that ion-selective electrodes are of merely fringe value in this field. For those of theoretical bent, Membrane Electrodes will be of greatest interest, and is useful in having the relevant background theory neatly in one place. For the practical analyst and, for general instruction purposes, Dr. Bailey's book must be the choice.

In a subject which is still expanding — albeit at a slower rate than 5 years ago — not every reader will agree with all that each author says. But, at last, readers can select the book which seems closest to their own requirements.

A. M. G. Macdonald

H. W. van der Marcel and H. Beutelspacher, *Atlas of Infrared Spectroscopy of Clay Minerals and their Admixtures*, Elsevier, Amsterdam, 1976, viii + 396 pp., price $65.95, Dfl. 165.00.

The interpretation of infrared spectra of clays and associated minerals, oxides, hydroxides, carbonates, sulphates, rock-forming silicates and humic substances is still a relatively young science. The spectra provide a useful technique for identifying clay structures and especially for observations of impurities associated with the structures.

The Atlas provides a 30-page introduction to infrared spectroscopy and includes a chapter on the assignment of clay absorption bands. Spectra, which cover the range 4000—420 cm^{-1}, are generally of acceptable quality. Replication for certain minerals, especially kaolinite and montmorillonite, would appear to be excessive, although this focuses attention on the extents to which impurities can dominate the spectra of naturally occurring deposits of clay minerals. In their commentaries the authors draw attention to some errors in interpretations of the originally published spectra. Inevitably, in a work of this magnitude, some inaccurate interpretations will have escaped their notice and the intending user might be advised to follow the guiding principles provided before using some of the spectra data as reference material.

This Atlas is a good beginning, and will inevitably be followed by more definite selections and interpretations. It does provide at this time a very important addition to the library of workers in the field of clay science.

M. H. B. Hayes

Roger Perry and Robert J. Young (Eds.), *Handbook of Air Pollution Analysis*, Chapman and Hall, London, 1977, xvi + 506 pp., price £20.00.

This is a good book, and most reasonably priced. The general standard of production is excellent, with particularly fine diagrams, but Eugene Sawicki will not like the spelling of his name on p. 339, and those who try to trace the entry on x-ray fluorescence from the subject index will have difficulty.

The editors, members of the staff of the Department of Public Health and Water Resource Engineering at Imperial College, London, have had the assistance of one Canadian, two American, and six other British contributors in the preparation of this book, which is intended primarily as a practical manual for postgraduate students and those employed in civil and public health engineering. This book is therefore not written by analytical chemists for analytical chemists, but it does contain a great deal of modern analytical chemistry and the mode of presentation, different in emphasis to that encountered routinely in analytical chemistry texts, is refreshing and interesting.

The chapters deal with General Sampling Techniques, Analysis of Particulate Pollutants, Metal Analysis, Nitrogen and Sulphur Compounds, Secondary Pollutants, Hydrocarbons and Carbon Monoxide, Halogen-containing Compounds, Remote Monitoring Techniques, and Planning and Execution of an Air Pollution Study. Each chapter gives many references to the literature, including material published in 1976.

This book achieves its purpose. It will be a useful acquisition for all those engaged in air pollution analysis, and it could also go on to the list of books recommended to students and teachers of environmental chemistry.

D. M. W. Anderson

John G. Stockham and Edward G. Fochtman (Eds.), *Particle Size Analysis*, Ann Arbor Science, Michigan, 1977, xi + 140 pp., price £15.60, $26.40.

This neat little book presents papers prepared by members of the Fine Particles Research Section of the I.I.T. Research Institute, Chicago, and presented at a one-day symposium held to celebrate "Filtration Day" on October 24, 1975. Accordingly, the text refers little to work published more recently than 1974. The editors have been successful, misprints are few, and the treatment is clear and uniform throughout. Good lists of figures, tables and references, and a comprehensive subject index make it easy to locate specific items. The twelve chapters are mostly short, of 8—15 pp.; they give concise, clear discussions of topics such as Sizing with the Microscope, Sizing with Modern Image Analysers, Simple Sedimentation Methods, Optical Sizing Techniques, The Electrozone Counter, Inertial Analysers for Particle Size Measurement of Aerosols, Size Analysis by Elucidation and Centrifugation, The Effect of Particle Shape, and Selections of a Particle Size Measurement Instrument.

Particle size analysis is of great importance in fundamental studies and in the technological development and optimization of many products. It is a specialized branch of analysis; this publication is unlikely to contain much information for the specialist, but it offers a useful introduction to many aspects of the subject for students.

Howard E. Hesketh, *Fine Particles in Gaseous Media*, Ann Arbor Science, Michigan, 1977, x + 214 pp., price £15.60, $26.40.

This book can be regarded as a useful companion volume to that reviewed immediately above, but it was written primarily for the practising engineer and air pollution control specialist and therefore falls outside the area of direct interest for analytical chemists, other than those concerned with atmospheric environmental problems.

The treatment is mathematical, but there is a good blend of theory and practice; following an introductory chapter, there are chapters on Unidirectional Motion of Particles, Non-steady Motion of Particles, Effects of Other Forces, Particle Collection, and Size Measurement. An interesting feature is the inclusion of a chapter that presents Experiments and Problems; these deal with topics such as particle velocity and acceleration, collection efficiencies of rough spheres, Reynolds Numbers etc., and may be of interest to teachers of physics, physical chemistry, or chemical engineering.

Lawrence H. Keith (Ed.), *Identification and Analysis of Organic Pollutants in Water*, Ann Arbor Science, Michigan, 1976, x + 718 pp., price £17.90, $30.25.

The analysis of waters for organic pollutants has fallen far behind trace inorganic analysis, and is still commonly done by BOD, COD, and TOC tests. The application of computer-assisted g.c.-m.s. may change this state of affairs; apparently, 400—500 organic compounds have already been identified in potable waters, and it is estimated that some 100,000 more may yet be found.

This book contains 32 papers read at a symposium in Mexico City in 1975, with four other papers added, and indicates current development in this area. It comprises three parts: the chemistry of pollutants; methods of analysis, particularly g.c.-m.s. and separation techniques; and identification techniques, again with a preponderance of g.c.-m.s. Most types of waters, including domestic and trade wastes, are covered. There is certainly useful information in these papers, but they would more usefully have appeared in condensed form in environmental journals. As has come to be expected from this publisher, the cover blurb is less than ethical, and the fact that this book comprises Symposium Proceedings appears only at the end of the preface. No doubt those interested in water analysis who can afford computerized g.c.-m.s. will want to buy a copy, but it is difficult to find reasons why anyone else should do so.

C. L. Wilkins, S. P. Perone, C. E. Klopfenstein, R. C. Williams and D. E. Jones, *Digital Electronics and Laboratory Computer Experiments*, Plenum Press, New York, 1976, viii + 283 pp., price, $15.00.

This book is based on several years of experience with teaching a laboratory course on computer-assisted experimentation in the Universities of Nebraska and Oregon, Purdue University and Western Maryland College. After a short introduction, the student is taken through five experiments which outline the principles of digital logic and which are essential for those with no prior experience of computer work. The bulk of the book

contains descriptions of the principles of interfacing, and twelve experiments which illustrate these principles, starting with logic chip tests, A/D conversion, graphic display and ensemble averaging, and ending with potentiometric titrations, gas chromatography, kinetic analysis and spectrophotometry (Job plots). Modified BASIC language is used, and the experiments are designed around Varian 620 and HP 2100 computers. Useful appendices give details of the realtime language modifications and of the equipment needed. The laboratory time involved is about 90 hours for the complete course, but it is not clear for which grade of student the course is intended.

This is certainly an interesting text, and is recommended not only for student use, but for those teachers who feel that their practical classes should be more computer-orientated.

Printed in The Netherlands

CONTENTS

Short Communications